

UNIVERSITA' VITA-SALUTE SAN RAFFAELE

**CORSO DI DOTTORATO DI RICERCA
INTERNAZIONALE
IN MEDICINA MOLECOLARE**

Curriculum in Neuroscience and Experimental Neurology

Development of an *in vitro* functional platform to discover new drugs for progressive multiple sclerosis and translation to preclinical animal models

DoS: Prof. Gianvito Martino 

Second Supervisor: Jun.-Prof. Dr. Michela Deleidi

Tesi di DOTTORATO di RICERCA di Svetlana Bezukladova
Matr. 013835
Ciclo di dottorato XXXIV
SSD BIO/13

Anno Accademico 2020/2021

RELEASE OF PHD THESIS

La sottoscritta/*I, the undersigned* Svetlana Bezukladova

Matricola / *registration number* 013835

nata/ *born in* Balakovo, Russia

il/on 29/06/1992

autore della tesi di Dottorato di ricerca dal titolo / *author of the PhD Thesis titled*

Development of an in vitro functional platform to discover new drugs for progressive multiple sclerosis and translation to preclinical animal models

AUTORIZZA la Consultazione della tesi / *AUTHORIZE the public release of the thesis*

NON AUTORIZZA la Consultazione della tesi per 12 mesi / *DO NOT AUTHORIZE the public release of the thesis for 12 months*

a partire dalla data di conseguimento del titolo e precisamente / *from the PhD thesis date, specifically*

Dal / *from* 03/03/2022 Al / *to* 03/03/2023

Poiché / *because*:

X l'intera ricerca o parti di essa sono potenzialmente soggette a brevettabilità / *The whole project or parts of it may be the subject of a patent application;*

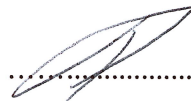
ci sono parti di tesi che sono già state sottoposte a un editore o sono in attesa di pubblicazione / *Parts of the thesis have been or are being submitted to a publisher or are in the press;*

X la tesi è finanziata da enti esterni che vantano dei diritti su di esse e sulla loro pubblicazione / *the thesis project is financed by external bodies that have rights over it and its publication.*

E' fatto divieto di riprodurre, in tutto o in parte, quanto in essa contenuto / *reproduction of the thesis in whole or in part is forbidden*

Data / *Date* 25/02/2022

Firma / *Signature*



DECLARATION

This thesis has been composed by myself and has not been used in any previous application for a degree. Throughout the text I use both 'I' and 'We' interchangeably.

All the results presented here were obtained by myself, except for:

- 1) **Reprogramming and iPSC lines characterization** was performed by Dr. Francesca Ruffini and Dr. Linda Ottoboni, Neuroimmunology unit, Division of Neuroscience, San Raffaele Scientific Institute, Milan, Italy.
- 2) **Electrophysiological analyses** (Results, chapter 3.5.1.4, figure 40), were performed by Dr. Stefano Taverna, Division of Neuroscience, San Raffaele Scientific Institute, Milan, Italy.
- 3) **Flow cytometry experiments readout and data analysis** (Results, chapter 3.5.1.6, figures 43- 44) and neurofilament (Nfl) measurement (Results, chapter 3.3.5, figure 25) were performed by Dr. Alessandra Mandelli, Clinical Neuroimmunology unit, Division of Neuroscience, San Raffaele Scientific Institute, Milan, Italy.
- 4) **The hSOX10-inducible system** was previously set up by Annamaria Cafarella and hiOL differentiation experiment and FACS readout (Results, chapter 3.3.2, figure 17), was performed by Dr. Akram Mokhtarzadeh and Dr. Valentina Murtaf. Neuroimmunology unit. Division of Neuroscience, San Raffaele Scientific Institute, Milan, Italy.
- 5) **The pharmacokinetic analyses of Bavisant and Casopitant** (Results, chapter 3.3.5, figure 23) were performed by IRBM, Pomezia, Italy.
- 6) **Histopathological evaluation and data interpretation** (Results, chapter 3.3.5, figure 27) were performed by Anatomical Pathology Unit, San Raffaele Scientific Institute, Milan, Italy.
- 7) **RNA-sequencing and data analysis** (Results, chapter 3.5.2, figures 45-47) was performed by a group of Prof. Sergio Baranzini, University of California, San Francisco, United States.

All sources of information are acknowledged by means of reference.

This thesis might contain copyrighted material, the use of which may not have been specifically authorised by the copyright owner. This material is available in an effort to explain the biological processes relevant to the understanding of the experimental procedures and results or to illustrate the biological composition or functions. The material contained in this thesis is reported without profit for research and educational purposes. Only small portions of the original work are being used and those could not be used easily to duplicate the original work. This should constitute a "fair use" of any copyrighted material (referenced and provided for in section 107 of the US Copyright Law). If you wish to use any copyrighted material from this site for purposes of your own that go beyond "fair use", you must obtain expressed permission from the copyright owner.

In loving memory of my mother,
who passed away at the age of 42 from progressive multiple sclerosis.

ACKNOWLEDGEMENTS

This thesis would not have been possible without support of my mentors, laboratory and administrative staff members, and the collaborators of the BRAVEinMS project.

I would like to express my gratitude to Prof. Gianvito Martino and Prof. Paola Panina for the opportunity to join the lab and for the endless support during the last three years.

This dissertation would not have been possible without the support of the collaborators of the BRAVEinMS project and the Progressive Multiple Sclerosis Alliance funding agency.

I especially would like to thank Dr. Linda Ottoboni for being a mentor and a friend, for believing in me. This work would not be possible without her.

I would like to thank my second supervisor Prof. Michela Deleidi for valuable suggestions and support.

I would like to thank all members of the lab, especially Francesca Ruffini and Elena Brambilla, Alessandra Mandelli, Akram Mokhtarzadeh, Annamaria Cafarella, Valentina Murtaj, Martina Absinta, Carolina Peri, Jessica Perego, Giulia Di Sabato, Claudia Giglione for help with the experiments and for the useful suggestions.

I would like to acknowledge Desiree Zambroni, Valeria Berno and Stefano Taverna for help with imaging and electrophysiology experiments.

Finally, I would like to thank my family, and especially my husband Enzo for the endless support and encouragement, for being with me through every step of this journey.

ABSTRACT

Multiple sclerosis (MS), an inflammatory autoimmune disease characterised by myelin and axonal damage, is the major cause of progressive neurological disability in young adults. Most MS patients have a continuous accumulation of disability throughout their lifespan leading to progressive MS (PMS), still an incurable disease. The urgent challenge is the development of novel effective therapies for progressive forms of MS, which could slow or prevent ongoing neurodegeneration by targeting neuroprotection and remyelination. One of the rational approaches to achieve this goal is drug repurposing. Drug repurposing focuses on identifying novel targets for generic medications with the indication for other diseases. In addition to drug repurposing, *in silico* drug prediction offers a complementary approach for the efficient selection of successful drug candidates. To better reproduce the human biological tissue, iPSCs can provide a valuable tool for *in vitro* disease modelling and almost an infinite cellular source with the preserved genetic background of the donor. The iPSC-derived oligodendrocyte and neuronal cultures represent a unique patient-specific “disease-in-a-dish” tool for evaluating drug candidates’ pro-myelinating and neuroprotective effects. The aim of the project is to design and conduct a comprehensive and well-characterized pharmacological screening to ultimately identify a handful of lead compounds with therapeutic potential for PMS. Therefore, *in vitro* phenotypic drug screening of drug repurposing library using primary murine and hiPSC-derived neuronal cultures was set up. The library of repurposed drugs in this project was selected by machine learning-based tool SPOKE in collaboration with S. Baranzini lab at UCSF. The pharmacological activity of two selected drugs was evaluated *in vivo* in the preclinical model of MS (EAE). Target identification and mechanism of action of hit compounds neuroprotective/remyelinating properties are currently ongoing. In addition, we have characterized the molecular profiles and functional phenotypes of hiPSC-derived neurons from three twin pairs discordant for MS that will provide additional knowledge on the potential impact of genetic and epigenetic changes on neuronal susceptibility to damage in MS. By better understanding the underlying causes of progressive nerve damage and impaired myelin regeneration, the development of novel treatments for people with PMS will be eventually accelerated.

TABLE OF CONTENTS

ACRONYMS AND ABBREVIATIONS.....	11
LIST OF FIGURES AND TABLES	15
1. INTRODUCTION	17
1.1 MULTIPLE SCLEROSIS.....	17
1.2 PATHOGENESIS OF PROGRESSIVE MULTIPLE SCLEROSIS.....	18
1.3 MECHANISMS LEADING TO PROGRESSION IN MS.....	22
1.4 PROGNOSTIC RISK FACTORS AND EVALUATION OF PROGRESSION.....	25
1.5 CURRENT THERAPIES AND CLINICAL TRIALS IN PMS	27
1.5.1 Therapies approved for PMS management	27
1.5.2 Therapies targeting neuroprotection and remyelination.....	30
1.5.3 Stem cell therapies.....	33
1.6 NOVEL APPROACHES IN DRUG DEVELOPMENT FOR PMS.....	36
1.6.1 Drug repurposing	36
1.6.2 Drug prioritization in silico.....	37
1.6.3 iPSCs for disease modelling and drug discovery	37
2. AIMS OF THE STUDY	41
3. RESULTS.....	42
3.1 SETUP OF THE MULTISTAGE STEPWISE DRUG SCREENING PLATFORM.....	42
3.1.1 Overview of screening approach.....	42
3.1.2 Drug library selection via bioinformatic in silico prioritization.....	43
3.2 IN VITRO PHENOTYPIC SCREENING	47
3.2.1 Evaluation of compounds cytotoxicity effect	47
3.2.1.1 Cytotoxicity assays identified 160/273 non-toxic compounds on primary murine cortical neurons	48
3.2.1.2 Secondary cytotoxicity evaluation identified 148/160 compounds non-toxic on hiPSC-derived neuronal cultures	51
3.2.2 Evaluation of compounds neuroprotective efficacy in 2D in vitro models.....	53
3.2.2.1 Neuroprotective assay setup on primary murine cortical neurons: selection of NMDA and NAC as a stressor and neuroprotective control respectively.....	53
3.2.2.2 Identification of 17 compounds with neuroprotective efficacy against NMDA-mediated excitotoxicity in survival assay on primary murine cortical neurons	56
3.2.2.3 Identification of 23 compounds with neuroprotective efficacy against NMDA-mediated excitotoxicity on primary murine cortical neurons.....	57
3.2.2.4 Identification of 9 out of 32 “front runners” with neuroprotective efficacy against TBHP-mediated oxidative stress in hiPSC-derived neuronal cultures.....	60

3.2.3	<i>Compounds ranking and prioritization</i>	62
3.3	VALIDATION OF SELECTED HIT-COMPOUNDS BAVISANT AND CASOPITANT	64
3.3.1	<i>Dose-response experiments of Bavisant and Casopitant confirm their neuroprotective properties</i>	64
3.3.2	<i>Bavisant and Casopitant show promyelinating efficacy in hiOL</i>	66
3.3.3	<i>Bavisant and Casopitant confirm their neuroprotective efficacy in 3D neural spheroids</i>	69
3.3.4	<i>Bavisant-and Casopitant-treated EAE mice show lower demyelination and lower axonal loss of the spinal cord but no amelioration of the clinical score</i>	74
3.4	IN SILICO AND IN VITRO HIT-COMPOUNDS TARGET VALIDATION	82
3.4.1	<i>In silico target/pathway analysis identifies NK1R and SIGMAR1 as potential targets of Casopitant, and HRH3 as a potential target of Bavisant</i>	82
3.4.2	<i>In vitro target validation</i>	84
3.4.2.1	<i>TACR1 transcript is expressed in hiPSC-derived and mouse cortical neurons but not in N2A cells, while SIGMAR1 and HRH3 transcripts are expressed in all tested cell types</i>	85
3.4.2.2	<i>TACR1 protein is expressed in hiPSC-derived and mouse cortical neurons but not in N2A cells, while SIGMAR1 and HRH3 proteins are expressed in all tested cell types</i>	86
3.4.3	<i>Casopitant confirms its neuroprotective and antioxidant effect in N2A cells</i>	89
3.4.4	<i>SIGMAR1 small RNA interference modulation</i>	92
3.5	MS-SPECIFIC NEURONAL CELL CHARACTERIZATION.....	95
3.5.1	<i>Characterization of hiPSC-derived glutamatergic neurons from three twin pairs discordant for MS</i>	95
3.5.1.1	<i>Immunofluorescence characterization</i>	96
3.5.1.2	<i>RT-qPCR identifies highly expressed VGLUT1 in hiPSC-derived neurons from MS patients</i>	99
3.5.1.3	<i>hiPSC-derived glutamatergic neurons from twin pairs comparably release glutamate during differentiation</i>	100
3.5.1.4	<i>Patch-clamp electrophysiology identifies decreased potassium and sodium currents in hiPSC- derived neurons from MS patients</i>	102
3.5.1.5	<i>hiPSC-derived neurons voltage-gated ion channels expression profile</i>	105
3.5.1.6	<i>Functional oxidative CellROX assay identifies increased oxidative stress response in hiPSC-derived neurons from MS patients</i>	108
3.5.2	<i>RNA-seq transcriptional profiles of NPCs and hNeu from three twin pairs discordant for MS</i>	111
4.	DISCUSSION	118
5.	CONCLUSIONS AND FUTURE PERSPECTIVES	131
6.	MATERIALS AND METHODS	133
6.1	ANIMALS	133

6.1.1 Ethics, Consent, and Permission	133
6.2 PREPARATION OF THE COMPOUNDS.....	133
6.3 DIFFERENTIATION OF PRIMARY MURINE CORTICAL NEURONS AND ASTROCYTES	133
6.4 DIFFERENTIATION OF NEURO2A CELLS	134
6.5. iPSC GENERATION	134
6.5.1 hiPSC differentiation into neural progenitors (NPCs) and neurons	135
6.5.2 hiPSC differentiation into hSOX10 oligodendrocytes	136
6.5.2.1 hSox10 inducible vector.....	136
6.5.2.2 Neural precursor generation	136
6.5.2.3 hSOX10 oligodendrocyte differentiation	136
6.6 3D NEURAL SPHEROIDS (BRAINSPHERES)	137
6.6.1 Neuroprotective assay and sholl analysis of neurite outgrowth of 3D neural spheroids (BrainSpheres)	138
6.7 CYTOTOXIC AND NEUROPROTECTIVE ASSAY ON PRIMARY MURINE CORTICAL NEURONS	138
6.8 MORPHOLOGICAL INTEGRITY EVALUATION OF PRIMARY MURINE CORTICAL NEURONS	139
6.9 CYTOTOXIC AND NEUROPROTECTIVE ASSAY ON HUMAN hiPSC-DERIVED NEURONS	139
6.10 FUNCTIONAL OXIDATIVE STRESS ASSAY (CELLROX)	139
6.11 CYTOTOXIC AND NEUROPROTECTIVE ASSAY ON NEURO2A CELL LINE.....	140
6.12 CELLULAR CHARACTERISATION.....	141
6.12.1 Immunofluorescence	141
6.12.2 BrainSpheres immunocytochemistry	142
6.12.3 EAE spinal cords immunohistochemistry	142
6.12.3.1 Hematoxylin and Eosin (H&E) staining.....	142
6.12.3.2 Luxol fast blue staining.....	142
6.12.3.3 Bielschowsky's silver stain	143
6.12.4 RNA extraction and reverse transcription.....	143
6.12.5 Polymerase Chain reaction (PCR) and Real-Time Polymerase Chain reaction (RT-qPCR)	144
6.12.6 Patch-clamp electrophysiology	146
6.12.7 Glutamate release measure	146
6.12.8 Western blot and SDS-page analysis.....	147
6.13 SMALL RNA INTERFERENCE	148
6.14 INDUCTION OF MOG-EAE AND CLINICAL FOLLOW-UP	149
6.15 SIGNALING PATHWAYS NETWORK ANALYSIS VIA SPOKE	149

6.16 STATISTICAL ANALYSES	150
7. REFERENCES.....	151

ACRONYMS AND ABBREVIATIONS

2D, Two-Dimensional
3D, Three-Dimensional
3NP, 3-Nitropropionic Acid
9HPT, 9-Hole Peg Test
ACSF, Artificial Cerebrospinal Fluid
ADCC, Antibody-Dependent Cellular Cytotoxicity
ADHD, Attention-Deficit Hyperactivity Disorder
ADME/PK, Absorption, Distribution, Metabolism, Excretion, and Pharmacokinetics
AIMS, Astrocytes Inflamed in MS
ALA, Alpha-Lipoic Acid
ALS, Amyotrophic Lateral Sclerosis
AP, Action Potential
APC, Antigen-Presenting Cell
ATP, Adenosine Triphosphate
b.i.d., twice daily
BBB, Brain-Blood Barrier
BTK, Bruton's Tyrosine Kinase
C1q, Component 1q
CACNG3, Calcium Voltage-Gated Channel Auxiliary Subunit Gamma 3
CCL2, Chemokine (C-C motif) Ligand 2
CCR7, C-C chemokine receptor type 7
CETSA, Cellular Thermal Shift Assay
CGRP, Calcitonin Gene Related Peptide
CIS, Clinically Isolated Syndrome
CNS, Central Nervous System
CSF, Cerebral Spinal Fluid
DC, Dendritic Cell
DEG, Differentially Expressed Genes
DIV, Days In Vitro
DMSO, Dimethyl sulfoxide
DMT, Disease-Modifying Treatment
DNA, Deoxyribonucleic Acid
DTI, Diffusion Tensor Imaging
DWPC, Degree-Weighted Path Count
EAE, Experimental Autoimmune Encephalomyelitis
EDSS, Expanded Disability Status Scale
EPO, Erythropoietin
ER, Endoplasmic Reticulum
ES, Embryonic Stem cell
FC, Fold Change

FeSO₄, Iron Sulphate
FDA, Food and Drug Administration
FDR, False Discovery Rate
GalC, Galactosylceramidase
GFAP, Glial Fibrillary Acidic Protein
GFP, Green Fluorescent Protein
GluA1/2, Glutamate ionotropic receptor AMPA type subunit 1
GO, Gene Ontology
GM-CSF, Granulocyte-Macrophage Colony-Stimulating Factor
GWAS, Genome-Wide Association Study
H₂O₂, Hydrogen peroxide
H&E, Haematoxylin and Eosin
HIF-PDI, Hypoxia-Inducible Factor-Proline Dioxygenase Inhibitors
hiOL, Human iPSC-derived Oligodendrocytes
hiPSC, Human-Induced Pluripotent Stem Cells
HMGB1, High-Mobility Group Box-1
hNeu, human neurons
HRH3, Histamine H3 receptor
HSC, Hematopoietic Stem Cell
HTS, High-Throughput Screening
IFN γ , Interferon- γ
IL-17, Interleukin-17
IL-6, Interleukin-6
IL-1 α , Interleukin-1 α
INPP5D, Inositol Polyphosphate-5-Phosphatase D
iPSC, Induced Pluripotent Stem Cell
ISC, Immunosenescence
K_i, receptor binding affinity
K2P, Two-pore-domain potassium channels
KCNK9 (or TASK-3), Potassium Two Pore Domain Channel Subfamily Member 9
LDH, Lactate Dehydrogenase
LIF, Leukaemia-Inhibiting Factor
LPA, Lysophosphatidic Acid
MAIT, Mucosal-Associated invariant T cell
MAM, Mitochondria-Associated Membrane
MBP, Myelin Basic Protein
MIMS, Microglia Inflamed in MS
MitoQ, Mitochondrial-targeted coenzyme Q10
mNeu, mouse neurons
MoA, Mechanism of Action
MOG, Myelin Oligodendrocyte Glycoprotein
MRI, Magnetic Resonance Imaging

MS, Multiple Sclerosis
MSC, Mesenchymal Stromal Cell
MSC-NPs, Mesenchymal Stem Cell-derived Neural Progenitors
mtDNA, Mitochondrial DNA
MW, multiwell
NAC, N-acetyl Cysteine
NAWM, Normal-Appearing White Matter
NfL, Neurofilament Light Chain
NK1R, Neurokinin-1 Receptor
NMDA, N-methyl-D-aspartic Acid
NMDAR1, The N-methyl-D-aspartate Receptor
NO, Nitric Oxide
NOS, Nitric Oxide species
NPC, Neural Precursor Cell
NSC, Neural Stem Cell
OL, Oligodendrocyte
OPC, Oligodendrocyte Precursor Cell
PASAT, Paced Auditory Serial Addition Test
PBMC, Peripheral Blood Mononuclear Cell
PBVC, Percentage Brain Volume Change
PCA, Principal Component Analysis
PDGF, Platelet-Derived Growth Factor
PET, Positron-Emission Tomography
PMS, Progressive Multiple Sclerosis
PO, per os
POL, Polyornithine/Laminin
PMS, Progressive Multiple Sclerosis
PPMS, Primary-Progressive Multiple Sclerosis
PRDX, Peroxiredoxin
q.d., once daily
QC, Quality Control
qMTR, Quantitative Magnetization Transfer
QSM, Quantitative Susceptibility Mapping
RIS, Radiologically Isolated Syndrome
RNA, Ribonucleic Acid
RNS, Reactive Nitrogen Species
ROS, Reactive Oxygen Species
RRMS, Relapsing-Remitting Multiple Sclerosis
S1P, Sphingosine-1 Phosphate
S1R/SIGMAR1, Sigma non-opioid Intracellular Receptor 1
SAS, Subarachnoid Space
SCC, Spinal Cord Culture

scRNA-seq, single-cell RNA sequencing
SEM, Standard Error of the Mean
SIMOA, Single-Molecule Array Immunoassay
siRNA, small interfering RNA
snRNA-seq, single-nucleus RNA-sequencing
SPMS, Secondary Progressive Multiple Sclerosis
SPOKE, Scalable Precision Medicine Open Knowledge Engine
SYN1, Synapsin 1
SYT1, Synaptotagmin 1
T25FW, Timed 25-Foot Walk
TBHP, Tert-Butyl Hydrogen Peroxide
TF, Transcription Factor
TGF- β 2, Transforming Growth Factor β 2
TH1, T helper 1 cell
TH17, T helper 17 cell
TNF α , Tumour Necrosis Factor α
TSPO, Translocator Protein
T β 4, Thymosin beta-4
UPLC-MS, Ultraperformance Liquid Chromatography-tandem Mass Spectrometry
UPR, Unfolded Protein Response
VGIC, Voltage-Gated Ion Channel
VGLUT1, Vesicular Glutamate Transporter 1
WM, White Matter
WST-8, Water-Soluble Tetrazolium salt

LIST OF FIGURES AND TABLES

Figure 1. Immune processes dysregulation is involved in MS pathogenesis and progression. ...	19
Figure 2. Factors influencing the development of progressive MS.....	22
Figure 3. Schematic of multistage phenotypic screening pipeline.	43
Figure 4. Compounds analysis.	46
Figure 5. List of compounds target genes from pathway enrichment analysis.	47
Figure 6. Characterization of primary murine cortical neurons culture.	48
Figure 7. Results of the cytotoxicity assay of 273 in silico prioritized compounds evaluated on primary murine cortical neurons.....	50
Figure 8. hiPSC-derived glutamatergic neurons as a cellular model for secondary (hit-to-lead validation) phenotypic screening.....	51
Figure 9. Evaluation of compounds cytotoxicity in hiPSC-derived neurons.	52
Figure 10. Neuroprotective assay setup on primary murine cortical neurons: selection of toxic stressor.....	54
Figure 11. Neuroprotective assay setup with NMDA as a stressor on primary murine cortical neurons: selection of positive neuroprotective control.	56
Figure 12. Primary screening of 160 non-toxic compounds in NMDA-mediated and neuroprotective assay settings.....	57
Figure 13. Evaluation of compounds neuroprotective efficacy from NMDA-mediated excitotoxicity: morphological integrity.	59
Figure 14. Validation of 32 “front runners” compounds in hiPSC-derived neuronal cultures.	61
Figure 15. Compounds ranking and prioritization.	64
Figure 16. Validation of hit-compounds Bavisant and Casopitant neuroprotective properties in vitro: dose-response assay.....	65
Figure 17. Validation of pro-myelinating properties of Bavisant and Casopitant in hiOL.	67
Figure 19. 3D neural spheroids (BrainSpheres).	70
Figure 20. Oxidative stressor dose-response assay in the 3D neural spheroids.	71
Figure 21. Evaluation of Bavisant and Casopitant neuroprotective efficacy in the 3D neural spheroids.....	72
Figure 22. Summary of Bavisant and Casopitant neuroprotective efficacy in the 3D neural spheroids.....	73
Figure 23. In vivo validation of hit-compounds in EAE animal model: clinical score evaluation	75
Figure 24. Immunohistochemical evaluation of EAE spinal cord tissue demyelination.....	77
Figure 25. Immunohistochemical evaluation of EAE spinal cord tissue axonal loss.	78
Figure 26. Immunohistochemical evaluation of EAE spinal cord tissue immune cell infiltrates	79
Figure 27. Histopathological evaluation of EAE mice organs treated with Bavisant, Casopitant, or Methocell.....	82
Figure 28. Casopitant pathway interaction and target prediction analysis via SPOKE	83
Figure 29. Bavisant pathway interaction and target prediction analysis via SPOKE.....	84
Figure 31. In vitro target validation: HRH3 protein expression profile.....	87
Figure 32. In vitro target validation: NK1R and SIGMAR1 protein expression profiles	87
Figure 33. Neuroprotective assay setup on N2A cell line.	91
Figure 34. SIGMAR1 siRNA modulation.	94
Figure 35. Effect of Casopitant and PRE-084 on SIGMAR1 protein levels.....	95
Figure 36. hiPSC-derived glutamatergic neurons from three twin pairs clinically discordant for MS: immunofluorescence characterisation.	98

<i>Figure 37. hiPSC-derived glutamatergic neurons from three twin pairs clinically discordant for MS: RT-qPCR characterisation.</i>	100
<i>Figure 38. hiPSC-derived glutamatergic neurons from two twin pairs comparably release glutamate during differentiation.</i>	101
<i>Figure 39. Scheme of patch-clamp electrophysiology in hiPSC-derived neurons.</i>	103
<i>Figure 40. hiPSC-derived neurons electrophysiological characterisation.</i>	105
<i>Figure 41. hiPSC-derived neurons voltage-gated ion channel expression profile.</i>	107
<i>Figure 42. Summary on differentially expressed genes encoding voltage-gated ion channels in neurons from two twin pairs clinically discordant for MS.</i>	108
<i>Figure 43. Setup of a functional oxidative stress assay CellROX in hiPSC-derived neurons by FACS readout.</i>	109
<i>Figure 44. Functional CellROX assay identifies increased oxidative stress response in hiPSC-derived neurons from MS patients.</i>	111
<i>Figure 45. Principal Component Analysis (PCA) of RNA-seq performed on fibroblasts, iPSC, NPCs, and neurons from three twin pairs discordant for MS.</i>	112
<i>Figure 46. Differential gene expression and GO enrichment analysis in MS vs. HC NPC cluster</i>	113
<i>Figure 47. Differential gene expression and GO enrichment analysis in MS vs HC neuronal cell cluster.</i>	114
<i>Figure 48. Protein-protein interaction network analysed by STRING 9.0 software.</i>	117
<i>Table 1. Selected clinical trials in multiple sclerosis.</i>	33
<i>Table 2. The list of the biological process terms utilised in silico drug prioritization algorithm</i>	44
<i>Table 3. The list of keywords utilised in silico drug prioritization algorithm</i>	45
<i>Table 4. Summary of EAE incidence, maximum disease severity, the cumulative and average score for each treatment group.</i>	76
<i>Table 5. Clinical and anagraphic information of twin pairs donors</i>	96

1. INTRODUCTION

1.1 Multiple sclerosis

Multiple sclerosis (MS) is a chronic inflammatory and neurodegenerative immune-mediated disease of the central nervous system that leads to demyelination and establishment of focal lesions in the brain and the spinal cord (Thompson *et al*, 2018). The demyelinating inflammatory lesions are the hallmarks of the disease, and their accumulation leads to a plethora of neurological dysfunctions including fatigue, ataxia, visual and gait disturbances, cognitive symptoms, muscle weakness, and paralysis. Although the initial trigger that causes the disease remains unknown, MS results from a combination of multiple pathological processes in one individual, altered by a great number of genetic, biological, and environmental factors (O’Gorman *et al*, 2012; Ramagopalan *et al*, 2010; Olsson *et al*, 2016). Among the multiple risk factors associated with MS are genetic variants (Baranzini & Oksenberg, 2017), viral infections (Reich *et al*, 2018), obesity (Gianfrancesco & Barcellos, 2016), microbiome changes (Berer *et al*, 2017; Takewaki *et al*, 2020; Jangi *et al*, 2016), diet (Mannino *et al*, 2022) vitamin D deficiency (Simon *et al*, 2012; Kočovská *et al*, 2017), environmental toxins (Wheeler *et al*, 2019; Rumah *et al*, 2013) and tobacco exposure (O’Gorman *et al*, 2012).

The disease mainly manifests during young adulthood (18-40 years old), and in 85% of cases starts with a relapsing-remitting form (RRMS) (Thompson *et al*, 2018). In 2-10% of cases, MS can manifest before the age of 16 years, recognized as paediatric or juvenile multiple sclerosis (Alroughani & Boyko, 2018; Yan *et al*, 2020). The incidence of MS is higher in women compared to men, with a 3:1 ratio (Thompson *et al*, 2018). Within 20 years from the onset, the majority of RRMS patients advance to a secondary progressive form of the disease (SPMS). The progressive form is characterized by the absence of relapses and a steady accumulation of symptoms, eventually leading to irreversible disability. The remaining subset of patients (10-15%) develops a progressive disease course from the onset, namely primary-progressive multiple sclerosis (PPMS). Almost 3 million people are estimated to live with MS worldwide (Walton *et al*, 2020), and at least 1.5 million people will receive a diagnosis of progressive MS (PMS).

Progressive multiple sclerosis remains one of the leading causes of non-traumatic neurological disability in young adults, therefore sustaining a substantial socioeconomic burden for patients, their families, and the healthcare system (Hartung, 2021; Nicholas *et*

al, 2020). Despite the significant progress in the development of disease-modifying treatments (DMT) for RRMS in the last decade, treatment options for progressive MS are limited or poorly effective (Faissner & Gold, 2019). Therefore, the major challenge is the development of novel effective therapies for progressive forms of MS, which could slow or prevent ongoing neurodegeneration by targeting neuroprotection and remyelination.

1.2 Pathogenesis of progressive multiple sclerosis

The clinical manifestations and the course of multiple sclerosis are heterogeneous among patients and often unpredictable. Although RRMS and SPMS are classified as distinct subtypes of MS, certain pathologic features and underlying disease mechanisms partially overlap, but with a variable degree. Historically, MS has been defined as an autoimmune inflammatory disease that manifests with an acute inflammatory attack driven by T- and B-lymphocytes and plasma cells that enter the CNS and spread to the white matter (WM), where the immune response is targeted against myelin antigens (Steinman, 1996; Reich *et al*, 2018). White matter damage results from complex interactions of infiltrating immune cells, microglia, astrocytes, oligodendroglia, and neurons (Domingues *et al*, 2016; Absinta *et al*, 2021). In RRMS, such attacks lead to demyelination, acute axonal transection, and formation of focal white matter lesions that MRI identifies as gadolinium-enhancing due to a disruption of the blood-brain barrier (BBB) (Filippi, 2000). The formation of new lesions often correlates with clinical manifestations or relapses, determined by a lesion location; however, some of the plaques are formed silently. Although in RRMS lesions are mainly formed in the WM, cortical and deep grey matter lesions can be also detected but with a lower incidence. On the other hand, the increased quantity of the cortical lesions is a characteristic feature of the progressive MS (Kutzelnigg *et al*, 2005). Several types of grey matter lesions have been described, such as leukocortical lesions that form in the proximity of white-grey matter border, intracortical lesions confined to a cortical ribbon, and subpial lesions or superficial lesions of the neocortex (Kutzelnigg & Lassmann, 2005). In progressive MS, the subpial cortical lesions are often associated with the presence of leptomeningeal lymphoid-like structures or B-cell follicles (Griffiths *et al*, 2020; Gh Popescu & Lucchinetti, 2012).

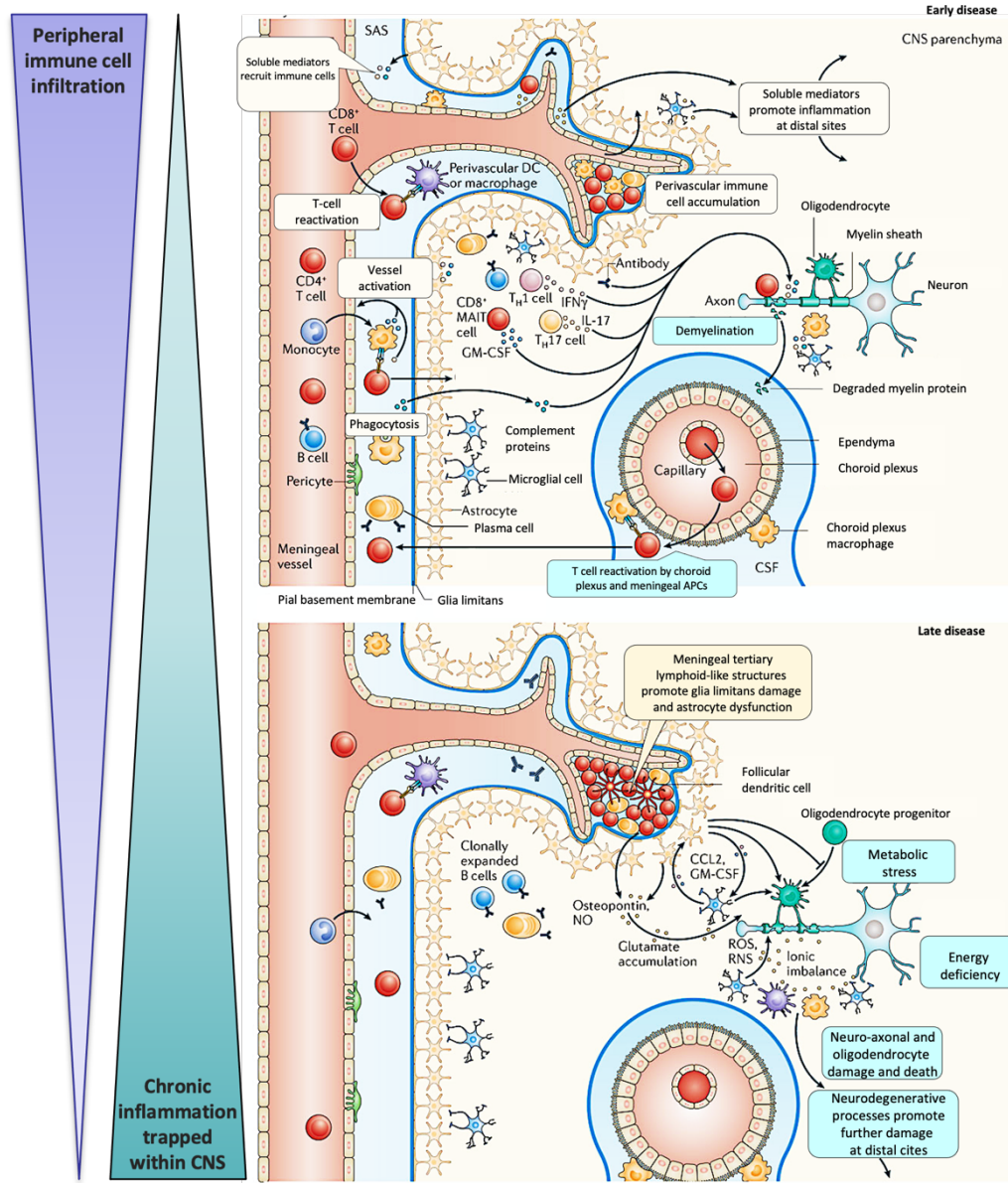


Figure 1. Immune processes dysregulation is involved in MS pathogenesis and progression. Infiltration of peripheral innate and adaptive immune cells such as CD4+ and CD8+ T cells, B cells, and myeloid cells from the periphery into the central nervous system (CNS) takes place during the early stages of MS through blood vessels of the blood-brain barrier (BBB), the subarachnoid space (SAS) and the choroid plexus (top panel). During the relapse or the acute immune attack, these cells enter the CNS parenchyma and accumulate in perivascular spaces and around post-capillary venules of the BBB. The antigen-specific immune cells create a local inflammatory environment secreting pro-inflammatory cytokines and activating CNS-resident microglia and astrocytes. Subsequent activation of innate immune cells amplifies inflammatory response and secondary adaptive and immune cells recruitment. The inflammatory wave of immune infiltrating and activated CNS-resident cells contributes to oligodendrocyte damage, demyelination, and neuro-axonal injury by soluble inflammatory and neurotoxic mediators. In progressive MS (bottom panel), the episodic peripheral infiltration of immune cells into the CNS is declining; however, compartmentalized CNS inflammation becomes predominant. Meningeal immune B-cell infiltrates potentially mediate a constant low-grade inflammatory insult by forming lymphoid-like structures, while CNS-resident innate cells (for example, astrocytes)

produce CC-chemokine ligand 2 (CCL2) and granulocyte-macrophage colony-stimulating factor (GM-CSF). The secretion of pro-inflammatory factors promotes microglial activation, fuelling a hostile inflammatory environment that prevents the differentiation of oligodendrocyte progenitor cells into mature oligodendrocytes. Other mechanisms contributing to ongoing tissue injury are the decreased repair capacity of the damaged neuro-axon-glial unit, chronic oxidative stress promoted by innate and adaptive immune cell activation and disrupted iron metabolism, mitochondrial dysfunction, hypoxia, altered glutamate homeostasis, and potential contribution of complement system activation. APC, antigen-presenting cell; DC, dendritic cell; IFN γ , interferon- γ ; IL-17, interleukin-17; NO, nitric oxide; RNS, reactive nitrogen species; ROS, reactive oxygen species; MAIT cell, mucosal-associated invariant T cell; TH1, T helper 1 cell; TH17, T helper 17 cell. Figure adapted from references (Filippi *et al*, 2018; Dendrou *et al*, 2015).

Meningeal inflammation is linked to increased grey matter atrophy, an additional source of sustained compartmentalized humoral immunity. Both phenomena have been associated with a poorer prognosis and faster progression in MS (Magliozzi *et al*, 2007; Howell *et al*, 2011). With disease development, the newly formed lesions in PMS become less frequent, while compartmentalized chronic inflammation and widespread diffuse axonal damage become predominant (Seewann *et al*, 2009; Vrenken *et al*, 2010). Chronic low-grade inflammation is sustained by activated microglia/macrophages and astrocytes, which are often found at the periphery of chronic active lesions (Absinta *et al*, 2021). Smouldering plaques or slowly expanding lesions are a distinct hallmark of progressive MS, and their evolvement is a result of a sustained inflammatory process driven by activated iron-rich microglia. The source of iron in chronic active MS lesions is unknown, however, the leading hypothesis is that activated microglia ingest iron-rich myelin and dying oligodendrocytes that release iron in the extracellular space (Dal-Bianco *et al*, 2017). It has been shown that iron accumulation in activated macrophages is driven by the pro-inflammatory cytokines IL-6 and IL-1beta which promote microglia polarization towards a pro-inflammatory phenotype (Mehta *et al*, 2013). Several histopathological studies showed (Luchetti *et al*, 2018; Frischer *et al*, 2015) that this type of lesion has a destructive core with a pronounced axonal loss and presence of activated microglia at the border of the lesion but an almost complete absence of microglia/macrophages in the centre of the lesion (Kuhlmann *et al*, 2017). Due to high iron content, the iron rims of chronic active lesions are detectable by high field 7T MRI (Absinta *et al*, 2016) or quantitative susceptibility mapping (QSM) technique (Stüber *et al*, 2016) and therefore can be used as an imaging biomarker to monitor disease evolution. A longitudinal study with QSM showed (Dal-Bianco *et al*, 2017) that chronic active lesions with iron rim increase in size and enlarge for an average of six to eight years, potentially driving disease

progression. In addition, increased numbers of slowly-expanding lesions have been associated with higher disability in SPMS (Absinta *et al*, 2019).

Complementary to MRI-based techniques, the presence of invisible widespread chronic inflammation and activated microglia in the lesions and normal-appearing white matter (NAWM) in MS is detectable by positron-emission tomography (PET) imaging, targeting 18-kDa translocator protein (TSPO) (Airas *et al*, 2018; Vivash & OBrien, 2016; Janssen *et al*, 2018). The increased TSPO activity, linked to a higher level of neuroinflammation, has been associated with clinical disability and widespread structural disruption in the NAWM of PMS patients (Sucksdorff *et al*, 2020; Bezukladova *et al*, 2020).

Another critical feature of progressive MS is the exhaustion of the remyelination capacity (Hagemeyer *et al*, 2012). Although the completely remyelinated lesions or shadow plaques are detectable in MRI and present among all courses of the disease with similar frequencies, the extent of remyelination is highly variable among the patients, and the cause of such differences is unknown (Patrikios *et al*, 2006). Neuropathological analyses have identified that oligodendrocyte precursor cells (OPC) mainly remain in their progenitor state within the plaques in progressive MS either due to maturation failure or axonal exhaustion for remyelination (Patrikios *et al*, 2006; Kuhlmann *et al*, 2008; Chang *et al*, 2000). Interestingly, the latest research by T. Kuhlmann and colleagues showed that human iPSC-derived oligodendrocytes (hiOL) from twins discordant for the disease, which have been transplanted into Shi/Shi Rag2^{-/-} mice successfully myelinate *in vivo* confirming the notion that oligodendrocyte differentiation block may arise from extrinsic, but not intrinsic oligodendroglia properties (Mozafari *et al*, 2020). Further research confirmed that one of the extrinsic factors inhibiting oligodendrocytes differentiation is the inflammatory environment and the secretion of IFN γ sustained by activated peripheral blood mononuclear cells (PBMCs). Interestingly, while the pro-remyelinating drugs clemastine, benztropine, and miconazole did not affect oligodendrocyte differentiation when applied together with activated PBMC supernatants, the treatment with immunomodulatory drug teriflunomide could partially restore the impaired hiOL differentiation capacity (Starost *et al*, 2020). These results indicate that future therapeutic approaches in progressive MS should consider the

possibility of combinatory treatments targeting both myelination and inflammation to effectively promote remyelination.

1.3 Mechanisms leading to progression in MS

Despite the significant progress achieved in the last decades in the MS field, the exact mechanisms responsible for the transition from RRMS to SPMS are not well understood. Two main hypotheses propose that progressive MS may evolve either due to accumulation of extensive neuronal damage and exhaustion of repair mechanisms associated with ageing and immune and cellular senescence or can be triggered by a certain level of chronic inflammation within the CNS caused by a lifelong tissue injury (Leray *et al*, 2010; Absinta *et al*, 2020).

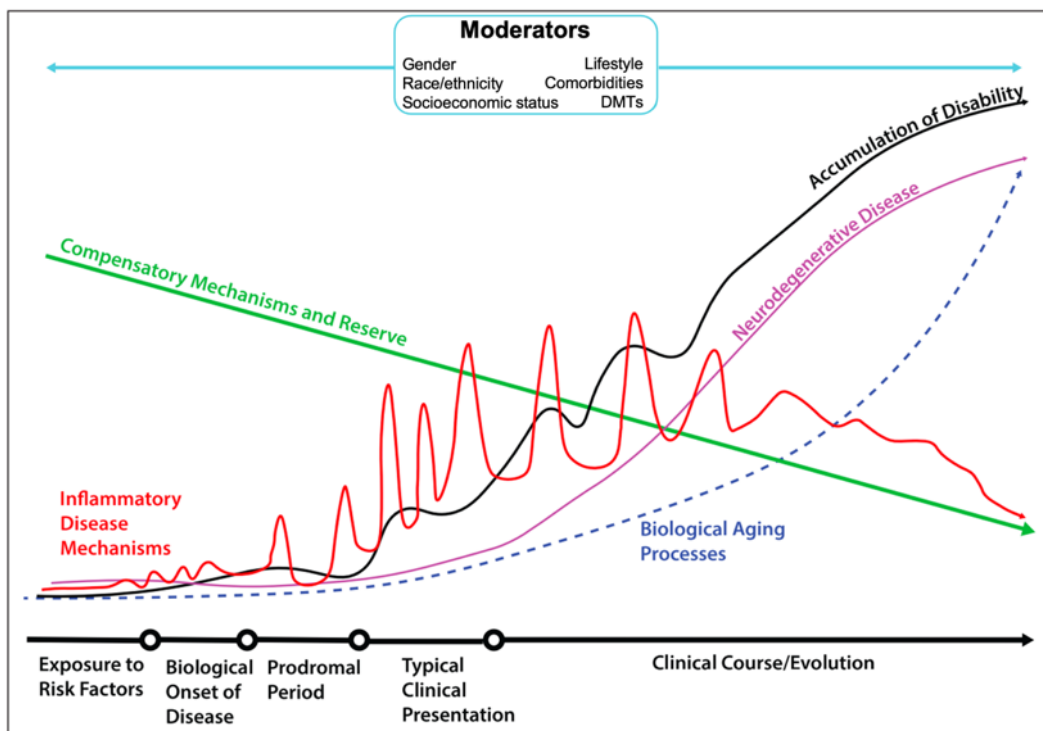


Figure 2. Factors influencing the development of progressive MS. The combination of several pathological factors, including inflammatory-induced damage, neurodegenerative mechanisms, and biological ageing, influence the gradual accumulation of disability that eventually leads to the development of progressive MS. Compensatory mechanisms and brain functional reserve likely attenuate these processes during the early disease stages, however, with disease evolution, the accumulation of damage exceeds the system’s compensatory capacity to repair. Gender, socioeconomic status, diet, lifestyle, environmental factors, viral exposures, comorbidities, and the utilization of DMTs are the significant moderators in the development of PMS. Figure adapted from (Thompson *et al*, 2022).

In RRMS, the episodic inflammation and demyelination followed by a recovery phase are predominant, while axonal loss and neuronal dysfunction are the key features in SPMS. Although RRMS has been historically considered mainly as an inflammatory disease while SPMS has been considered as a neurodegenerative process independent of inflammatory responses, numerous studies in the last decade show that sustained compartmentalized inflammation plays a significant role in the progressive MS evolution (Machado-Santos *et al*, 2018; Meisl *et al*, 2008; Michel *et al*, 2015; Matthews, 2019). The pathogenic mechanisms underlying PMS include chronic demyelination and axonal damage sustained by prominent oligodendrocyte and neuronal loss, which advance mitochondrial exhaustion and ion channel imbalance, favouring astrogliosis and chronic microglial activation (Lassmann *et al*, 2012; Immitola *et al*, 2006; Cree *et al*, 2021). Once the balance between tissue injury and repair exceeds a certain threshold, a progressive MS stage initiates.

In both hypotheses, ageing plays a significant role in driving MS progression. Several studies have demonstrated that progression to a secondary phase happens on average around 45 ± 10 years of age (Koch *et al*, 2010; Tutuncu *et al*, 2012), and later age at the onset is a strong predictor for progressive MS (Stankoff *et al*, 2007). While both immune and cellular senescence are being associated with increasing age (Eschborn *et al*, 2021; Baden *et al*, 2019; Papadopoulos *et al*, 2020), age-related immune dysfunctions play a significant role in the development of many neurological diseases, including MS. During ageing, both phenomena sustain the persistent low-grade neuroinflammation – or “inflammaging”, fuelling-up an oxidative environment and the build-up of mitochondrial injury. Mitochondrial dysfunction, accumulation of mitochondrial DNA (mtDNA) mutations, and decline in mitochondrial energetics are the hallmarks of ageing. Impaired mitochondria are the primary source of increased ROS production (Starkov, 2008), inflammation, and subsequent axonal injury, which contribute to neurodegeneration in MS (Witte *et al*, 2014; de Barcelos *et al*, 2019; Dutta *et al*, 2006). Mitochondrial damage is observed in all stages of MS, but particularly evident in progressive MS where high levels of NOS and ROS produced by activated microglia promote injury to neuronal mitochondria (Campbell & Mahad, 2018). Excitotoxicity and increased energy demands in demyelinated axons lead to $\text{Na}^+/\text{Ca}^{2+}$ ionic imbalance, increasing axonal Ca^{2+} concentration that activates Ca^{2+} -dependent apoptosis mechanisms, leading to neuronal

death (Nicholls & Budd, 1998). Therefore, targeting cellular senescence together with mitochondrial dysfunction, oxidative stress, and ion channel imbalance are the promising neuroprotective strategies in MS (Rosenkranz *et al*, 2021; Licht-Mayer *et al*, 2020; Shirani *et al*, 2016; Mendiola *et al*, 2020; Enders *et al*, 2020; Arun *et al*, 2013; Subedi *et al*, 2017; Villoslada, 2016; Oost *et al*, 2018; Rivellini *et al*, 2021).

Cellular senescence and alterations in the peripheral immune system are associated with ageing. The immune system senescence (ISC) affects both innate and adaptive immune systems, leading to dysregulation of a repertoire of immune functions and an imbalance between pro-and anti-inflammatory responses. In progressive MS, the premature ageing of the immune system is evidenced by somatic and leukocyte telomere shortening (Hecker *et al*, 2021; Guan *et al*, 2015) that is associated with disability and higher oxidative stress in the progressive MS stage (Krysko *et al*, 2019).

Additionally, cellular senescence of progenitor cells potentially contributes to OPC's ability to remyelinate damaged neurons, affecting action potential propagation and increasing neuronal vulnerability. The suggested mechanism causing OPC cellular senescence is a high-mobility group box-1 (HMGB1)-mediated transcriptomic changes (Nicaise *et al*, 2019). OPCs sensitivity to a highly inflammatory and hostile oxidative environment has been confirmed by the latest single-cell RNA sequencing (scRNA-seq) studies (Domingues *et al*, 2016; Witte *et al*, 2014). Transcriptomics analysis of nuclei isolated from post-mortem MS brain tissue identified (Jäkel *et al*, 2019) a loss of both fully mature oligodendrocyte (OL) and intermediate OPC populations, indicating that only specific subsets of oligodendrocytes may contribute to remyelination, and their restoration should be targeted in the future therapeutic approaches. The remaining “stressed OPCs” and myelinating OLs have shown lower expression of genes responsible for OL differentiation and myelin synthesis (e.g. *BCAS1* (Fard *et al*, 2017), *SGMS1*). Instead, genes involved in oxidative and cellular stress responses (e.g. the unfolded protein response (UPR), heat-shock response) were highly upregulated, indicating severe stress of OLs in MS (Schirmer *et al*, 2019). Stressed OLs were specifically enriched at the periplaque and the edge of chronic active lesions in the post-mortem progressive MS brain tissue (Absinta *et al*, 2021).

Moreover, the signature of stressed microglia, so-called “microglia inflamed in MS” (MIMS), comprised of “foamy” phagocytosing microglia and “iron-rich” microglia

clusters expressing high levels of inflammatory and complement genes (Morgan *et al*, 2021) has been identified within smouldering plaques suggesting a pathogenic role of these cells in disease progression (Absinta *et al*, 2021). Concomitant with microglia, the presence of “astrocytes inflamed in MS” (AIMS) (Absinta *et al*, 2021) with upregulated *GFAP*, *APOE*, *VIM*, *S100B*, *SOD1*, *FTL/FTH1* genes, and MAFG/MAT2 α -driven pro-inflammatory astrocytes have also been identified (Wheeler *et al*, 2020) at the peri-plaque area of chronic active lesions in PMS. This clear signature of highly inflammatory microglia and astrocytes in progressive MS has led to the hypothesis of their failure to modulate the inflammatory response and inability to return to the homeostatic state after CNS insult. This impairment has been supported by evidence of several age-related changes in the microglia and astrocytes (Zhang *et al*, 2021b; Palmer & Ousman, 2018; Costa *et al*, 2021). Aged microglia become dysfunctional to efficiently clear myelin debris and therefore are defective in phagocytosis. Activated senescent microglia produce higher levels of ROS (Lu *et al*, 2000) and pro-inflammatory cytokines (Marschallinger *et al*, 2020; Cantuti-Castelvetri *et al*, 2018). Similarly, activated astrocytes are pro-inflammatory in the aged, induced by microglia through secretion of interleukin-1 α (IL-1 α), tumour necrosis factor α (TNF α) cytokines, and complement component 1q (C1q) (Liddelow *et al*, 2017). It has been suggested that neurotoxicity triggered by activated astrocytes is sustained via secretion of saturated lipids, where lipo-apoptosis of oligodendrocytes is mediated through activation of endoplasmic reticulum-regulated stress response pathways (Guttenplan *et al*, 2021).

Altogether, the complex interplay of aged-driven immune and cellular changes together with the accumulation of lifelong tissue injury and persistent inflammation may lead to disease progression in MS. Novel therapies targeting neurodegeneration and axonal dysfunction via neuroprotection and promoting remyelination together with suppression of compartmentalized CNS inflammation might be beneficial in treating progressive MS.

1.4 Prognostic risk factors and evaluation of progression

Prevention of transition to progressive MS is the primary clinical goal for patients with MS diagnosis and physicians. Conversion to SPMS is associated with poor prognosis, shorter life expectancy, increased disease burden, and cognitive impairment (Cree *et al*, 2021). To date, no standardized definition for SPMS has been concluded (Lorscheider *et*

al, 2016), partially due to retrospective diagnosis of SPMS, which is mainly based on a clinical history of slow accumulation of disability during the relapsing-remitting phase. The moment when progression initiates is ambiguous: overall, it is a part of a disease continuum, and the exact mechanisms driving the transition from RRMS to SPMS have not yet been well-established.

To date, there are no reliable biomarkers for early detection and assessment of progression, and there is no universal consensus on diagnostic criteria defining the disease progression (Ziemssen *et al*, 2020). The latest definition of criteria for progressive MS diagnosis was recently established and include three factors: the worsening of the Expanded Disability Status Scale (EDSS) ≥ 4 ; a functional impairment of the pyramidal system of ≥ 2 ; and the clinical reconfirmation of disability during a three months follow up (Lorscheider *et al*, 2016). Although EDSS evaluation, based on neurological examination, is a gold standard and the most used system to evaluate disease progression in MS, it does not distinguish between mild, moderate, and severe symptoms and has a poorly stratified evaluation scale. To improve sensitivity in evaluating worsening of a multifactorial disease like MS, additional performance tests e.g., 9-Hole Peg Test (9HPT) (Feys *et al*, 2017) for upper limb function assessment, Timed 25-Foot Walk (T25FW) (Kalinowski *et al*, 2021) for ambulatory performance test, and Paced Auditory Serial Addition Test (PASAT) (Tombaugh, 2006) for cognitive evaluation, together with neuropsychological questionnaires (Meca-Lallana *et al*, 2021) should be used in routine clinical assessment in patients, especially at the age of 45-55 years old when patients are at higher risk to progression. Age is considered to be the most common risk factor for conversion to SPMS together with the disease duration (Tutuncu *et al*, 2012; Fambiatos *et al*, 2020). Other prognostic factors include higher EDSS and older age at disease onset (Fambiatos *et al*, 2020; Scalfari *et al*, 2014; Barzegar *et al*, 2020), higher relapse frequency (Fambiatos *et al*, 2020; Scalfari *et al*, 2014), male sex (Scalfari *et al*, 2014; Koch *et al*, 2010), accelerated brain volume loss without evident disease activity (Cree *et al*, 2019), grey matter volume loss and cortical grey matter lesions (Eshaghi *et al*, 2018; Kutzelnigg & Lassmann, 2005; Scalfari *et al*, 2018), brainstem and spinal cord lesions, or motor impairment (Koch *et al*, 2010; Barzegar *et al*, 2020) and higher number of chronic active or “slowly-expanding” lesions (Elliott *et al*, 2019; Luchetti *et al*, 2018; Absinta *et al*, 2016, 2019). These pathological brain and spinal cord changes can be

detected in a retrospective manner with MRI-based techniques, but radiological data alone has limitations for the efficient diagnosis and monitoring of progressive MS. Complementary to the most common clinical MRI-based assessment (Kaunzner & Gauthier, 2017) of disease activity, the additional biomarkers may provide earlier identification of real-time pathological changes leading to progression (Meca-Lallana *et al*, 2021). The development of extremely sensitive single-molecule detection-based techniques (e.g., single-molecule array immunoassay, SIMOA) allows to monitor disease activity by measuring levels of neurofilament light chain (NfL)(Uphaus *et al*, 2021; Cantó *et al*, 2019; Kuhle *et al*, 2019; Thebault *et al*, 2020) and glial fibrillary acidic protein (GFAP)(Ayrignac *et al*, 2020; Axelsson *et al*, 2011; Högel *et al*, 2020) in the blood and cerebral spinal fluid (CSF) of the patients, and correlate them to neuroimaging findings (Saraste *et al*, 2021a, 2021b), although these biomarkers are not yet applied in routine clinical practice (Bittner *et al*, 2021). Only with careful monitoring of disease evolution and optimized disease-modifying treatment selection (Brown *et al*, 2019; Comi, 2013; Ciotti & Cross, 2018), it will be possible to prevent or slow down progressive MS.

1.5 Current therapies and clinical trials in PMS

1.5.1 Therapies approved for PMS management

Decades of research of inflammatory components underlying MS pathology led to the development of an armamentarium of effective therapies for RRMS, although the progress achieved in the last decade in developing therapeutical strategies in progressive MS is as well encouraging. Nevertheless, genuinely effective therapies targeting mechanisms responsible for disability accumulation in PMS are still missing. The failure in many PMS clinical trials is partially driven by an incomplete understanding of the complex pathogenic mechanisms that advance patients to a progressive disease phase. Four drugs, namely ofatumumab, ocrelizumab, siponimod, and cladribine, have been FDA-approved for patients with active SPMS experiencing clinical relapses without MRI activity. Siponimod, so far, is the only drug that showed efficacy in reduction of brain atrophy and reduction of disability accumulation in SPMS patients in phase III clinical trial (EXPAND, NCT01665144) (Kappos *et al*, 2018), while ocrelizumab (ORATORIO, NCT01194570) (Montalban *et al*, 2017) was only moderately effective in primary progressive MS. Both ofatumumab and ocrelizumab belong to the group of drugs targeting B-cells. Ocrelizumab is a humanized anti-CD20 monoclonal antibody depleting

B-cells mainly through antibody-dependent cellular cytotoxicity (ADCC). At the same time, ofatumumab is a monoclonal immunoglobulin 1 κ (IgG1 κ) lytic antibody that aims at decreasing B-cell levels in a dose-response manner through the CD20 binding (Faissner & Gold, 2019). CD20 is expressed by B-cells lineage, including naïve B-cells, pre-B cells, and memory B-cells, allowing their specific targeting. The development of B-cell depleting therapies arose from the evidence of B-cell tertiary follicles in the meninges of chronic MS patients, correlative with clinical score severity and grey matter cortical thinning (Magliozzi *et al*, 2007). The memory subset of B-cells and plasmablasts infiltrating CNS represents the pathogenic pool producing high levels of antigen-presenting immunoglobulins and pro-inflammatory cytokines (Amit *et al*, 2010), cytotoxic to oligodendrocytes and neurons (Lisak *et al*, 2012, 2017). B-cell accumulation in meningeal and perivascular cuffs is shown to drive compartmentalized inflammation contributing to MS worsening; therefore, depletion of circulating B-cells (and T-cells) may indirectly reduce their contribution to smouldering inflammatory activity in progressive MS.

In addition, other B-cell targeting therapies, including rituximab, atacicept, obinutuzumab, ublituximab, and various Bruton's tyrosine kinase (BTK) inhibitors (evobrutinib, ibrutinib, fenebrutinib) have been developed (Cencioni *et al*, 2021). The main disadvantage of anti-CD20 monoclonal antibodies is their inability to cross BBB, therefore limiting their efficacy in the direct effect on CNS-resident B cells and plasmablasts. The development of BBB-penetrant drugs such as idealisib, a PI3 kinase inhibitor (Greenfield & Hauser, 2018), is a favourable option for implementing novel small molecules targeting B-cell signalling.

Another potential therapeutic target in PMS treatment is a family of sphingosine-1 phosphate (S1P) receptors. Several molecules targeting S1P were developed in the last decade and received regulatory approval for treating multiple sclerosis, including fingolimod, siponimod, ponesimod, and ozanimod. S1Ps are high-affinity G-protein coupled receptors comprised of five distinct subtypes (McGinley & Cohen, 2021). Each subtype has heterogeneous tissue and immune cell expression, involved in various functions, including immune cell trafficking, neurogenesis, regulation of neuronal excitability, oligodendrocyte survival, angiogenesis, endothelial and blood-brain barrier function (McGinley & Cohen, 2021). S1PR₁ receptor subtype is mainly expressed by

most immune cells, while S1PR₂-S1PR₅ expression patterns are not limited to the immune system only, being expressed by CNS-resident cells including microglia, astrocytes, and oligodendrocytes (Karunakaran & van Echten-Deckert, 2017). The S1P signalling cascade plays an important role in immune cell trafficking and secretion of immune mediators, therefore regulating local and systemic immune responses. The proposed S1PRs modulators' mechanism of action is mainly through their binding to S1P receptors expressed on CCR7-positive lymphocytes that lead to receptor internalization and loss of S1P gradient function (from low S1P levels in tissues to high S1P levels in vascular compartments), regulating lymphocytes egress from lymph nodes (Thompson *et al*, 2022). Naïve and central memory T-cells expressing CCR7 chemokine receptor retained in lymphoid tissues limit the migration of inflammatory cells into the CNS, reducing annualized relapse rate and disease progression in MS (McGinley & Cohen, 2021). Although fingolimod showed good clinical efficacy in decreasing MRI lesion activity, relapse rate, and brain volume loss in RRMS, it has failed to reduce confirmed disability in PPMS patients (INFORMS, NCT00731692) (Lublin *et al*, 2016). Despite the similarity in the peripheral effect of S1PR modulators, their potential direct effect in the CNS is not yet well-understood. Both fingolimod and siponimod can cross the BBB and directly affect the CNS, reducing astrogliosis and microglial activation, exerting a neuroprotective function, and enhancing remyelination via the S1P₅ signalling (Kipp, 2020; Hunter *et al*, 2016). Although S1P modulators have both direct anti-inflammatory effects in addition to their central action in the CNS, the benefit of S1PR modulators was so far only moderately effective in progressive MS.

The latest approved drug for active SPMS is cladribine, a synthetic deoxyadenosine (purine nucleoside analogue) targeting circulating T and B lymphocytes. Cladribine acts through deoxycytidine kinase phosphorylation expressed at high levels by B-cells and T lymphocytes, leading to DNA strands break and eventual gradual over weeks-to-months lymphocyte apoptosis (Leist & Weissert, 2011). The drug showed efficacy in selective depletion of memory B-cell population and decreasing T-cell lymphocyte population by 40-50%. Cladribine was investigated in phase III clinical trial CLARITY (NCT00213135) in patients with RRMS and confirmed its efficacy in reducing relapse rate and reducing the risk of disability progression. In the additional clinical trial ONWARD (NCT00436826), cladribine combined with interferon-beta showed

encouraging clinical benefit in reducing the relapse rate by 63% and reducing by 90% T1 gadolinium-enhancing lesions in active RRMS and SPMS with relapses (Montalban *et al*, 2018). Despite the promising clinical efficacy, treatment with cladribine is associated with the risk of developing solid tumours, lymphopenia, risk of infections, and may cause congenital disabilities if used during pregnancy. Notwithstanding a long route to regulatory approval and potential side effects, cladribine is a unique oral therapy with the long-term efficacy of reducing disability progression in the active MS (Patti *et al*, 2020). Besides few medications with proven but limited efficacy in moderation of disability progression, novel therapeutic approaches focusing on enhancing neuronal resilience and promoting remyelination are currently under development.

1.5.2 Therapies targeting neuroprotection and remyelination

Two promising drugs targeting neuroprotection that showed efficacy in either primary or secondary progressive MS phase II clinical trials are simvastatin (MS-STAT, NCT00647348) (Chataway *et al*, 2014) and ibudilast (SPRINT-MS, NCT01982942) (Fox *et al*, 2018). Simvastatin, a widely used medication for hypercholesterolemia, showed anti-inflammatory and neuroprotective effects in preclinical experimental autoimmune encephalomyelitis (EAE) studies (de Oliveira *et al*, 2015; Zamvil & Steinman, 2002), as well reducing by 43% brain tissue loss in SPMS patients. Ibudilast is a phosphodiesterase inhibitor used for asthma treatment that was able to slow down the whole-brain atrophy by 20% over 96 weeks period in patients with progressive MS but did not reduce the development of new T2 or T1 lesions, indicating its neuroprotective but not anti-inflammatory mechanism of action (Naismith *et al*, 2021). Both drugs have been identified through repurposing approaches (Pushpakom *et al*, 2019), screening already approved drugs with indications for other diseases. In addition, other repurposed drugs with neuroprotective efficacy, including alpha-lipoic acid (Spain *et al*, 2017), riluzole, fluoxetine, and amiloride have been investigated (Chataway *et al*, 2020) for the treatment of secondary progressive MS. Alpha-lipoic acid is an endogenous antioxidant used for diabetic neuropathy treatment; riluzole is a medication for treating amyotrophic lateral sclerosis, modulating glutamate-mediated excitotoxicity; fluoxetine is an antidepressant drug targeting astrocytic lactate release and providing neuronal energy support; amiloride is an acid-sensing ion channel blocker targeting calcium overload. Even though their efficacy was reported (Waslo *et al*, 2019) in various preclinical studies, treatment with

riluzole, fluoxetine and amiloride did not meet the primary outcome of the MS-SMART clinical trial (96 weeks percentage brain volume change (PBVC) compared with placebo); however, treatment with alpha-lipoic acid could reduce by 68% annualized PBCV in SPMS patients (Spain *et al*, 2017).

An alternative approach to target neuroprotection is through remyelination enhancement, function restoration, and axonal degeneration prevention. Remyelination is a spontaneously occurring process, although it is drastically decreased in the ageing brain (Cantuti-Castelvetri *et al*, 2018), particularly in the SPMS (Nicaise *et al*, 2019; Bramow *et al*, 2010). Evidence from human neuropathology and experimental studies show that myelin sheaths wrapping the axon facilitate the saltatory conduction, provide axonal support by lactate production, protect axons from inflammatory and immune mediators, therefore offering neuroprotection (Nave, 2010a, 2010b; Lee *et al*, 2012). Various approaches to enhance remyelination have been addressed by targeting the recruitment, survival, differentiation, and maturation of OPCs, promoting neuronal electrophysiological activity, suppressing remyelination inhibitors, or targeting declined phagocytosis function in microglia (Plemel *et al*, 2017; Cunniffe & Coles, 2021). Several remyelination clinical trials have been conducted in the last years (Lubetzki *et al*, 2020), mostly in RRMS patients, and fewer clinical trials had investigated the capacity of drugs such as opicinumab (anti-LINGO1 antibody) (Cadavid *et al*, 2019), high-dose biotin (Sedel *et al*, 2015; Tourbah *et al*, 2016; Cree *et al*, 2020), erythropoietin (EPO) (Schreiber *et al*, 2017; Ehrenreich *et al*, 2007) and domperidone (Koch *et al*, 2021) (NCT02308137) to enhance remyelination in progressive MS. Unfortunately, none of these studies achieved significant results in PMS, lacking clinical efficacy (Huntemann *et al*, 2021). The failure of clinical trials may indicate that exclusively targeting axonal resilience or only enhancing remyelination might not be sufficient to achieve neuroprotection and revert or delay MS progression. Instead, a combination of immunomodulation, neuroprotection, and enhancement of remyelination, or polytherapy, altogether may provide a promising strategy for PMS.

Although major progress has been made in understanding remyelination biology that led to the discovery of over 50 candidate molecules promoting myelin repair (Plemel *et al*, 2017; Lubetzki *et al*, 2020), only moderate efficacy has been achieved in PMS clinical trials. The potential pitfalls of remyelination trials in PMS are the contribution of ageing

and ageing-associated innate immune system changes to the remyelination capacity (Sim *et al*, 2002; Goldschmidt *et al*, 2009; Rist & Franklin, 2008). Novel therapies targeting senescence, for example, the combination of an antihyperglycemic drug metformin and pro-myelinating agents have been shown to enhance the remyelination capacity of aged OPCs (Neumann *et al*, 2019). Similarly, the therapeutic usage of metformin alone or in combination with R- α -lipoic acid was proposed by the UK MS society lead experts for the treatment of progressive MS (Cunniffe *et al*, 2021).

Another potential challenge in clinical trials of remyelination is highly heterogeneous regional (e.g., periventricular vs. subcortical lesions) and intraindividual variations in the remyelination patterns (Zeis *et al*, 2018; Heß *et al*, 2020). Consequently, the longitudinal follow-up of complex patterns of remyelination in living individuals requires sensitive imaging techniques to quantify myelin content changes. Several MRI-based techniques were developed, including quantitative magnetization transfer (qMTR) and myelin water imaging techniques (Granziera *et al*, 2021), the inversion recovery ultrashort TE imaging (Jang *et al*, 2021), diffusion tensor imaging (DTI) (Fox *et al*, 2011) and novel PET-based molecular imaging techniques (Zhang *et al*, 2021a; Bauckneht *et al*, 2019), although the absence of unique consensus on clinical evaluation of remyelination and lack of standardized protocols are still the critical limiting factors.

The incomplete understanding of complex pathophysiology of progressive MS together with the contribution of ageing to disease development gave rise to the set of questions addressed by researchers designing clinical trials for remyelination, for example: “What type of lesions have to be evaluated for remyelination: active or chronic lesions?”; “What are the optimal clinical outcome measures of remyelination?”; “Which population should be included in the clinical trial: patients in the early disease phase or chronically-stable patients, given that the potential of CNS repair declines with age and accumulation of disability?” These and other urgent questions (Plemel *et al*, 2017; Neumann *et al*, 2020; Klistorner & Barnett, 2021) are to be addressed for the powerful design of future clinical trials.

Drug	Type ^a	Major outcome measures (study duration)	Drug class/mechanism of action	Phase	Trial status	N	NCT number
Evobrutinib	RMS	Active lesions (12-24 wks)	Bruton TKI	2	ANR	267	NCT02975349
Evobrutinib	RMS	Annualized relapse rate (96 wks)	Bruton TKI	3	Recruiting	950	NCT04032158
SAR442168	RMS	New active lesions (12 wks)	Bruton TKI	2	Recruiting	127	NCT03889639
SAR442168	RMS	New active lesions (12 wks)	Bruton TKI	2	Recruiting	105	NCT03996291
Masitinib	PMS	Disability progression (96 wks)	TKI	3	ANR	656	NCT01433497
Imatinib	RRMS	Functional system score (28 d)	TKI	2	Recruiting	200	NCT03674099
Ibudilast	PMS	Brain atrophy and safety (96 wks)	Anti-inflammatory	2	Completed	255	NCT01982942
BIB033	RMS	Disability and safety (72/96 wks)	antiLINGO-1 MAb	2	ANR	263	NCT03222973
Elezanumab	RMS	Disability progression (52 wks)	antiRGMA MAb	2	Recruiting	165	NCT03737851
AHSCT	RRMS	Disease activity and disability (5 yrs)	Immune reset	3	Recruiting	100	NCT03477500
AHSCT	RRMS	Disease activity and disability (5 yrs)	Immune reset	3	Recruiting	200	NCT03342638
AHSCT	MS	Disease disability change (5 yrs)	Immune reset	2	ANR	110	NCT00273364
Simvastatin	SPMS	Disability progression (3 yrs)	Statin	3	Recruiting	1180	NCT03387670
Vitamin D ₃	CIS	Conversion of clinically isolated syndrome to multiple sclerosis (2 yrs)	Vitamin D ₃	3	Recruiting	316	NCT01817166
Vitamin D ₃	RRMS	Annualized relapse rate (2 yrs)	Vitamin D ₃	3	ANR	172	NCT01490502
MD1003	PMS	Disability progression (15-27 mos)	High dose biotin	3	ANR	642	NCT02936037
Lipoic acid	PMS	Brain atrophy progression (2 yrs)	Multiple	2	Recruiting	118	NCT03161028
Nanocrystalline gold	RRMS	VEP and MS disability (48 wks)	Under investigation	2	Recruiting	150	NCT03536559
Laquinimod	PPMS	Brain volume change (24 mos)	Anti-inflammatory	2	Completed	374	NCT02284568
GNbAC1 mAb	RRMS	Active lesions (12 and 24 wks)	To target HERV	2	Completed	270	NCT02782858
IMU-838	RRMS	Number of active lesions (24 wks)	DHODH inhibitor	2	Recruiting	195	NCT03846219
Erythropoietin alfa	ON	Visual acuity and RNFLT-G (6 mos)	Neurotrophic agent	3	ANR	100	NCT01962571
Pioglitazone, montelukast, hydroxy-chloroquine, losartan	MS	Disability progression (1.5 yrs)	Under investigation	2	Recruiting	250	NCT03109288
Balloon venoplasty	RRMS SPMS	Clinical and safety outcomes (48 wks)	To improve CCSVI	2	Completed	104	NCT01864941
SPARC1103	MS	Muscle spasticity (24 d)	GABA _B receptor agonist	2	Completed	142	NCT02027025
VSN16R	MS	Spasticity (26 days)	BKCa calcium activated K ⁺ channel modulator	2	Completed	160	NCT02542787
Amantadine, modafinil, methylphenidate	MS	Fatigue (5 wks)	Stimulants	3	Completed ^a	140	NCT03185065
BX-1 (dronabinol)	MS	Spasticity (16 wks)	Cannabis	3	Recruiting	384	NCT03756974
ADS-5102	MS	Walking speed (12 wks)	Amantadine ER	3	Recruiting	540	NCT03436199
ADS-5102		Walking speed (52 wks)	Amantadine ER				NCT03567057
Arbaclofen ER	RRMS SPMS	Muscle spasticity and disability (1 yr)	R enantiomer of baclofen	3	ANR	323	NCT03319732
Arbaclofen ER	MS	Muscle spasticity and global function (84 d)	R enantiomer of baclofen	3	Completed ^a	536	NCT03290131
Intranasal insulin	MS	Cognitive function (24 wks)	Insulin	2	Recruiting	105	NCT02988401
Adderall XR	MS	Cognitive function (12 wks)	Stimulant	3	Recruiting	180	NCT02676739

^a Study population as reported by study authors at clinicaltrials.gov; ^b Results not posted. Abbreviations: AHSCT, autologous hematopoietic stem cell transplantation; ANR, active nonrecruiting; CCSV, chronic cerebrospinal venous insufficiency; CIS, clinically isolated syndrome; DHODH, dihydroorotate dehydrogenase; ER, extended release; HERV, human endogenous multiple sclerosis-associated retrovirus; LINGO-1, leucine rich repeat and immunoglobulin-like domain-containing protein 1; MS, multiple sclerosis; PMS, progressive MS; PPMS, primary progressive MS; ON, optic neuritis; RMS, relapsing MS; RRMS, relapsing-remitting MS; SPMS, secondary progressive MS; RGMA, repulsive guidance molecule A; RNFLT-G, retinal ganglion nerve fiber layer thickness; TKI, tyrosine kinase inhibitor; VEP, visual evoked potentials.

Table 1. Selected clinical trials in multiple sclerosis. Adapted from (Balashov, 2020).

1.5.3 Stem cell therapies

Stem cell therapy is a broad concept of regenerative medicine that involves transplantation of stem cell progenitor or their derivatives in recipient patients to achieve a therapeutic effect. Stem cell therapeutic effect can be mediated by restoring the stem

cell pool reserve by direct cell replacement or by a bystander effect of beneficial trophic factors release. Therefore, stem cell therapy might serve as a suitable alternative or as complement to current drug therapies in MS. Three main types of adult stem cells transplantation have been investigated in the last decade: hematopoietic stem cells (HSCs), mesenchymal stromal cells (MSCs), and neural stem cell transplantation (NSCs), including fetal NSCs, induced pluripotent stem cell (iPSC) derived NSCs, and directly reprogrammed iNSCs. HSC transplantation is a largely clinically validated procedure routinely used for blood and bone malignancies treatment. The rationale behind autologous HSC transplantation in MS is to eliminate autoantigen reactive CD4+ lymphocytes, restore T cell receptor diversity and function, and immune reconstitution to a naïve, self-tolerant state. The benefits of hematopoietic stem cell transplantation are limited only to patients with high disease activity failing to respond to conventional therapies. HSC transplantation did not show a clear benefit in PMS patients, despite the aggressive immune ablation (Boffa *et al*, 2021; Casanova *et al*). Instead, mesenchymal stem cell transplantation remains of great interest in PMS for immunomodulatory, neurotrophic, and tissue repair functions that have been investigated in numerous experimental *in vivo* preclinical studies (Genc *et al*, 2018). Mesenchymal stem cells are pluripotent, in contrast to the hematopoietic precursors, and can be isolated from various tissues, including adipose tissue, bone marrow, umbilical cord blood, placenta, and dental pulp. The potential mechanisms of action of mesenchymal stem cells involve the combination of peripheral immune system modulation and protection of the CNS tissue through the secretion of soluble trophic factors, such as growth factors, cytokines, and chemokines. Another important feature of MSCs is their pluripotent potential to differentiate towards mesodermal lineage cells, inducing neuronal axon protection and the regeneration of inflamed tissues in the EAE model (Uccelli *et al*, 2011; Yanwu *et al*, 2020). Several studies on mesenchymal stem cell transplantation have been conducted in patients with PMS, demonstrating safety and tolerability of the procedure and short-term benefits inhibiting disease progression, especially in patients with previously active disease (Petrou *et al*, 2020; Smith *et al*, 2021). Additional progressive MS-specific trials are currently ongoing (NCT04749667 (SMART-MS), NCT03696485, NCT03799718) to evaluate neurophysiological and functional outcomes in PPMS and SPMS patients. Two phase-II clinical trials (NCT03355365, NCT03822858) will investigate potential benefits

of autologous mesenchymal stem cell-derived neural progenitors (MSC-NPs), a specific MSC subpopulation primed towards neuroectodermal lineage, in PMS patients. Phase I safety clinical study by Harris and colleagues demonstrated improvement in EDSS in a subset of ambulatory SPMS patients ($EDSS \leq 6.5$), together with improvement in bladder and muscle strength functions after intrathecal administration of MSC-NPs (Harris *et al*, 2018). The transplantation was well-tolerable and safe, resulting in sustained EDSS improvement or disease stabilization in 13 out of 20 patients over a 2-year follow-up period (Harris *et al*, 2021).

Finally, the transplantation of fetal NSCs has several advantages compared to other stem cell sources due to their inherent commitment to the neural lineage, lack of pluripotency, and therefore low tumorigenicity. Among the major drawbacks of fetal NSCs are the low proliferation rate *in vitro* and therefore limited accessibility, and their fetal tissue source of origin which brings major ethical issues. Patient-specific iPSC-derived cells and iNSCs are the alternative cellular therapy candidates to overcome ethical concerns. iPSC-derived cells and iNSC demonstrated the preclinical evidence in MS-relevant animal models ameliorating chronic neuroinflammation, reducing astrogliosis and demyelination through release, for instance, of leukaemia-inhibiting factor (LIF) and transforming growth factor (TGF)- β 2, confirming their “bystander” effect activity (Smith *et al*, 2021; De Feo *et al*, 2017; Laterza *et al*, 2013). Regarding clinical evidence of NSCs and pluripotent stem cell derivatives transplantation in PMS, two safety Phase I studies have been conducted so far (NCT03269071, NCT03282760); however, public reports on trials’ clinical outcome are not yet available. There are several challenges in iPSC-derived stem cell therapy clinical application, including immunogenicity, tumorigenicity and heterogeneity (Yamanaka, 2020; Frederiksen *et al*, 2021), which should be carefully addressed to advance iPSC-based technology into routine clinical settings.

Although stem cell therapies showed encouraging results in preclinical and early clinical studies in the last years (Mansilla *et al*, 2021), the field of stem cell-based regenerative medicine is still in its relative infancy, and more advanced, well-designed, and rigorously controlled studies are required to establish the stem cell repair potential in PMS (Pluchino *et al*, 2020).

1.6 Novel approaches in drug development for PMS

1.6.1 Drug repurposing

Significant advancements were achieved in anti-inflammatory and immunomodulatory therapies development for early MS; however, the neurodegenerative component and the compartmentalized inflammation have remained largely untargeted in progressive forms of MS. Novel effective disease-modifying therapies are the unmet need in treating progressive MS that cannot be delayed any further. One of the rational approaches to achieve this goal is drug repurposing. Drug repurposing focuses on identifying novel targets for generic medications with the indication for other diseases. Drug repurposing, or repositioning, is an attractive approach offering overall lower costs and shorter time to drug approval, bypassing potential safety concerns (Pushpakom *et al*, 2019). Repositioned drugs have already been tested preclinically and clinically, and their safety, tolerability, and pharmacological interactions are mostly known, thus increasing the probability of success in future clinical studies.

A plethora of potential drug candidates able to promote remyelination or neuroprotection *in vitro* and *in vivo* were recently identified by repurposed drugs screening approach, such as antidepressant clomipramine (Faissner *et al*, 2017), antimuscarinic and antihistaminic drugs clemastine, benztropine, and antipsychotic quetiapine (Mei *et al*, 2014), steroids methoxyisoflavone (Eleuteri *et al*, 2017) and clobetasol (Najm *et al*, 2015), antioxidant edaravone (Eleuteri *et al*, 2017), cholesterol-lowering drug lovastatin (Eleuteri *et al*, 2017), estrogen receptor modulators bazedoxifene (Rankin *et al*, 2019) and danazol (Manousi *et al*, 2021), antifungal miconazole (Najm *et al*, 2015) and anthelmintic parbendazole (Manousi *et al*, 2021). Few of these drugs have been already evaluated in MS early phase clinical trials. For example, remyelinating properties of clemastine were confirmed in ReBUILD clinical trial (NCT02040298) in early RRMS patients with optic neuritis. Quetiapine fumarate was not tolerable to MS patients (Metz *et al*, 2020; Green *et al*, 2017). In addition, bazedoxifene is currently in the recruitment phase of ReWRAP clinical study (NCT04002934).

1.6.2 Drug prioritization in silico

Drug repurposing can be addressed by experimental approaches such as phenotypic high-throughput screening (HTS) or binding assay to identify novel targets, with the support of a computational approach, for example, by network analysis (Lotfi Shahreza *et al*, 2018) or data mining. Network analysis investigates the complex relationships between drugs, diseases, genes, proteins, or adverse drug reactions, enabling discoveries and increasing drug discovery success rate. While still considered a new field in computational biology, successful examples of heterogeneous network use are starting to emerge (Himmelstein *et al*, 2017; Center *et al*, 2015; Yan *et al*, 2016). Although drug repurposing is a promising strategy, screening thousands of compounds without specific prioritization is extremely time-inefficient and may lead to high failure risks. The computational prediction, whether a specific drug or a class of drugs could treat a disease, may significantly improve the success of drug discovery. Various computational methods enabling systematic approaches for precise drug stratification and prioritization of combinatorial strategies have been recently developed (Guney *et al*, 2016; Pushpakom *et al*, 2019; Shameer *et al*, 2018).

The *in silico* machine-learning-based approach integrating worldwide biomedical knowledge in a unique database was employed in this study to increase the success rate in identifying novel drug candidates for PMS (Himmelstein *et al*, 2017). The Scalable Precision Medicine Open Knowledge Engine (SPOKE) (<https://spoke.ucsf.edu>) integrates 29 publicly available databases of genes, compounds, diseases, proteomics, etc. combining over 50 years of biomedical knowledge into a single resource, allowing to explore interconnected pathways and to predict novel targets for existing compounds. Integration of different sources that accurately represent the domain knowledge in the MS field (e.g., the human protein interactome, expression profiles of drug-perturbed genes, disease genetics, and pathophysiology, etc.) via machine learning represents a powerful strategy to prioritize compounds with the potential to influence a phenotype of interest i.e., neuroprotection and remyelination.

1.6.3 iPSCs for disease modelling and drug discovery

Relevant systems closely recapitulating human MS phenotype are required to efficiently evaluate the neuroprotective and pro-remyelinating properties of *in silico* prioritized compounds. Drug screenings based on pure biochemical assays (purified

protein, drug-target interaction) do not fully reproduce the complex *in vivo* situation, while *in vivo* assays based on animal models are unsuitable for screening libraries of compounds. Cellular models became a valuable alternative, and indeed, cell-based assays have a broad range of applications in basic research and drug discovery, although cell lines used to test CNS-targeting compounds are often unspecific. Alternative models such as primary cells of rodent origin often cannot provide enough material required for high-throughput screening settings and are inherently variable. Instead, human cells are more suitable for screening assays due to their potential for rapid intraspecies translation. *In vitro* models that resemble human disease conditions remarkably increase drug screening efficiency and accuracy, as the target subtypes or drug-target affinities of the same drug can be fundamentally different in humans versus rodents. While primary patient cells (e.g., biopsy, surgical material) are directly used to model the effects of a drug in a patient-specific personalized manner, their availability and capacity for expansion are limited compared to immortalized cell lines.

A revolutionary advent of human-induced pluripotent stem cells (hiPSC) by Shinya Yamanaka (Takahashi & Yamanaka, 2006) provided almost an infinite cellular source with the preserved genetic background of the donor for disease-relevant modelling and drug discovery. The reprogramming (Fusaki *et al*, 2009) of somatic cells, including skin fibroblasts (Takahashi *et al*, 2007) or blood cells (Staerk *et al*, 2010), enables the generation of numerous pluripotent stem cell lines representing desirable disease genotypes and phenotypes. The hiPSC cells have similar characteristics of blastocyst-derived embryonic stem (ES) cells and infinite capacity to differentiate to any desired cell type, including not accessible otherwise neural precursor cells (NPCs), neurons, oligodendroglia, astrocytes, microglia, and non-CNS cell types. hiPSC-derived cells have been reported to recapitulate phenotypes of several neurodegenerative diseases (Garcia-Leon *et al*, 2019), and therefore represent a so-called “disease-in-a-dish” system (Tiscornia *et al*, 2011). A study by D.Pitt and colleagues recently showed the evidence of enhanced pro-inflammatory response driven by a common genetic MS risk variant in MS-specific hiPSC-derived astrocytes (Ponath *et al*, 2018). Interestingly, *in vitro* and *in vivo*, oligodendrocytes generated from MS hiPSCs showed no functional or morphological abnormalities and could myelinate to the same extent as oligodendrocytes derived from healthy controls (Mozafari *et al*, 2020; Starost *et al*, 2020). Future studies using patient-

specific hiPSC-derived neurons or microglia may shed a light on potential CNS-intrinsic mechanisms contributing to MS susceptibility.

Besides implementation in disease-modelling, hiPSC-derived cells are also suitable for drug screening or toxicology studies, thanks to their great self-renewal and differentiation capacity. In the context of MS, hiPSC-derived oligodendrocyte and neuronal cultures obtained from the same individual provide a unique opportunity to validate the pro-myelinating and neuroprotective effects of novel drug candidates and to identify druggable therapeutic targets for the treatment of MS. Although hiPSC-differentiated cells exhibit morphological and functional features of primary human cells, they are considered relatively immature compared to their original counterparts (Passier *et al*, 2016). A further disadvantage of hiPSC cells is the potential genetic and epigenetic alterations that may occur during *in vitro* reprogramming process (Perrera & Martello, 2019); however, several studies reported preserved age-related (Mertens *et al*, 2015) and disease-associated (de Boni *et al*, 2018) epigenetic signatures in hiPSC-derived cells.

While two-dimensional (2D) cell culture systems have been considered the most simplistic and reproducible for drug screening purposes, more sophisticated hiPSC-derived 3D cellular models such as organoids or spheroids, able to better recapitulate the complex cellular environment of the human brain, have been recently developed (Amin & Paşca, 2018). 3D organoids are the preferential models to study neurodevelopmental and neuropsychiatric disorders that capture complex structural and functional deficiencies of the diseased human brain. In contrast, brain spheroids, 100-500 nm spheres lacking complex structural organization, are more suitable for low and middle-scale drug screening since reproducibility and automation are the key features for screening approaches (Pamies *et al*, 2017; Renner *et al*, 2020). Brain spheroids contain all three cell types, including neurons, astrocytes, and oligodendrocytes, and are reproducible in size, shape, and cellular composition. The presence of oligodendrocytes within spheroids makes them an essential test system for quantitative evaluation of the myelination (Chesnut *et al*, 2021). In addition, the development of 3D culture systems incorporating microglia provides a versatile tool to model neuroinflammation and study neuro-immune interactions *in vitro* (Abreu *et al*, 2018).

Although a human iPSC-based 3D cell culture system is a unique tool in drug discovery and disease modelling “in a dish”, brain organoids do not recapitulate the

complex human brain tissue, lacking vasculature, cerebral spinal fluid flow and immune system component. The relative immaturity of cells within 3D brain structures is another shortcoming in model ageing and age-related aspects of neurodegenerative diseases, including MS. Advancements in generating more complex 3D systems (Sharma *et al*, 2020) and improvement in cell maturation have been recently made to overcome these limitations (de Leeuw *et al*, 2021; Odawara *et al*, 2016). A novel chimaera model with engrafted hiPSC-derived oligodendrocytes that significantly improves the system physiological relevance (Mozafari & Baron-Van Evercooren, 2021) has been proposed to study the remyelination of human oligodendroglia *in vivo*.

2. AIMS OF THE STUDY

Progressive multiple sclerosis is one of the major causes of advanced neurological disability in young adults that remains untreatable. The relapsing-remitting form of MS, primarily an inflammatory disease, is successfully targeted by various immunomodulatory and anti-inflammatory treatments. The progressive form, associated with CNS-compartmentalized inflammation and widespread neurodegeneration, still lacks effective therapies that promote remyelination and neuroprotection. Traditional processes of drug discovery based on molecular target or phenotypic screen-based approaches usually take a decade and approximately 2.6 billion dollars (Freedman, 2019) for successful drug development making these approaches extremely time and economically inefficient. Instead, a novel drug repurposing approach based on identifying a new application for approved drugs may provide patients with therapies in a relatively short time and within a contained budget. Repositioned drugs have known safety, pharmacokinetics, and pharmacodynamic data, therefore reducing the risk of failure in early clinical trials. In addition to drug repurposing, *in silico* drug prediction offers a complementary approach for the efficient selection of successful drug candidates. To better reproduce the human biological tissue, iPSCs can provide a valuable tool for *in vitro* disease modelling and almost an infinite cellular source with the preserved genetic background of the donor. The hiPSC-derived oligodendrocyte and neuronal cultures represent a unique patient-specific “disease-in-a-dish” tool for evaluating drug candidates’ pro-myelinating and neuroprotective effects. The goal of the project is to develop an *in vitro* functional platform to discover new drugs for progressive MS with translation to preclinical models, therefore following study aims were established:

- 1) To set up an *in vitro* phenotypic drug screening of a drug repurposing library using primary murine and hiPSC-derived neuronal cultures.
- 2) To provide *in vivo* evidence of pharmacological activity of a small number of drugs in an efficacy study in a preclinical model of MS (EAE).
- 3) To identify the molecular targets of the neuroprotective/remyelinating hit compounds.
- 4) To characterize and evaluate potential functional and molecular differences in hiPSC-derived neurons from three twin pairs discordant for MS.

3. RESULTS

3.1 Setup of the multistage stepwise drug screening platform

3.1.1 Overview of screening approach

This project, named **Bioinformatics and cell Reprogramming** to develop an **IN vitro** platform to discover new drugs for progressive **Multiple Sclerosis (BRAVEinMS)**, is an effort of a multi-national consortium supported by the Progressive Multiple Sclerosis Alliance. The platform is based on a stepwise phenotypic screening approach combining *in vitro* and *in vivo* assays and human validation protocols – on both neural and oligodendrocyte cells from MS patients and the “MS-dedicated” bioinformatic system. This novel approach may help to overcome the limitations of a classic drug discovery pipeline, speeding up and optimizing the process of drug discovery for PMS. First, the drug library of approximately 1500 compounds was prioritized by SPOKE by predicting the interactions of compounds related to the process of myelination or neuroprotection (S. Baranzini lab, UCSF, San Francisco, US). As a result, about 511 compounds were selected and further proceeded to quality control (QC) of chemical entities uniqueness, drug purity analysis by ultraperformance liquid chromatography-tandem mass spectrometry (UPLC-MS), and selection of reliable providers for the available compounds (IRBM, Italy). In summary, 295 compounds were purchased, whereas 22 compounds were excluded after QC, resulting in 273 compounds included in the BRAVEinMS library collection.

The following steps included in *in vitro* evaluation of compounds cytotoxicity on primary murine neuronal and oligodendrocyte cultures, including primary murine oligodendrocytes (Agresti lab, ISS, Rome, Italy), CG4 rat OPC line (Nait-Oumesmar lab, INSERM, Paris, France), primary murine cortical neurons, and hiPSC-derived neurons (Martino lab, San Raffaele Scientific Institute, Milan, Italy), resulting in the selection of 160 non-toxic compounds. The non-toxic compounds were further screened in various functional assays to identify compounds with neuroprotective and promyelinating functions. Functional assays included differentiation of murine and human oligodendrocytes (CG4 OPC line, primary rat OPCs cultures (Nait-Oumesmar lab); morphological integrity evaluation of murine cortical and striatal neurons upon excitotoxic injury (IRBM & Martino lab); neuroprotective experiments on primary murine cortical neurons upon excitotoxic injury (Martino lab). The hit-compounds

validated in several biological systems assessing different phenotypes for the specific outcomes (neuroprotection and/or myelination) were passed to further screening. Validation assays were performed on hiOLs (Kuhlmann lab, WWU, Münster, Germany) and human fetal OPCs (Annik Baron-Van Evercooren lab, INSERM, Paris, France), evaluating myelination function. At the same time, the neuroprotective efficacy of hit-compounds was validated on hiPSC-derived neurons upon oxidative stress injury (Martino lab) and differentiated embryonic human neurons (Zipp lab, JGU, Mainz, Germany). In addition, murine spinal cord cultures (SCC) were used to evaluate both myelination and axonal quantification (Goebels lab, HHU, Dusseldorf, Germany). As a result, a shortlist of selected hit-compounds underwent *in silico* absorption, distribution, metabolism, excretion, and pharmacokinetics (ADME/PK) evaluation to select drug candidates suitable for *in vivo* evaluation. Two compounds, namely Bavisant and Casopitant, were selected to provide *in vivo* evidence of their pharmacological activity in several preclinical models of MS: EAE (Martino lab), model of non-immune demyelination (lyssolecithin model, Nait-Oumesmar lab), and humanized chimaera model (Shi/Shi: Rag2^{-/-}, Annik Baron-Van Evercooren lab).

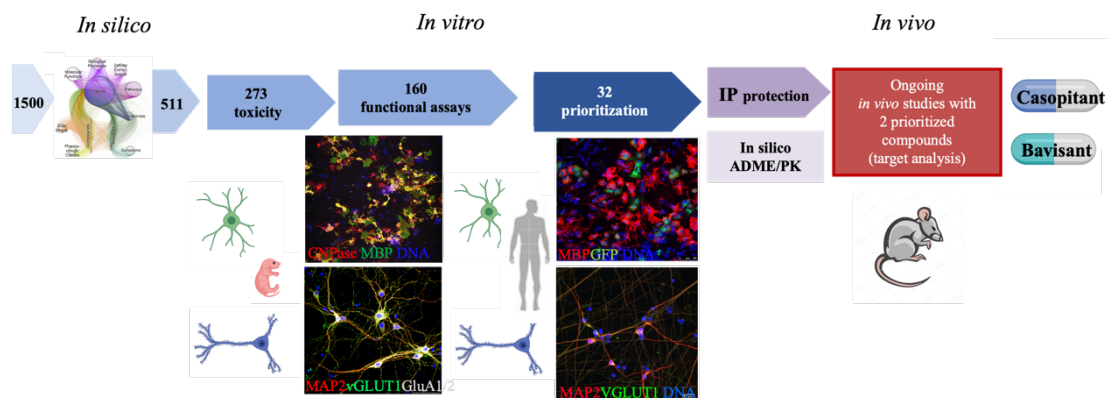


Figure 3. Schematic of multistage phenotypic screening pipeline.

3.1.2 Drug library selection via bioinformatic *in silico* prioritization

To predict novel molecules with neuroprotective and promyelinating properties with potential therapeutic efficacy in the context of PMS, about 1500 repurposed drugs underwent prioritization through the SPOKE algorithm by computing the probability of the interactions between the drugs, disease-associated pathways, and biological processes. In detail, the algorithm was set up to identify drug-gene-biological process relationships according to a query of multiple sclerosis-associated pathways (or

keywords) and multiple sclerosis genetic associated risk factors. The software identified "metapaths" (or connections), whose relevance is quantified through the degree-weighted path count (DWPC). The DWPC was calculated by identifying the existing connections between the nodes of interest, and subsequently, each of the identified connections was "weighed" considering the type of connection in relationship to other connections and the linked nodes.

<i>axon ensheathment in central nervous system</i>	<i>neuron migration</i>
<i>brain-derived neurotrophic factor receptor signaling pathway</i>	<i>neuron projection development</i>
<i>branching morphogenesis of a nerve</i>	<i>neuron recognition</i>
<i>cell morphogenesis involved in neuron differentiation</i>	<i>neuron-neuron synaptic transmission</i>
<i>ensheathment of neurons</i>	<i>neuronal stem cell population maintenance</i>
<i>forebrain generation of neurons</i>	<i>neuropeptide signaling pathway</i>
<i>GABAergic neuron differentiation</i>	<i>neurotransmitter transport</i>
<i>motor neuron axon guidance</i>	<i>neurotransmitter-gated ion channel clustering</i>
<i>Myelination</i>	<i>neurotrophin signaling pathway</i>
<i>nerve development</i>	<i>positive regulation of neuroepithelial cell differentiation</i>
<i>neural crest cell differentiation</i>	<i>regulation of calcineurin-NFAT signaling cascade</i>
<i>neural nucleus development</i>	<i>regulation of glial cell-derived neurotrophic factor secretion</i>
<i>neural precursor cell proliferation</i>	<i>regulation of neural precursor cell proliferation</i>
<i>neuroblast differentiation</i>	<i>regulation of neurological system process</i>
<i>neuroepithelial cell differentiation</i>	<i>regulation of neuron death</i>
<i>neuromuscular process</i>	<i>regulation of neuronal synaptic plasticity</i>
<i>neuromuscular synaptic transmission</i>	<i>regulation of neurotransmitter levels</i>
<i>neuron death</i>	<i>regulation of neurotransmitter transport</i>
<i>neuron fate commitment</i>	<i>response to nerve growth factor</i>
<i>neuron maturation</i>	<i>transmission of nerve impulse</i>

Table 2. The list of the biological process terms utilised in silico drug prioritization algorithm.

<i>AKT</i>	<i>IGF1</i>
<i>D-aspartate</i>	<i>Insulin</i>
<i>Propionate metabolism</i>	<i>Interferonβ</i>
<i>5-Hydroxymethyl cytosine</i>	<i>JAB1</i>
<i>ADP-ribosylation</i>	<i>Ketone bodies</i>
<i>AMBRA1</i>	<i>KIR4.1</i>
<i>Amino acid metabolism</i>	<i>KRAB</i>
<i>ASIC1</i>	<i>MAP1β</i>
<i>ASRGL1</i>	<i>MdM2</i>
<i>Autophagy</i>	<i>miR-125-3p</i>
<i>BAFF</i>	<i>MIR125a</i>
<i>CASPR</i>	<i>MS susceptibility associated genes</i>
<i>CCL20</i>	<i>mTOR</i>
<i>CCR6</i>	<i>Myelin oligodendrocyte glycoprotein</i>
<i>CD39</i>	<i>NCX3</i>
<i>CD73</i>	<i>NRF2</i>
<i>CXCL13</i>	<i>Oxidative stress</i>
<i>EBNA2</i>	<i>Pyruvate metabolism</i>
<i>EBV</i>	<i>SDF1</i>
<i>Epstein-Barr virus</i>	<i>SOX17</i>
<i>Experimental autoimmune encephalomyelitis</i>	<i>TACE</i>
<i>Fatty acid oxidation</i>	<i>TCA cycle</i>
<i>Glutamate</i>	<i>TGFβ</i>
<i>Glycolysis</i>	<i>TNFR2</i>
<i>GPR17</i>	<i>TNFRSF14</i>
<i>GRK2</i>	<i>Vitamin D</i>

Table 3. The list of keywords utilised in silico drug prioritization algorithm.

As a result, the selection of keywords focused on pathways associated with neuroprotection and pathways or biological processes targeting myelination allowed to prioritize the list of 511 compounds sorted based on the absolute parameter DWPC with a cut-off value of DWPC>0.0005. The 511 unique selected drugs were analysed, identified 177 target genes and 47 associated pathways. In addition, 118/511 molecules were predicted to have a PK permissive to BBB.

The final list of 273 molecules used in *in vitro* phenotypic screening in this project was characterized as 46% of kinase inhibitors modulators (mainly with anti-tumour activity); 11 % are modulators of neurotransmitter receptors; 4% are modulators of ion

channel receptors, and 4% are the modulators of hormone receptors (Figure 4). Altogether, the target genes of the selected molecules are involved in the modulation of signalling pathways linked to IL8, STAT3, or NF-kB signalling pathways, or linked to the CNS biological processes such as "axonal guidance", "neuregulin", or "reelin signalling" (Figure 5).

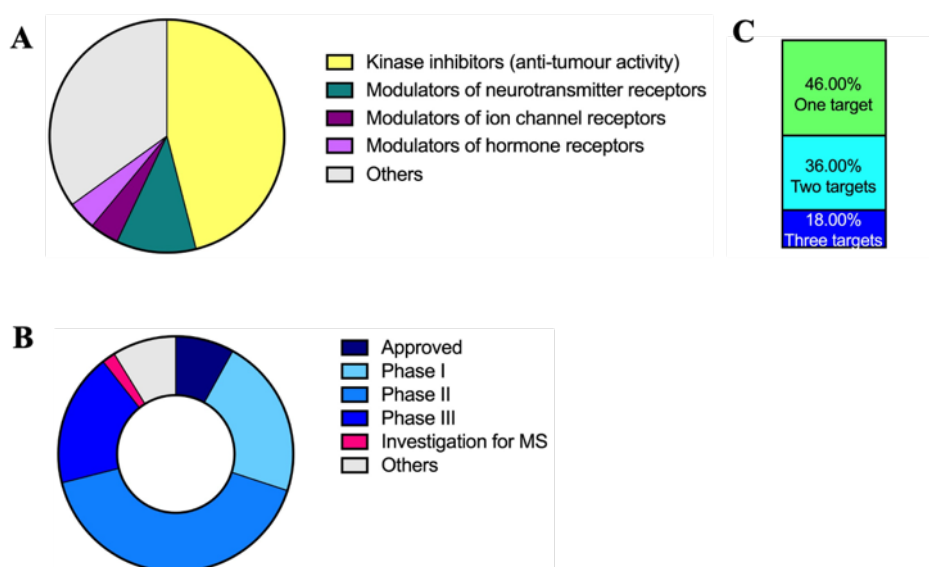


Figure 4. Compounds analysis. (A) The pie chart shows the main classes of compounds. (B) The doughnut graph shows the proportion of each category for compound approval status. (C) Target analysis.

Further detailed analysis of the compounds identified that 36% of compounds have two targets and 18% have three targets. Eight percent (8%) of the 273 compounds are approved by FDA; 18% are in Phase III, 41% are in Phase II, 22% are in Phase I, 54% are discontinued. To note, 5/273 compounds are under investigation for MS, including siponimod, ponesimod and lipoic acid, which have been identified as molecules with anti-inflammatory and neuroprotective properties (Faissner & Gold, 2019; Baldassari & Fox, 2018).

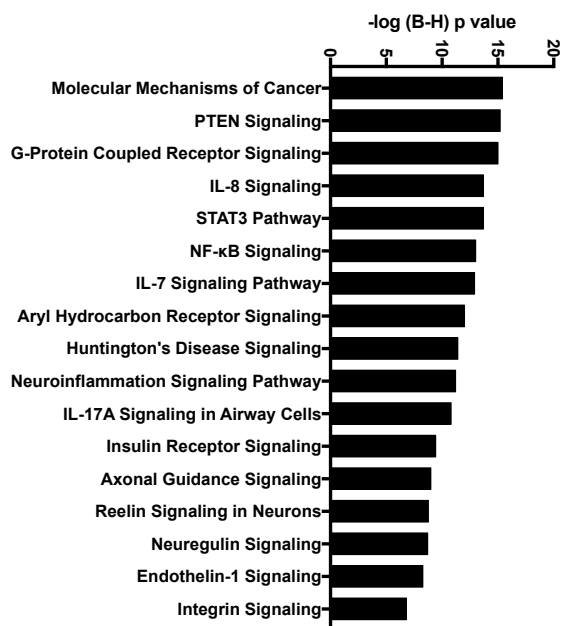


Figure 5. List of compounds target genes from pathway enrichment analysis. Ingenuity Pathway analysis identified 177 target genes and 47 associated pathways. The graph shows the list of significantly enriched pathways. The reported p-value has been corrected according to the Benjamini-Hochberg method.

3.2 In vitro phenotypic screening

3.2.1 Evaluation of compounds cytotoxicity effect

As the first step of most pharmacological screenings, we first evaluated the compounds' toxicity. The cytotoxicity of compounds was evaluated on primary murine cortical neurons as a suitable cellular source for large and mid-throughput screening. Murine cortical neurons can be obtained in relatively large amounts ($\sim 1 \times 10^6$ /embryo) from C57BL/6J pregnant females at E16.5-E17.5 gestational day that become fully mature in 10-14 days of *in vitro* differentiation. First, we characterized cortical neurons by immunofluorescence evaluating the expression of neural (MAP2), synaptic (vGLUT1, Glua1/2, SYN1, SYT1), and astrocyte (GFAP) markers by confocal imaging at 7DIV, 11DIV, and 14DIV to identify the optimal time point of full neuronal maturation with minor contamination of astrocytic cells (Figure 6). Neurons stably expressed MAP2 throughout differentiation, while synaptic markers were maximally expressed at the end of two weeks differentiation period. Finally, we have selected 13-14 days *in vitro* (DIV) as an appropriate time point for evaluating compounds' cytotoxicity and neuroprotective activity.

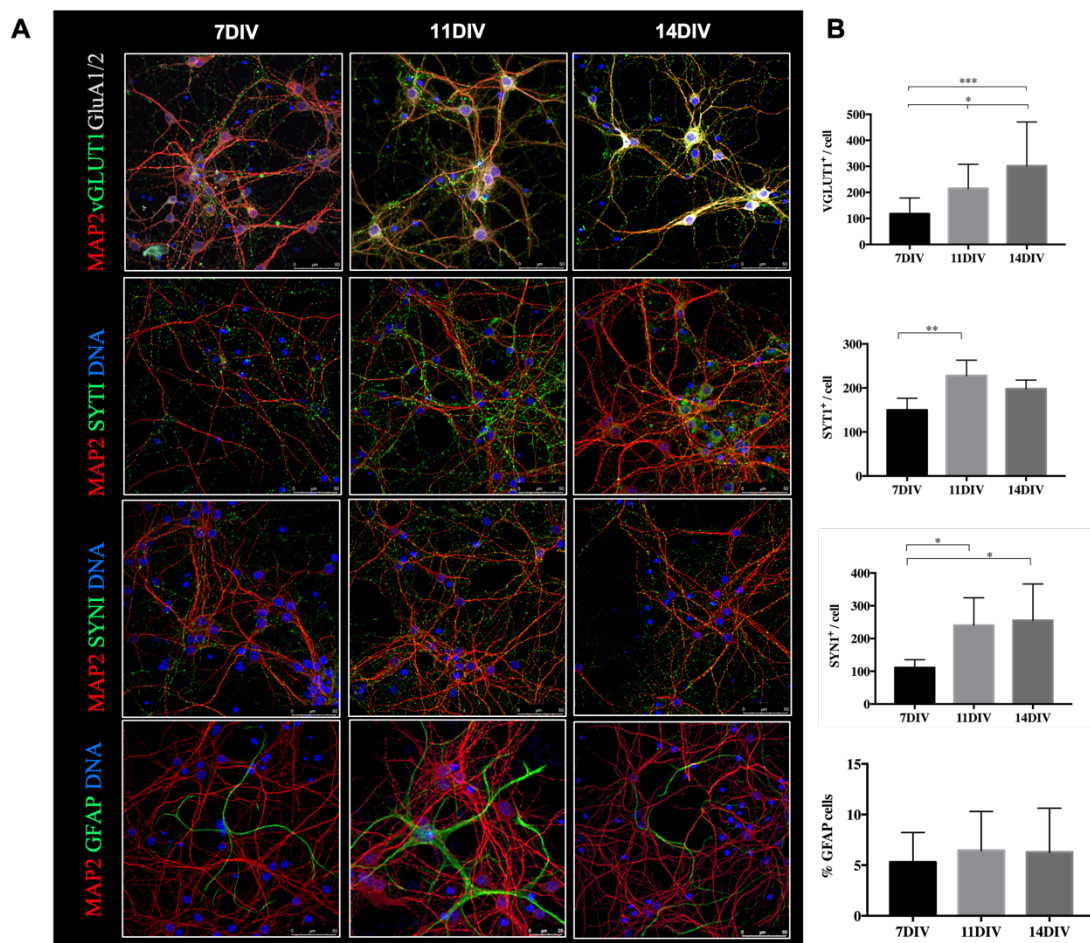


Figure 6. Characterization of primary murine cortical neurons culture. (A) Representative expression of neural (MAP2), synaptic (vGLUT1, GluA1/2, SYNI, SYTI) and astrocyte (GFAP) markers of mouse cortical neurons at 7DIV-11DIV-14DIV evaluated by immunofluorescence and confocal imaging. (B) Quantification of the expression of synaptic markers vGLUT1, SYTI, SYNI, and GFAP⁺ cells normalized by a total number of cells. Mean values are reported with standard deviation (SD). Stat. test performed with one-way ANOVA, * $p < 0.05$; ** $p < 0.01$; *** $p < 0.001$.

3.2.1.1 Cytotoxicity assays identified 160/273 non-toxic compounds on primary murine cortical neurons

Cytotoxicity of 273 compounds was evaluated at two pharmacological concentrations (1 μ M and 10 μ M) on primary cortical neurons at DIV13-14, plated in the multiwell (MW) 96 plates. Each plate contained non-treated cells, DMSO (or vehicle)-treated cells, and the positive control of cytotoxicity staurosporine, a broad-spectrum kinase inhibitor, and known neurotoxin (Deshmukh & Johnson, 2000). Each compound was tested in triplicate, and 47 compounds were re-tested twice in two independent experiments to ensure the reproducibility of the results. A moderate positive linear correlation ($0.3 < r < 0.7$) between two independent experiments indicated the reproducibility of the assay (Figure 7, B-C).

The neuronal viability was evaluated with colorimetric CCK8 assay based on the reduction of water-soluble tetrazolium salt (WST-8) by dehydrogenase activities in the cells, which reflects the metabolic activity of the viable cells. The CCK8 assay is far superior compared to the other enzyme-based methods (e.g. MTT) because it is easy-to-use, safe, has a high reproducibility, and is non-toxic for the cells (Riss *et al*, 2016). Since WST-8 assay is non-toxic and doesn't require cells lysis, additional experiments may be carried out using the same cells after CCK8 readout, for example the neuronal morphology integrity readout. A threshold of 80% viability (compared to DMSO) and $p < 0.05$ stat. significance was selected as an indication of cytotoxicity. As a result of compounds cytotoxicity evaluation, 134 compounds were non-toxic at both 1 μ M and 10 μ M concentrations, 25 compounds were non-toxic at 1 μ M but were toxic at 10 μ M, and one compound was not toxic at the higher 10 μ M concentration, while 19 compounds were identified as toxic at both concentrations and thus were excluded from further evaluation (Figure 7F). As a result, the 160/273 compounds which were not toxic on primary murine cortical neurons at both concentrations or at the lower 1 μ M concentration, and non-toxic on primary oligodendrocyte cultures (cytotoxicity evaluation was performed by external collaborators) were selected for further stepwise functional assays.

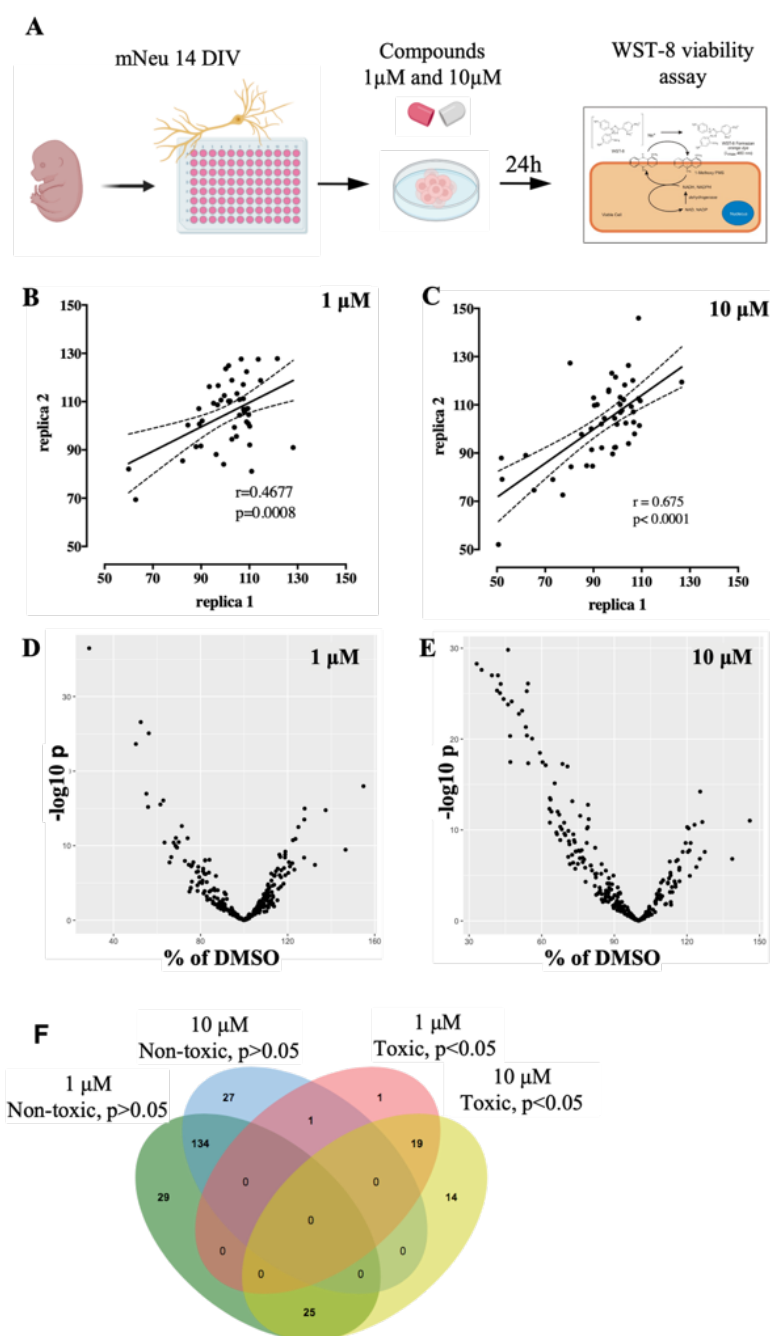


Figure 7. Results of the cytotoxicity assay of 273 in silico prioritized compounds evaluated on primary murine cortical neurons. (A) Schematic representation of compounds cytotoxicity evaluation. (B-C) Correlation plot of 47 molecules tested twice to evaluate the reproducibility of toxicity at 1 μM (B) and 10 μM (C). The correlations are visualized with linear regression lines with confidence intervals and Spearman correlation coefficient, significant at the level of $p < 0.05$ (D-E) Volcano plots of 273 compounds tested at 1 μM and 10 μM. Y-axis expressed as $-\log_{10} p$ -value; x-axis is expressed as % to DMSO. (F) Venn's diagram of 273 compounds tested at the two different doses grouped by 80% viability threshold and $p < 0.05$ stat. significance.

3.2.1.2 Secondary cytotoxicity evaluation identified 148/160 compounds non-toxic on hiPSC-derived neuronal cultures

The potential toxicity of 160 non-toxic to murine cell compounds was also evaluated on hiPSC-derived neurons from one control line to exclude the possibility that human cells have a different degree of toxicity susceptibility. The protocol for differentiation of hiPSC-derived glutamatergic neurons, originally developed at Lorenz Studer's lab, was adapted for this purpose. The protocol scheme employs a two-step process: induction phase driven by dual SMAD inhibition (Chambers *et al*, 2009) and differentiation phase guided by the combinatorial application of six pathway inhibitors (Qi *et al*, 2017). Fifteen days of induction phase resulted in the generation of rosette-forming neuroepithelial state NPCs, followed by approximately forty days of differentiation leading to generation of mature neuronal network with established electrophysiological activity evaluated by the patch-clamp technique. This protocol produced nearly pure neuronal cultures without glial cell contamination (detailed characterization is shown in 3.5.1.1-3.5.1.2), therefore making this cellular model favourable for drug screening and setup of neurotoxic injury assays. The choice of glutamatergic lineage is justified by the evidence of the particular vulnerability of cortical grey matter in MS, where cortical thinning and selective cortical neuron damage contribute to the formation of MS lesions and potentially is a driving force of neurodegeneration in the chronic MS stage (Schirmer *et al*, 2019). The schematic of the differentiation protocol is represented in Figure 8.

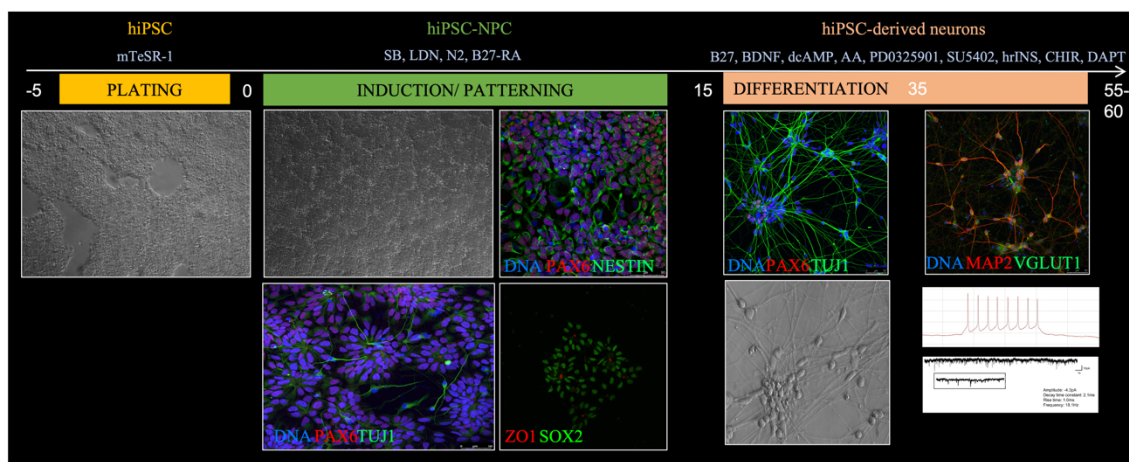


Figure 8. hiPSC-derived glutamatergic neurons as a cellular model for secondary (hit-to-lead validation) phenotypic screening. Timeline of differentiation protocol of human iPSCs to glutamatergic neurons and the composition of the media at different stages. Protocol based on dual SMAD inhibition method and small molecules inhibition approach optimized from Qi *et al*. 2017.

160 compounds selected from cytotoxicity evaluation on primary murine cultures were tested at 1 μ M on hiPSC-derived neurons from one control line at DIV45 of differentiation, plated in MW96 plates (Figure 9). Each plate contained non-treated cells, 0.02% DMSO (or vehicle)-treated cells and a positive control of cytotoxicity staurosporine. Cell viability/metabolic activity was evaluated by CCK8 (WST-8) viability assay. As a result, most compounds (148/160) were non-toxic to hiPSC-derived neurons, of which 85 compounds promoted cellular metabolic activity (potentially influencing the enzymatic dehydrogenase activity), while 12/160 compounds reduced neuronal viability by 20-30% compared to DMSO.

In conclusion, 92.5% of the compounds were not toxic for hiPSC-derived neurons and were further proceeded for evaluation of their neuroprotective function.

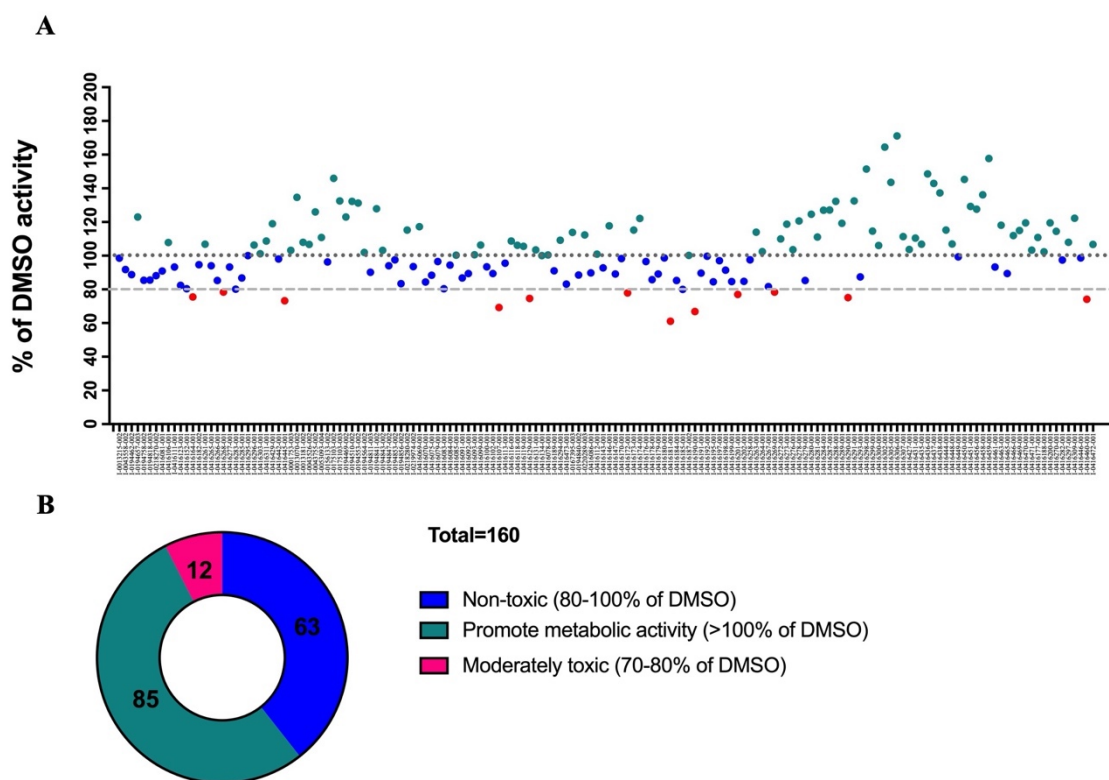


Figure 9. Evaluation of compounds cytotoxicity in hiPSC-derived neurons. Cytotoxicity of 160 compounds evaluated on hiPSC-derived neurons (DIV45) by WST-8 viability assay. (A) Cell viability/metabolic activity is expressed in percentage relative to DMSO activity. The dotted line marks a threshold of 80% viability/metabolic activity, where each dot reports a mean value of a triplicate readout. (B) 148/160 compounds were considered non-toxic (>80% of metabolic activity relative to DMSO), while 12/160 compounds were moderately toxic.

3.2.2 Evaluation of compounds neuroprotective efficacy in 2D in vitro models

3.2.2.1 Neuroprotective assay setup on primary murine cortical neurons: selection of NMDA and NAC as a stressor and neuroprotective control

The next objective was to evaluate the neuroprotective capacity of selected compounds on primary murine cortical neurons by reproducing neurotoxic conditions *in vitro* that partially mimic the neurodegenerative environment of brain parenchyma in MS. Loss of neuronal function is an important pathological feature of progressive MS, and typically, MS lesions contribute to axonal degeneration responsible for the clinical disability (Singh *et al*, 2017). Axonal swellings or axonal retraction bulbs are the histological hallmarks of transected axons, eventually occurring in chronically demyelinated axons. Therefore, we aimed to identify molecules that interfere with the pathological processes and potentiate the adaptive and neuroprotective compensatory mechanisms (Chang *et al*, 2008) to delay neuronal degeneration.

To reproduce stressor conditions *in vitro*, we identified a series of compounds with toxic activity (stressor) and empirically evaluated the possible effective stimulus concentrations for a group of neurotoxic molecules, namely stressors inducing excitotoxicity, for example, glutamate (Azevedo *et al*, 2014), kainic acid (Wang *et al*, 2005), NMDA (Liu *et al*, 2007). In addition, we have tested the agents inducing oxidative stress, for example, FeSO₄ (Hametner *et al*, 2013), 3-nitropropionic acid (3NP) (Geddes *et al*, 2000), tert-butyl hydrogen peroxide (TBHP) (Görlach *et al*, 2015), and H₂O₂ (Ohl *et al*, 2016). We also have tested the acidosis (pH=6.8) condition and a toxicity effect of inflammatory cytokines such as TNF α (Blaser *et al*, 2016), IFN- γ (Mizuno *et al*, 2008), IL-6 (Göbel *et al*, 2018) and IL-1 β (Rossi *et al*, 2014), however we could not identify a clear dose response relation upon cytokine stimulation (Figure 10A).

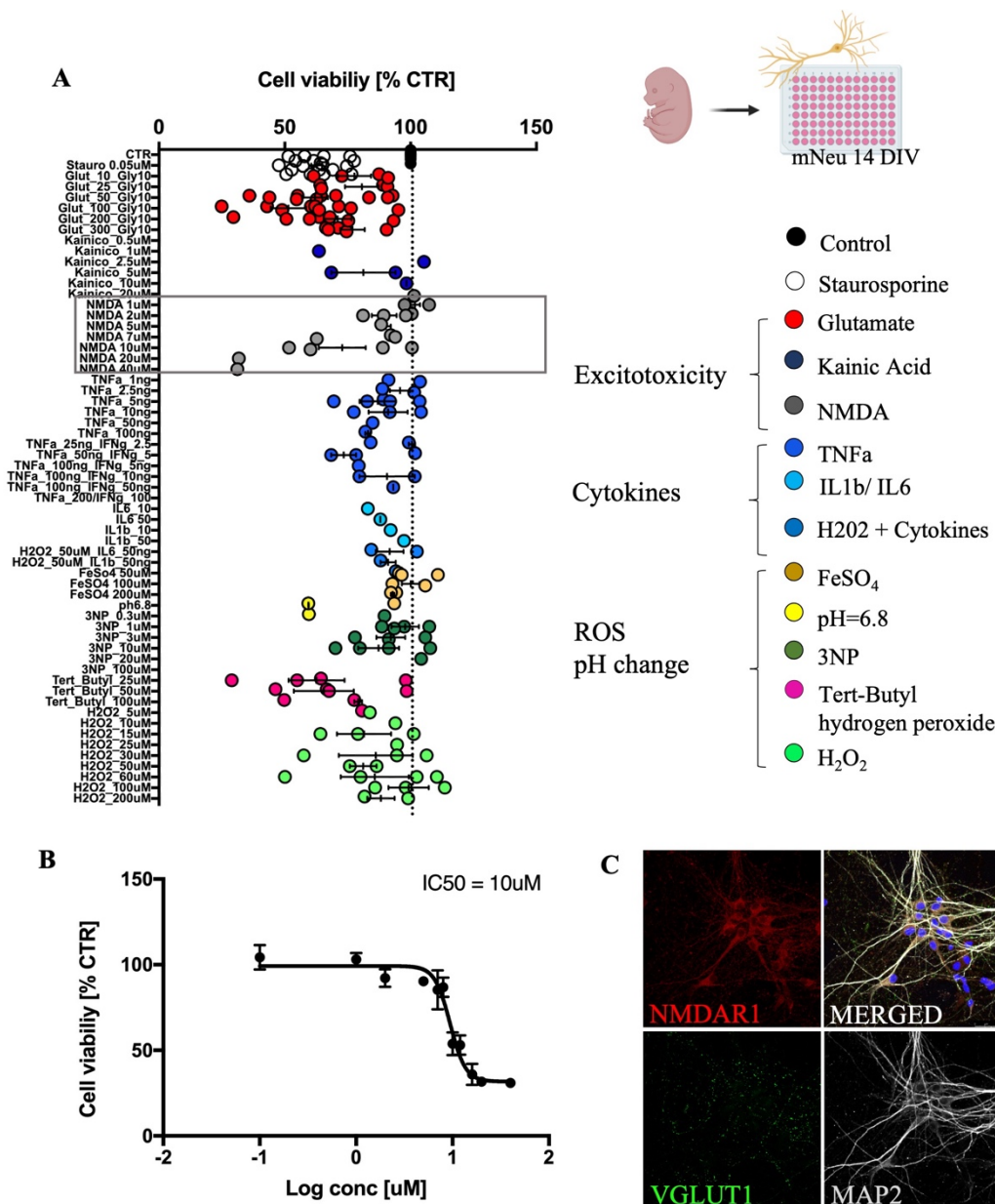


Figure 10. Neuroprotective assay setup on primary murine cortical neurons: selection of toxic stressor. (A) Mouse cortical neurons at 14DIV were treated with various concentrations of excitotoxicity-inducing stressors (glutamate, kainic acid, NMDA), oxidative stressors (FeSO₄, 3NP, TBHP, H₂O₂), and pH change (pH=6.8). Staurosporine was used as a positive control of cytotoxicity. The normalized viability/metabolic activity is expressed in percentage compared to the non-treated control (CTR). Each dot reports a mean value \pm SEM obtained from independent experiments run in sextuplicate. (B) The normalized dose-response curve demonstrates the dependence of cytotoxicity on NMDA concentrations. The percentage of cytotoxicity is plotted against the logarithmic micromolar concentrations of NMDA. Data from each point were obtained from 3 independent experiments performed in sextuplicate. The identified IC₅₀ for NMDA is 10 μ M. (C) Representative expression of neural (MAP2), pre-synaptic (vGLUT1), and NMDAR1 markers of mouse cortical neurons at 14DIV evaluated by immunofluorescence and confocal imaging.

Exposure of cortical neurons to neurotoxic concentrations of NMDA leads to overactivation of NMDA receptors and subsequently to intracellular calcium overload, mitochondrial depolarization and excitotoxic neuronal injury (Dong *et al*, 2009). Chronic (24h) treatment of primary cortical neurons with NMDA demonstrated a dose-response relationship ($IC_{50}=10\mu M$) dependence of cytotoxicity on increasing NMDA concentrations (Figure 10B). NMDARs and VGLUT1 receptors expression was validated on 14DIV mouse cortical neurons by immunofluorescence and confocal imaging (Figure 10C).

The next step was to identify a neuroprotective agent able to protect from NMDA-induced excitotoxicity. The molecules with known neuroprotective potential such as resveratrol (Bastianetto *et al*, 2015), alpha-lipoic acid (ALA) (Rocamonde *et al*, 2012), N-acetyl cysteine (NAC) (Stanislaus *et al*, 2005), mitochondrial-targeted coenzyme Q10 (MitoQ) (Mao *et al*, 2013), calpain inhibitor calpeptin (Guyton *et al*, 2010), and nicotinamide (Yoshino *et al*, 2018) were tested in preventive regimen followed by NMDA exposure (Figure 11). The most potent molecule with neuroprotective effect against NMDA excitotoxicity was NAC (300 μM), which was chosen as a positive control for further neuroprotective assays. As a result, we have setup the cell viability assay to evaluate the neuroprotective efficacy of the 160 selected compounds using NMDA as a stressor and NAC as a positive neuroprotective control.

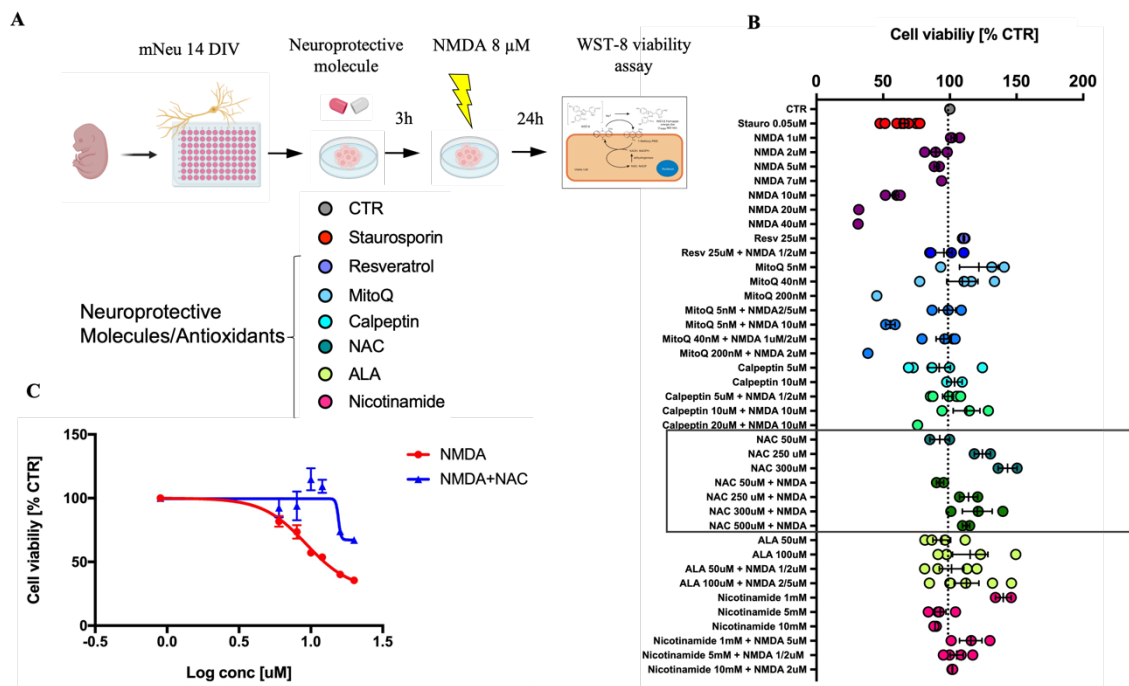


Figure 11. Neuroprotective assay setup with NMDA as a stressor on primary murine cortical neurons: selection of positive neuroprotective control. (A) Schematic representation of neuroprotective experimental on mouse cortical neurons. Mouse cortical neurons (14DIV) were pre-treated with various concentrations of known neuroprotective molecules (resveratrol, MitoQ, calpeptin, NAC, alpha-lipoic acid (ALA), and nicotinamide) and then stressed with NMDA for 24h. (B) The normalized viability/metabolic activity is expressed in percentage compared to the non-treated control (CTR). Staurosporine was used as a positive control of cytotoxicity. Each dot reports a mean value \pm SEM obtained from $n > 3$ independent experiments run in sextuplicate. (C) Normalized dose-response curve demonstrates the neuroprotective effect of NAC from NMDA-induced cytotoxicity. The percentage of cytotoxicity is plotted against the logarithmic micromolar concentration of NMDA with or without 300 μ M NAC pre-treatment. Data from each point were obtained from 3 independent experiments performed in sextuplicate.

3.2.2.2 Identification of 17 compounds with neuroprotective efficacy against NMDA-mediated excitotoxicity in survival assay on primary murine cortical neurons

We performed a mid-scale screening of 160 non-toxic compounds selected in the first stage of the screening. To evaluate the neuroprotective activity of selected compounds, murine cortical neurons (13DIV) were pre-treated with 1 μ M compounds or NAC (300 μ M) for 3 hours, followed by 24 hours chronic stimulation with NMDA (8 μ M) to induce neuronal damage. All experiments were performed in triplicate in MW96 plates, with at least three independent biological experiments. Each plate contained a set of controls, including non-treated cells (NC), DMSO-, NMDA-, NAC-, NAC+NMDA-treated cells, and staurosporine as a positive control of cytotoxicity. As a result, 17 potentially neuroprotective molecules were identified (stat. significant at $p < 0.05$, Kruskal-Wallis test with multiple comparison correction by controlling FDR). The secondary validation was performed with a longer pre-treatment (24h) to evaluate the neuroprotective efficacy of compounds with a potential long-lasting action. The secondary screening did not include a full set of six controls; therefore, a standardized Z score was applied for normalization. Longer pre-treatment resulted in the identification of 31 compounds scored with $Z > 0.5$, among which five compounds were re-confirmed from 3h pre-treatment screening, and two compounds were identified as hits ($Z > 2$). Interestingly, the identified hits were adenosine A_{2A} receptor and muscarinic acetylcholine M1 receptor antagonists, both reported to modulate NMDARs functionality (Franco *et al*, 2020; Galvin *et al*, 2021).

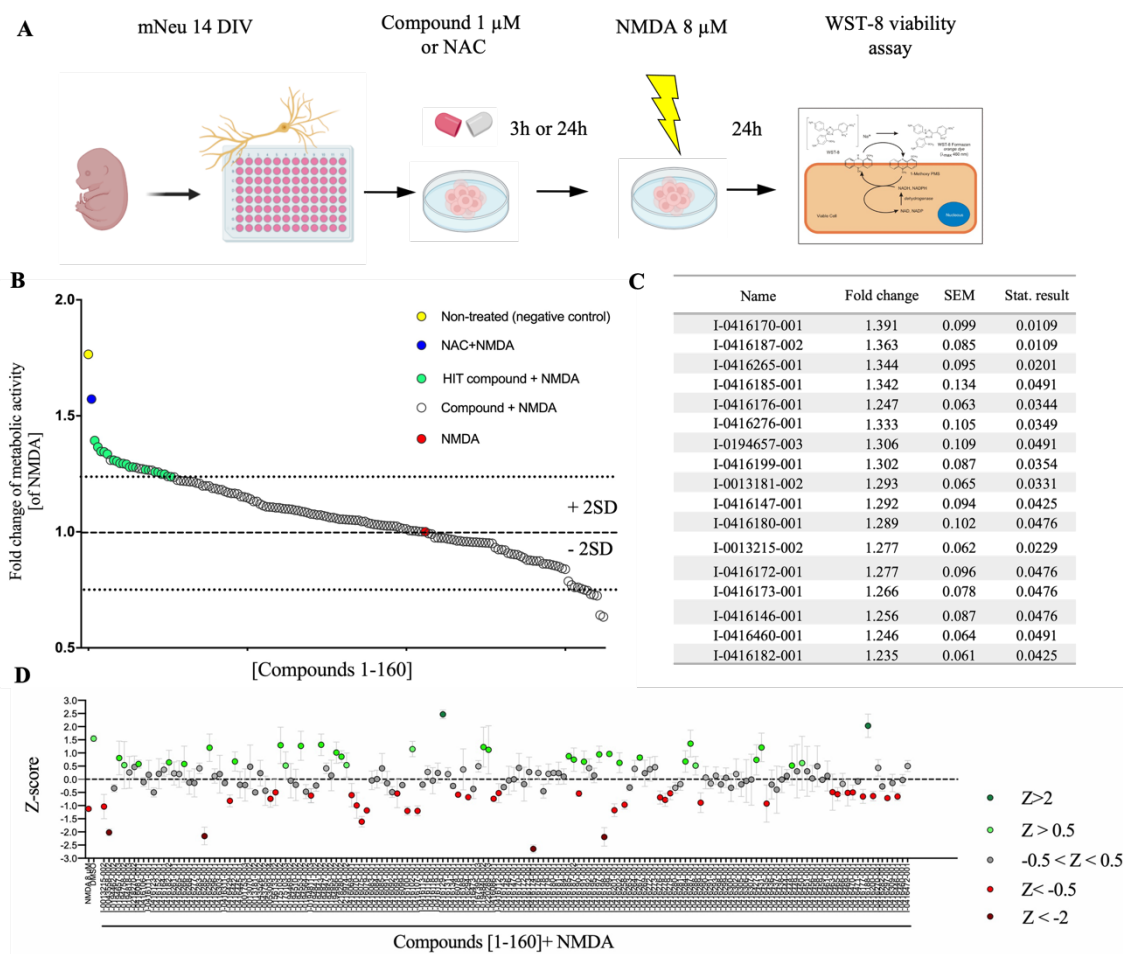


Figure 12. Primary screening of 160 non-toxic compounds in NMDA-mediated and neuroprotective assay settings. (A) Schematic representation of neuroprotective experimental setup on mouse cortical neurons. (B) Neuroprotective effect of 160 non-toxic compounds was evaluated on murine cortical neurons at 14 DIV in the NMDA-mediated cytotoxic assay upon 3h pre-treatment with compounds. The normalized viability/metabolic activity is expressed compared to the NMDA-treated control. Each dot reports a mean value \pm SEM obtained from $n > 3$ experiments run in triplicates. (C) Table of 17 hit-compounds significantly protecting from NMDA-mediated cytotoxicity. Stat. test performed with Kruskal-Wallis test with the post hoc two-stage linear step-up procedure of Benjamini, Krieger and Yekutieli multiple comparison correction, stat. significant $p < 0.05$. (D) Neuroprotective effect of 160 non-toxic compounds was evaluated on murine cortical neurons at 14 DIV in NMDA-mediated cytotoxic assay with 24h compounds pre-treatment. The normalized viability/metabolic activity is expressed with a Z score. Each dot reports a mean value \pm SEM obtained from the triplicate readout of a single or duplicate experiment.

3.2.2.3 Identification of 23 compounds with neuroprotective efficacy against NMDA-mediated excitotoxicity on primary murine cortical neurons

Next, we performed phenotypic image analysis of primary murine cortical neurons after stimulation with the stressor (NMDA) to evaluate the consequences of the neurotoxic stimulus and the protective effect of compounds. Besides the

viability/metabolic readout, neuronal structural integrity is another measure outcome of neuronal health that can be evaluated by MAP2 immunofluorescent staining and high-content imaging (Sherman & Bang, 2018). Microscopy was performed using ArrayScanTMXTI (ThermoFisher) imaging platform, and images were analysed by an in-house built image analysis pipeline (CellProfiler). The total neurite length and the total number of non-trunk branches were measured, and the measures were converted to a standardized Z-score. As a result of morphological integrity evaluation, 28 compounds scored with $Z > 0.5$ were shown to preserve total neurite length (Figure 13C) and 27 compounds scored with $Z > 0.5$ in preserving the total number of branches (Figure 13D), while 23 compounds preserved both neurite length and network integrity (Figure 13F). Both parameters correlated to each other, indicating a direct relationship between the total neurite length and the integrity of the neuronal network (Figure 13E). Among the identified compounds, 10 were both neuroprotective from NMDA-induced cytotoxicity in cell survival assay (with 3h or 24h pre-treatment) and could also preserve neurite length and dendritic branching. Interestingly, among the ten compounds, one was identified as a NMDA receptor antagonist with known neuroprotective function (Kalia *et al*, 2008; Danysz & Parsons, 2002). The identification of a NMDA antagonist as one of the hit compounds furthermore reinforces the validity of the screening approach. Among the other nine compounds we could identify positive GABA_A receptor modulators (Li *et al*, 2016), $\alpha 7$ nicotinic receptors partial agonists (Shen *et al*, 2010), CDK inhibitors (Li *et al*, 2001), sodium channel blockers (Yang *et al*, 2015) and ASK-1 inhibitors (Takenaka *et al*, 2020). Modulation of these pathways has been well-documented to be involved in neuroprotection.

In parallel to the functional assays on primary neuronal cultures, the project collaborators have evaluated the effect of compounds on differentiation and myelination of the OPC CG4 line and on a primary rat OPC line in basal conditions. Altogether, the evaluation of compounds' neuroprotective function on primary cortical neurons and promyelinating function on primary OPCs resulted in the selection of 32 "front runners" molecules for further validation on human cells.

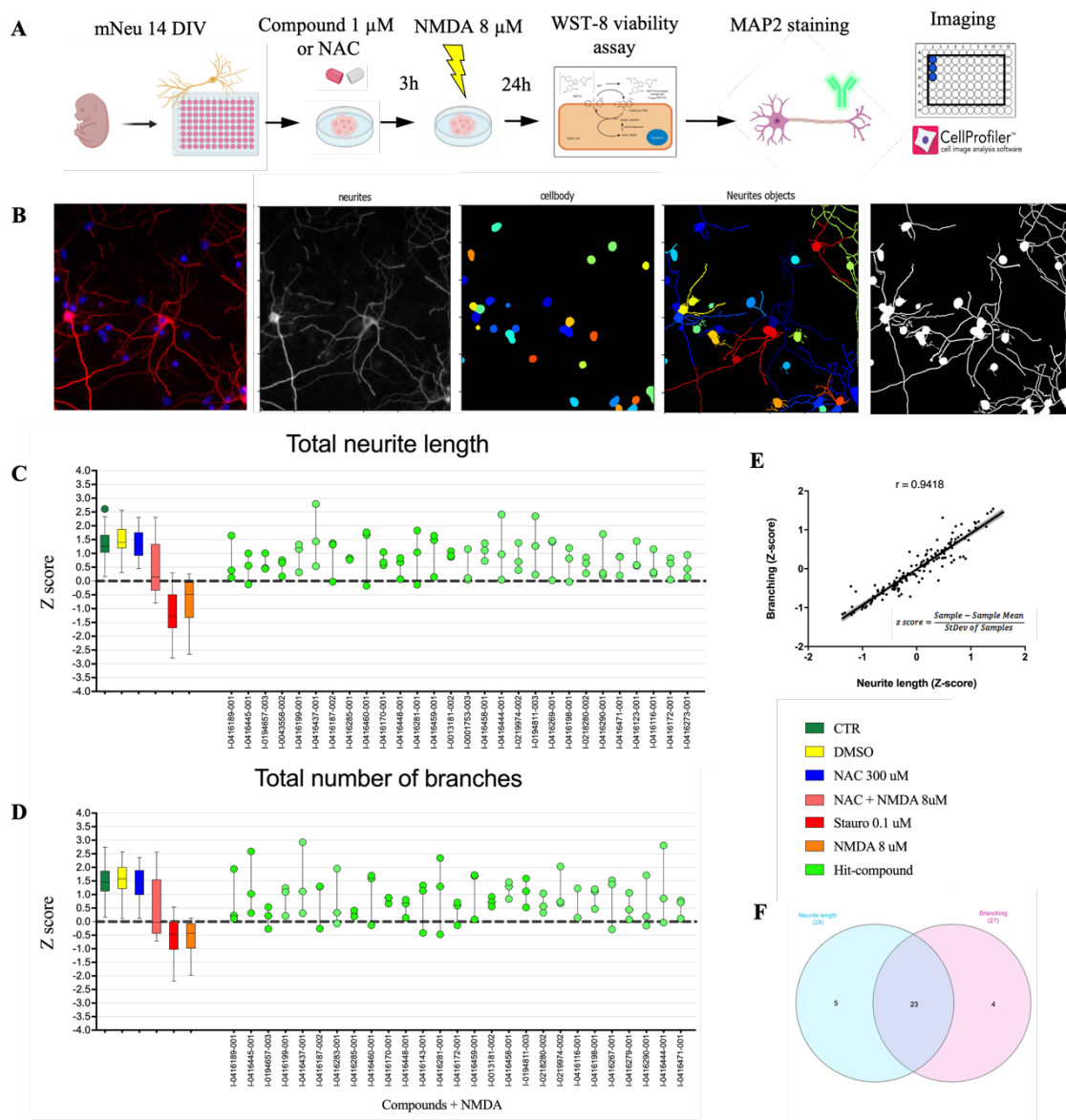


Figure 13. Evaluation of compounds neuroprotective efficacy from NMDA-mediated excitotoxicity: morphological integrity. (A) Schematic representation of the morphological integrity experimental setup. Mouse cortical neurons were pre-treated with 1 μM of compounds of NAC 300 μM and then challenged with NMDA to induce excitotoxic stress. After evaluating cell viability, neurons were fixed and evaluated for MAP2 by immunofluorescence imaging. Forty-five images were acquired for each condition with Arrayscan XTI microscope and analysed in CellProfiler. (B) Step-by-step example of CellProfiler in-house built image analysis pipeline. The analysis starts with nucleus identification, expanding to the cell body (soma) and the neurites segmentation. Total neurite length (C) and the total number of branches (D) expressed as Z-scores were evaluated from 15 images/well, and each compound/control was tested in triplicates. (E) Correlation plot of neurite length and branching parameters. Z score was calculated for each compound. (F) Morphological integrity evaluation identified 28 compounds preserving the total neurite length and 27 compounds preserving the dendritic branching.

3.2.2.4 Identification of 9 out of 32 “front runners” with neuroprotective efficacy against TBHP-mediated oxidative stress in hiPSC-derived neuronal cultures.

In vitro models that resemble human disease conditions remarkably increase the drug screening efficiency and accuracy, as the target subtypes or drug-target affinities of the same drug can be fundamentally different for humans versus rodents. In addition, screening on human cells may accelerate the identification of compounds for translation into clinical use. Accordingly, we have differentiated three control hiPSC-NPC lines, namely CTR4, CTR7, and CTR8, into functional mature glutamatergic neurons to validate the neuroprotective function of a prioritized list of 32 compounds. The protocol for differentiation of hiPSC-derived glutamatergic neurons was applied as described in 3.2.1.2, Figure 8. First, we have evaluated the cytotoxicity effect of chronic exposure (24h) of glutamate at various concentrations on hiPSC-derived glutamatergic neurons obtained from a control line at DIV35 (Figure 14A); however, we could not reach the optimal level of glutamate-induced cytotoxicity (IC50). This can be explained by the relative neuronal immaturity at this time point of differentiation and by the low expression of glutamatergic receptors. Moreover, the line-to-line variations in the expression of glutamate receptors due to the intrinsic heterogeneity of hiPSC-derived neurons could further influence the assay readout, therefore we have selected a more general stressor that did not depend on the expression of a specific receptor. As an alternative stress inducer, we used TBHP, a pro-oxidant molecule that model organic hydroperoxides production observed in pathological conditions. TBHP is reported to induce oxidative stress, lipid peroxidation, ferroptosis, inhibition of axonal transport, and mitochondrial depolarization in neuronal cells, eventually leading to apoptosis and cell death (Isonaka *et al*, 2011; Wu *et al*, 2018). We have performed a dose-response assay of various concentrations of TBHP on three control lines of hiPSC-derived glutamatergic neurons to evaluate its cytotoxicity effect (Figure 14B). hiPSC-derived neurons were differentiated for 30-40 DIV, and cell viability was evaluated 24h after acute exposure (2h) to TBHP. Although three lines had a variable response to TBHP-induced stress, e.g., neurons of the CTR8 line were the most susceptible to oxidative stress, the TBHP 100 μ M concentration was selected for the following neuroprotective experiments. hiPSC-derived neurons from three control lines (CTR4, CTR7, CTR8) were differentiated for 30-40 DIV, pre-treated with 1 μ M compounds or MitoQ (a positive antioxidant control) for 24h,

and challenged with 100 μ M of TBHP for 2h, followed by media replacement, to evaluate the neuroprotective efficacy of 32 compounds from TBHP-induced oxidative stress. Cell viability was evaluated after 24h with WST-8 viability assay (Figure 14C). The experiment was performed on three independent neuronal differentiation attempts for each line, while each compound was tested in sextuplicate. As a result of the screening, nine compounds showed significant neuroprotective efficacy against TBHP-induced oxidative stress (Figure 14D).

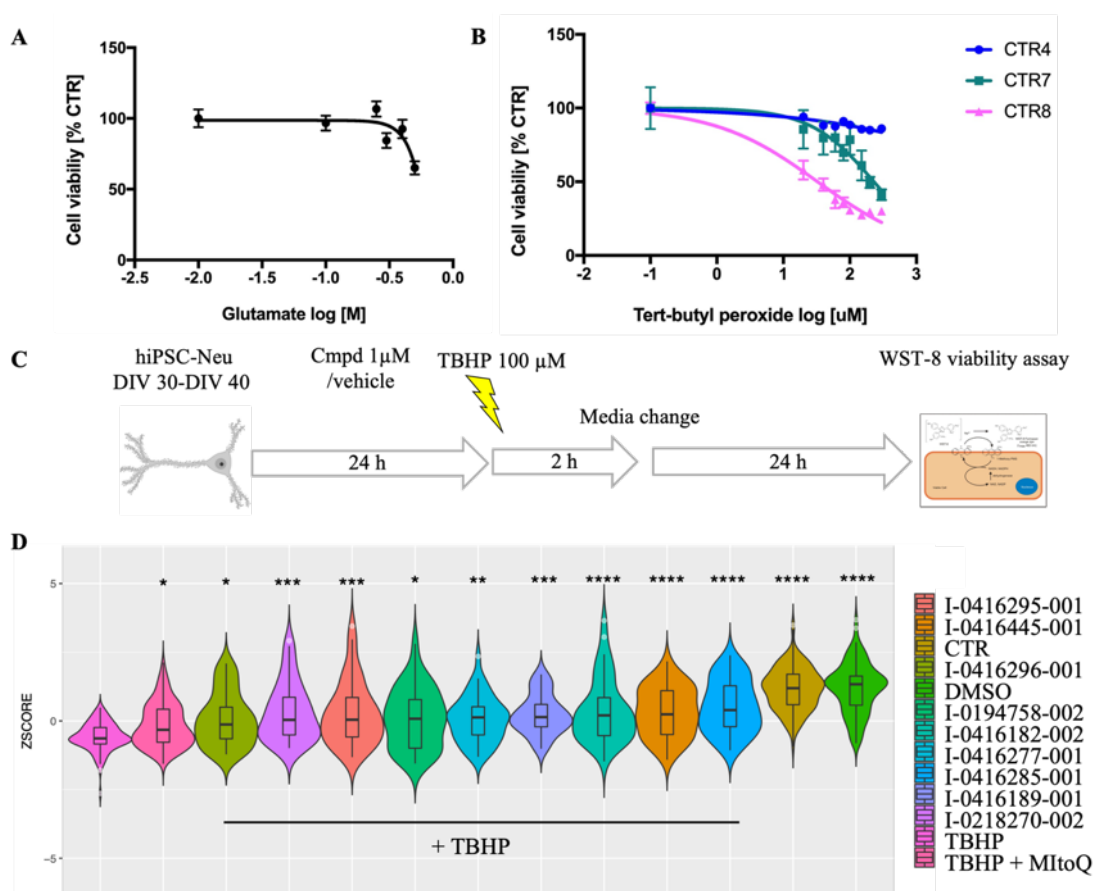


Figure 14. Validation of 32 “front runners” compounds on hiPSC-derived neuronal cultures. Various concentrations of glutamate (A) and TBHP (B) were tested on hiPSC-derived neuronal cultures to evaluate the cytotoxicity effect. The percentage of cytotoxicity is plotted against the logarithmic micromolar concentrations of glutamate/TBHP. (C) Schematic representation of the neuroprotective experimental setup on hiPSC-derived neurons. hiPSC-derived neurons were differentiated for 30-40 DIV, pre-treated with 1 μ M compounds for 24h and challenged with 100 μ M of TBHP for 2h, followed by media replacement. Cell viability was evaluated after 24h with WST-8 viability assay. (D) Compounds were tested on hiPSC-derived neurons from three control lines (CTR4, CTR7, CTR8) in three independent experiments (n=9 total); each compound was tested in sextuplicate. Boxplot shows the median value, outliers shown as single dots. Each 96 well plate included controls: 0.02% DMSO, CTR (non-treated), TBHP (stressor) and combination of TBHP+MitoQ as a neuroprotective rescue control. Stat. test performed with ordinary non-parametric Kruskal-Wallis test, followed by Dunn's multiple comparison correction, stat. significant $p < 0.05$. * $p < 0.05$, ** $p < 0.01$, *** $p < 0.001$, **** $p < 0.0001$.

3.2.3 Compounds ranking and prioritization

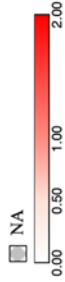
Prior to preclinical validation of the neuroprotective/repair and promyelinating properties of promising compounds, several criteria need to be addressed both to ensure that the studies provide interpretable data but also to minimize the ethical impact of animal testing; therefore, a careful selection and prioritization must be performed to identify the best drug candidate/s eventually. The selection criteria that we used included evaluation of the following parameters: 1) overall compound performance in neuronal and oligodendrocyte-based assays; 2) *in silico* ADME analysis of CNS activity, BBB permeability, P-glycoprotein substrate binding (Li *et al*, 2021) performed by external collaborators (CNR, UniMi); 3) evidence for brain penetration and data sources; 4) drug formulation and route of administration; 5) highest stage of development; CNS trials; 6) safety comments based on clinical data; 7) patentability and regulatory issues.

It is essential to assess that the compounds:

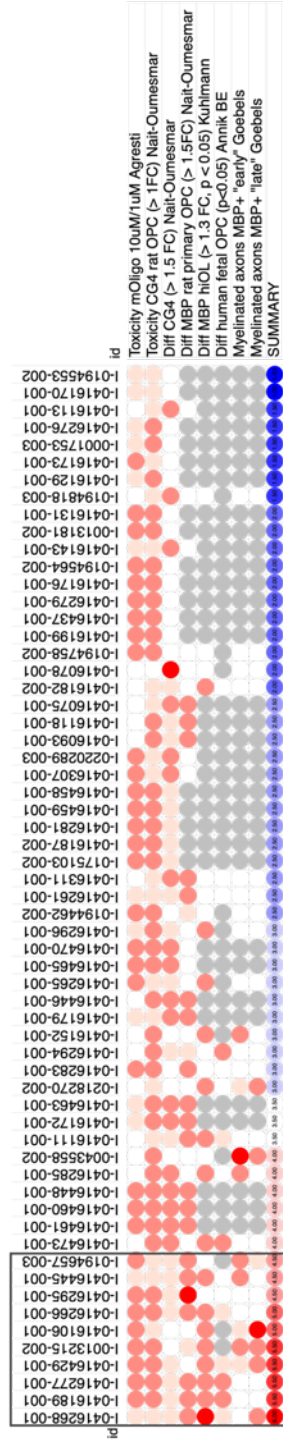
1. can be formulated and administered to achieve systemic exposure;
2. have sufficient half-life and permeability to allow distribution to the target organ (CNS);
3. do not show toxicity at the dose under consideration for the potential target of interest.

The overall compound performance in various neuronal (n=13) and oligodendrocyte-based-assays (n=8) was evaluated by ranking, or score assignment, accordingly to each experimental setting significance threshold, and visualized as a heatmap (Figure 15). The best compounds scored in neuronal- and oligodendrocyte-based assays were then assessed for an additional evaluation of drugs' ADME-PK properties (QikProp, SwissADME). As a result of the evaluation, two compounds, namely Bavisant (I-0416266-001), a histamine H3 (HRH3) antagonist, and Casopitant (I-0416445-001), a neurokinin-1 receptor (NK1R) antagonist, were selected for preclinical validation *in vivo*. Both compounds are among the top-10 ranked compounds in both neuronal- and oligodendrocyte-based assays, are orally available, CNS-penetrant, and with a good safety profile.

Score assignment
 0 - do not correspond to threshold
 0.5 - borderline to threshold
 1 - correspond to threshold
 2 - hit-compound in assay

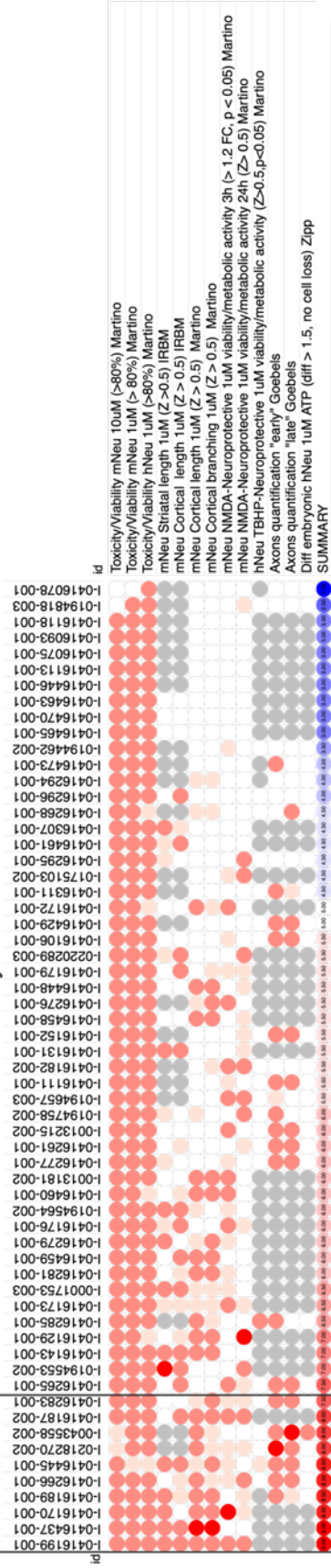


Oligodendrocyte-based assay



Toxicity mOligo 10uM/1uM Agresti
 Toxicity CG4 rat OPC (> 1FC) Nait-Oumesmar
 Diff CG4 (> 1.5 FC) Nait-Oumesmar
 Diff MBP rat primary OPC (> 1.5FC) Nait-Oumesmar
 Diff MBP hiOL (> 1.3 FC, p < 0.05) Kuhlmann
 Diff human fetal OPC (p<0.05) Annik BE
 Myelinated axons MBP+ "early" Goebels
 Myelinated axons MBP+ "late" Goebels
 SUMMARY

Neuronal-based assay



Toxicity/Viability mNeu 10uM (>80%) Martino
 Toxicity/Viability mNeu 1uM (> 80%) Martino
 Toxicity/Viability hNeu 1uM (>80%) Martino
 mNeu Striatal length 1uM (Z > 0.5) IRBM
 mNeu Cortical length 1uM (Z > 0.5) IRBM
 mNeu Cortical length 1uM (Z > 0.5) Martino
 mNeu Cortical branching 1uM (Z > 0.5) Martino
 mNeu NMDA-Neuroprotective 1uM viability/metabolic activity 3h (> 1.2 FC, p < 0.05) Martino
 mNeu NMDA-Neuroprotective 1uM viability/metabolic activity 24h (Z > 0.5) Martino
 hNeu TBHP-Neuroprotective 1uM viability/metabolic activity (Z > 0.5, p < 0.05) Martino
 Axons quantification "early" Goebels
 Axons quantification "late" Goebels
 Diff embryonic hNeu 1uM ATP (diff > 1.5, no cell loss) Zipp
 SUMMARY

Figure 15. Compounds ranking and prioritization. Heatmap shows the ranking of 160 compounds evaluated in multi-staged screening comprised of various neuronal-based and oligodendrocyte-based assays performed by the BRAVEinMS consortium. Toxicity evaluation included toxicity assay on primary murine oligodendrocytes (Agesti lab), CG4 rat OPC line (Nait-Oumesmar lab), primary murine cortical neurons, and hiPSC-derived neurons (Martino lab). Functional assays included differentiation of murine and human oligodendrocytes: CG4 OPC line, primary rat OPCs, (Nait-Oumesmar lab), embryonic human neurons (Zipp lab), hiOLs (Kuhlmann lab), and human fetal OPCs (Annik Baron-Van Evercooren lab); morphological integrity evaluation of murine cortical and striatal neurons upon excitotoxic injury (IRBM & Martino lab); neuroprotective experiments on primary murine cortical neurons upon excitotoxic injury, and hiPSC-derived neurons upon oxidative stress injury (Martino lab); evaluation of axonal myelination and axons of murine spinal cord cultures (SCC) Goebels lab. Compound performance was scored corresponding to the significance threshold of each experimental setting. The best compounds scored in oligodendrocyte and neuronal-based assays (black rectangle) were selected for further investigation.

3.3 Validation of selected hit-compounds Bavisant and Casopitant

3.3.1 Dose-response experiments of Bavisant and Casopitant confirm their neuroprotective properties.

Hit validation studies, including dose-response curves and assessment of compounds mechanism of action, are the established procedures to de-risk drug discovery. Compounds were tested at low-to-mid nanomolar range concentrations on primary murine cortical neurons in excitotoxic or oxidative stress conditions to evaluate the effectiveness of compounds in inducing neuroprotection and to estimate the minimal effective dose for further translation *in vivo*. The settings of the neuroprotective experiment are shown in Figure 16A. Interestingly, Bavisant showed a neuroprotective efficacy in a dose-response manner in NMDA-mediated assay (Figure 16B), but not in the oxidative stress-mediated experiment (Figure 16D). On the contrary, Casopitant showed prominent antioxidant activity protecting neurons from TBHP-mediated oxidative stress in a dose-response manner (Figure 16E) but was not active in NMDA-mediated experimental settings (Figure 16C). In addition, we tested the compound Orvepitant that has a chemical structure analogue to that of Casopitant (Figure 16F), confirming its neuroprotective properties under oxidative stress conditions (Figure 16G). Therefore, both drugs confirmed their neuroprotective properties in dose-response experiments under oxidative stress or excitotoxic conditions, predicting 500nM and 1uM as the effective doses for Casopitant, and 1uM dose - for Bavisant.

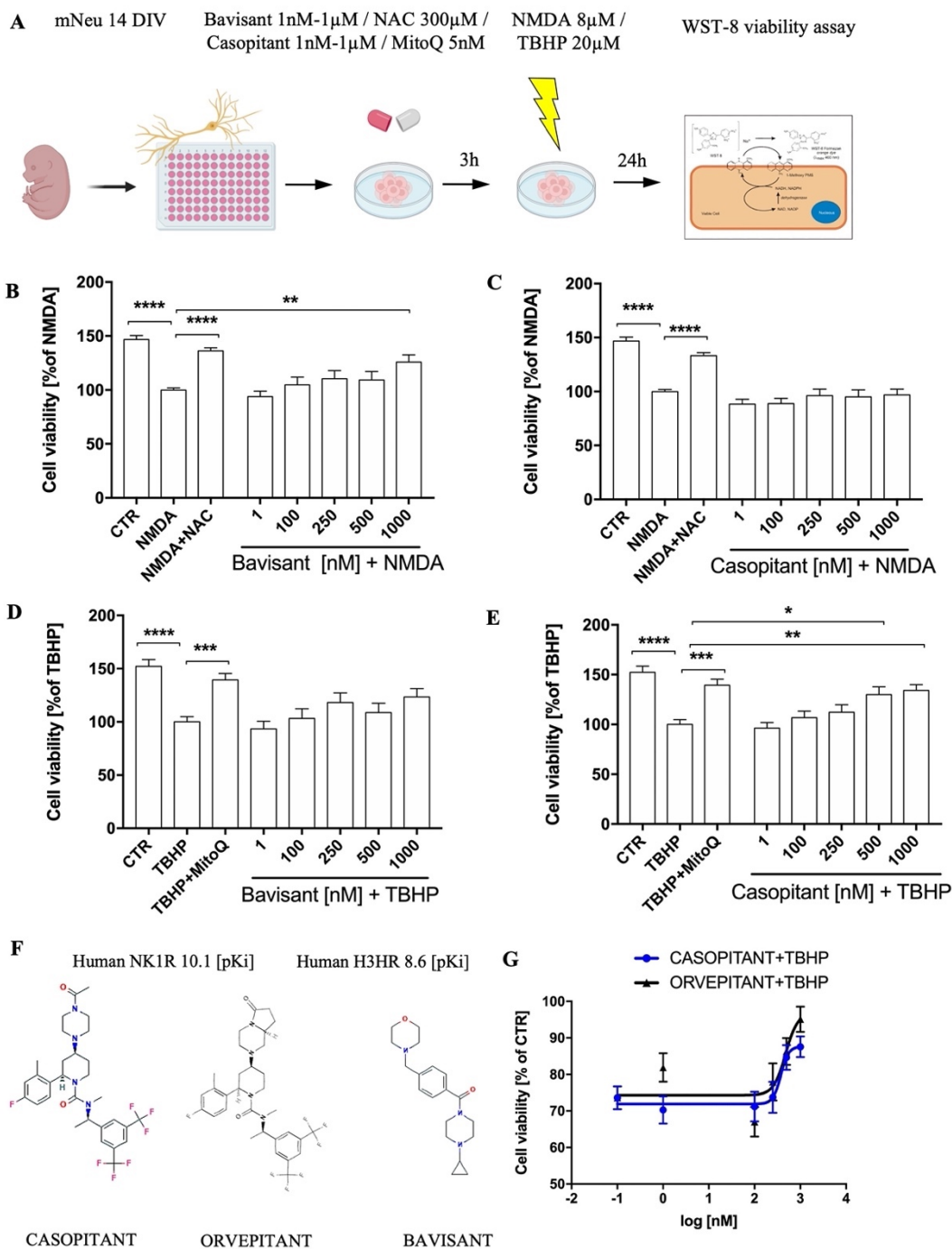


Figure 16. Validation of hit-compounds Bavisant and Casopitant neuroprotective properties in vitro: dose-response assay. (A) Schematic representation of neuroprotective experimental setup. (B) Dose-response assay demonstrates the neuroprotective effect of Bavisant from NMDA-induced excitotoxicity. Cell viability/metabolic activity is expressed in percentage relative to NMDA-treated cells. Each bar reports mean value \pm SEM obtained from five independent experiments run in sextuplicate. (C) Dose-response assay demonstrates the absence of protective effect of Casopitant in NMDA-induced excitotoxicity assay. Cell viability/metabolic activity is expressed in percentage relative to NMDA-treated cells. Each bar reports mean value \pm SEM obtained from three independent experiments run in sextuplicate. (D) Dose-response assay demonstrates the absence of Bavisant protection from TBHP-induced cytotoxicity. Cell viability/metabolic activity is expressed in percentage relative to TBHP-treated cells. Each bar

reports mean value \pm SEM from three independent experiments run in sextuplicate. (E) Dose-response assay demonstrates the neuroprotective effect of Casopitant from TBHP-induced cytotoxicity. Cell viability/metabolic activity is expressed in percentage relative to TBHP-treated cells. Each bar reports mean value \pm SEM from five independent experiments run in sextuplicate. Stat. test performed with one-way ANOVA, followed by Dunnett multiple comparison correction, * p <0.05; ** p <0.01; *** p <0.001; **** p <0.0001. (F) Chemical structures for Casopitant, Orvepitant and Bavisant. (G) Normalized dose-response curve demonstrates the neuroprotective effect of Casopitant and Orvepitant from TBHP-induced oxidative stress cytotoxicity. The percentage of cytotoxicity is plotted against the logarithmic nanomolar concentration of compounds challenged with TBHP 20 μ M. Data from each point were obtained in sextuplicate from 3 independent experiments.

3.3.2 Bavisant and Casopitant show promyelinating efficacy in hiOL

In addition to neuroprotective properties, both drugs have been validated for their promyelinating effects on human iPSC-derived oligodendrocytes (hiOL). The generation of hiOL cultures is a complex task that requires a prolonged culture (>3 months) to obtain mature oligodendroglia cultures. One of the latest approaches to accelerate hiOLs differentiation employs overexpression of three transcription factors (TFs) highly enriched in OLs (Ehrlich *et al*, 2017). A novel approach to generate SOX10-bearing hiOLs by overexpression of the single TF hSOX10 in iPSC-derived NPCs by an inducible lentiviral vector harbouring a GFP reporter was implemented in our laboratory (work of Annamaria Cafarella). After transduction, iPSC-NPCs differentiate into O4+ OPCs and matured into MBP+ oligodendrocytes within 26-28 days

hiOL were differentiated according to the protocol described in 6.5.2, and myelin basic protein (MBP) expression was evaluated by FACS analysis and immunofluorescence to validate Bavisant and Casopitant promyelinating efficacy. After 26 days of differentiation, including 14 days of treatment with Bavisant at 1 μ M, Casopitant at 1 μ M, DMSO 0.01% (vehicle), or a thyroid hormone (T3) at 60ng/mL, Bavisant-treated cells expressed the highest MBP level evaluated by immunofluorescence (Figure 17B), while the area occupied by MBP+ cells was comparable to Casopitant-treated cells (Figure 17C). In both conditions, the MBP+ area was significantly more extended than the MBP+ area of T3-treated cells. In the evaluation by FACS analysis, we have identified a slight discrepancy in the percentage of MBP+ cells, with Casopitant being more efficient than Bavisant in promoting oligodendrocyte differentiation. Also, the effect on MBP expression induced by T3 was unexpectedly weak, despite that T3 is a widely used positive control for oligodendrocyte differentiation and maturation (Farsetti *et al*, 1991).

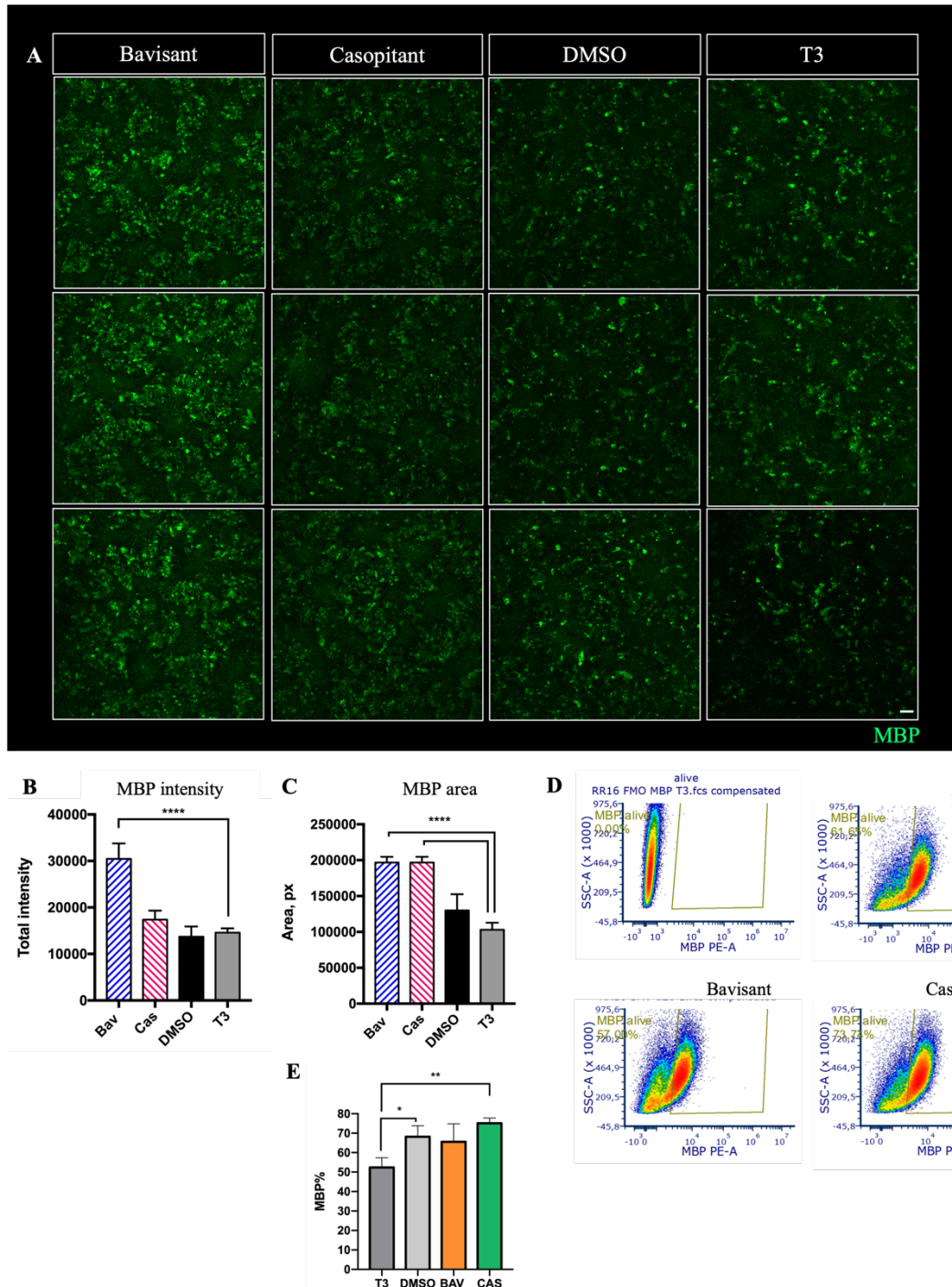


Figure 17. Validation of pro-myelinating properties of Bavisant and Casopitant in hiOL.

(A) Three representative images of MBP staining of hiOLs differentiated from one MS patient-specific line treated with Bavisant, Casopitant, T3, or DMSO. MBP intensity (B) and MBP area (C) were analysed with CellProfiler in-house built pipeline. Scale bar = 100 μ m. (D) The gating strategy for FACS analysis. Doublets and dead cells (positively stained with LiveDead assay kit) were excluded from the analysis. Gates applied for population discrimination were based on the control population (T3) sample. (E) Quantification of mean fluorescence MBP intensity obtained by FACS analysis. Each bar represents mean value \pm SD from three independent wells. Stat. test performed with one-way ANOVA, followed by Dunnett multiple comparison correction, * $p < 0.05$; ** $p < 0.01$.

Therefore, preliminary results show a positive effect of both drugs on human oligodendrocyte myelination properties, however additional experiments are still required (a new batch of T3 must be tested) to confirm these findings.

Additionally, we have characterized the effect of compounds treatment on the expression of the oligodendrocyte markers O4 and GalC, and the effect on astrocyte (GFAP) proliferation. The GFAP expression and astrocytes morphology were comparable between all the treatments, while expression of O4 and GalC was reduced in T3-treated cells. The hiOL SOX10-inducible system represents a tri-culture system comprised of neurons, astrocytes, and oligodendrocytes, which can serve as a scalable platform for screening compounds that target the crosstalk between CNS cells as well as to evaluate myelination. In addition, SOX10-overexpressing NPCs can be used for the differentiation of a complex 3D cellular system like neural spheroids (Brain Spheres).

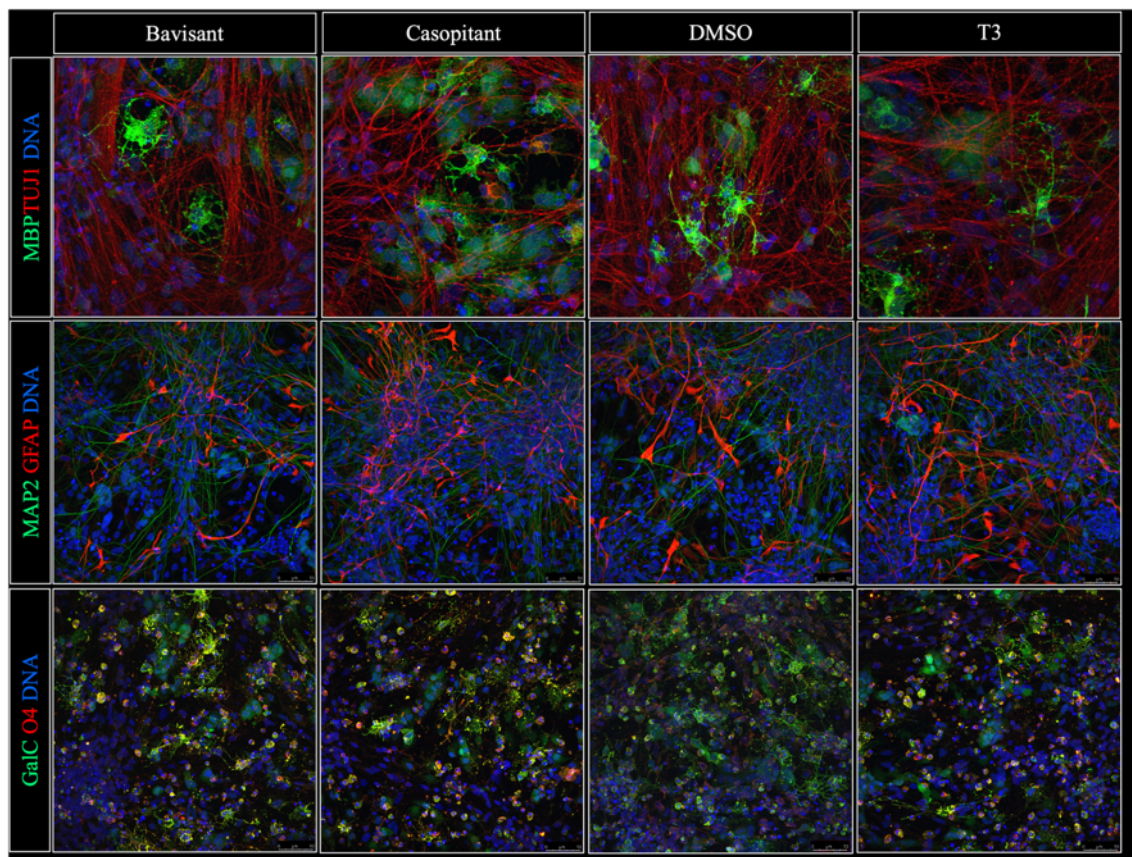


Figure 18. *hiOL is a tri-culture system comprised of neurons, oligodendrocytes, and astrocytes. Representative images of oligodendrocyte MBP, GalC, O4, neuronal TUJ1, MAP2, and astrocyte GFAP immunofluorescence staining on hiOLs at DIV26 of differentiation of each treatment condition (Bavisant, Casopitant, DMSO and T3).*

3.3.3 Bavisant and Casopitant confirm their neuroprotective efficacy in 3D neural spheroids.

The hiPSC-derived oligodendrocyte and neuronal co-cultures obtained from the same individual provide a unique opportunity to evaluate the promyelinating effects of hit-compounds. A co-culture system is superior in reproducing the human biological tissue and allows testing of drugs with dual neuroprotective and promyelinating functions. The 3D human iPSC-derived neural spheroid model is a more physiologically relevant paradigm for testing the efficacy of drug candidates and is a valuable research tool capable of complementing animal models of neurodegeneration and live human brain tissue (Pamies *et al*, 2017).

In this project, we set up the 3D neural spheroid model to validate the neuroprotective efficacy of Bavisant and Casopitant under neurotoxic and oxidative stress conditions. About 120-150 spheroids were differentiated in a single well of the 6-well plate. Spheroids had a homogenous size (~500 μm) and shape between weeks 6 and 12 of differentiation (Figure 19, B-C), which has been identified as an optimal experimental time window. From the preliminary characterisation, spheroids were comprised of neurons (TUJ1+), astrocytes (GFAP+), and oligodendrocyte precursor cells (O4+) at week 7 of differentiation (Figure 19D), and a low percentage (~6.3%) of GalC and 3.4% of MBP+ oligodendrocytes at week 12 of differentiation (Figure 19E).

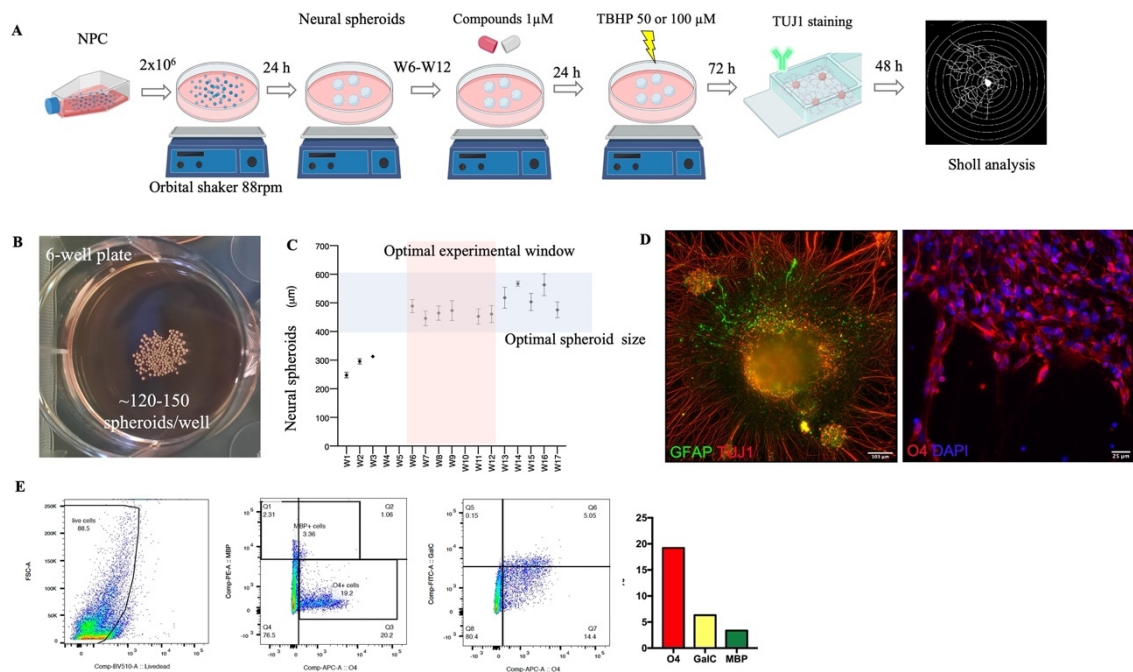


Figure 19. 3D neural spheroids (BrainSpheres). (A) Schematic of spheroids differentiation protocol and neurite outgrowth readout. (B) An image of the well with spheroids at week 6 of differentiation with an average diameter of 500 μm . (C) The size of spheroids was measured between weeks 1-17 of differentiation. Spheroids ($n = 10$) were randomly selected at each time point for obtaining pictures and measuring size using AxioCam ZenLite software. Results are expressed as mean \pm SD. (D) hiPSC-derived brain spheroids were characterized by IF at week 7 and FACS analysis (E) at week 12 confirming the presence of oligodendrocyte precursor cells expressing O4 (19.2%), and low percentage of MBP+ (3.4%) and GalC+ (6.3%) oligodendrocytes.

To evaluate TBHP toxicity effect on spheroids, we performed a dose-response assay to assess neurite outgrowth at week 6 of differentiation. Three doses of TBHP were applied for 2h to the antioxidant-deprived Neurobasal media and spheroids were then plated on polyornithine/laminin (POL)-coated chamber slides. After 72h, neurite outgrowth was evaluated by TUJ1 immunofluorescence staining, and Sholl analysis was performed with Fiji plugin. Neurite outgrowth analysis showed a dose-response toxicity effect of TBHP on neurite density, where TBHP 50 μM reduced the number of neurite intersections by 37%, TBHP 100 μM – by 73.5%, while TBHP 200 μM was 100% toxic to neural spheroids (no attachment of spheroids to the glass surface was observed). The area under the curve was used to compare TBHP treatment with non-treated control (Figure 20B).

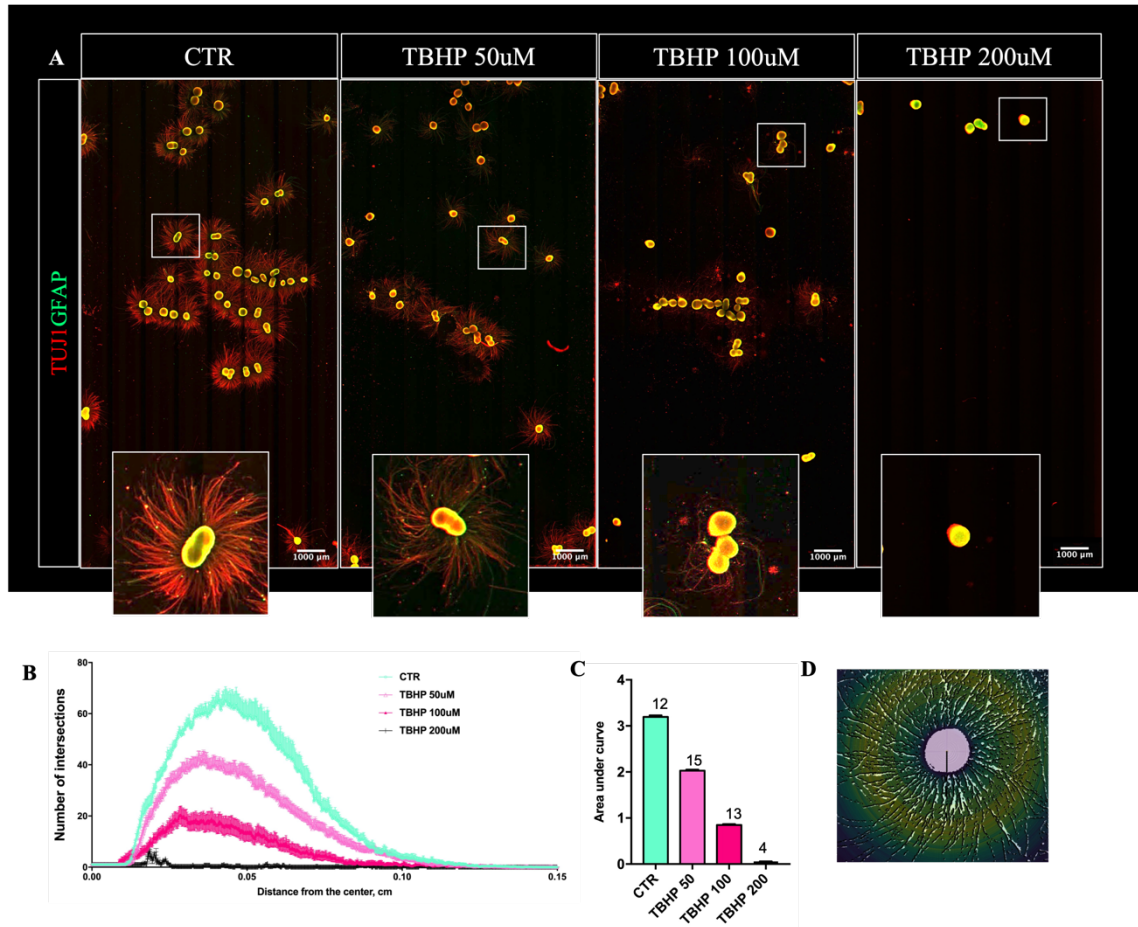


Figure 20. Oxidative stressor dose-response assay in the 3D neural spheroids. (A) Representative images of oxidative stressor dose-response on hiPSC-derived spheroids neurite outgrowth at week 6 of differentiation. (B) Neurite outgrowth quantification of TBHP dose-response assay performed with Sholl analysis in Fiji software. The x-axis represents a distance from the spheroid centre, while the Y-axis represents the number of intersections with the concentric circles produced by the software. (C) The area under curve analysis of graph B. Each bar represents mean value \pm SD and the number of analysed spheroids. (D) Example of Sholl analysis image output.

Next, we evaluated Bavisant and Casopitant neuroprotective effect on spheroids neurite outgrowth at week 8.5 of differentiation in TBHP-mediated oxidative stress conditions. In detail, the day before the experiment, spheroids were pre-treated for 24h with 1 μ M Bavisant or Casopitant and were acutely stressed (two hours) with 50 μ M or 100 μ M of TBHP at the next day (Figure 21A). Spheroids' capability to outgrow neurites was evaluated by plating them on POL-coated surface for 72h and assessed by TUJ1 immunostaining and Sholl analysis. Application of a higher concentration of TBHP (100 μ M) for two hours reduced neurite outgrowth by approximately 50%, while 24h pre-treatment with drugs rescued TBHP-induced toxicity, resulting in 16.4% recovery in the number of intersections (neurites) in Bavisant-treated condition and 43% improvement in

neurite outgrowth in Casopitant-treated condition, compared to TBHP 100 μ M treated spheroids (Figure 21C).

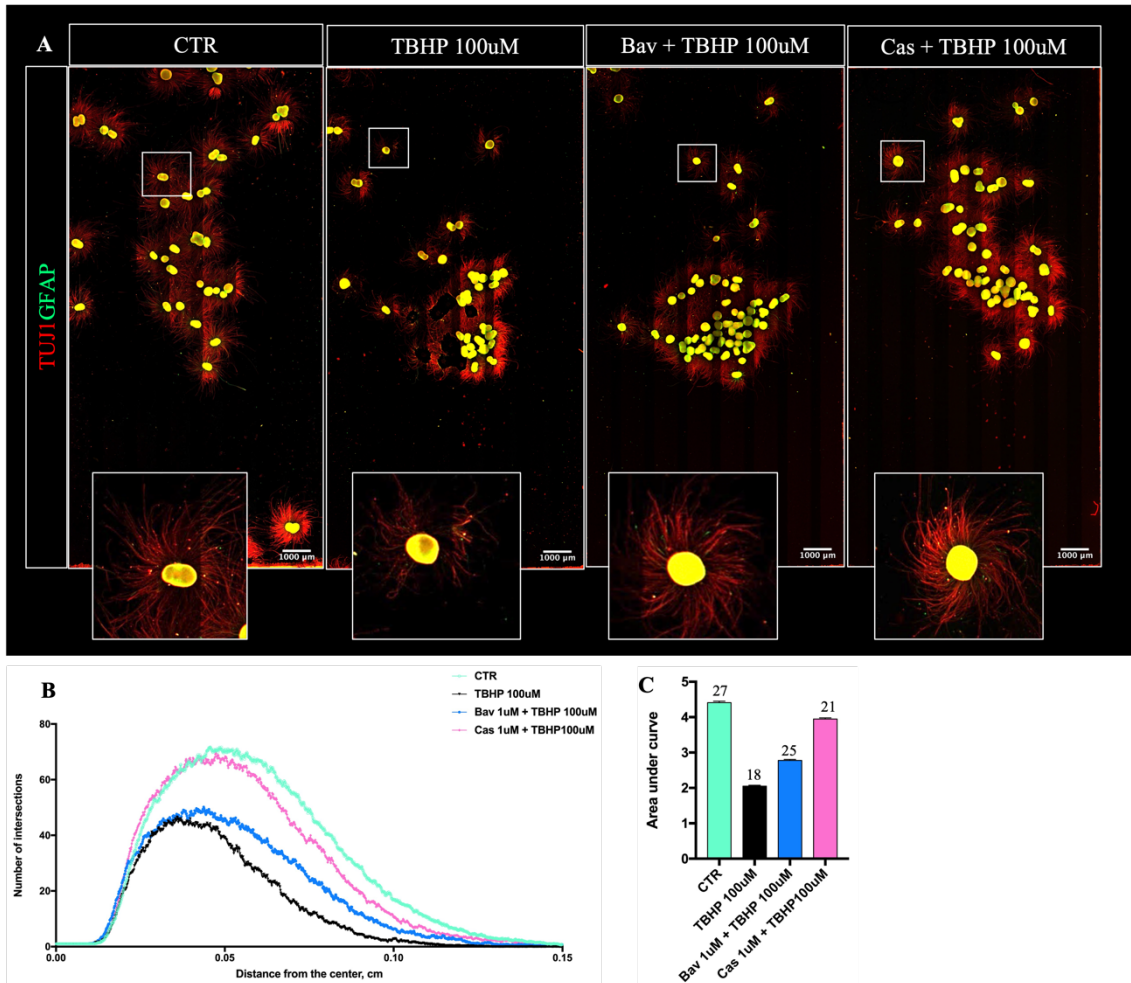


Figure 21. Evaluation of Bavisant and Casopitant neuroprotective efficacy in the 3D neural spheroids. (A) Representative images of hiPSC-derived spheroids neurite outgrowth assay in neuroprotective and stressor conditions at week 8.5 of differentiation. (B) Neurite outgrowth quantification of the images shown in A by Sholl analysis. The x-axis represents a distance from the spheroid centre, while the Y-axis represents the number of intersections with the concentric circles produced by the software. (C) The area under curve analysis of graph B. Each bar represents mean value \pm SD and the number of analysed spheroids.

Three independent experiments were performed for Bavisant and Casopitant at weeks 7.5, 8.5, and 12 of spheroids differentiation, as shown in the summary graphs (Figure 22).

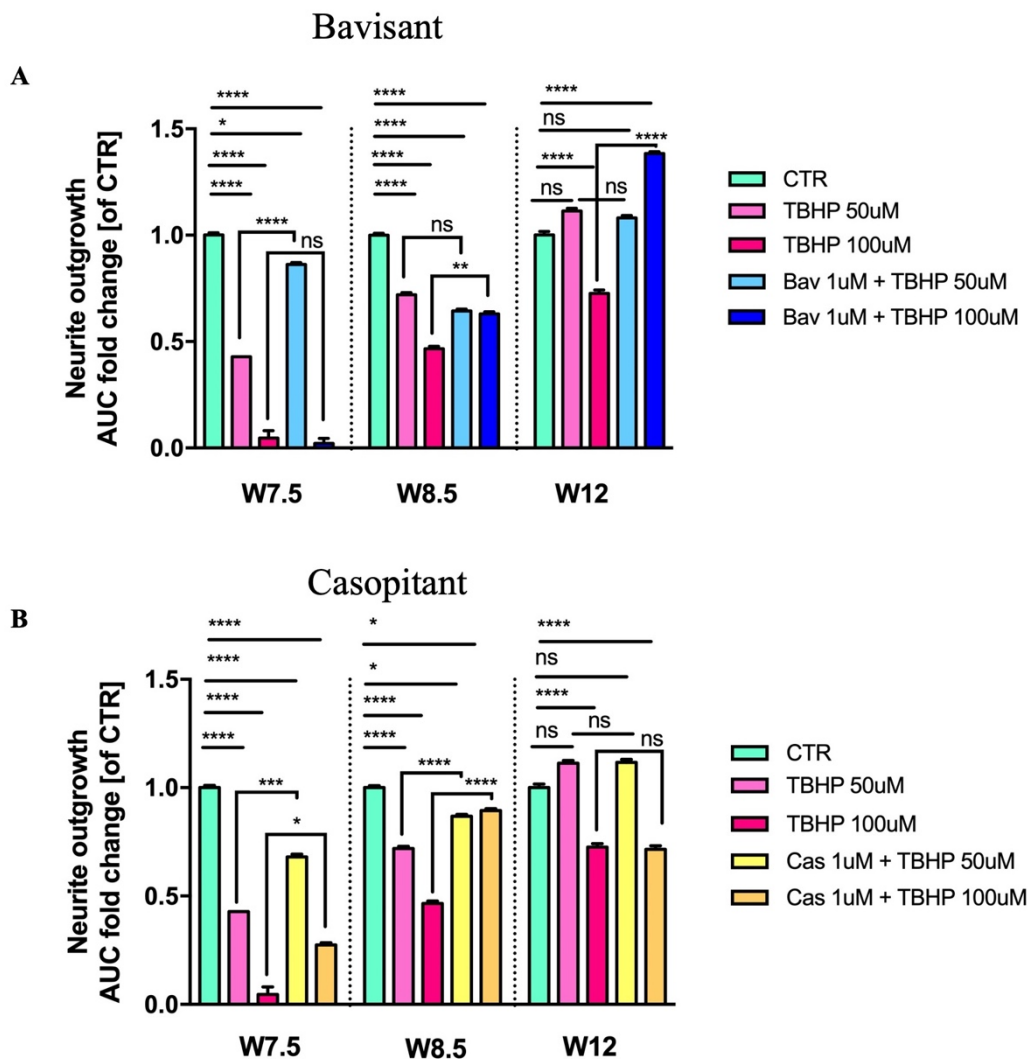


Figure 22. Summary of Bavisant and Casopitant neuroprotective efficacy in the 3D neural spheroids. The neuroprotective potential of Bavisant (A) and Casopitant (B) was evaluated in oxidative stress condition on hiPSC-derived spheroids from one control line at 7.5, 8.5, and 12 weeks of differentiation. The area under the curve (AUC) of neurite outgrowth was evaluated by Sholl analysis and normalised to the AUC of respective non-treated spheroids (CTR). Each bar reports mean \pm SD value. Stat. test performed with one-way ANOVA, followed by Dunnett multiple comparison correction, * $p < 0.05$; ** $p < 0.01$, *** $p < 0.001$; **** $p < 0.0001$.

Both drugs showed significant neuroprotective effect against oxidative stress in the 3D neural spheroids. However, the antioxidant effect of Casopitant was more pronounced at week 7.5 (23 % recovery from TBHP induced oxidative stress vs no recovery by Bavisant pre-treatment) and at week 8.5 (42.9% recovery by Casopitant vs only 16.4% improvement by Bavisant compared to TBHP-treated spheroids). Nevertheless, Bavisant showed superior neuroprotective efficacy at week 12 of differentiation, improving by 66% the number of neurite outgrowth, while Casopitant did not show any protective

effect. Interestingly, 50 μ M TBHP did not induce any decrease in spheroids neurite outgrowth at week 12, potentially due to a protective effect induced by astrocytes (higher GFAP expression was observed at week 12, data not shown).

In conclusion, both drugs confirmed their neuroprotective properties in the complex 3D cellular model of BrainSpheres upon oxidative stress. Additional experiments evaluating compounds' effect on myelination of spheroids differentiated from SOX10-transduced NPCs will be performed.

3.3.4 Bavisant-and Casopitant-treated EAE mice show lower demyelination and lower axonal loss of the spinal cord but no amelioration of the clinical score

To evaluate the clinical efficacy of the compounds, we have selected the well-established animal model of MS experimental autoimmune encephalomyelitis (EAE). The chronic phase of EAE is characterized by the presence of progressive ascending paralysis caused by damage and inflammation mainly in the peripheral white matter of the spinal cord (Constantinescu *et al*, 2011). Chronic EAE was induced in seventy 7-8 weeks old C57BL/6J female mice as described in 6.14. Myelin Oligodendrocyte Glycoprotein (MOG)-immunized mice were randomized in five treatment groups: EAE, Bavisant (30 mg/kg) once daily (q.d.), Casopitant (100 mg/kg) once or twice daily (q.d./b.i.d.), or 0.5% Methocell (vehicle) twice daily (b.i.d.). The treatment was started at the peak of the disease (3-4 days after onset). Oral gavage administration was performed in a blinded fashion for 28 days (from the peak of the disease until the sacrifice). Bodyweight change and EAE clinical score were evaluated daily (Figure 23A).

The optimal dose and route of administration were selected based on the preliminary pharmacokinetics analysis of Bavisant and Casopitant performed by an external collaborator (IRBM, Italy). Plasma and brain PK/PD analyses of both drugs were carried out in healthy 6-8 weeks old C57BL/6J female mice, suggesting a longer half-life time for Bavisant (~24h) compared to Casopitant (~8h) (Figure 23, B-C). The dosing regimen decision was based on PK/PD parameters, such as receptor binding affinity (K_i), clearance, protein binding and bioavailability. Based on the lower potency of Casopitant for the mouse NK1 receptor, 100 mg/kg per os (PO) administration (q.d. or b.i.d.) was selected as a reasonable dosing regimen. Based on sub-optimal PK data and high bioavailability of Bavisant, 30 mg/kg PO q.d. dose was suggested. Bavisant was

developed to treat excessive insomnia; therefore, treatment longer than 28 days was not recommended to avoid sleep/wake cycle alterations. After 28 days of treatment, blood from three EAE mice from each treatment group was collected one hour after the last drug administration. Blood was centrifuged to separate the plasma. Immediately after sacrifice, the brains of the same mice were collected, flash-frozen, and sent for PK analysis (IRBM, Italy). Unbound plasma and brain concentrations of Bavisant and Casopitant in EAE mice were comparable to compounds PK/PD in healthy mice (Figure 23, B-C).

No amelioration in EAE clinical score was observed after 28 days of Bavisant or Casopitant administration compared to the vehicle treated (Methocell) or EAE mice (Figure 23D). The weight of animals treated with Casopitant q.d. or b.i.d. doses was significantly decreased, compared to EAE mice. No difference in mortality incidence was observed (Table 4).

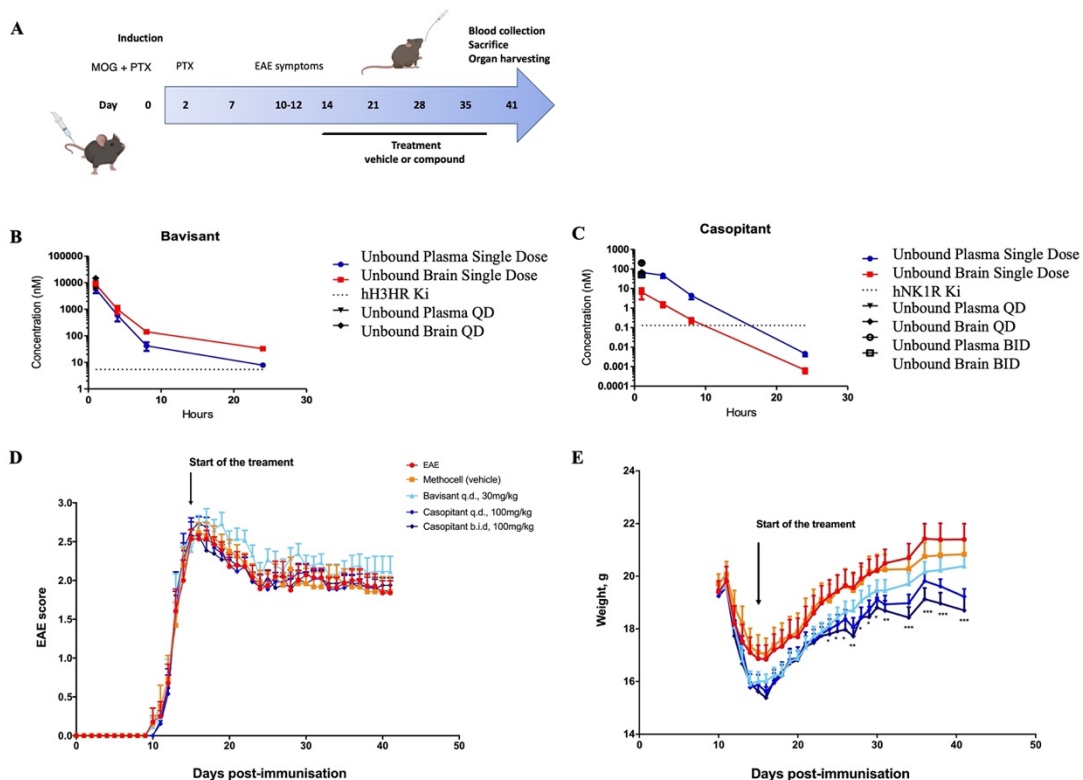


Figure 23. In vivo validation of hit-compounds in EAE animal model: clinical score evaluation. (A) Schematic representation of EAE immunization and treatment protocol (as described in Materials and Methods). (B-C) Pharmacokinetic analysis for Bavisant (q.d.) and Casopitant (q.d./b.i.d.) was performed on plasma and brain of healthy C57BL6/J mice after 1-4-8-24h administration (blue and red lines) and EAE mice (black symbols) 1h after administration. The clinical score (D) was comparable between all treatment conditions, while the weight (E) of the animals treated with Casopitant (q.d./b.i.d.) was significantly decreased compared to non-treated

EAE mice. Data are shown as mean ± SEM. Stat. test was performed with two-way ANOVA, followed by Dunnett multiple comparison corrections.

Group	Score max	Score min	Mortality	Cumulative score	Average score
EAE	3	0	0/14	60.89	1.84 ± 0.16
Methocell (b.i.d.)	2.5	0.5	1/13	61.56	1.89 ± 0.20
Bavisant (q.d.)	3.5	0.5	0/13	67.06	2.09 ± 0.18
Casopitant (q.d.)	3	0.5	0/13	61.04	1.90 ± 0.11
Casopitant (b.i.d.)	3.5	0.5	1/13	60.52	1.92 ± 0.10
EAE incidence: 66/70 mice					

Table 4. Summary of EAE incidence, maximum disease severity, the cumulative and average score for each treatment group. The average score is shown as mean ± SEM.

Although we could not observe the therapeutic effect of compounds on chronic EAE clinical scores, mild amelioration in demyelination (Figure 24) and axonal loss (Figure 25) of Bavisant- and Casopitant (q.d.)-treated mice were observed in histopathological analyses of the spinal cord. Histopathological analyses of spinal cords of five representative mice (with low, mild, and pronounced clinical scores) from each treatment group were performed by Luxol fast blue (demyelination), Bielschowsky silver staining (axonal damage) and H&E (immune cell infiltrates) staining.

Luxol fast blue staining identified a lower rate of demyelination in Bavisant and Casopitant (q.d.) treatment groups compared to EAE or vehicle-treated mice (Figure 24B). Interestingly, mice with a higher clinical score of 2.5 (dragging of hind legs, limp tail) had two-fold lower demyelination than EAE, Methocell- or Casopitant b.i.d.-treated mice with the exact clinical representation.

In axonal damage evaluation, we observed a similar trend of amelioration in Bavisant and Casopitant (q.d.) treatment groups (Figure 25B). In addition to histopathological analysis, we measured neurofilament light chain (Nfl) levels after 28 days of treatment from the plasma of four out of five animals used in the immunohistology examination as a biomarker of axonal/neuronal injury. No significant Nfl level differences were identified among the treatment groups (Figure 25C). The correlation analysis between the axonal damage rate and EAE clinical score revealed that mice with higher clinical scores

had a two-fold lower axonal loss than EAE or Casopitant b.i.d.-treated mice with the same clinical features (Figure 25D).

No significant differences were observed in the number of the immune infiltrates evaluated by H&E staining among the treatment groups (Figure 26).

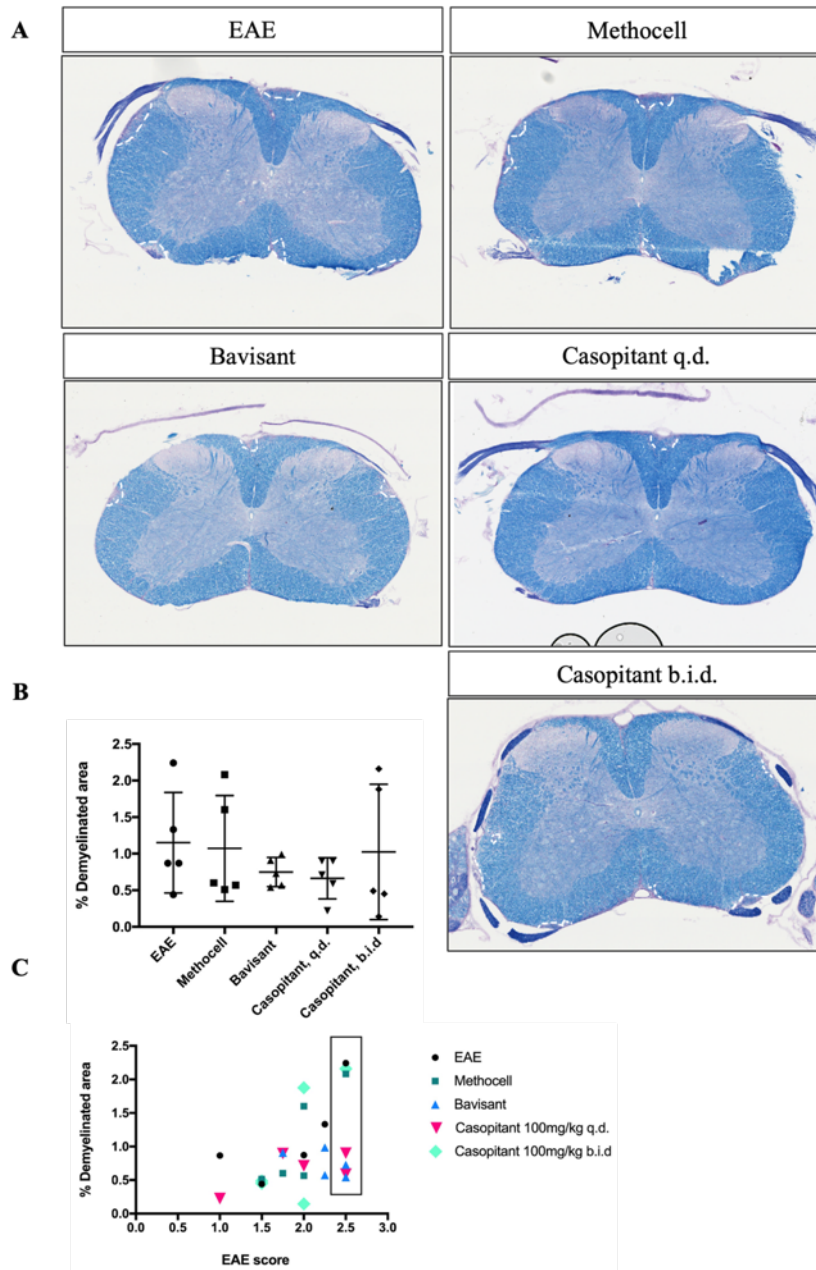


Figure 24. Immunohistochemical evaluation of EAE spinal cord tissue demyelination. Spinal cord sections were obtained from five EAE, Methocell-treated, Bavisant, or Casopitant-treated mice at day 41 post immunisation (28 days of treatment) and analysed by Luxol Fast Blue staining for demyelination. (A) Representative images of lumbar spinal cord sections show areas of demyelination, indicated by a white dashed outline. (B) The demyelinated area was normalized to the total area of each spinal cord section and expressed in percentage. The sections of the whole spinal cord were analysed. Treatment with Casopitant (q.d.) and Bavisant showed a trend

in lower demyelination compared to EAE or vehicle-treated mice. The scatter plot shows mean value \pm SD; each dot represents an individual animal. (C) Mice with the highest EAE clinical score of 2.5 treated with Casopitant (q.d.) or Bavisant had a lower demyelination rate than EAE or vehicle-treated mice.

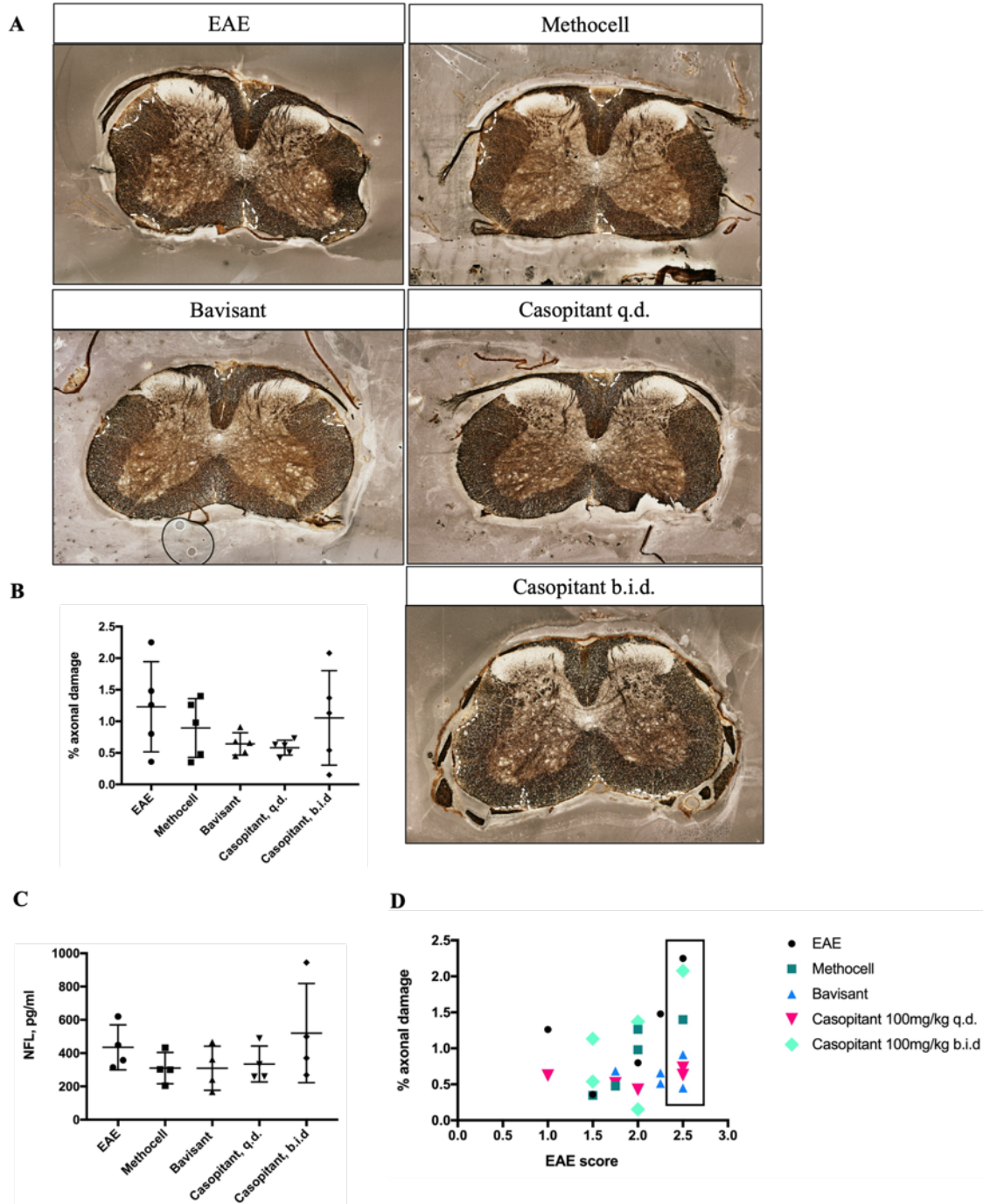


Figure 25. Immunohistochemical evaluation of EAE spinal cord tissue axonal loss. Spinal cord sections were obtained from five EAE, Methocell-treated, Bavisant, or Casopitant-treated mice at day 41 post immunisation (28 days of treatment) and analysed by Bielchowsky silver staining. (A) Representative images of lumbar spinal cord sections show areas of axonal damage, indicated by a white dashed outline. (B) Axonal loss area was normalized to the total area of each spinal cord section and expressed in percentage. The sections of the whole spinal cord were analysed.

Treatment with Casopitant (*q.d.*) and Bavisant showed a trend in reduced axonal damage compared to EAE or vehicle-treated mice. The scatter plot shows the mean value \pm SD; each dot represents an individual animal. (C) Neurofilament light chain (Nfl) levels were measured from the plasma of four animals from each treatment group. The scatter plot shows the mean value \pm SD, each dot represents an individual animal. (D) Mice treated with Casopitant (*q.d.*) or Bavisant had a lower axonal damage rate than EAE or vehicle-treated mice.

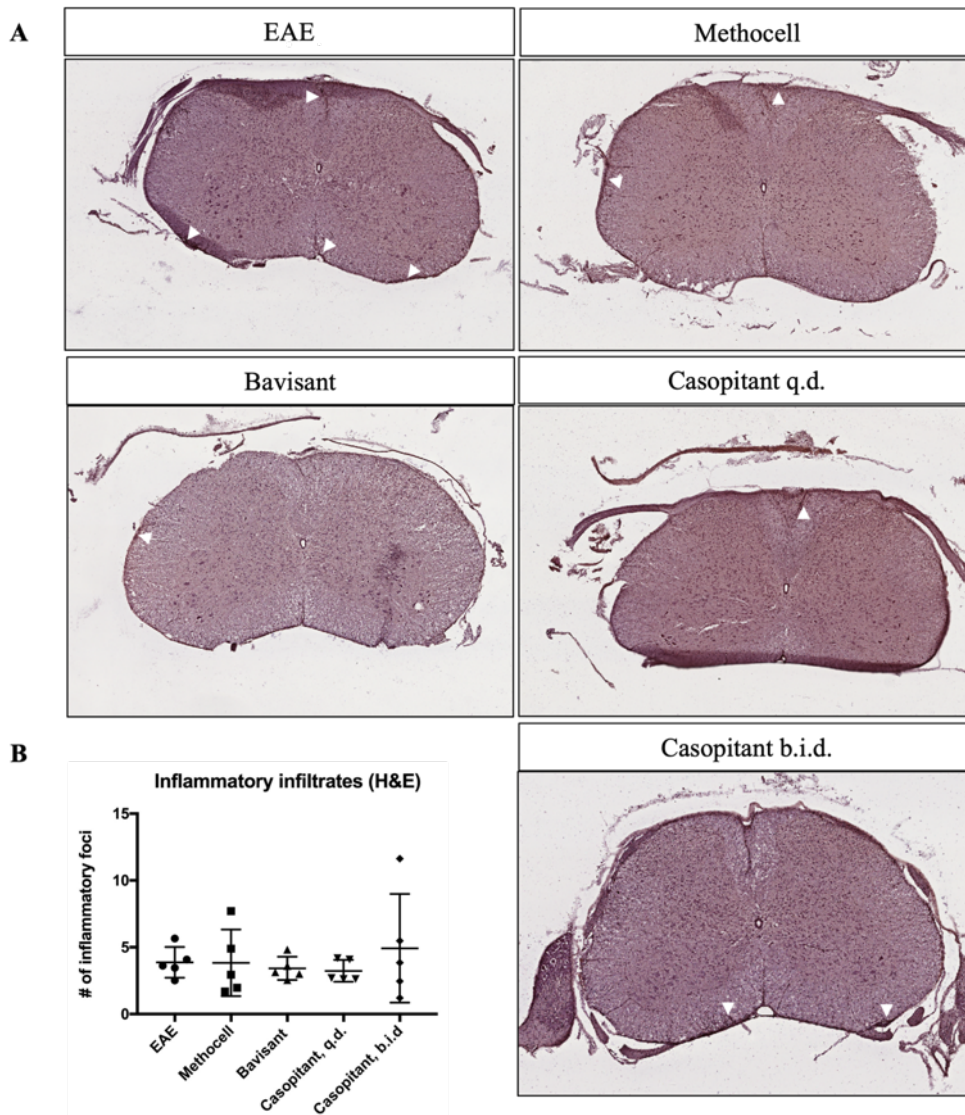
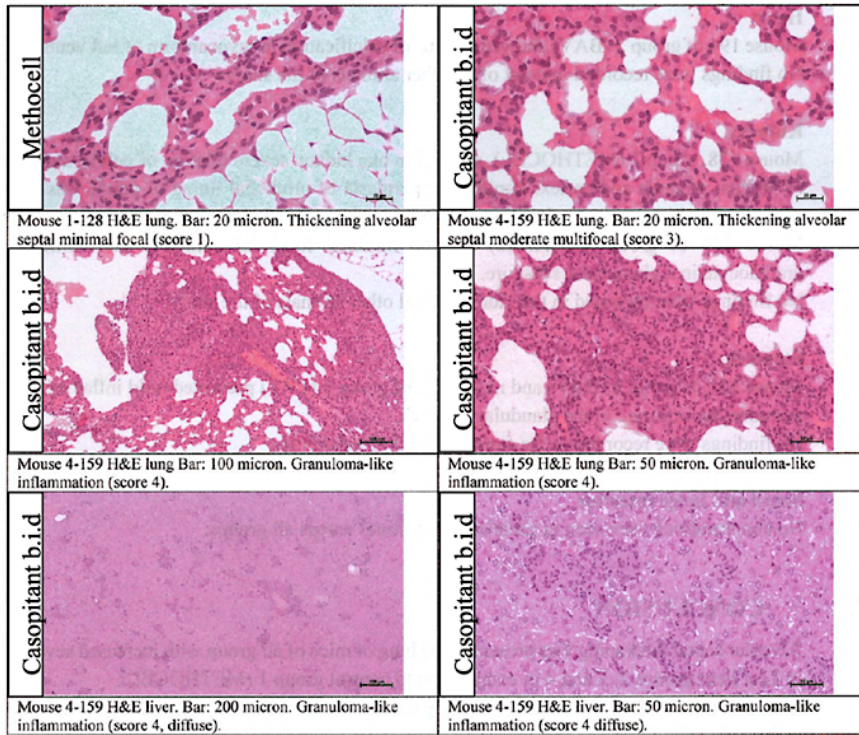


Figure 26. Immunohistochemical evaluation of EAE spinal cord tissue immune cell infiltrates. Spinal cord sections were obtained from five EAE, Methocell-treated, Bavisant, or Casopitant-treated mice at day 41 post immunisation (28 days of treatment) and analysed by H&E for immune infiltration. (A) Representative images of lumbar spinal cord sections with solid white arrows indicate infiltrating areas. (B) The mean number of inflammatory foci from entire spinal cord sections from five animals. No significant difference was identified in the number of immune cell foci between treatment groups. The scatter plot shows the mean value \pm SD; each dot represents an individual animal.

In conclusions, we could not observe clinical efficacy of Casopitant or Bavisant in the chronic EAE model, but we detected a subtle effect on pathology (lower demyelination and axonal loss). The regimen of the compounds administration e.g., treatment after 40 days post-immunisation, when EAE displays a more chronic phase and lower inflammation, or in combination with anti-inflammatory treatments (dexamethasone/teriflunomide) are under consideration for the future experiments.

To rule out a possible toxic effect of the compounds caused by systemic administration, we have performed histopathological evaluation of the vital organs. The histopathological staining and the data analysis were performed by an external collaborator Dr. Francesca Sanvito (Anatomical Pathology Unit, San Raffaele Scientific Institute, Milan, Italy). Bone marrow, colon, heart, kidneys, liver with gall bladder, lungs, mesenteric lymph nodes, spleen, stomach, small and large intestine were obtained from two EAE, Methocell-treated, Bavisant, or Casopitant-treated mice at day 41 post immunisation (28 days of treatment) and analysed by haematoxylin and eosin (H&E) staining. The slides (including controls) were randomized (shuffled), and relevant pathological features were scored without prior information on the treatment groups. Two trained pathologists independently reviewed the slides to reach a consensus on the findings and scores. As a result of the evaluation, diffuse marked granulomatous-like inflammation (characterized by the aggregates of macrophages, lymphocytes, monocytes, and occasionally granulocytes) was identified in the liver, spleen, mesenteric lymph nodes, bone marrow, and kidneys of Casopitant-treated (b.i.d.) mice. Alveolar septal thickening characterized by increased granulocytic cellularity, haemorrhages, and emphysema in lung parenchyma was present in the lungs of mice from all groups, potentially due to oral gavage procedure-related inflammation or terminal procedure (cervical dislocation). One animal treated with Bavisant showed a focus calcification in the myocardium of the left ventricle, while no findings were recorded in the hearts of other animals. No abnormalities were detected in the samples of intestines across all groups, except one Bavisant-treated animal and animal 152 from the Casopitant q.d. treatment group, which showed mild inflammatory granulocytic infiltrates in the stomach. The representative images (Figure 27A) and individual animal data (Figure 27B) are shown below.

A



B

R&D PATH 134. Pathology Individual Animal Data								
GROUP-ANIMAL ID	1-128	1-144	2-151	2-194	3-152	3-197	4-159	4-198
Number of Animal	2	2	2	2	2	2	2	2
Liver								
<i>Inflammation, granulomatous-like</i>							4 diffuse	
<i>Inflammatory cell infiltrate, mixed cell</i>	2	2	2	2	2	2		2
Spleen								
<i>Extramedullary hematopoiesis</i>	1	1	1	1	1	1	2	1
<i>Predominance, granulocytes</i>	1	1	1	1	1	1	1	1
<i>Inflammation, granulomatous-like</i>							2	
<i>Prominence germinal centre</i>							2	
Lungs								
<i>Inflammatory cell infiltrate, lymphohistiocyte, perivascular</i>	1	1		1				1
<i>Thickening/increased cellularity, alveolar septa</i>	1	1	2	2	1	2	3	2
<i>Inflammation, granulomatous-like</i>				2	1	3	4	2
<i>Emphysema</i>	1	1	2	1	1	2	2	1
<i>Hemorrhages</i>	1 focal		2 focal		1 focal	1 focal		1 focal
Kidneys		NAD	NAD	NAD	NAD	NAD		NAD
<i>Inflammatory cell infiltrate, granulocyte, glomerulus</i>							1 focal	
<i>Dilation, pelvic</i>	P monolateral							
<i>Atrophy, papilla, medulla and cortex</i>	4 monolateral							
<i>Hyperplasia papillary, urothelium, pelvis</i>	P monolateral							
<i>Inflammation, granulocyte, pelvis</i>	4							
Bone marrow femur								
<i>Increased cellularity, myelo-granulocytic</i>	4	2	3	3	3	2	4	3
Heart	NAD	NAD	NAD		NAD	NAD	NAD	NAD
<i>Mineralization</i>				P				
Mesenteric lymph nodes								
<i>Increased cellularity, lymphoplasmacellular, medulla</i>	2	2	2			1	3 granulocytes	
<i>Prominence germinal centre</i>	1	2	1	1	1		1	1
Stomach	NAD	NAD		NAD		NAD	NAD	NAD
<i>Inflammatory cell infiltrate, granulocyte, glandular stomach</i>			2		2			
Small and large intestine	NAD	NAD	NAD	NAD	NAD	NAD	NAD	NAD

Figure 27. Histopathological evaluation of EAE mice organs treated with Bavisant, Casopitant, or Methocell. (A) Representative H&E images of several organs of Methocell and Casopitant b.i.d.-treated mice with reported scores of pathological changes. (B) Summary table for an individual animal processed for histopathological analysis. NAD: no abnormality detected; P: present; Grade1: minimal; Grade2: mild; Grade 3: moderate; Grade 4: marked. Mouse IDs correspond to Methocell (128, 144), Bavisant (194, 151); Casopitant q.d. (152, 197) and Casopitant b.i.d. (159, 198).

Therefore, Casopitant administered twice daily by oral gavage induces a severe systemic toxicity. Alternative routes of administration e.g., mini-osmotic pump intracerebroventricular infusion (Hampton *et al*, 2020) will be considered for future experiments.

3.4 *In silico* and *in vitro* hit-compounds target validation

3.4.1 *In silico* target/pathway analysis identifies NK1R and SIGMAR1 as potential targets of Casopitant, and HRH3 as a potential target of Bavisant

To identify targets for Casopitant and Bavisant through which the hit compounds exert their neuroprotective/remyelinating properties, we performed an *in silico* bioinformatic analysis via the SPOKE tool. Neurokinin 1 receptor (NK1R) is the main known target for Casopitant (Navari, 2008) that was confirmed by SPOKE analysis. Interestingly, sigma non-opioid intracellular receptor 1 (S1R) was predicted as an additional target for Casopitant, as well as for other drugs used in MS clinical trials, e.g. lamotrigine (Kapoor *et al*, 2010), donepezil (Christodoulou *et al*, 2006), fluoxetine (Chataway *et al*, 2020), clemastine fumarate (Green *et al*, 2017) (Figure 28).

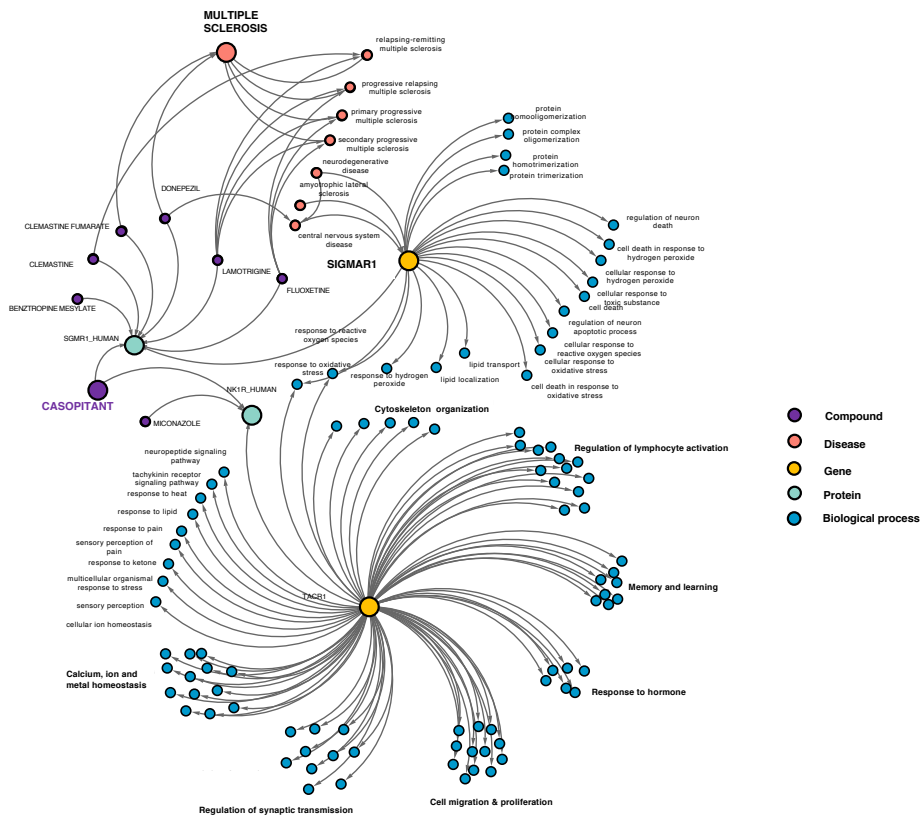


Figure 28. Casopitant pathway interaction and target prediction analysis via SPOKE.

The second hit compound Bavisant is a histamine H3 (HRH3) antagonist indicated for treating attention-deficit hyperactivity disorder (ADHD), alcoholism, and excessive daytime sleepiness. Pathway and drug target analysis with SPOKE showed a potential relationship between Bavisant and MS-related drugs Fingolimod (Ingwersen *et al*, 2012) and Mitoxantrone (Scott & Figgitt, 2004) as well as with MS-related pathways (S1PR signalling (McGinley & Cohen, 2021) and STAT3 (Jakkula *et al*, 2010)), thus making Bavisant a potential drug candidate for future MS clinical trials. Although HRH3 is not a novel target for MS treatment (Schwartzbach *et al*, 2017), further investigation of the MoA and *in vivo* validation of Bavisant in demyelinating animal models of multiple sclerosis (cuprizone/lysolecithin) may provide additional knowledge for HRH3 role in myelination and neuroprotection.

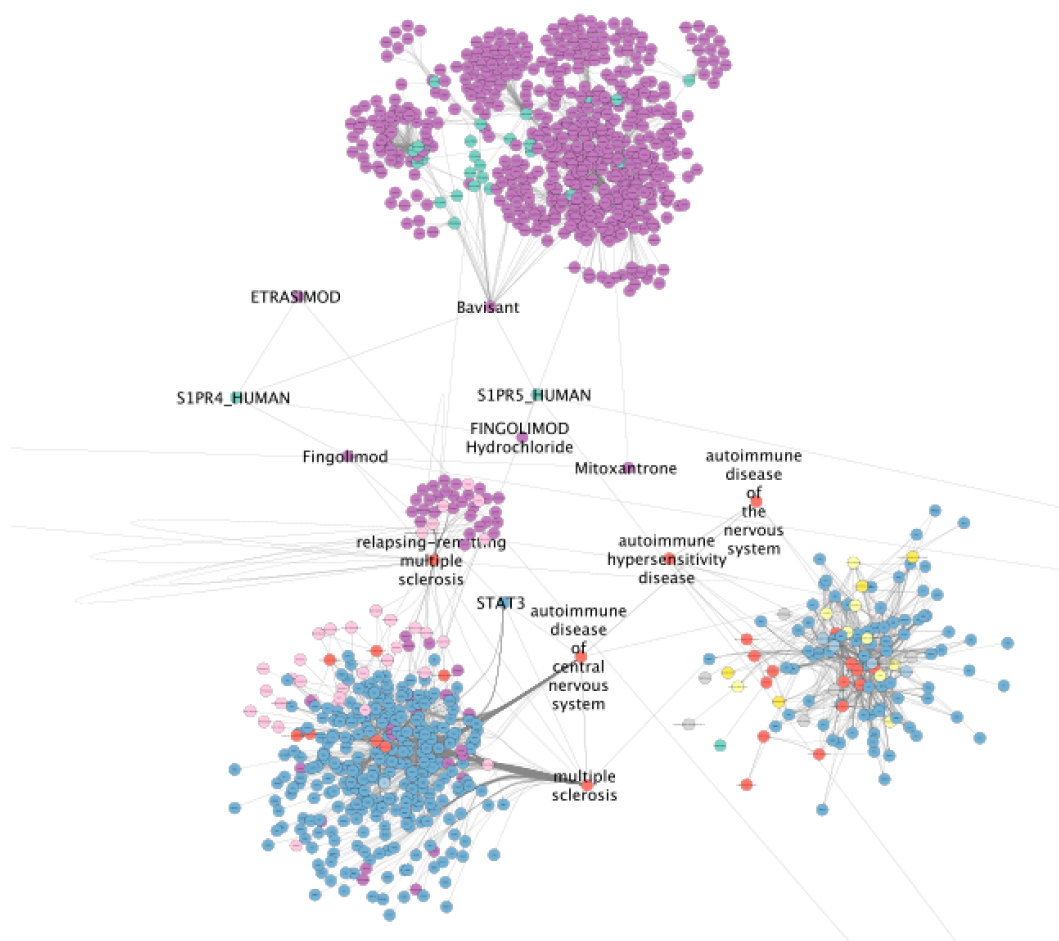


Figure 29. Bavisant pathway interaction and target prediction analysis via SPOKE. Purple=drugs, blue=genes, green=proteins, red=disease, yellow = biological processes.

Since target prediction analysis could not identify additional targets for Bavisant potentially novel for MS treatment, we focused our attention exclusively on Casopitant drug-target validation.

3.4.2 *In vitro* target validation

In vitro target validation was performed by evaluating target expression profiles at mRNA and protein levels in the cellular models of the screening (mouse cortical neurons and hiPSC-derived neurons). The target deconvolution was performed via *in vitro* modulation of target protein S1GMAR1 by small interfering RNA (siRNA) in the Neuro2A cell line.

3.4.2.1 TACR1 transcript is expressed in hiPSC-derived and mouse cortical neurons but not in N2A cells, while SIGMAR1 and HRH3 transcripts are expressed in all tested cell types.

Target transcripts levels were assessed by RT-PCR to determine the expression of predicted target genes for Casopitant *TACR1* and *SIGMAR1* and Bavisant target gene *HRH3*. *SIGMAR1* was identified to be expressed in hiPSC-derived NPCs, hiPSC-derived mature neurons, mouse cortical neurons, and Neu2A. Instead, *TACR1* was expressed at a low level in hiPSC-derived neurons (Figure 30A) and at a higher level in mouse cortical neurons (Figure 30C). Additionally, *TACR1* expression was not detected in Neu2A (Figure 30B). *HRH3* was expressed by human and mouse cortical neurons, as well as in N2A, but not in hiPSC-NPCs. In conclusion, we showed that cellular models used in stepwise screening express the Casopitant target genes *SIGMAR1* and *TACR1* and Bavisant target gene *HRH3*. N2A cell line instead is an appropriate cellular model to corroborate the role of *SIGMAR1* in mediating Casopitant neuroprotective function.

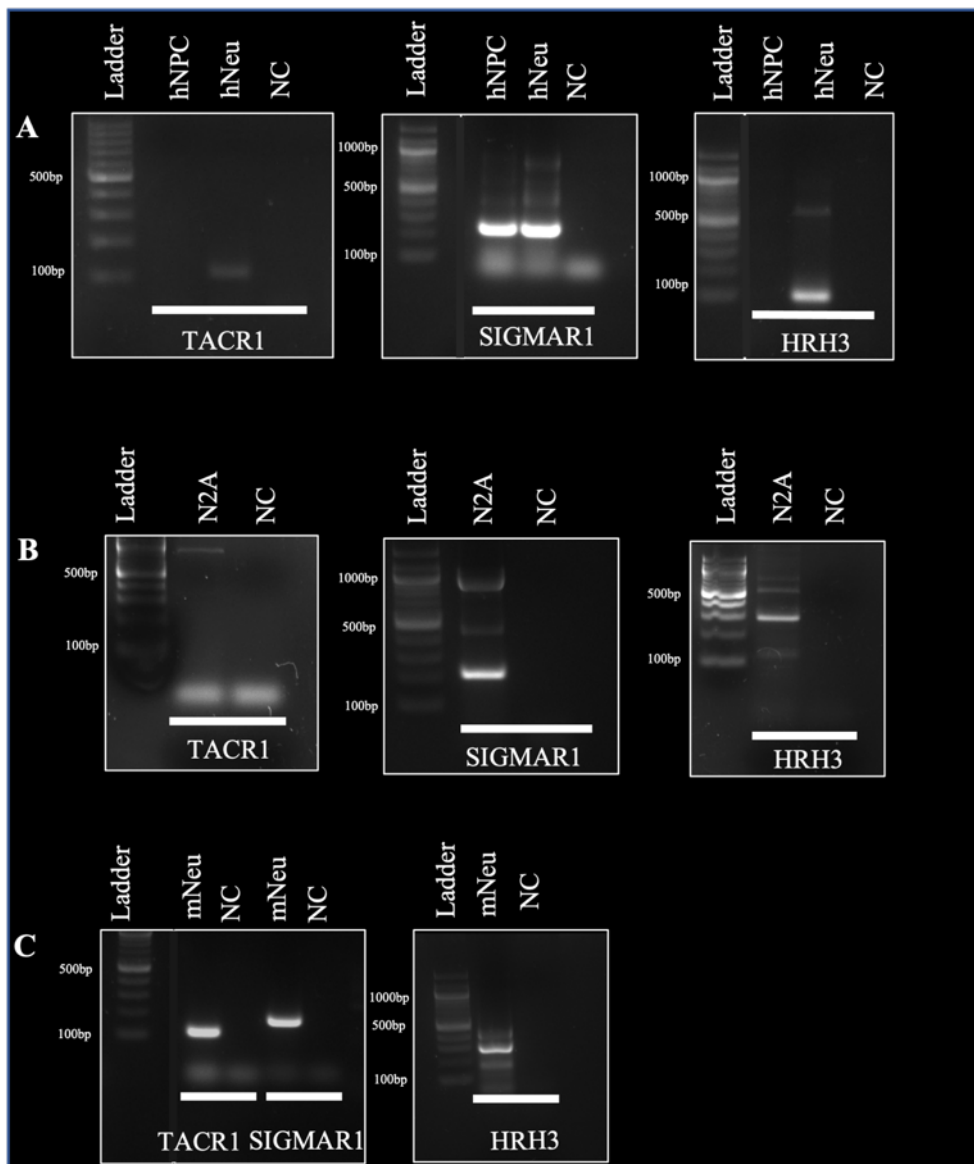


Figure 30. In vitro target validation: mRNA expression profile of the target genes. Agarose gel electrophoresis of RT-PCR-amplified *TACR1*, *SIGMAR1*, and *HRH3* cDNA validated target gene expression in (A) hiPSC-NPCs and hiPSC-neurons, (B) N2A cell line, and (C) primary mouse cortical neurons. Predicted size of amplified PCR products for human *TACR1* = 156bp; human *SIGMAR1* = 162bp; human *HRH3* = 127bp; mouse *TACR1* = 147bp; mouse *SIGMAR1* = 209bp; mouse *HRH3* = 285bp. 100bp DNA ladder was used in all gel electrophoresis experiments. A sample containing primers and reagents for PCR reaction but not cDNA was used as negative control (NC).

3.4.2.2 *TACR1* protein is expressed in hiPSC-derived and mouse cortical neurons but not in N2A cells, while *SIGMAR1* and *HRH3* proteins are expressed in all tested cell types.

The second step of target validation was to characterise target protein expression in three cellular models by immunofluorescence and confocal imaging.

Histamine H3 receptor was highly expressed in mature mouse cortical neurons and N2A and at a lower level in hiPSC-derived neurons, confirming RT-PCR results (Figure 31). Immunofluorescence staining was performed for SIGMAR1 and KDEL, an ER-resident protein, to validate the cellular localization of SIGMAR1. SIGMAR1 is mainly expressed in mitochondria-associated membrane sites (MAMs), an interface between ER and mitochondria (Hayashi & Su, 2007), while the KDEL receptor localizes in the ER and Golgi complex (Capitani & Sallese, 2009). Immunofluorescence confirmed the expression of SIGMAR1 in Neu2A cells and its colocalization with KDEL (Figure 32C). Immunostaining on mature mouse cortical neurons at 14DIV and hiPSC-derived neurons confirmed NK1R and SIGMAR1 expression (Figure 32, A-B). NK1R was mainly expressed in neuronal soma, while SIGMAR1 expression was also detected along the axons and dendrites, reflecting complex axonal ER distribution (Öztürk *et al*, 2020). NK1R was not detected in N2A cells, confirming RT-PCR data.

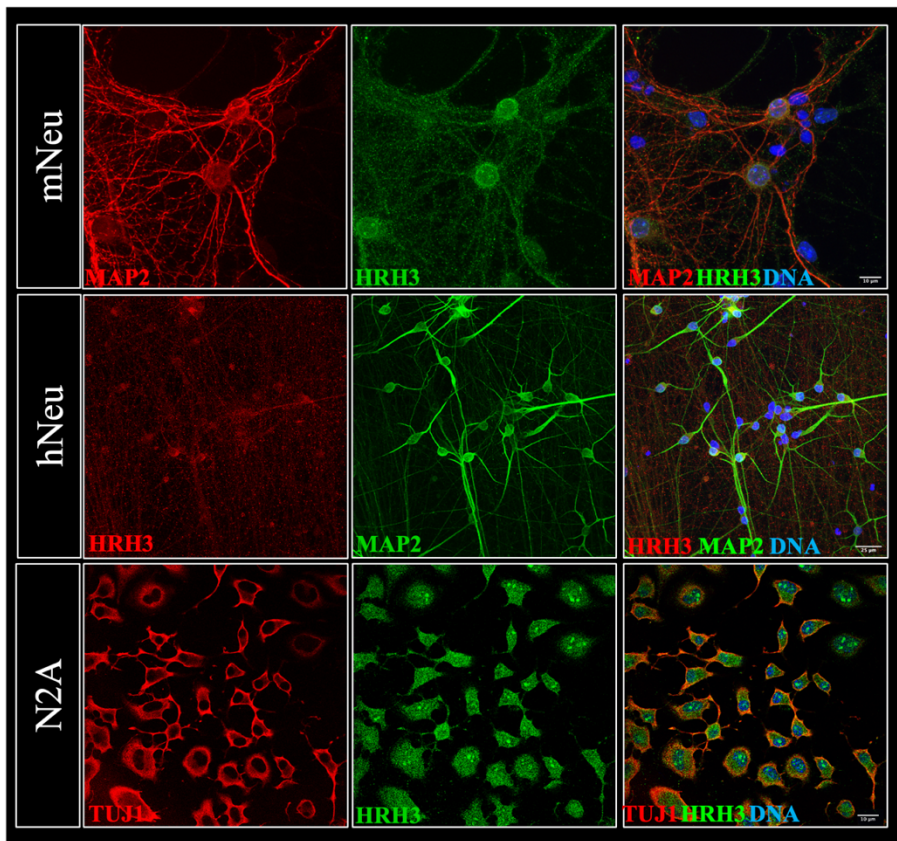


Figure 31. In vitro target validation: HRH3 protein expression profile. Representative expression of HRH3 by mouse cortical neurons (mNeu), hiPSC-derived neurons (hNeu), and N2A cell line evaluated by immunofluorescence and confocal imaging.

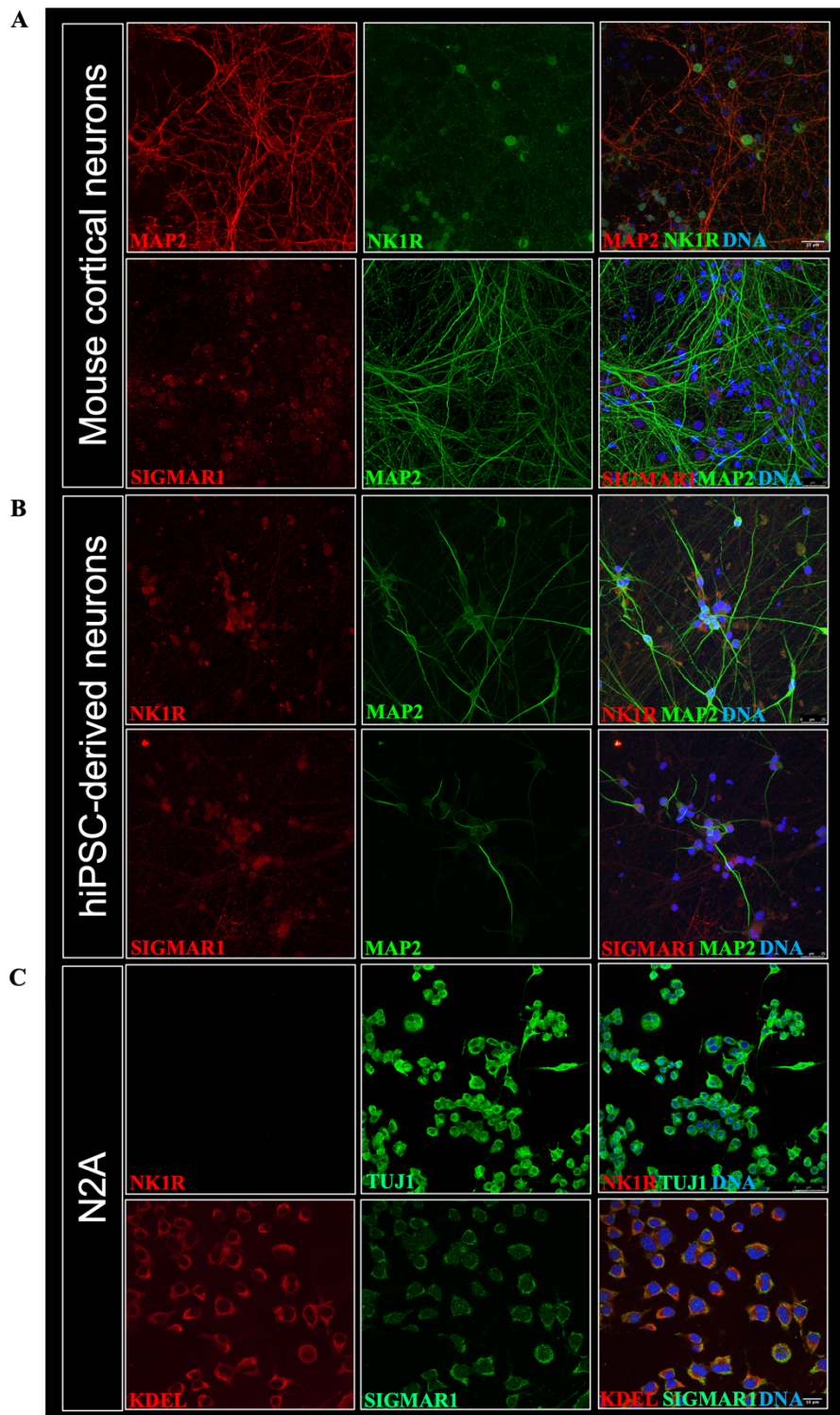
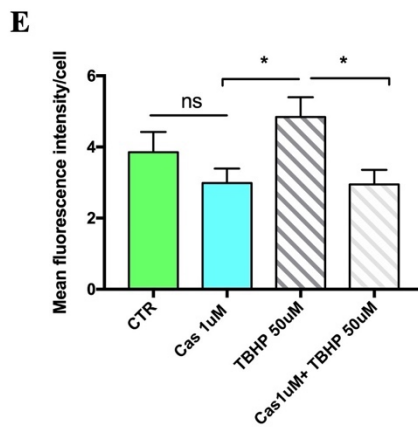
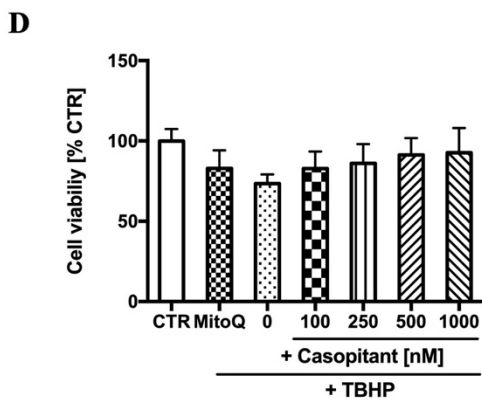
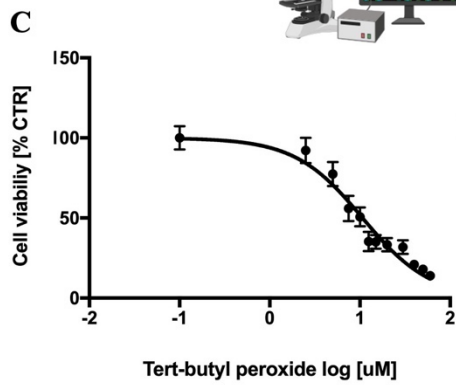
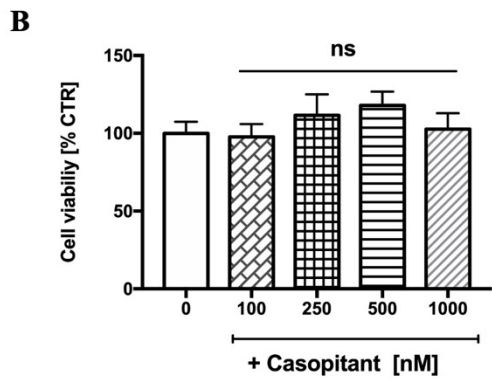
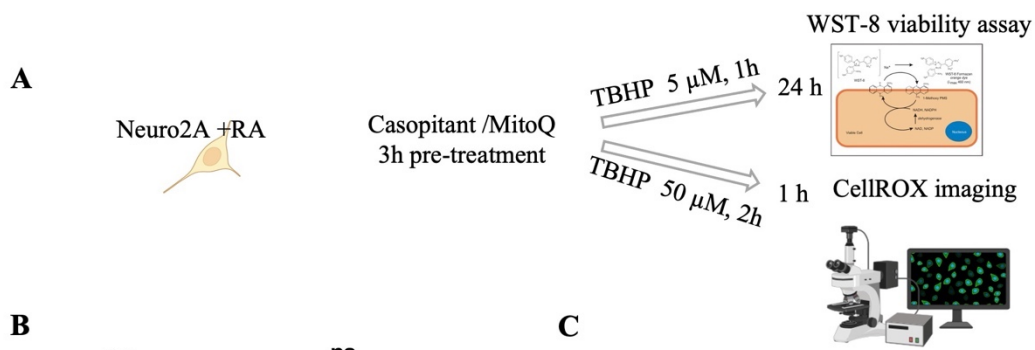


Figure 32. In vitro target validation: NK1R and SIGMAR1 protein expression profiles. Representative expression of NK1R and SIGMAR1 by mouse cortical neurons (A), hiPSC-derived neurons (B), and N2A cell line (C) evaluated by immunofluorescence and confocal imaging. SIGMAR1 co-localise with ER-resident peptide KDEL in N2A cell line (C).

3.4.3 Casopitant confirms its neuroprotective and antioxidant effect in N2A cells

A neuroprotective assay under oxidative stress conditions was set to evaluate the Casopitant neuroprotective and antioxidant effect in the N2A cell line. Neu2A cells were differentiated by reducing serum (0.1% FBS) and application of retinoic acid (Kumar & Katyal, 2018). Differentiated N2A were pre-treated with MitoQ or Casopitant for 3h and then exposed to acute oxidative stress (TBHP). Cell viability was evaluated 24h after stressor exposure by WST-8 assay, or functional oxidative stress CellROX assay was performed immediately after TBHP application by live-cell imaging (Figure 33A). Casopitant itself did not affect N2A cell viability (Figure 33B), while TBHP induced cell cytotoxicity in a dose-response manner (Figure 33C). We identified a half-maximal inhibitory concentration (IC50) dose of 10 μ M resulted in ~50% reduction of N2A cell viability upon acute TBHP application. As shown in Figure 33D, Casopitant induced a detectable rescue of N2A cell viability in a dose-response manner from TBHP-induced cytotoxicity. To confirm Casopitant antioxidant effect, a CellROX assay was performed to assess intracellular ROS levels by measuring CellROX dye fluorescence intensity via live-cell imaging. Casopitant showed the ability to decrease endogenous ROS levels, since CellROX intensity in Casopitant-treated cells was lower than in CTR (non-treated cells), and to protect N2A cells from TBHP-induced oxidative stress (Figure 33, E-F).



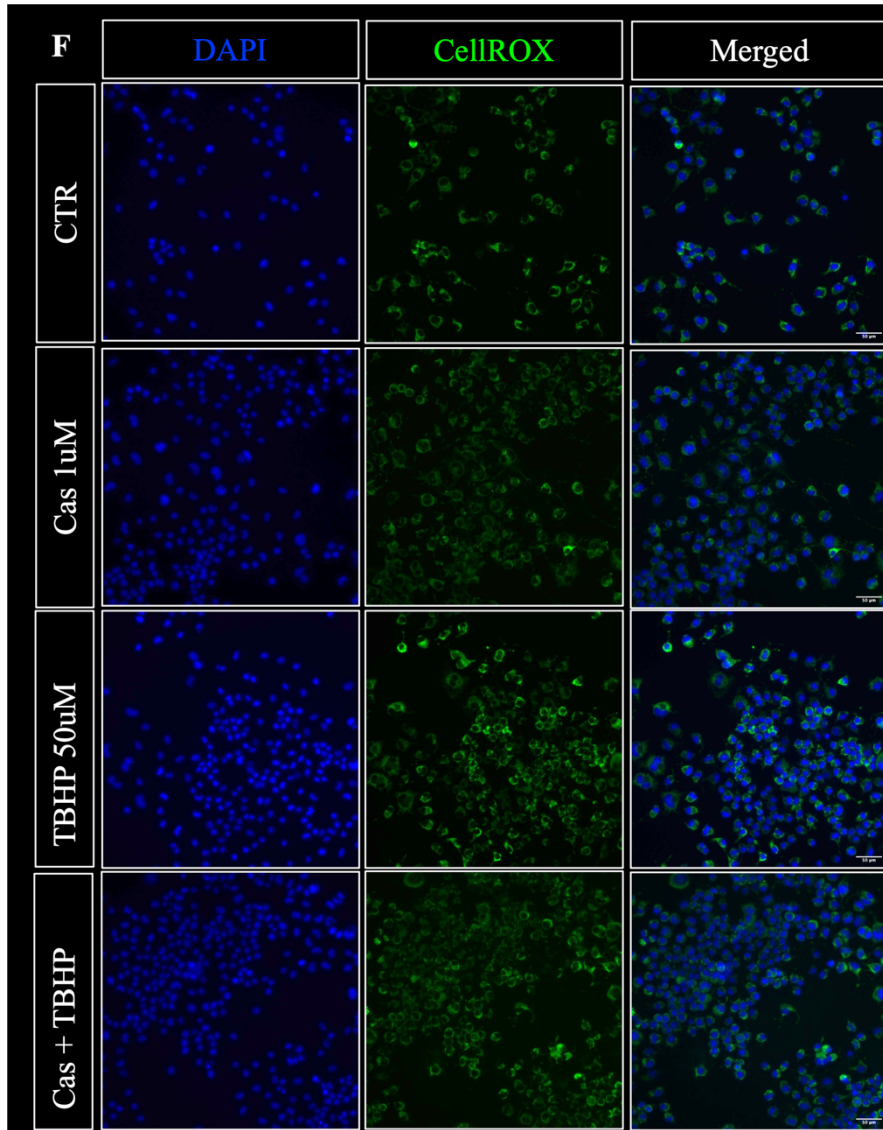


Figure 33. Neuroprotective assay setup on N2A cell line. (A) Schematic representation of the experimental setup. N2A were differentiated with retinoic acid (RA), pre-treated with Casopitant 1 μ M or MitoQ 5nM, and then challenged with TBHP 5 μ M for 1h for cell viability evaluation or with TBHP 50 μ M for 2h for live CellROX imaging. Cell viability was evaluated after 24h with WST-8 viability assay. (B) Various concentrations of Casopitant were tested on N2A to evaluate the potential cytotoxicity effect. The percentage of cytotoxicity is normalized to non-treated (CTR) cells. (C) Normalized dose-response curve demonstrating the dependence of cytotoxicity on TBHP concentrations. The percentage of cytotoxicity is plotted against the logarithmic micromolar concentration of TBHP. Data from each point were obtained in sextuplicate from 3 independent experiments. IC₅₀ is 10 μ M. (D) Dose-response assay demonstrates the neuroprotective effect of Casopitant from TBHP-induced cytotoxicity. Cell viability/metabolic activity is expressed in percentage relative to CTR cells. Each bar reports mean value \pm SEM obtained from three independent experiments run in sextuplicate. (E) Quantification of Casopitant effect on intracellular oxidative stress level measured with CellROX fluorescence dye (shown in F). Each bar reports mean fluorescence intensity \pm SD normalized to total cell count within an image. Ten images were obtained for each condition. Stat. test performed with one-way ANOVA, followed by Dunnett multiple comparison correction, * p <0.05. (F) Representative

images of intracellular ROS-labelled N2A cells in oxidative stress conditions (TBHP-treated), with or without Casopitant pre-treatment.

The protective and antioxidant properties of Casopitant in N2A cells was confirmed even in the absence of expression of its known target NK1 receptor. Therefore, we hypothesize that Casopitant activity might be modulated through the predicted target SIGMAR1 receptor.

3.4.4 SIGMAR1 small RNA interference modulation

To validate the Casopitant mechanism of action with a hypothesis that the compound mediates its antioxidant and neuroprotective function through SIGMAR1, we performed transient *SIGMAR1* gene silencing by siRNA in Neu2A cells, as described in Materials and Methods. We tested three siRNA targeted to *SIGMAR1* and one non-targeting control. *SIGMAR1* mRNA expression level was evaluated with SYBR Green RT-PCR at 72 hours post-transfection by normalization to expression level of histone 3 (H3) housekeeping gene and comparison to the expression level of basal (lipofectamine-treated) cells by the $2^{-\Delta\Delta CT}$ method. siRNA2 alone, or a combination of siRNA1 and siRNA2, resulted in the most efficient *SIGMAR1* downregulation by 62% (Figure 34A). Western blot analysis showed 50.5% SIGMAR1 downregulation at 72h post-transfection with 15pmol of siRNA2 (Figure 34, B-C).

N2A were transfected with siRNA2 for 72h to validate the effect of SIGMAR1 silencing on oxidative stress levels in N2A cells, and a dose-response TBHP-mediated toxicity assay was performed. The ROS levels were determined by CellROX fluorescence intensity measurement by live imaging in mock (lipofectamine only) and siRNA2-transfected cells. Fluorescence intensity analysis was performed by an in-house built CellProfiler image analysis pipeline. Although TBHP induced a significant increase in ROS levels in a dose-response manner (Figure 34D), we could not observe a difference in ROS induction between mock-treated and SIGMAR1-silenced cells. The neuroprotective assay settings from the previous chapter were repeated to evaluate ROS levels in mock (lipofectamine only) and siRNA2-transfected cells at 72h post-silencing. We again could observe a significant antioxidant effect of Casopitant protecting mock-treated cells (Figure 34E), but not siRNA-silenced cells from TBHP-induced oxidative stress. The fluorescence intensity levels were slightly higher in all siRNA2-silenced

conditions (e.g., 12.65 vs 9.4 in non-treated cells; 5.6 vs 4.5 in Casopitant-treated cells; 22.5 vs 20.75 in TBHP-treated cells; 15 vs 12.9 in Casopitant/TBHP-treated cells), although the difference was not significant. This could be potentially explained by insufficient downregulation of SIGMAR1 protein levels since it has been previously demonstrated that oxidative stress levels are significantly increased in SIGMAR1-silenced 661W photoreceptor cells (Wang *et al*, 2019).

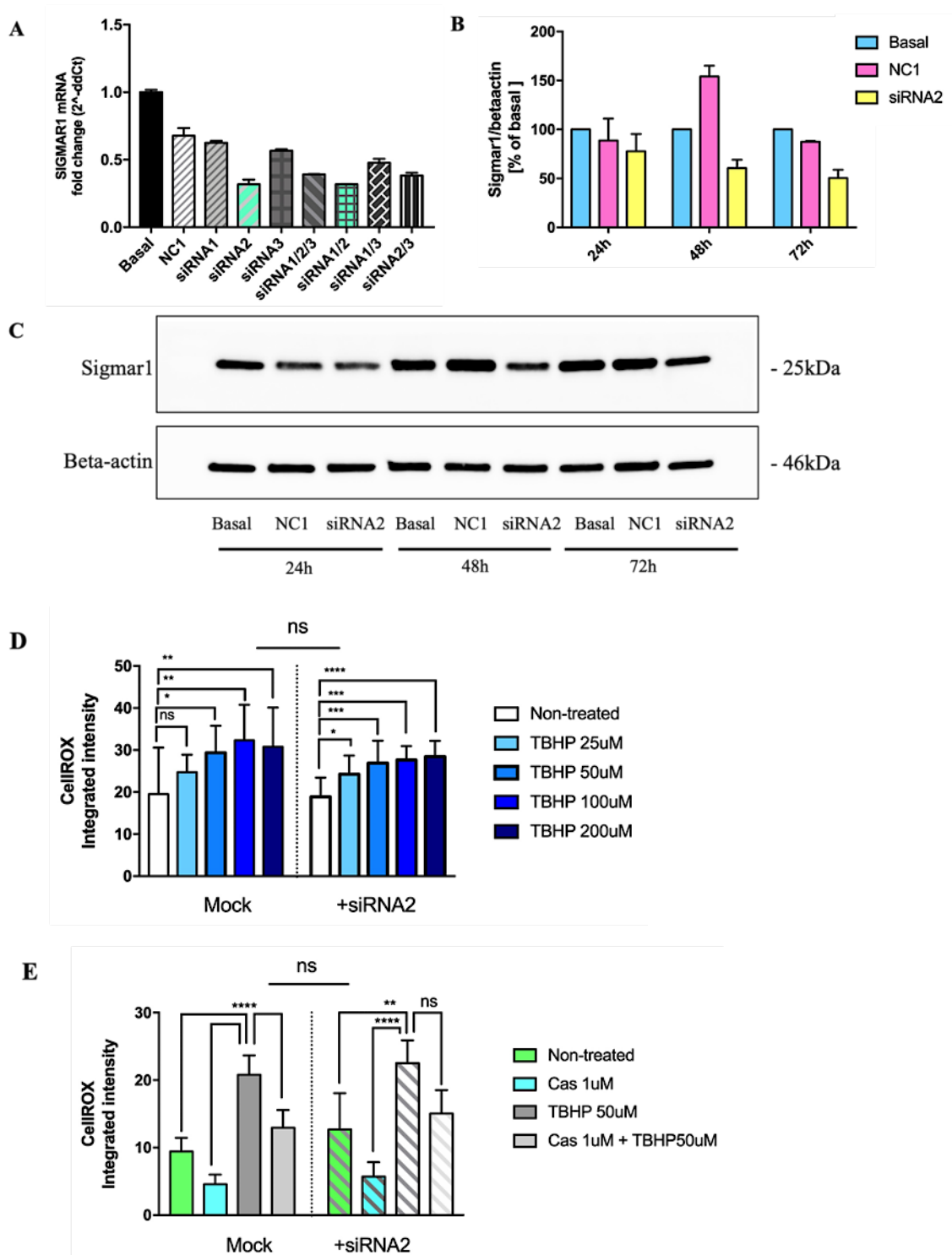


Figure 34. SIGMAR1 siRNA modulation. (A) RT-qPCR detection of Sigmar1 knockdown 72 hours post-transfection. Sigmar1 mRNA level was downregulated by 62% at 72h post-transfection. Each bar reports mean \pm SD value from two replicate wells. (B) Immunoblot shows the Sigmar1 protein levels normalized to beta-actin in cells collected 24-48-72 hours post-transfection with NCI/siRNA2 or in non-transfected cells (basal). (C). Quantification of the immunoblot from panel B was performed by densitometry image analysis. Sigmar1 protein levels were normalized to beta-actin and compared to the SIGMAR1 basal level (mock-treated) of each time point. Each bar reports mean \pm SD value from two independent blots. Sigmar1 protein level was downregulated to 50.5% at 72h post-transfection. (D) ROS levels of TBHP dose-response in mock and siRNA2-silenced N2A cells were determined by CellROX fluorescence intensity measurement and quantified by CellProfiler image analysis. Each bar represents mean value \pm SD from 10 images obtained from two replicate wells. Stat. test for siRNA2 condition was performed with one-way ANOVA, followed by Dunnett multiple comparison correction. Mock condition (non-normally distributed data, Shapiro-Wilk normality test) was analysed by non-parametric Kruskal-Wallis test with Dunn's multiple comparison correction. Pairwise comparisons between all mock and all siRNA conditions were performed with the Mann-Whitney test. * $p < 0.05$; ** $p < 0.01$; *** $p < 0.001$; **** $p < 0.0001$. (E) Neuroprotective assay performed on mock and SIGMAR1 siRNA2-silenced N2A cells. Oxidative stress was measured by CellROX fluorescence intensity measurement by CellProfiler image analysis. Each bar represents mean value \pm SD from 10 images obtained from two replicate wells. Stat. test for the mock condition was performed with one-way ANOVA, followed by Dunnett multiple comparison correction, and for siRNA2 condition with non-parametric Kruskal-Wallis test with Dunn's multiple comparison correction (non-normally distributed data, Shapiro-Wilk normality test). Pairwise comparisons between all mock and siRNA conditions were performed with the Mann-Whitney test. * $p < 0.05$; ** $p < 0.01$; *** $p < 0.001$; **** $p < 0.0001$.

The SIGMAR1 protein levels in N2A cells were assessed after 24h treatment with 1 μ M Casopitant or known high-affinity selective SIGMAR1 agonist PRE-084 at 1 μ M to evaluate whether Casopitant regulates SIGMAR1 expression. PRE-084 increased the SIGMAR1 protein levels in a dose-response manner compared to non-treated or DMSO-treated wells, while no increase in SIGMAR1 levels was observed after Casopitant treatment (Figure 35).

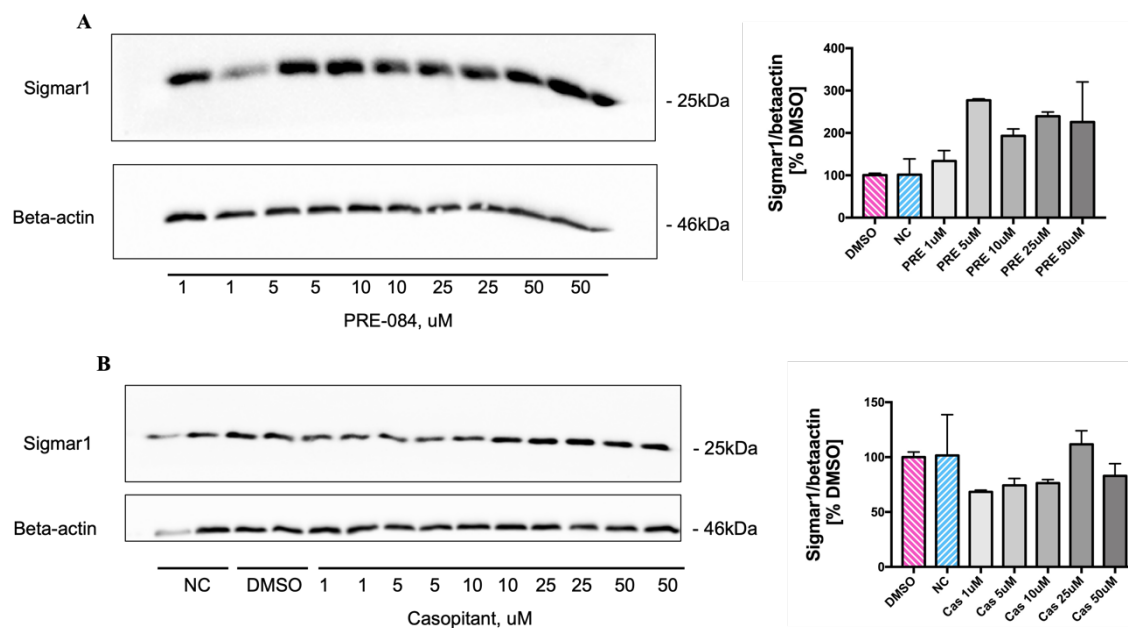


Figure 35. Effect of Casopitant and PRE-084 on SIGMAR1 protein levels. Representative immunoblots for Sigmar1 protein in N2A cells lysates collected 24h post-treatment with PRE-084 (A) or Casopitant (B). Beta-actin was used as a loading control. Quantification of the immunoblots was performed by densitometry image analysis. Sigmar1 protein levels were normalized to beta-actin and compared to the SIGMAR1 endogenous level (non-treated cells). Each bar represents mean value \pm SD from densitometric analysis of two replicate wells.

In conclusion, additional experiments such as cellular thermal shift assay (CETSA) (Jafari et al, 2014) are necessary to understand the potential interaction of Casopitant with SIGMAR1 receptor. More efficient SIGMAR1 siRNA modulation or CRISPR-Cas9-driven SIGMAR1 knockout (Yang *et al*, 2019) are required for better characterization of Casopitant mechanism of action.

3.5 MS-specific neuronal cell characterization

3.5.1 Characterization of hiPSC-derived glutamatergic neurons from three twin pairs discordant for MS

Our laboratory (Martino lab) has previously reprogrammed fibroblasts from three twin pairs discordant for MS (healthy, HC and relapsing-remitting, RRMS) into pluripotent stem cells with Sendai virus (Fusaki *et al*, 2009). Two of these twin pairs are monozygotic (Table 5). In addition, in the past two years we have completed the reprogramming of iPSC lines from three additional twin pairs with the help of Dr. Francesca Ruffini and Dr. Barbara Clissi (OSR, Milan, Italy).

hiPSC-derived cells have been shown to recapitulate features of several other neurodegenerative diseases (Nagel *et al*; Mehta *et al*, 2018) being useful for *in vitro*

disease modeling. While only a few recent publications demonstrated pathological features of MS in the hiPSC-derived astrocytes (Ponath *et al*, 2018; Perriot *et al*, 2018), no phenotypic differences were identified in the hiPSC-derived oligodendrocytes (Mozafari *et al*, 2020). Nevertheless, no documented evidence is yet available for MS-specific hiPSC-derived neuronal cells. The recent findings by Schirmer *et al*, 2019 report a selective vulnerability of upper layer excitatory cortical neurons, and upregulation of stress pathway genes in MS cortical tissue identified by single-nucleus RNA-sequencing (snRNA-seq), emphasizing the molecular changes associated with MS pathogenesis. Based on these data, we aimed to characterize the molecular signature and functional phenotype of hiPSC-derived neurons from twin pairs discordant for disease, to understand the potential impact of genetic and epigenetic changes on neuronal susceptibility to damage in MS.

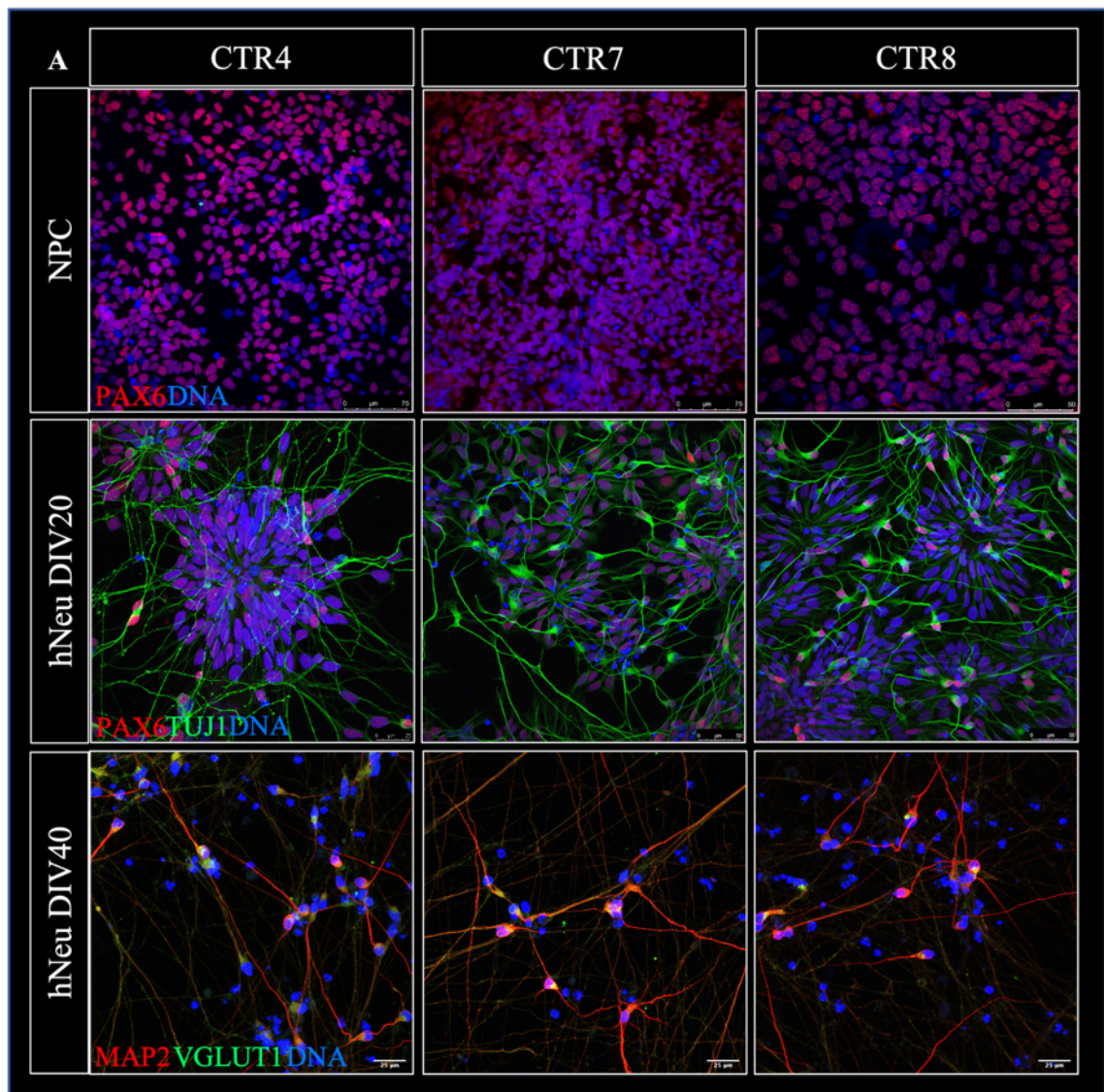
ID	Disease	Disease duration	Gender	Age at biopsy	Treatment prior to biopsy	Relapse prior to biopsy	Genetic definition
CTR4	CTR	NA	F	32	NA	NA	Monozygotic
CTR7	CTR	NA	F	37	NA	NA	Dizygotic
CTR8	CTR	NA	F	35	NA	NA	Monozygotic
RR16	RRMS	11y	F	32	Rebif 44	30 days	Monozygotic
RR24	RRMS	16mo	M	37	Rebif 22	16 months	Dizygotic
RR25	RRMS	15mo	F	35	Rebif 44	6 months	Monozygotic

Table 5. Clinical and anagraphic information of twin pairs donors.

3.5.1.1 Immunofluorescence characterization

I have setup and performed the differentiation of all six iPSC lines to NPCs and subsequently to neuronal lineage by protocol adapted from (Qi *et al*, 2017). The first step of neuronal culture characterization was performed by immunostaining for neural progenitor marker (PAX6) at NPC stage, pan-neuronal markers (TUJ1, MAP2), glutamatergic synaptic marker (VGLUT1) at earlier (DIV20) and more mature (DIV40) stages of neuronal differentiation. No differences were observed in PAX6 expression nor

in cell morphology since NPCs from all twin pairs formed rosette-like structures characteristic of the early neuroectoderm differentiation (Townshend *et al*, 2020).



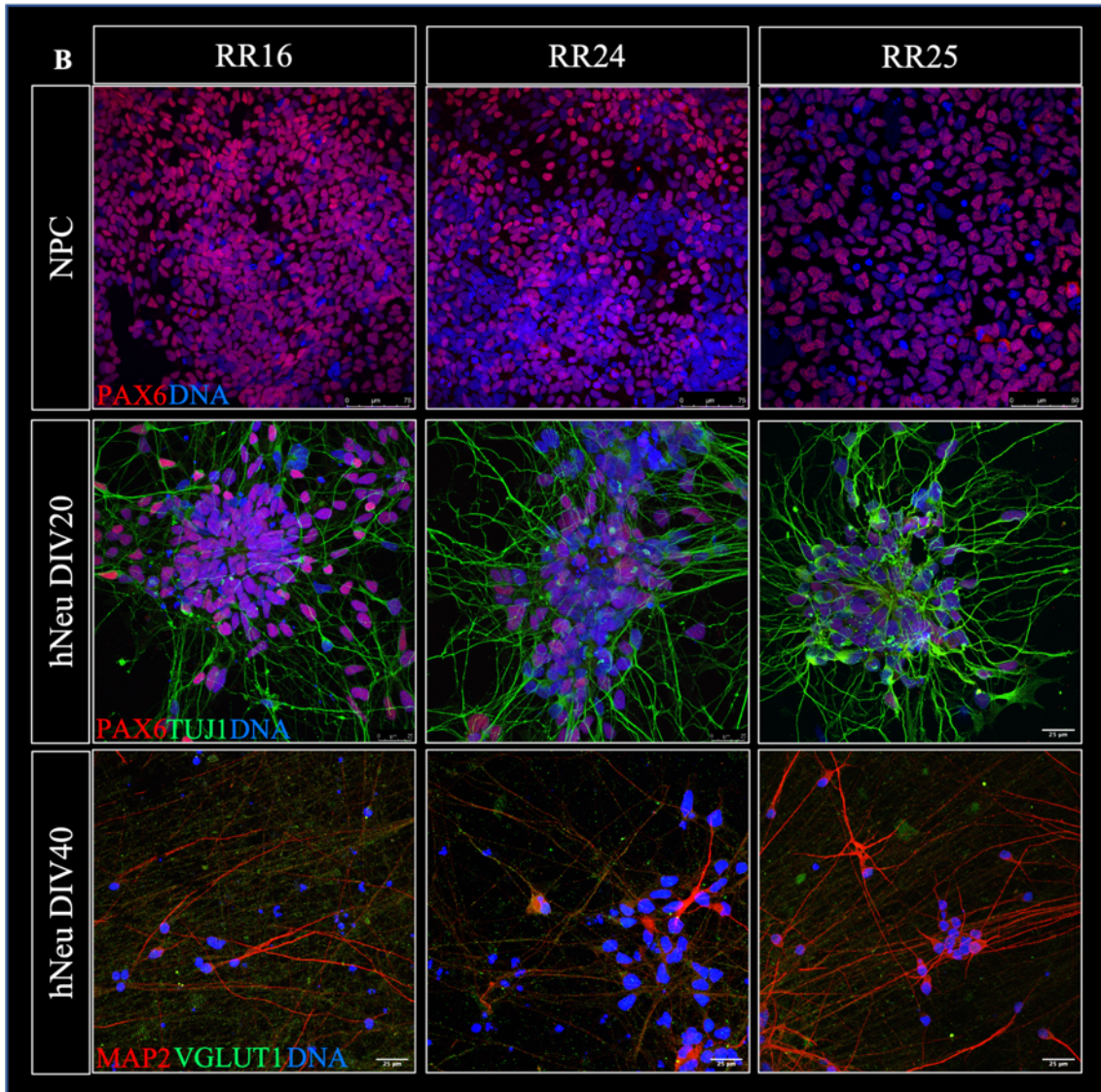


Figure 36. hiPSC-derived glutamatergic neurons from three twin pairs clinically discordant for MS: immunofluorescence characterisation. Representative images of neural precursor cells (NPCs), young neurons at 20DIV, and mature neurons at 40DIV from healthy controls (A) and their respective MS-affected twins (B) characterized by immunofluorescence and confocal imaging. Immunostaining was performed for neural precursor marker PAX6 and neuronal markers TUJ1, MAP2, and VGLUT1.

Higher VGLUT1 protein expression was observed in mature neurons (DIV40) from RRMS patients (Figure 36B). Interestingly, a genome-wide association study (GWAS) analysis identified genetic polymorphisms relevant to glutamate biology in individuals diagnosed with MS. These patients had elevated glutamate brain levels and a higher rate of brain tissue loss (Baranzini *et al*, 2010b). The overexpression of VGLUTs in drosophila resulted in increased release of glutamate, causing progressive neurodegeneration (Daniels *et al*, 2011a), corroborating the evidence that expression of

VGLUT1 can affect quantal size that is directly linked to the amount of glutamate released per single vesicle (Wilson *et al*, 2005).

3.5.1.2 RT-qPCR identifies highly expressed VGLUT1 in hiPSC-derived neurons from MS patients

TaqMan RT-qPCR analysis was performed to characterize neuronal cultures at the NPC stage, early neuronal (DIV20), and mature stage (DIV40) of differentiation. The mRNA expression levels were normalized to the housekeeping gene GAPDH and compared to the expression level at the NPC stage ($2^{-\Delta\Delta CT}$ method).

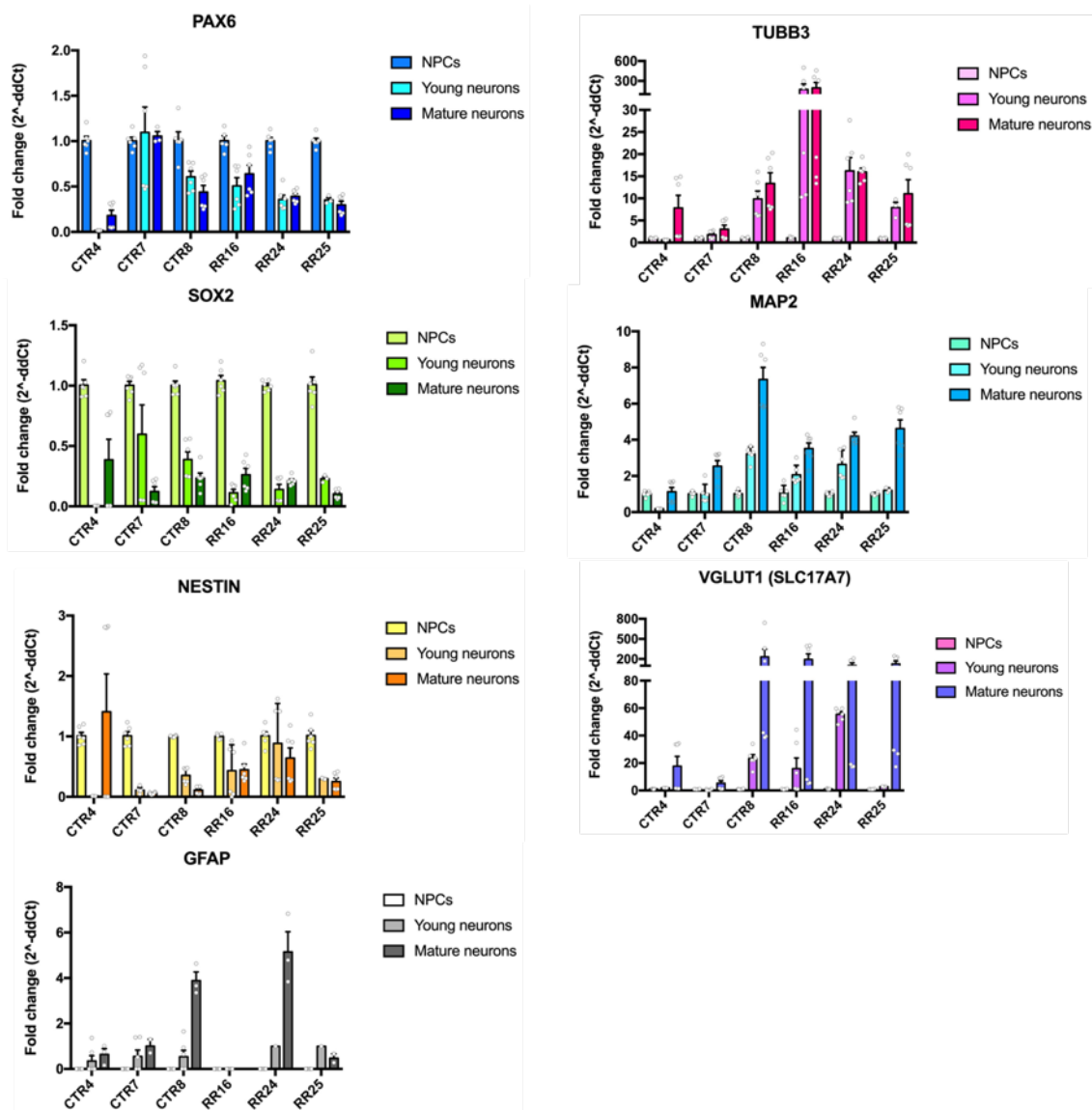


Figure 37. hiPSC-derived glutamatergic neurons from three twin pairs clinically discordant for MS: RT-qPCR characterisation. Neural precursor cells (NPCs), young neurons at 20DIV, and mature neurons at 40DIV from three twin pairs discordant for the disease were characterized by RT-qPCR. mRNA expression levels for neural precursor *PAX6*, *SOX2*, *NESTIN*, neuronal *TUBB3*, *MAP2*, *VGLUT1*, and astrocytic *GFAP* markers for each line were normalized to the *GAPDH* and compared to the expression level at NPC stage ($2^{-\Delta\Delta CT}$ method). Mean values are reported with a standard error of the mean (SEM). Two independent experiments were performed, while RT-PCR readout for each gene was done in triplicate.

We observed variability between differentiation attempts reflected in the distribution of single dots in bar graphs of Figure 37 (two independent neuronal differentiations were performed, while each RT-qPCR readout for a single gene was done in triplicate). As expected, we identified a decrease in expression of NPC markers *PAX6*, *SOX2*, and *NESTIN* throughout differentiation, except for CTR7 that had stably expressed *PAX6*. *TUBB3* and *MAP2* expression levels increased in young and mature neurons compared to NPC, whereas astrocyte marker *GFAP* was notably expressed in CTR8 and RR24 lines, as expected only at the late differentiation stage (DIV40). A striking difference was observed in *VGLUT1* (*SLC17A7*) expression 10-fold higher in all RRMS and CTR8 lines. We cannot exclude that these differences might be influenced by line-to-line variation in neuronal differentiation speed, resulting in relative neuronal immaturity of CTR4 and CTR7 lines compared to twin RRMS counterparts at the same differentiation stage. Nevertheless, high *VGLUT1* mRNA transcript levels correlated with high *VGLUT1* protein expression in three RRMS lines, shown in Figure 36, although this relationship is not necessarily direct (Liu *et al*, 2016).

3.5.1.3 hiPSC-derived glutamatergic neurons from twin pairs comparably release glutamate during differentiation

To further corroborate the findings, we measured the extracellular glutamate release at DIV30, 40 and 50 of neuronal differentiation from two twin pairs CTR4-RR16 and CTR7-RR24, respectively, in which we have identified distinct *VGLUT1* mRNA and protein expression levels. Extracellular glutamate levels were measured by luminescence-based Glutamate-Glo assay (Promega) in basal conditions and after depolarization with high potassium solution (KCl 60mM). High potassium solution depolarizes neurons, increasing their firing rate and increasing vesicular release of glutamate. The glutamate release caused by high potassium depolarization is Ca^{2+} dependent and biphasic process,

with about 20% of glutamate exocytosed within 2s and the remaining 80% released within approximately 70 seconds (Hackett & Ueda, 2015; Nicholls & Attwell, 1990). The Glutamate-Glo assay combines the process of glutamate oxidation by glutamate dehydrogenase catalysis leading to reduction of NAD⁺ to NADH. In the presence of NADH, reductase converts pro-luciferin reductase substrate to luciferin which Ultra-Glo rLuciferase and ATP use to produce light proportional to the glutamate levels (Figure 38A).

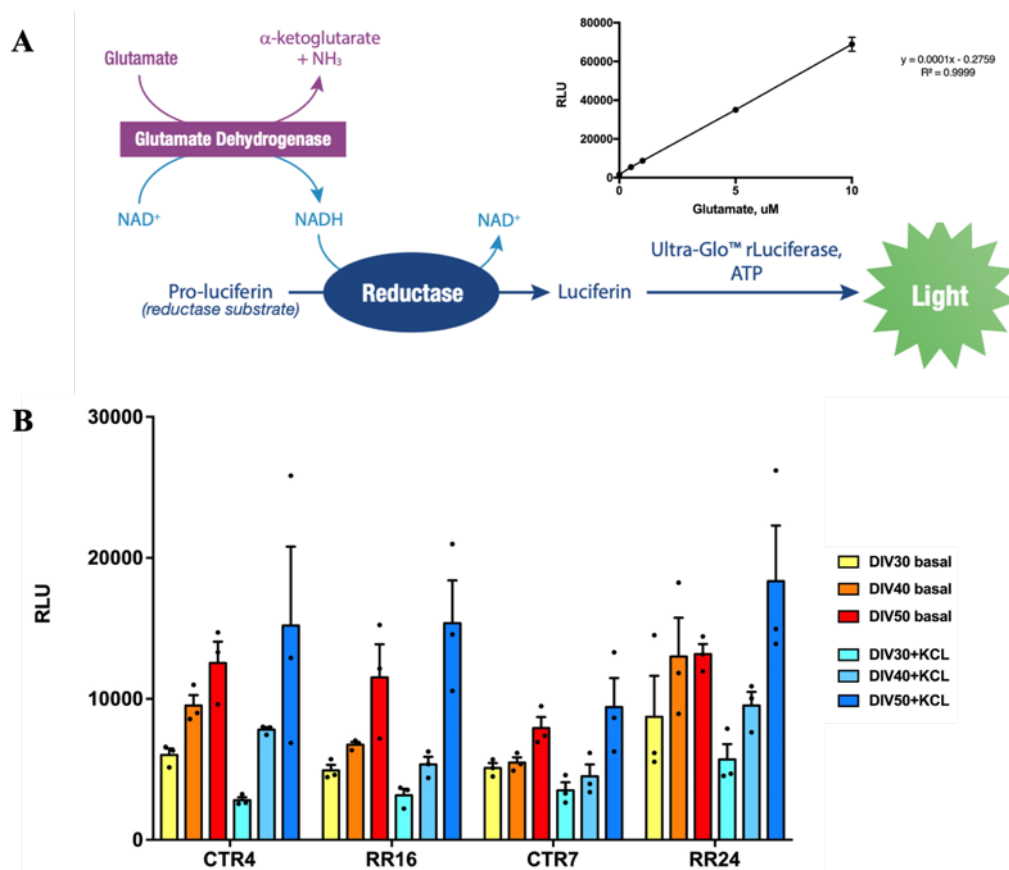


Figure 38. hiPSC-derived glutamatergic neurons from two twin pairs comparably release glutamate during differentiation. (A) A schematic diagram of the Glutamate-Glo assay principle and glutamate titration curve performed before each glutamate measurement readout. Twofold serial dilutions of glutamate were prepared in PBS, starting from 10 μ M. Data represent the average of three replicates from readings using a Berthold Tech Mithras luminometer. (B) Glutamate extracellular levels measured with Glutamate-Glo assay kit (Promega) at basal level and after 60mM KCl challenge in neurons from two twin pairs discordant for MS at 30DIV, 40DIV, and 50DIV. The y-axis is expressed in a relative light unit (RLU).

We identified the ability of hiPSC-derived neurons to release glutamate in extracellular space during differentiation, implying on neuronal cultures maturation process; however, no significant differences were observed in glutamate levels at baseline and after KCL

stimulation between CTR lines and their respective twins. Extracellular glutamate levels were higher although not significant at DIV50 of differentiation in the RR24 line compared to CTR7, at baseline and after KCL-evoked depolarization (Figure 38B).

To confirm the data, additional experiments on glutamate release will be performed by the intensity-based glutamate-sensing fluorescent reporter iGluSnFR (Marvin *et al*, 2013) and live imaging.

3.5.1.4 Patch-clamp electrophysiology identifies decreased potassium and sodium currents in hiPSC- derived neurons from MS patients

Whole-cell patch-clamp recordings were used to access the electrophysiological properties of hiPSC-derived neurons from three twin pairs. The recordings were performed by an experienced electrophysiologist (Dr. Stefano Taverna, OSR, Milan, Italy), while I have differentiated the neuronal cultures. To enhance neuronal maturation, neurons differentiated for 30 days were co-cultured with primary murine cortical astrocytes for additional 30 days (total 60-65 days of differentiation), since cultures contained low level of endogenous astrocytes. It is known that astrocytes play an essential role in neuronal maturation, improving firing activity, increasing synaptic activity, neurotransmitter release, and the expression of Na⁺ and K⁺ channels (Tang *et al*, 2013). Rodent astrocytes are readily available and relatively easy to culture compared to hiPSC-derived astrocytes that require at least 60-70DIV for full maturation. Undoubtedly, a complete human co-culture system is considered superior in neuronal electrophysiological properties and maturation. Besides, it will provide the opportunity to study human astrocyte-to-neuron interactions and patient-specific disease pathological features (Hedegaard *et al*, 2020a).

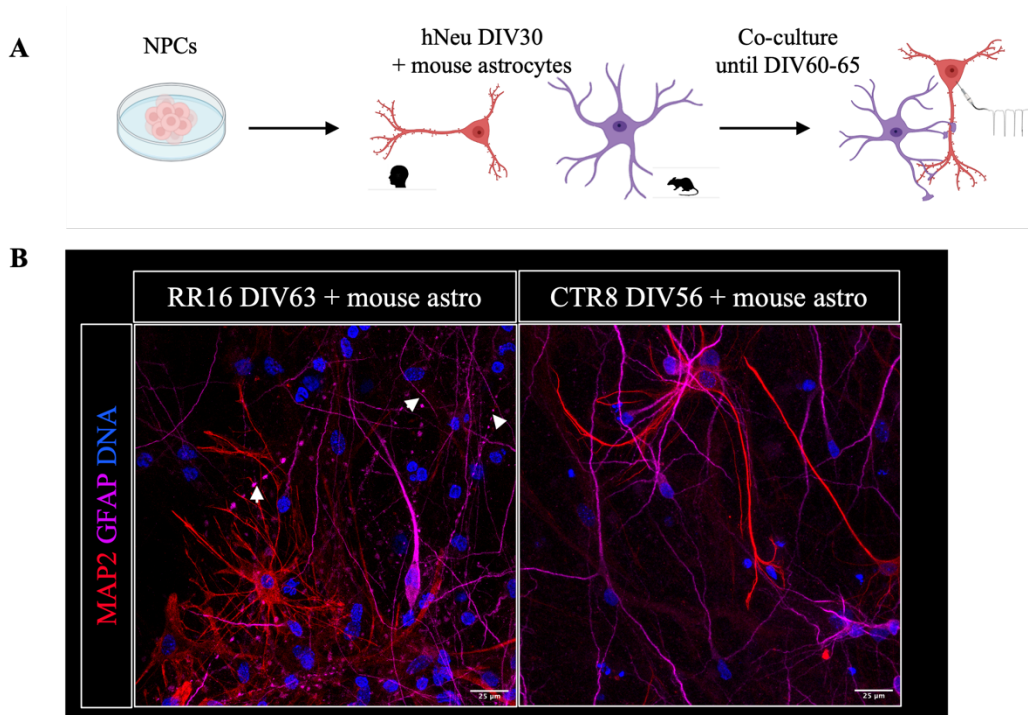
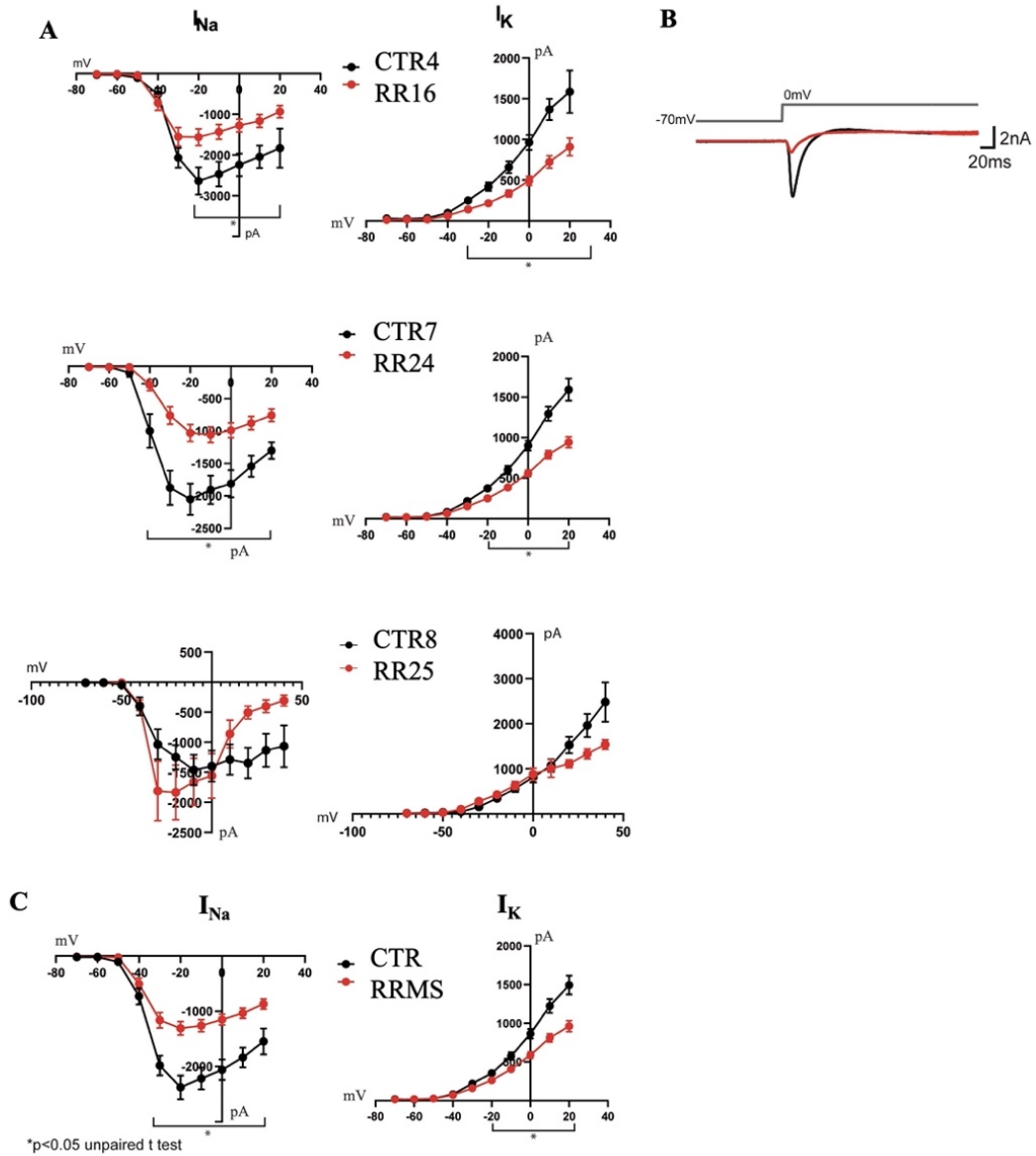


Figure 39. Scheme of patch-clamp electrophysiology in hiPSC-derived neurons. (A) Schematic representation of whole-cell patch-clamp experimental setup on hiPSC-derived neurons (hNeu) differentiated for 30 days and co-cultured with primary murine astrocytes for additional 30-35 days. (B) Representative immunofluorescence images of mature neurons (MAP2+) co-cultured with primary murine astrocytes (GFAP) at DIV63 from RR16 line and DIV56 for CTR8 line. White arrows indicate neuronal degeneration in the RR16 line.

Neurons from three twin pairs were differentiated for 30 days and co-cultured with primary murine astrocytes for additional 30 days. Whole-cell patch-clamp recordings were performed on the same day or the following day for each twin pair. Three independent differentiations were carried out for CTR4-RR16 and CTR7-RR24 lines, and only one differentiation was performed for CTR8-RR25 twin pair (in the long-term maintenance of the neurons from this twin pair). We identified a significant decrease in voltage-gated sodium (I_{Na}) and potassium (I_k) currents in neurons from RRMS patients RR16 and RR24, respectively, while only a trend was observed in the RR25 line, potentially due to a low number of patched cells (Figure 40A). The significant decrease was also robust when we pooled the data from all recordings ($n=57$ cells for CTR lines, $n = 58$ cells for RRMS lines) (Figure 40C). In addition, mature firing rates—characterized by the ability to fire repetitive action potentials in response to injection of suprathreshold current steps—were comparable between CTR4 and RR16 and dramatically decreased in the RR24 line compared to its respective twin CTR7 (Figure 40D, left panel). Overall,

the mature firing rate was decreased in RRMS-specific neurons versus their healthy cotwins (Figure 40D, right panel). Finally, spontaneous synaptic activity (mixed excitatory and inhibitory postsynaptic currents) was significantly decreased in neurons from RR16 and RR24 lines compared to their healthy twins, while CTR8 and RR25 were comparable. Summaries of all recordings and individual traces are shown in Figure 40F.



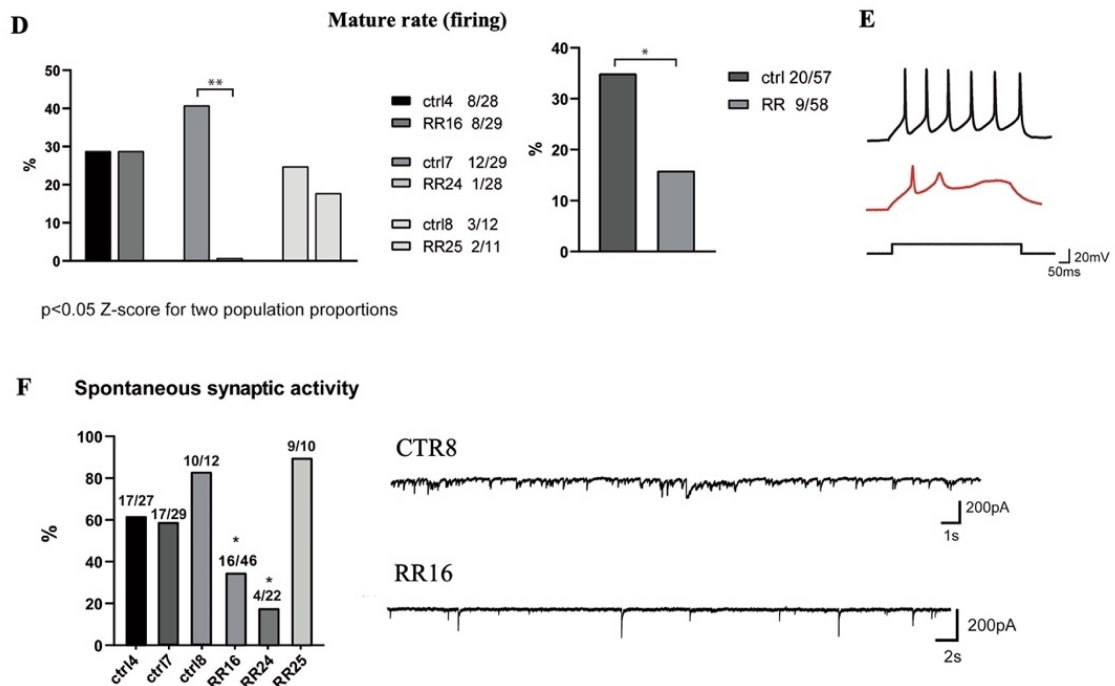


Figure 40. hiPSC-derived neurons electrophysiological characterisation. (A) Current-voltage plots obtained from whole-cell patch-clamp recordings of hiPSC-derived glutamatergic neurons from three twin pairs discordant for multiple sclerosis, co-cultured with primary murine astrocytes. Three independent differentiations were performed for CTR4-RR16 and CTR7-RR24 twin pairs, while only one differentiation was done for CTR8-RR25 lines. (B) Example of individual current traces in CTR and RRMS lines. (C) Summary of average INA and IK current-voltage relationship from all recordings ($n=57$ cells for CTR lines, $n = 58$ cells for RRMS lines). Statistical analysis was performed with unpaired t -test, $*p<0.05$. (D) Mature rate (firing) analysed separately for each twin pair (left panel) and the summary (right panel) of mature rate (firing) of all cells recorded from three twin pairs. Statistical analysis was performed with Z-score for two-population proportions (healthy vs. respective MS-affected twin), $*p<0.05$. (E) Examples of action potential trains induced by injection of 500-ms lasting suprathreshold current steps in CTR and RRMS lines. (F) Summary of spontaneous synaptic activity recordings (mixed excitatory and inhibitory postsynaptic currents) from three twin pairs. Each bar represents the percentage of cells displaying synaptic current activity normalized to the total number of the recorded cells. Statistical analysis performed with Z-score for two-population proportions (healthy vs. respective MS-affected twin), $*p<0.05$. Individual synaptic current traces from CTR8 (DIV57) and RR16 (DIV63) co-cultured with mouse astrocytes are shown in the right panel.

3.5.1.5 hiPSC-derived neurons voltage-gated ion channels expression profile

To understand whether electrophysiological differences between MS and healthy control neurons correlated with the gene expression profile of voltage-gated sodium and potassium channels, neurons from two twin pairs (CTR4-RR16 and CTR6-RR24) were differentiated and co-cultured with murine astrocytes for a total of 60 days. RNA was collected to quantitatively evaluate mRNA expression levels of 92 voltage-gated ion channels by TaqMan array and real-time PCR protocol. GAPDH-normalized expression

of each target gene in the RRMS line was compared to the expression level of the same target gene in the respective CTR twin line.

Although all four lines were simultaneously differentiated for the same time (60DIV) with identical differentiation protocol, the voltage-gated ion channel expression profile varied between twin pairs, since CTR7 and RR24 lines did not express 24 genes, whereas CTR4 and RR16 did not express the gene of only 9 ion channels. High cellular and functional variability in hiPSC-derived neuronal cultures were previously described (Bardy *et al*, 2016), highlighting a broad range of neuronal functional states, including the subtypes of “immature”, “transition state”, and “highly functional” neurons despite their maturation time *in vitro*. *CACNG3*, *KCNAB1*, *KCND3*, *KCNK1*, *KCNK12*, *KCNK9*, *KCNQ5* were down-regulated, while *KCNA5* and *KCNH6* were up-regulated in RRMS neurons compared to neurons from the respective healthy twins.

Additional studies will be performed to underline whether such differences are caused by MS-specific neuronal phenotypes or primarily caused by variations in neuronal maturation stage.

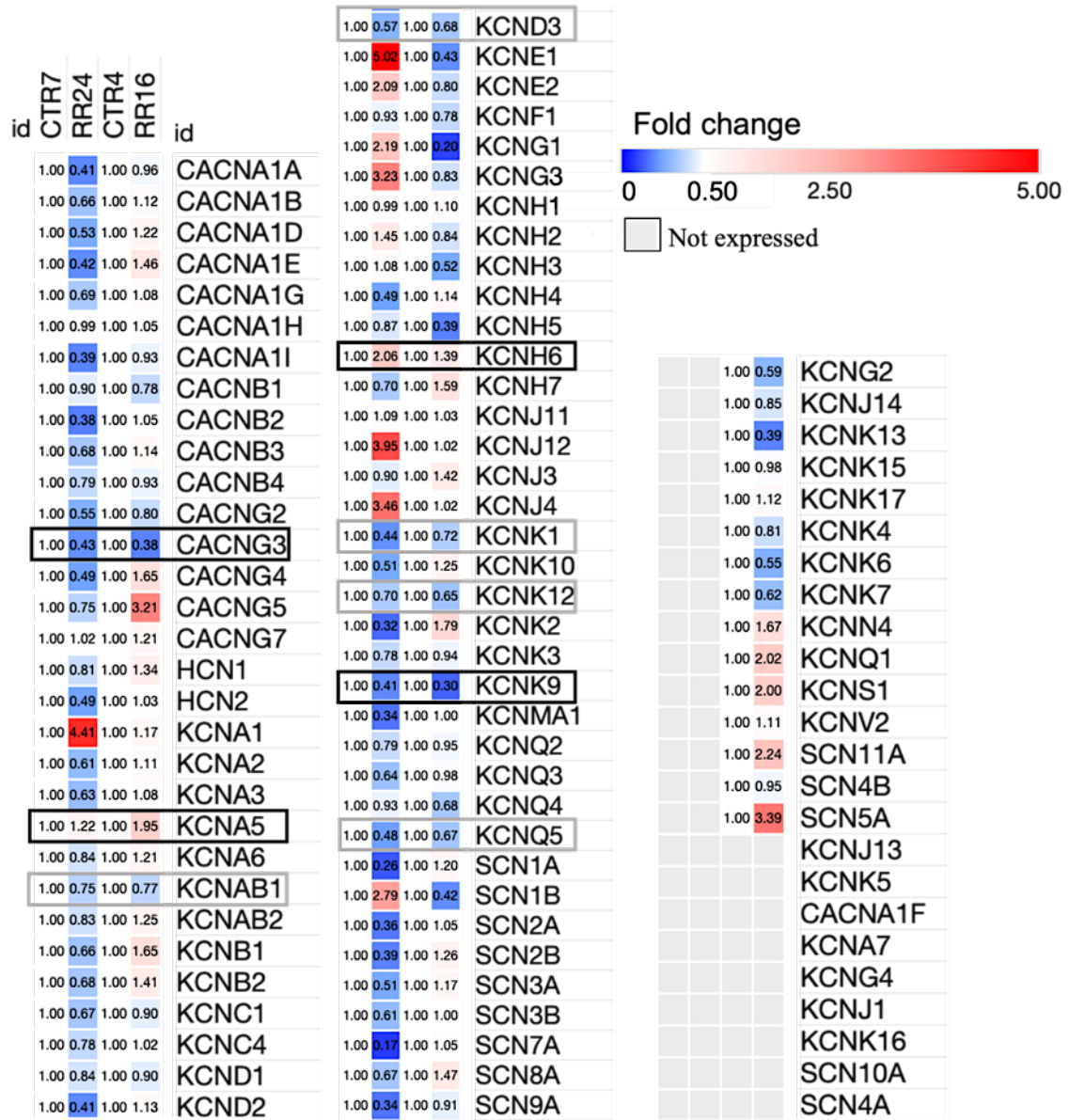


Figure 41. hiPSC-derived neurons voltage-gated ion channel expression profile. Neurons from two twin pairs MS discordant were differentiated for 30DIV and subsequently co-cultured for 30 days with primary murine astrocytes to enhance neuronal maturation. Gene expression was analysed by a human-specific voltage-gated ion channel TaqMan array card. The mRNA expression level of each target in the RRMS line was normalized to GAPDH and compared to the expression level of the same target gene in the respective CTR line. ($2^{-\Delta\Delta CT}$ method). The colour code corresponds to the fold change (FC) expression difference. Blue, negative FC indicates low expression; red, positive FC indicates high expression.

CACNG3 ↓↓	VOLTAGE-DEPENDENT CALCIUM CHANNEL GAMMA-3 SUBUNIT CACNG3 was significantly downregulated in iPSC-derived CHCHD10KO ALS motor neurons. (Harjuhaahto et al, 2020)
KCNK9 ↓↓	POTASSIUM CHANNEL, SUBFAMILY K, MEMBER 9; TWIK-RELATED ACID-SENSITIVE K⁺ CHANNEL 3; TASK3 In the absence of TASK3 channels, granule neurons do not maintain sustained repetitive firing. KCNK9 knockdown increased the frequency of spontaneous calcium transients in migrating cortical neurons. (Bando et al, 2014)
KCND3 ↓	POTASSIUM VOLTAGE-GATED CHANNEL, SHAL-RELATED SUBFAMILY, MEMBER 3; Kv4.3 First de novo KCND3 mutation causes severe Kv4.3 channel dysfunction leading to early onset cerebellar ataxia, intellectual disability, oral apraxia and epilepsy. (Smets et al, 2015)
KCNK1 ↓	POTASSIUM CHANNEL, SUBFAMILY K, MEMBER 1 POTASSIUM CHANNEL, WEAKLY INWARD-RECTIFYING, WITH TWIN P DOMAINS, 1; TWIK1 In astrocytes, the heterodimer formed by KCNK1 and KCNK2 is required for rapid glutamate release in response to activation of G-protein coupled receptors.
KCNQ5 ↓	POTASSIUM CHANNEL, VOLTAGE-GATED, KQT-LIKE SUBFAMILY, MEMBER 5 In neurons, Kv7.5 is important for regulation of the M-type current, and hence firing rates. Inhibition of M-currents leads to enhanced neuronal excitability associated with a wide spectrum of early-onset epileptic disorders. (Greene & Hoshi, 2017)
KCNAB1 ↓	POTASSIUM CHANNEL, VOLTAGE-GATED, SHAKER-RELATED SUBFAMILY, BETA MEMBER 1 KCNAB1 showed significantly reduced expression in samples from aged donors. (Voutetakis et al, 2015)
KCNK12 ↓	POTASSIUM CHANNEL, SUBFAMILY K, MEMBER 12; TANDEM PORE DOMAIN HALOTHANE-INHIBITED POTASSIUM CHANNEL 2; THIK2 Specific processes involving potassium channels have been described in non-autonomous glial mechanisms of ALS (Bataveljić et al., 2012; Sato et al., 2014).
KCNH6 ↑	POTASSIUM CHANNEL, VOLTAGE-GATED, SUBFAMILY H, MEMBER 6, KV11.2 In neurons, Kv11.1 regulates the spike frequency and controls the resting membrane potential. The isoforms Kv11.2 (hERG2) and Kv11.3 (hERG3) are primarily expressed in the brain. (Sahoo et al, 2014)
KCNA5 ↑	POTASSIUM CHANNEL, VOLTAGE-GATED, SHAKER-RELATED SUBFAMILY, MEMBER 5; Predominant expression of the Kv1.5 channel was found in astrocytes during EAE. (Bozic et al, 2019)

Figure 42. Summary on differentially expressed genes encoding voltage-gated ion channels in neurons from two twin pairs clinically discordant for MS. The arrow indicates either upregulated genes (upward direction) or down-regulated genes (downward direction). The colour reflects the relative degree of difference (dark blue – down-regulated with $FC < 0.5$; light blue – down-regulated in the range $0.5 < FC < 1$; light pink – up-regulated with $FC > 1.0$).

3.5.1.6 Functional oxidative CellROX assay identifies increased oxidative stress response in hiPSC-derived neurons from MS patients

As part of human-specific hit-validation, functional oxidative stress CellROX assay was set up to evaluate the antioxidant activity of the selected hit-compound Casopitant on hiPSC-derived neurons. The experiment aimed to validate neuroprotective and antioxidant properties of Casopitant in neurons from CTR lines and respective MS-affected twins under oxidative stress conditions. First, I set up a functional CellROX Deep Red assay for oxidative stress detection by FACS readout. CellROX Deep Red is a cell-permeable dye that becomes fluorescent upon oxidation by cytoplasmatic reactive oxygen

species including superoxide anion, nitroxides, and hydroxyl radicals in live cells. We performed a time-course experiment to determine the appropriate time frame for ROS detection induced by TBHP (Figure 43). The 1-2h was identified as the optimal time to detect an increase in ROS.

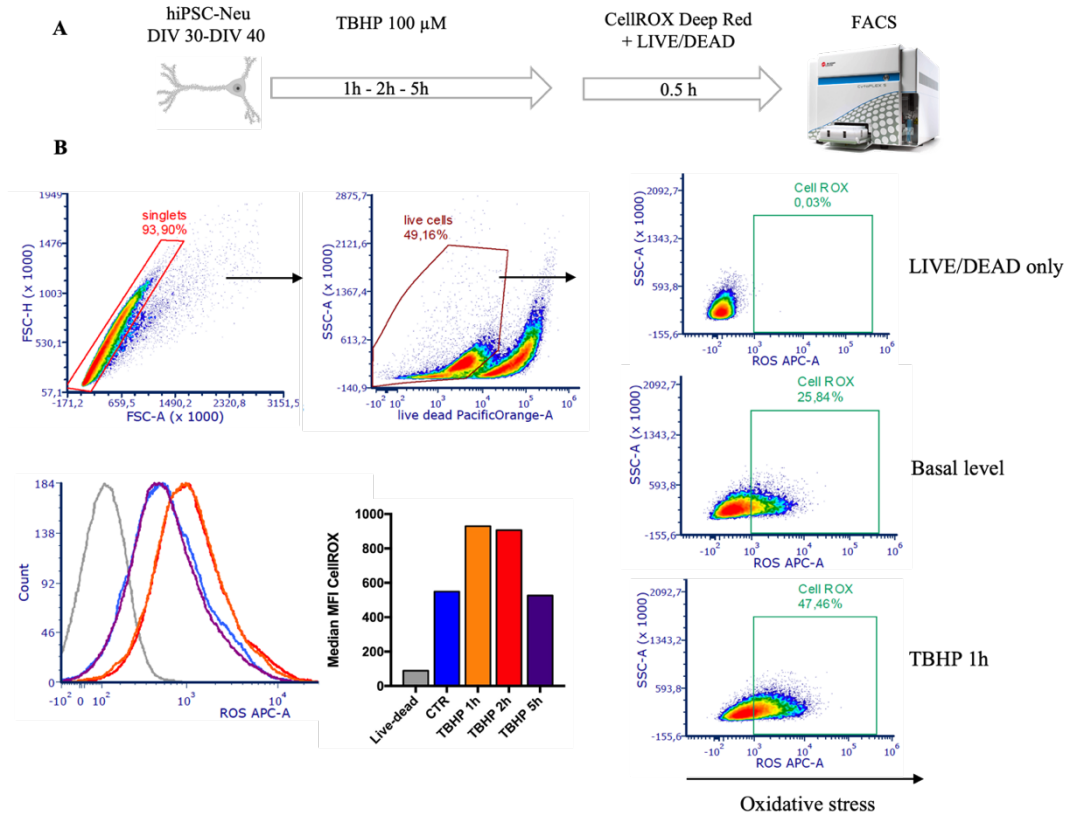


Figure 43. Setup of a functional oxidative stress assay CellROX in hiPSC-derived neurons by FACS readout. (A) Schematic representation of CellROX FACS experimental setup. hiPSC-derived neurons were differentiated for 30-40 DIV and challenged with 100 μ M tert-butyl hydrogen peroxide (TBHP) for 1-2-5h to evaluate the kinetics of oxidative stress by FACS analysis. (B) The gating strategy for FACS analysis. Doublets and dead cells (positively stained with LiveDead assay kit) were excluded from the analysis. Gates applied for population discrimination were based on the control population (CellROX-unstained) sample. (C) The representative fluorescence intensity distribution of each condition. (D) The median fluorescence intensity (MFI) of each condition.

The ability of neurons to cope with oxidative stress is limited due to high energy demands, making them particularly permissive to ROS-induced damage (Schirmer *et al*, 2019). This vulnerability augments in chronic oxidative stress environment in progressive MS (Choi *et al*, 2018; Lassmann & van Horssen, 2016). Among current MS drugs, only dimethyl fumarate (DMF) is associated with antioxidant activity through the Nrf2 induction (Yadav *et al*, 2021), while the majority of trials on endogenous or dietary

antioxidants in MS showed only short-term clinical benefits (Waslo *et al*, 2019). To date, lipoic acid, an endogenous antioxidant, and octanoic acid derivative showed a beneficial effect in preserving brain volume and improving walking speed in SPMS patients (Spain *et al*, 2017). Hence, it is crucial to identify novel efficient therapies to support redox status in MS.

To validate the neuroprotective and antioxidant properties of Casopitant in neurons from two CTR lines and their respective MS-affected twins under oxidative stress conditions, neurons differentiated for 30-40 DIV were pre-treated with 1 μ M Casopitant for 24h and applied an oxidative stressor TBHP for 1h followed by FACS readout (Figure 44A). Four independent experiments were performed on neurons from monozygotic twin pair CTR4 - RR16 and one on neurons from dizygotic twins CTR7 - RR24. We detected a significant antioxidant activity of Casopitant in CTR neurons that could effectively block TBHP-generated ROS comparable to the endogenous ROS levels (basal). However, oxidative stress in RRMS neurons was significantly higher, and Casopitant was no longer effective in scavenging ROS (Figure 44B). Interestingly, the basal level of oxidative stress was comparable between CTR and RRMS neurons (Figure 44C), suggesting that RRMS-specific neurons might have specific dysfunctions in the mechanisms regulating the response to the oxidative stress (Upadhayay & Mehan, 2021). A recent study identified genetic-driven targets linked to oxidative stress regulation potentially implicated in MS (Olla *et al*, 2021). Besides, the GWAS study conducted by the International Multiple Sclerosis Genetics Consortium does not exclude the CNS role in determining MS susceptibility, by reporting non-immune CNS cells variants (e.g., SLC12A5 locus-specific for neurons and variants associated with myelination processes)(Patsopoulos *et al*, 2019; Shepard *et al*, 2019).

To confirm these findings, additional experiments will be performed on hiPSC-derived neurons from the same twin pairs, by investigating the expression level of 92 oxidative stress related genes (TaqMan array) upon TBHP-induced challenge.

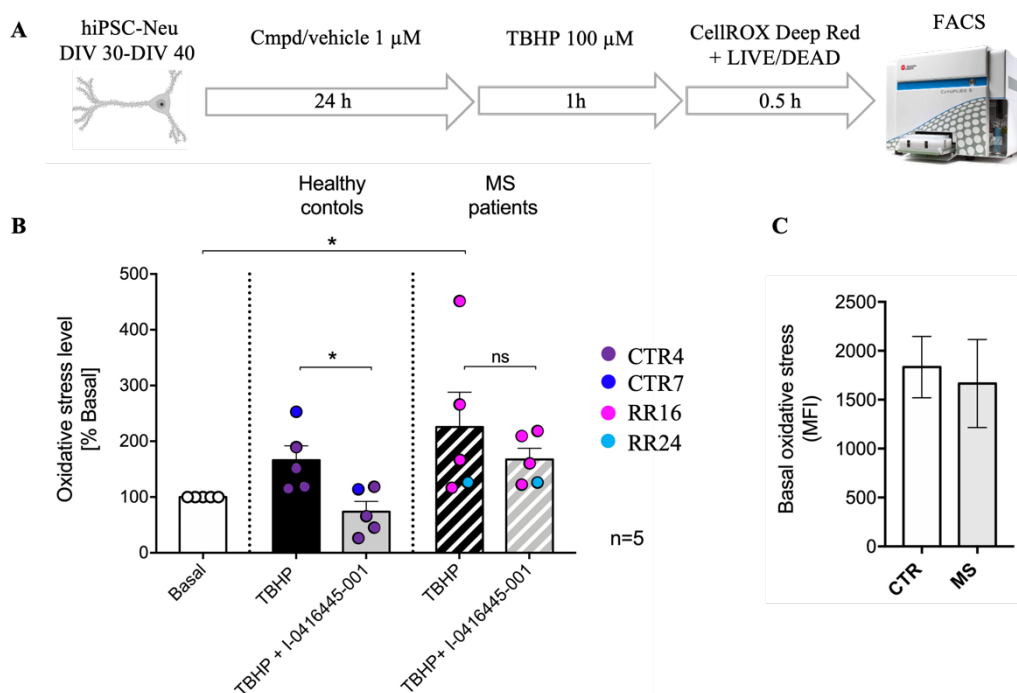


Figure 44. Functional CellROX assay identifies increased oxidative stress response in hiPSC-derived neurons from MS patients. (A) Schematic representation of CellROX FACS experimental setup. hiPSC-derived neurons from two twin pairs (CTR4-RR16, CTR7-RR24) were differentiated for 30-40 DIV, pre-treated with 1 μ M Casopitant (I-0416445-001) for 24h and then challenged with 100 μ M TBHP for 1h, followed by FACS readout. (B) Oxidative stress response was normalized to the basal level of endogenous oxidative stress evaluated by FACS analysis. Each bar shows mean value \pm SEM from five independent experiments. Stat. test performed with ordinary one-way ANOVA, followed by Dunnett multiple comparison correction, stat. significant at $*p < 0.05$. The pairwise comparisons between the stressor and drug treatment were performed separately for healthy control neurons and MS-specific neurons with the Mann-Whitney test, stat. significant at $*p < 0.05$. (C) The basal level of endogenous oxidative stress in CTR and MS neurons. The bar shows the mean value \pm SEM of fluorescence intensity (MFI) obtained in five independent experiments.

3.5.2 RNA-seq transcriptional profiles of NPCs and hNeu from three twin pairs discordant for MS

To get more insights into the molecular differences and to compare transcriptional profiles in HC and MS subjects, bulk RNA sequencing was performed with help of Dr. Sergio Baranzini lab (UCSF) on fibroblasts, hiPSC, hiPSC-NPCs, and young and mature neurons populations from three twin pairs discordant for disease. The RNA from all four cell types were prepared in our laboratory and samples were sent to UCSF for RNA sequencing and data pre-processing. After careful quality control of all samples with FastQC software (<http://www.bioinformatics.babraham.ac.uk/projects/fastqc>), principal component analysis (PCA) was performed to evaluate the associations between the

populations. PCA plot provides a map of clusters where distance reflects the difference in samples gene expression signature. As shown in Figure 45, a two-dimensional PCA plot revealed 61% variance between cell populations and 20% variance between the groups (CTR vs. MS). Distinct cell populations clustered away from each other suggest a good quality of hiPSC lines and their derivatives, supporting their phenotypic differences. Interestingly, the only clusters with minor separation between MS and CTR samples were NPCs and neurons (hNeu).

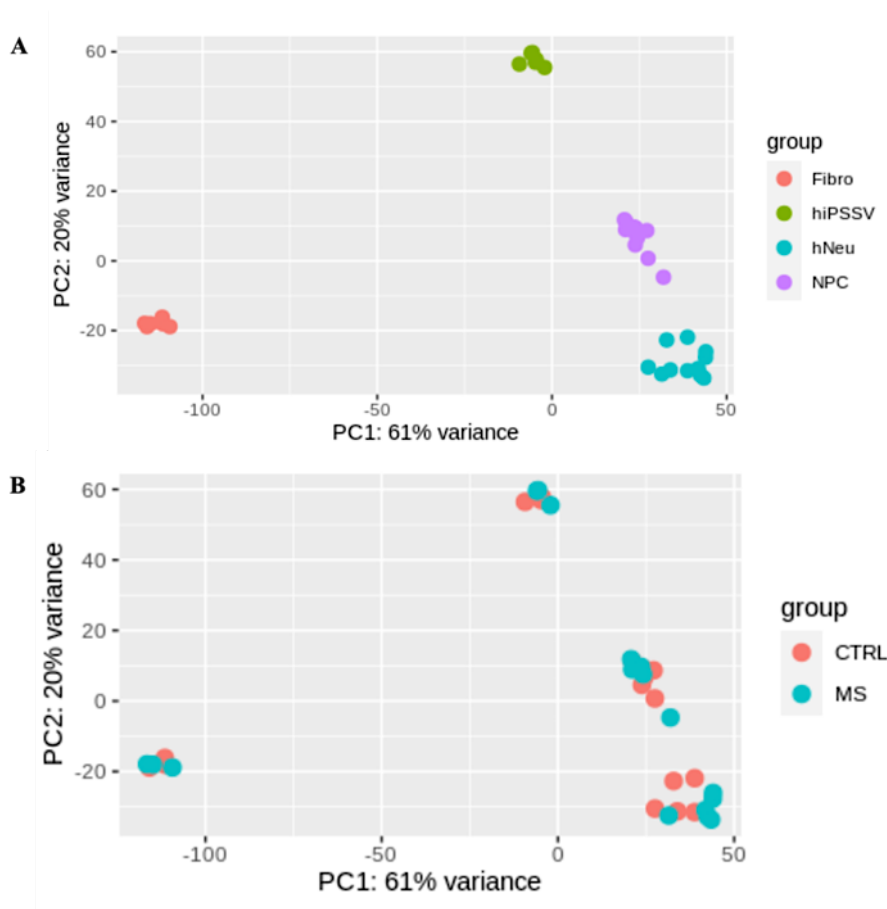


Figure 45. Principal Component Analysis (PCA) of RNA-seq performed on fibroblasts, iPSC, NPCs, and neurons from three twin pairs discordant for MS. (A) The top panel defines clusters of distinct cell populations (B) The lower panel shows the characteristic of the same clusters for CTRL and MS groups. Each dot indicates an individual sample. The proportion of variance is indicated in percentage.

Differentially expressed genes (DEG) analysis was performed for each cell type in CTR vs MS groups, resulting in no significant DEGs in the fibroblasts cluster, and only 16 significant DEGs were identified in the hiPSCs cluster (4 up-regulated and 12 down-regulated genes, false discovery rate (FDR) correction at $p < 0.05$). NPC cluster identified 33 significantly down-regulated and 44 up-regulated genes, false discovery rate-corrected (FDR 0.05) (Figure 46A). The gene ontology (GO) enrichment analysis was applied to all 77 DE genes in NPC cluster to identify biological attributes revealing associations with “cell-cell adhesion via plasma-membrane adhesion molecules”, “negative regulation of lymphocyte apoptotic process”, “cellular response to retinoic acid” and “axon guidance” GO terms (Figure 46C).

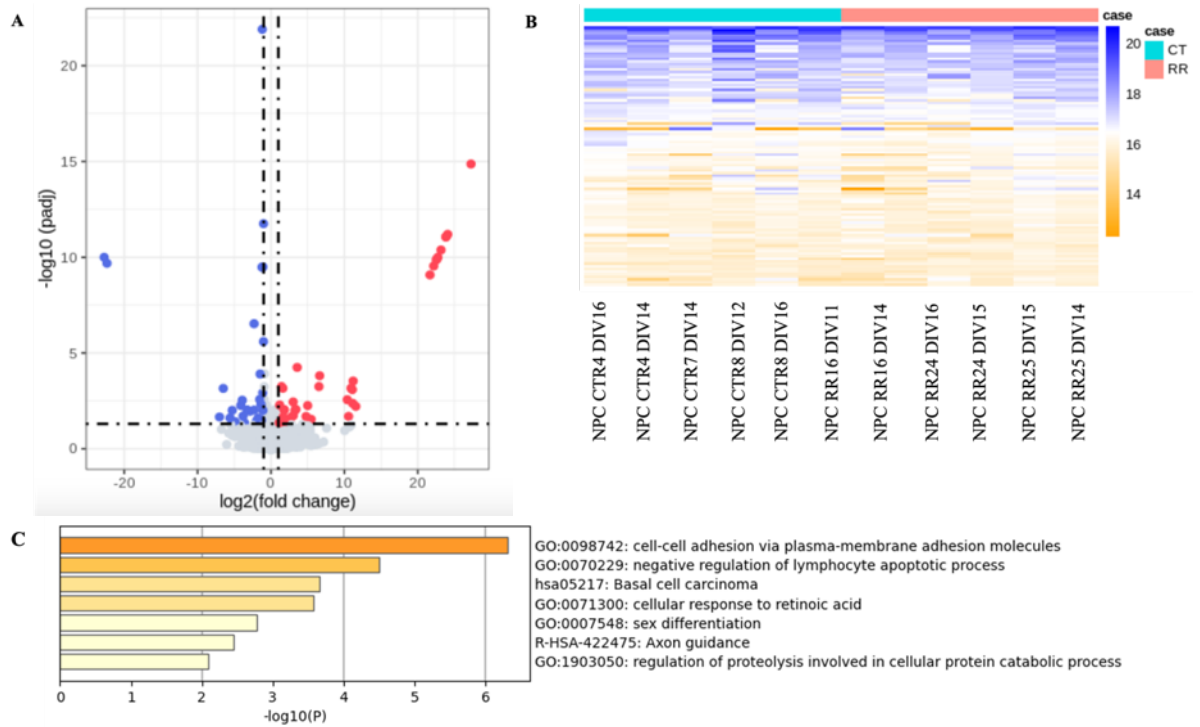


Figure 46. Differential gene expression and GO enrichment analysis in MS vs. HC NPC cluster. (A) Volcano plot of differentially expressed genes between the MS and HC NPCs, mapping 44 upregulated genes (red dots) and 33 downregulated genes (blue dots). The y-axis corresponds to the mean expression value of negative log 10 (adjusted p-value), and the x-axis displays the log2 fold change value, while dashed lines represent a significant cut-off. (B) Heatmap of all significantly differentially expressed genes (DEGs), where yellow colour denotes significantly upregulated genes and blue colour denotes significantly down-regulated genes. (C) Gene ontology enrichment analysis (Metascape) of biological processes on 77 DEGs of NPC cluster between HC and MS subjects. GO, gene ontology; neural precursor cell, NPC; multiple sclerosis, MS; healthy control, HC.

The 77 DEGs were as well identified in the cluster of MS vs HC neuronal cells (36 up-regulated and 41 down-regulated genes, FDR 0.05), (Figure 47A). Among the down-regulated genes, *ABCA8*, *LPAR3*, *CACNG3*, *INPP5D*, *SLIT3*, *SAT1*, and *PRDX4* are of particular interest for further investigation for their role in MS pathogenesis.

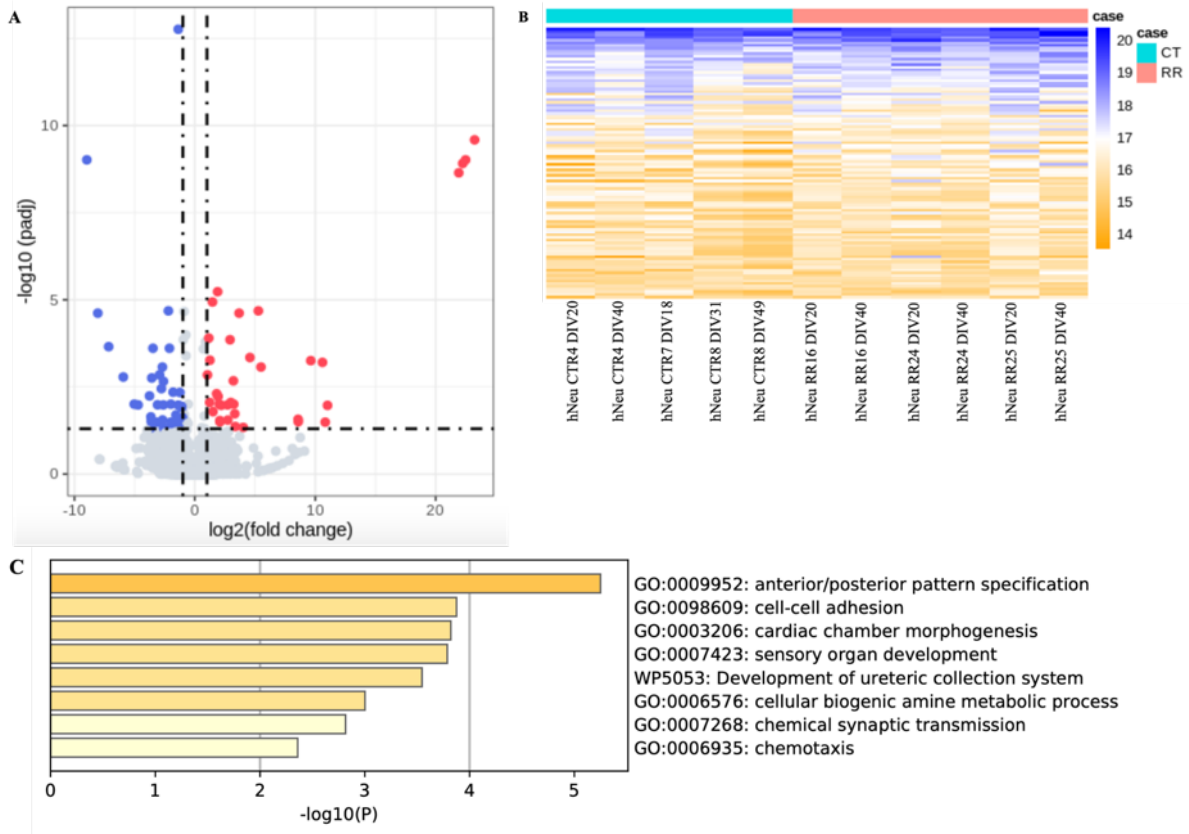


Figure 47. Differential gene expression and GO enrichment analysis in MS vs HC neuronal cell cluster. (A) Volcano plot of differentially expressed genes between the MS and HC hNeu, mapping 36 upregulated genes (red dots) and 41 downregulated genes (blue dots). The y-axis corresponds to the mean expression value of negative log 10 (adjusted p-value), and the x-axis displays the log2 fold change value, while dashed lines represent a significance cutoff. (B) Heatmap of all significantly differentially expressed genes (DEGs), where yellow colour denotes significantly upregulated genes and blue colour denotes significantly down-regulated genes. (C) Gene ontology enrichment analysis (Metascape) of biological processes on 77 DEGs of hNeu cluster between HC and MS subjects.

ABCA8 gene is a member of the ATP-binding cassette transporter family linked to susceptibility loci for the multiple sclerosis (Dugas *et al*, 2006). In addition, loss of *ABCA8* is associated with dysregulation of sphingomyelin synthesis and a decrease of myelination (Liu *et al*, 2022).

LPAR3 gene encodes a lysophosphatidic acid receptor 3 that binds lysophosphatidic acid (LPA). Dysregulation of LPAs is associated with MS and other autoimmune disorders (Schmitz *et al*, 2017). Moreover, LPA signalling is implicated in the regulation of oxidative stress response, while inhibition of LPARs aggravates EAE by inducing oxidative stress, neuroinflammation, and an increase in immune cell infiltrates (Choi *et al*, 2021).

Another candidate gene contributing to oxidative stress regulation is *PRDX4*, or peroxiredoxin 4. *PRDX4* belongs to a family of peroxiredoxins (PRDXs), ubiquitously expressed antioxidant enzymes playing a role in the detoxification process and managing hydrogen peroxide concentration. Among the six peroxiredoxins, PRDX4 is expressed by neurons, glia, and oligodendrocytes (Szeliga, 2020). In neurons, PRDX4 plays a neuroprotective and antioxidant role in regulating endoplasmic reticulum (ER) and oxidative stress response given the fact that PRDX4 silencing in HT-22 neurons induces ROS production, ER stress, and apoptosis (Kam *et al*, 2019). PRDXs levels are increased in serum and CSF of MS patients and have been linked with neuromyelitis optica and MS (Uzawa *et al*, 2020).

Significantly down-regulated gene *SATI* (Spermidine/Spermine N1-Acetyltransferase 1) is as well linked to ROS regulation controlling ferroptosis and lipid peroxidation processes (Li *et al*, 2020). In the context of autoimmune and neurodegenerative disorders, X-linked chromosome *SATI* loss-of-function is associated with systemic lupus erythematosus (Brooks & Renaudineau, 2015), at the same time decreased SAT1 expression were identified in Parkinson's disease brains (Ozawa, 2010).

Another significantly down-regulated gene in the MS neuronal cluster is *INPP5D*, or Inositol Polyphosphate-5-Phosphatase D. *INPP5D* plays role in various biological processes, including phosphoinositide and lipid metabolism, apoptosis and cell death, regulation of immune response, including lymphocyte and B cell-activation and production of cytokines (Raghu *et al*, 2019). *INPP5D* was suggested to be a part of the molecular network associated with chronic MS plaques (Satoh *et al*, 2009) and was identified as a susceptibility locus for the late-onset Alzheimer's disease (Tsai *et al*, 2021).

SLIT 3 (Slit Guidance Ligand 3) plays a role in axonal and dendritic patterning and is transiently expressed in the developing neocortex (Whitford *et al*, 2002). Interestingly,

SLIT3 was as well dysregulated in bulk NAWM MS tissue compared to healthy donor WM (Kular *et al*, 2019).

Additional gene closely regulating neuronal function is *CACNG3*, Calcium Voltage-Gated Channel Auxiliary Subunit Gamma 3. Notably, *CACNG3* down-regulation was as well identified by TaqMan array in both RR16 and RR24 mature neurons, confirming bulk RNA-seq findings. *CACNG3* polymorphism is linked to childhood absence epilepsy (Everett *et al*, 2007). Moreover, downregulation of *CACNG3* in amyotrophic lateral sclerosis (ALS) astrocytes led to neuronal support impairment (Ziff *et al*, 2022).

Eighteen genes were shared among the significant DEGs in NPC and hNeu clusters, including *KDM5D*, *DDX3Y*, *USP9Y*, *PRDX4*, *RPS4Y1*, *TMSB4Y*, *NLGN4Y*, *RPS6Ka3*, *NCRNA00185*, *TBX1*, *PCDHA7*, *PCDHA9*, *C21orf81*, *RP11-127B16.1*, *TTY15*, *C5orf17*, *PR11-138B4.1*, *F8A3*. These genes were either both up-or down-regulated in hNeu and NPC clusters. The most up-regulated genes shared between NPC and hNeu clusters were *KDM5D* (log2FoldChange= 11.01, padj= 0.01 for hNeu; log2FoldChange= 27.2, padj= 1.36E-15 for NPC) and *TMSB4Y* (log2FoldChange= 23.2, padj= 2.57E-10 for hNeu; log2FoldChange= 22.5, padj= 1.35E-10 for NPC). *KDM5D* is a lysine-specific demethylase 5D that regulates the activity of histone3 by tri-methylation and dimethylation at the Lys-4 residue (H3K4me3). H3K4me3 was decreased in neuronal nuclei in the MS cortex, whereas inhibition of H3K4me3 resulted in the reduced mitochondrial respiratory chain leading to impaired neuronal energetics and neurodegeneration in MS (Singhal *et al*, 2015). In addition, *KDM5D* was found to be significantly down-regulated in MS patient-derived monocytes (Almsned *et al*, 2021). This indicates that histone modifications might be linked to neurodegeneration and autoimmunity-related processes in MS (He *et al*, 2018).

TMSB4Y is a thymosin beta-4 (Tβ4) gene, Y-linked isoform, encoding for 5kD thymus gland peptide that plays a role in the organization of the cytoskeleton, actin polymerization, cell migration, tissue repair, and regeneration. Tβ4 has anti-inflammatory and neuroprotective properties and promote OPC differentiation and increase myelination in the MS demyelination models (Severa *et al*, 2019). Tβ4 targeting is a promising and versatile therapeutic approach to reduce neuroinflammation by inhibiting microglial activation and inhibiting inflammatory mediators secretion, promoting neuroprotection, and protecting oligodendrocytes from damage and death (Zhang *et al*, 2020; Santra *et al*,

2014). Interestingly, TMSB4Y, KDM5D, and DDX3Y are predicted to be linked in protein-protein interactions network (STRING) and are associated with major histocompatibility complex class I, A involved in the antigen presentation to the immune system.

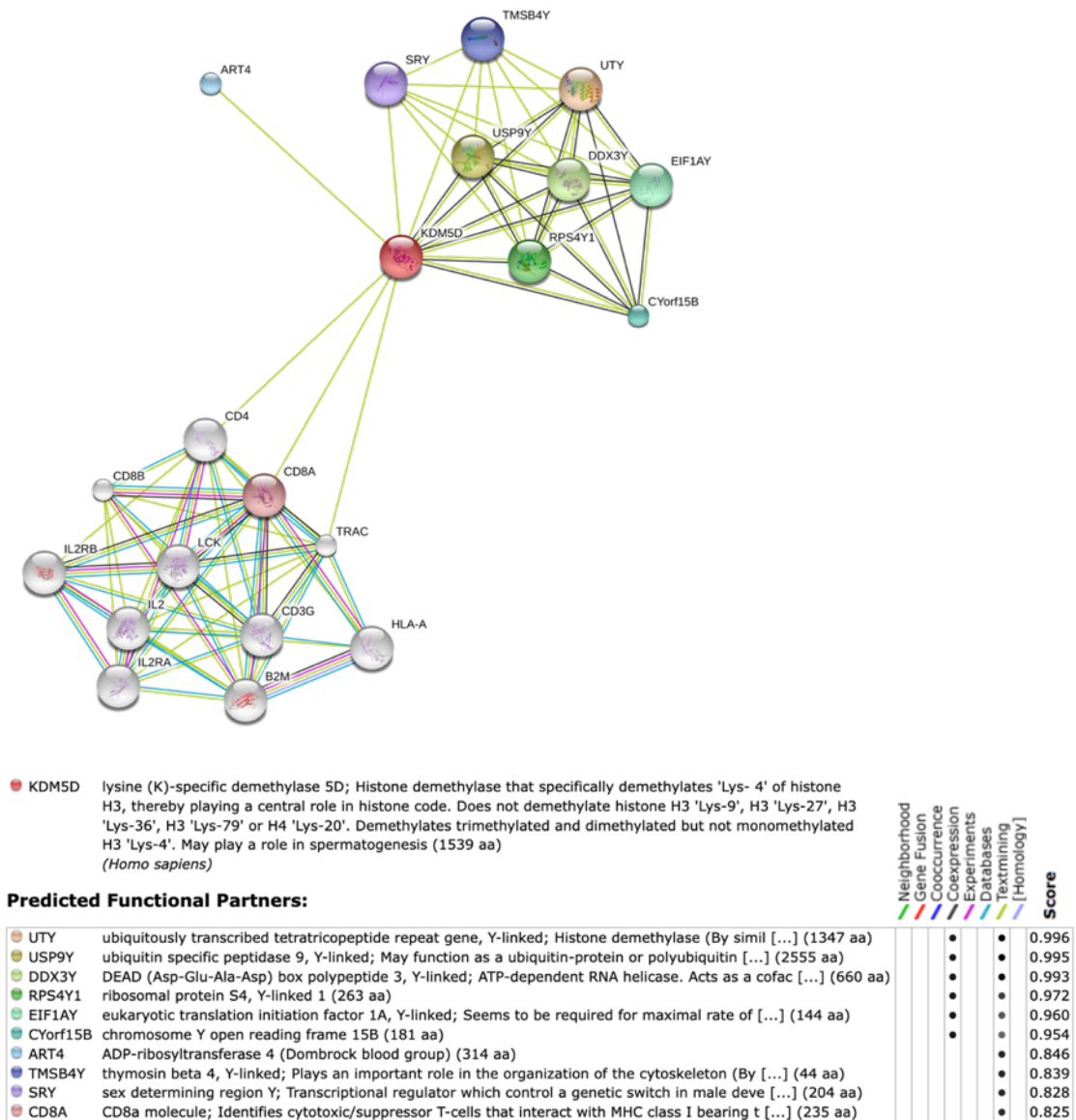


Figure 48. Protein-protein interaction network analysed by STRING 9.0 software. Network analysis results in predicting KDM5D, DDX3Y, and TMSB4Y interaction with a confidence cut-off of 0.7. Colours of the lines represent the types of evidence for the association: green line, neighbourhood evidence; red line, gene fusion evidence; blue line, co-occurrence evidence; black line, co-expression evidence; purple line, experimental evidence; light blue line, database evidence; and yellow line, text-mining evidence.

4. DISCUSSION

Progressive multiple sclerosis pathology is associated with widespread diffuse white matter damage, compartmentalised inflammation, the presence of chronic active smouldering lesions and persistent microglial activation. These factors, which remain untargeted and have been considered the pathological drivers of PMS, correlate with poor prognosis and higher MS disability (Giovannoni *et al*, 2022). The approved drugs for active RRMS and SPMS cannot effectively postpone disease progression and accumulation of irreversible disability. This implies that novel therapeutic strategies, including neuroprotective and promyelinating agents represent an urgent need for PMS. We hypothesize that therapeutics promoting brain repair through remyelination and neuroprotection, complementary to anti-inflammatory therapies, may prevent disease progression.

This project has employed novel methods and cutting-edge technologies to accelerate attempts to find effective treatments for PMS, including bioinformatics data integration and phenotypic drug screening on patient-specific cells. One of the project advantages is drug repurposing, which can provide novel treatment relatively quickly and with reduced costs, compared to the traditional drug discovery process. Repurposed drugs have already been tested preclinically and clinically, and their safety and pharmacodynamic profiles are mostly known. Another important advantage of this project is *ad hoc in silico* drug prioritisation. The *in silico* prediction of drug-to-gene interactions was performed with the SPOKE tool (Himmelstein *et al*, 2017) to efficiently stratify the selection of pharmacologically relevant compounds. Integrating different MS field knowledge domains, including the expression profiles of drug-perturbed genes, disease genetics and pathophysiology with a machine-learning approach is a powerful strategy to prioritise the compounds with the most significant potential to target MS-relevant pathways involved in neuroprotection and remyelination.

The methodological approach of the phenotypic screening consisted of stepwise multicellular *in vitro* assays on both primary rodent and human iPSC-derived neural and oligodendrocyte cells. This novelty may help overcome the limitations of a classic drug discovery pipeline, speeding up and optimising the process. A stepwise multicellular approach allows to validate compounds in more than one biological system and assess

more than one phenotype for the specific outcome (neuroprotection and myelination). We have selected murine cortical neurons as a suitable cellular model for primary cytotoxicity and neuroprotective screenings. The main advantages of using primary rodent cells are their relative availability, easy maintenance, and the possibility to extract the cells from animals with established neurodegenerative disease phenotype. Among the disadvantages are the inherent rodent genetics, increased sensitivity of neuronal cultures to death, disrupted 3D architecture, and inability to mimic the complexity of the human disease phenotypes (Belle *et al*, 2018). To better recapitulate the pathological features of MS, neurotoxic conditions were reproduced in neuronal *in vitro* assays to evaluate neuroprotective properties of a library of compounds. The excitotoxic damage, mitochondrial damage, oxidative stress injury and toxic iron accumulation are well-documented pathological features of progressive MS (Lassmann, 2018). Therefore, I evaluated the neurotoxic effects of three groups of stressors: molecules inducing excitotoxic damage (glutamate, NMDA, kainic acid), molecules inducing oxidative stress (TBHP, H₂O₂, 3-nitropropionic acid, FeSO₄), and cytokines. NMDA was selected as a suitable neurotoxic stressor that acts through overactivation of NMDA receptors (Dong *et al*, 2009), leading to intracellular calcium overload, mitochondrial depolarization and secondary axonal injury. We established a dose-response relationship of NMDA cytotoxicity and confirmed NMDAR1 expression in primary cortical neuronal cultures. Because NMDA administration alone cannot adequately reproduce MS neural tissue injury, a combination of multiple stressors should be tuned to model the inflammatory and neurotoxic milieu of the CNS in progressive MS. However, as assay reproducibility is essential for high-throughput and middle-scale screens, the neurotoxic conditions were set up using a unique stressor to minimize unnecessary assay variability. Moreover, compounds identified to be protective from NMDA-induced excitotoxicity might not be suitable to promote myelination, since decreased neuronal activity, partially due to NMDARs deactivation, has been reported to reduce remyelination processes (Gautier *et al*, 2015; Li *et al*, 2013).

Another critical point of the screening is the prophylactic regimen of the compound administration (pre-treatment) before application of the neurotoxic stressor. Although providing the drug preventively to the stressor when screening compounds *in vitro* may not reproduce the clinical settings of progressive MS, this approach significantly

increases drug discovery success and may lead to the discovery of potentially novel targets. Eventually, both prophylactic and therapeutic treatment regimens should be evaluated for the selected hit-compounds, as it was previously applied in the pharmacological screenings for ischemic stroke (Beraki *et al*, 2013). An early intervention is necessary to prevent or slow down brain damage before irreversible neural tissue injury accumulates and brain capacity to repair is diminished (Giovannoni *et al*, 2016; Cerqueira *et al*, 2018), therefore the modification of MS course with primary prophylaxis can be done for individuals at high-risk to develop MS (clinically isolated syndrome (CIS) or radiologically isolated syndrome (RIS).

In most drug screens, cell death assays are frequently used to identify potentially neurotoxic compounds prior to the phenotypic screening or to evaluate neuronal survival upon stressor exposure. Choosing the right cell-based method and appropriate readouts are essential to generate meaningful data (Kamiloglu *et al*, 2020; Kepp *et al*, 2011). The commonly used assays are applied to detect a direct neuronal death by binding to DNA or detecting DNA breakage (DAPI, Hoechst, Calcein-AM, TUNEL). Neuronal death represents a critical endpoint for screening assays and additional methods were developed to detect events that precede neuronal degeneration. For example, assays which measure caspase 3/7 activity are appropriate for apoptosis detection (e.g. Caspase-Glo 3/7 assay, Promega). In addition, the measurement of lactate dehydrogenase (LDH) release by the cells which lost membrane integrity can be used as indicator of irreversible cell death. Other surrogate marker of cell viability is the cellular metabolism. Several assays have been developed which can measure the changes in cellular metabolic activity (MTT/WST-8/ATP-based) or in mitochondrial function (JC-1, TMRM). However, since ATP- and WST-based assays are highly susceptible to metabolic interference and may generate false positive results, these tests are most suitable for primary medium- or high throughput cytotoxicity screenings. In this project, we have approached the evaluation of compounds toxicity and the evaluation of neuronal survival upon toxic stressor application via WST-8 (or CCK8) viability assay. The CCK8 is a colorimetric assay based on water-soluble tetrazolium salt (WST-8) reduction by dehydrogenase activities in the cells, which reflects the metabolic activity of viable cells. CCK8 assay method is far superior compared to the other enzyme-based methods (e.g., MTT). CCK8 assay is easy-to-use, non-toxic, and highly reproducible (Riss *et al*, 2016). We have attempted to setup

additional functional assays to assess neuronal properties after toxic stressor exposure, for example the change in mitochondrial membrane potential (JC-1) or calcium signaling (Fluo-4AM). These functional assays are useful for identification of compounds targeting the upstream secondary axonal injury cascade. However, JC1 or calcium imaging were technically not suitable for the testing of 160 compounds, as high readout variability was observed. Such functional assays might be more useful in validation studies for a smaller number of compounds.

The common way is to perform phenotypic screenings using immortalized tumor-derived cell lines or primary rodent cell cultures, however these cell types do not fully recapitulate human disease conditions and are often unspecific for CNS-targeting compounds (Brown & Wobst, 2020). Moreover, target subtypes or drug affinities of the same drug can be fundamentally different in humans versus rodents. On the other hand, using *in vitro* models that resemble human pathological features remarkably increases the efficiency and accuracy of drug screening. While primary patient cells (e.g., biopsy, surgical material) can be directly utilized to model the effects of a drug in a patient-specific personalized manner, their availability and expansion in culture are limited compared to *in vitro* derived or reprogrammed cell lines. In this regard, induced pluripotent stem cells (iPSCs) have revolutionized the field providing an almost infinite cellular source with the preserved genetic background of the donor (Ruscio *et al*, 2015), able to differentiate into cells not accessible otherwise (e.g., neurons, glial cells, etc). iPSC derived cells have been shown to recapitulate features of several pathological conditions being useful for *in vitro* disease modelling (Ghaffari *et al*, 2018), although only limited evidence is available for MS (Ghirotto *et al*, 2022). In this project, we performed the validation of selected molecules on hiPSC-derived neurons and oligodendrocytes from healthy controls and MS patients, providing the unprecedented opportunity of studying a disease-specific human *in vitro* system (disease-in-a-dish), enabling rapid clinical translation. One of the main issues with the use of iPSC-derived models is the variability within cell lines and derivation techniques (Volpato & Webber, 2020). To overcome this issue to some extent, the iPSC lines differentiation should follow standardised protocols and detailed characterization. Scarce expression of functional synapses expressing key receptors such as NMDA, GABA, AMPA or ion channels in iPSC-derived neurons is a common issue, therefore novel methods improving

electrophysiological activity and neuronal maturation have been developed, including the use of BrainPhys neuronal medium (Bardy *et al*, 2015), or co-culture with iPSC-derived astrocytes (Hedegaard *et al*, 2020b; Kuijlaars *et al*, 2016). iPSC-derived co-cultures can robustly model certain pathological features of neurodegenerative diseases, however important considerations should be made when developing co-culture systems, including cellular reproducibility and media/matrix compatibility. Although a big effort was made to establish protocols for terminal differentiation of functional neurons, to reduce the gap between *in vitro* models and *in vivo* brain physiological conditions, the development of methods promoting neuronal maturation and synaptic function to study disease mechanisms remains a challenge. While 2D systems have been considered the most simplistic and reproducible for drug screening purposes, more sophisticated hiPSC-derived 3D cellular models, such as organoids or spheroids, may overcome the two-dimensional co-culture system limitations. The complex cellular milieu of the human brain is better represented by 3D *in vitro* models (Amin & Paşca, 2018). Furthermore, recently developed 3D cellular models with microglia provide a versatile tool for modelling neuroinflammation and studying neuro-immune interactions *in vitro* (Abreu *et al*, 2018).

By stepwise phenotypic screening on primary murine and hiPSC-derived cells, two compounds, namely Bavisant and Casopitant, were selected, based on their overall performance in various neuronal (n=13) and oligodendrocyte-based assays (n=8) (Figure 15). In validation studies, Casopitant confirmed its neuroprotective property in hiPSC-derived neurons and Bavisant showed a promyelinating efficacy in hiPSC-derived oligodendrocytes. hiPSC-derived oligodendrocyte differentiation was implemented by overexpression of the single TF hSOX10 in iPSC-derived NPCs, using an inducible lentiviral vector harbouring a GFP reporter. In this way, SOX10-bearing hiOLs that matured into MBP⁺ oligodendrocytes were generated within 26-28 days. In addition to oligodendrocytes, neurons and astrocytes were also present within the hiOL SOX10-population, thus providing a useful tri-culture system. Such human iPSC-derived based multi-cellular system can serve as a scalable platform for screening compounds that target the crosstalk between oligodendrocytes, astrocytes, and neurons, and will enable to evaluate their promyelinating and neuroprotective properties within the same culture.

Prior to *in vivo* efficacy validation study, we estimated the safety and pharmacodynamic profiles of Bavisant and Casopitant based on previously published studies (Minthorn *et al*, 2008; Miraglia *et al*, 2010; Weisler *et al*, 2012). Both drugs are orally available, brain-penetrant and with a good safety profile. However, the predicted half-life of Casopitant in the brain is only 8 hours, which may impede the maintenance of effective drug concentration for the notable therapeutic effect. Both drugs were validated *in vivo* in the well-established animal model of MS, chronic EAE. Although we could not observe amelioration in the EAE clinical symptoms after 28 days of Casopitant and Bavisant administration (q.d.), both treatments resulted in reduced demyelination and axonal loss in the EAE spinal cord tissue (Figures 24-25). EAE is an imperfect but relevant animal model of MS, commonly used to effectively mimic the neuroinflammatory component of MS pathology with the presence of mild demyelination and axonal loss in the spinal cord. However, not all pathological features of the clinical MS settings can be modelled by EAE ('t Hart *et al*, 2011). Firstly, EAE is mainly characterized by pathological features within the spinal cord, while only mild inflammation can be detected in the cerebellum and optic nerve. Secondly, the lesions are characterized by significant axonal degeneration rather than primary demyelination, which distinguishes it from human MS. In contrast, EAE induced in Biozzi ABH mice more closely recapitulate the clinical features of progressive MS including the presence of chronic demyelination, neuro-axonal degeneration and ectopic follicles which represents the source of compartmentalized inflammation (Nishri *et al*, 2021). However, several pathological hallmarks of progressive MS such as smouldering and cortical lesions and diffuse NAWM and grey matter pathology still lack relevant animal models. The cuprizone model is an additional useful model to study demyelination and remyelination processes independent from adaptive immune system response (Zhan *et al*, 2020). Some of the aspects of progressive MS like diffuse white matter and axonal damage with minor immune cell infiltration, but presence of microglia activation and astrogliosis can be recapitulated in the cuprizone model. It is important to stress that a single animal model cannot possibly reproduce all pathological features of a complex and heterogenous disease as MS. Each animal model is useful for studying certain pathogenic elements rather than the disease overall complexity. Therefore, in addition to pre-clinical evaluation in EAE, the promyelinating capacity of Bavisant and Casopitant will be

evaluated by project's collaborators (Oumesmar and Baron-Van Evercooren labs, ICM, France) in the model of focal lysolecithin-induced demyelination and the humanized animal model of Shi/Shi Rag2^{-/-} mice transplanted with human iPSC-derived oligodendrocytes (Mozafari & Baron-Van Evercooren, 2021).

After evaluation the preclinical efficacy of the drugs *in vivo*, we have focused on the investigation the compounds' mechanism of action. The target/pathway analysis of hit-compounds was performed via SPOKE *in silico* bioinformatic tool. Bavisant is a histamine H3 antagonist investigated in clinical trials for the treatment of ADHD (Weisler *et al*, 2012) and excessive daytime sleepiness in Parkinson's disease (NCT03194217). The target/pathway analysis confirmed HRH3 as main target of Bavisant. In addition, we could identify the association of Bavisant with RRMS and other autoimmune diseases. By SPOKE analysis, Bavisant is predicted to interact with S1PR4 and S1PR5 receptors, however we could not identify additional potentially novel targets for MS. Even though no other targets for Bavisant have been identified so far, *in vivo* validation in demyelinating animal models of multiple sclerosis (cuprizone/lysolecithin) and further investigation of HRH3's role in myelination (Chen *et al*, 2017) and neuroprotection (Dai *et al*, 2007) may help to advance Bavisant as a novel drug for the treatment of MS and other CNS disorders by improving patients' cognitive functions and clinical symptoms (Imeri *et al*, 2021).

We have focused our main attention on the deconvolution of the Casopitant mechanism of action since HRH3 is not a novel target for MS treatment (Schwartzbach *et al*, 2017). Casopitant is an anti-emetic and anxiolytic drug recognised as a NK1R antagonist (Navari, 2008; Quartara *et al*, 2009). Literature search and *in silico* analysis confirmed that the primary target for Casopitant is NK1R. NK1R belongs to a family of tachykinin receptors widely distributed in the body, including nervous and immune systems. NK1R controls various physiological functions and plays a significant role in regulating inflammatory response by lymphocyte recruitment and activation mediated by NK1R ligand substance P (Mishra & Lal, 2021). Other NK1R-mediated functions are cell migration and proliferation regulation, cytoskeleton organisation, memory and learning, nociception, synaptic transmission regulation, and calcium and metal homeostasis maintenance. The involvement of NK1R in a wide range of mechanisms, including regulation of brain innate immune system response and neuroinflammation, make

tachykinins an attractive therapeutic target for neuroinflammatory disorders, including MS. The NK1R antagonism has been described to induce a therapeutic anti-inflammatory effect in various inflammatory and auto-immune CNS disorders (Johnson *et al*, 2017; Vilisaar *et al*, 2015; Eapen *et al*, 2019; Philipp, 2016; Mishra & Lal, 2021). The knockout of NK1R resulted in EAE amelioration during the chronic phase of the disease due to lower CD4+ T cells infiltration into the CNS (Reinke *et al*, 2006). However, the treatment with the NK1R antagonists SR140333 (Reinke *et al*, 2006) and CP-96,345 (Nessler *et al*, 2006) during the chronic EAE phase was ineffective in reducing EAE clinical symptoms. The protective effect was only observed when drugs were administered prophylactically before the disease onset. This evidence may potentially explain the absence of Casopitant clinical efficacy in the chronic EAE model (Figure 23). The other interpretation of the negative outcome of *in vivo* preclinical validation is the low potency of Casopitant on mouse NK1 receptors due to the drug's short half-life (~8h), resulting in insufficient drug availability in the CNS of treated EAE mice, which showed no evident therapeutical efficacy. Another critical issue is the potential side effects of Casopitant associated with high-grade inflammation in multiple organs, especially when animals were treated twice daily (Figure 27).

In addition to neuroprotective properties that both drugs exhibited *in vitro* and at some extent *in vivo* resulting in reduced axonal loss (Figure 25), Casopitant and Bavisant demonstrated promyelinating efficacy in primary murine and hiPSC-derived oligodendrocytes (Figure 15; Figure 17), and lower demyelination in the EAE model (Figure 24). While the role of HRH3 in myelination is well-known, NK1R role in myelination has never been described. Moreover, *TACRI* expression, which encodes NK1R, was not confirmed in the CG4 cell line. Based on this evidence, we performed an *in silico* analysis of Casopitant to evaluate potential novel targets that could mediate the promyelinating effect of Casopitant. As a result, the potential binding of Casopitant to NK1R receptor was confirmed by the SPOKE tool; besides, sigma non-opioid intracellular receptor 1 (S1R) was predicted as an additional target of Casopitant (Figure 28).

S1R, an endoplasmic reticulum (ER) chaperone protein, plays a role in regulating calcium signalling, oxidative and ER stress responses, and maintaining neuronal homeostasis (Mori *et al*, 2013). In addition, S1R regulates lipid metabolism and therefore

it is potentially involved in regulating oligodendrocyte differentiation and myelination (Hayashi & Su, 2004). Activation of S1R has been reported to sustain neuroprotection (Ryskamp et al, 2019), and it was proposed as a potential novel therapeutic target in MS (Lisak et al, 2020). The neuroprotective and antioxidant functions of Casopitant, likely modulated by Sigmar1, have been validated in primary murine cortical neurons (Figure 16), hiPSC-derived neurons (Figure 14) and 3D neural spheroids (Figure 22).

To address whether the neuroprotective effect of Casopitant was primarily modulated through SIGMAR1, we have selected N2A as a cellular model for drug-target validation. N2A cells neither express the NK1R protein nor the *TACR1* gene (Figure 30), but do express SIGMAR1, thus making N2A a proper model to define the SIGMAR1 role in mediating Casopitant neuroprotective function. Casopitant exhibited neuroprotective and antioxidant effects in N2A cells upon TBHP exposure (Figure 33, D-E), decreasing ROS levels and protecting N2A from TBHP-induced toxicity. We performed transient downregulation of Sigmar1 in N2A and evaluated the effect of silencing on the oxidative stress response. Although it has been previously demonstrated that oxidative stress levels significantly increase in Sigmar1-silenced 661W photoreceptor cells (Wang *et al*, 2019), we could not observe the same effect in N2A. The insufficient downregulation of Sigmar1 protein levels (~50%) can explain the obtained results. Future experiments will include titration of siRNA concentration to achieve more efficient Sigmar1 downregulation, or inducible knockdown of Sigmar1 in N2A cells will be set up by CRISPR/Cas9 gene editing (Yang *et al*, 2019). Although Bavisant and Casopitant have lacked clinical efficacy in the chronic EAE model, further investigation of the mechanism of action, targeting of upstream or downstream effectors of the original target or the optimization of drugs chemical structure are planned in future experiments. Alternatively, other four drugs with various targets e.g., calcitonin gene related peptide (CGRP) antagonists, JAK2/Src inhibitors, platelet-derived growth factor (PDGF) antagonists, and hypoxia-inducible factor-proline dioxygenase inhibitors (HIF-PDI) identified as hits in the drug screening, will be evaluated in future studies.

Finally, we have explored functional and molecular signatures of MS-specific hiPSC-derived neurons that offer a unique opportunity in recapitulating disease features for *in vitro* disease modelling (Ghaffari *et al*, 2018) and drug discovery (Qian & Tew, 2021). We took advantage of generating hiPSC lines from three twin pairs clinically discordant

for MS. Twin studies have been valuable for investigating complex genetic and environmental interactions and their contribution to disease susceptibility. So far, only three studies have demonstrated phenotypic differences in hiPSC-derived neurons from monozygotic twins clinically discordant for Parkinson's disease (Woodard *et al*, 2014), ALS (Seminary *et al*, 2020) and schizophrenia (Toritsuka *et al*, 2021). Several studies have previously investigated specific MS signatures in immune cell populations (Gerdes *et al*, 2020; Baranzini *et al*, 2010a) and hiPSC-derived oligodendrocytes (Starost *et al*, 2020), but could not identify significant differences. A study by Gerdes and colleagues (Gerdes *et al*, 2020) leads to the hypothesis that similarity in immune signatures and the signs of subclinical neuroinflammation identified in clinically healthy cotwins may indicate on prodromal MS. Therefore, twin studies should always be taken into careful consideration since the unaffected twin has the highest familial risk of developing MS (17.3% for monozygotic and 1.92% for dizygotic twins (Westerlind *et al*, 2014), and an increased probability of prodromal MS. Nevertheless, several studies identified differential gene expression and DNA methylation profiles in PBMCs from discordant monozygotic twins (Souren *et al*, 2019; Särkijärvi *et al*, 2006) highlighting the contribution of the genetic and epigenetic factors to MS development. The most recent study identified an inflammatory shift in monocyte populations and increased CD25 and Il-2 expression independent of individual genotype in the largest studied cohort of 61 monozygotic twin pairs, indicating immune dysregulation in twins with MS (Ingelfinger *et al*, 2022). In addition, a study by Berer *et al*, 2017 investigated gut microbiota signature in 34 monozygotic twins discordant for MS. The authors could not detect a significant difference in MS versus healthy individuals' microbial profiles but identified an increased incidence of spontaneous EAE in mice transplanted with microbiome from MS-affected twins. Most of the twin studies explored the MS-specific signatures in the peripheral blood or in the microbiota of the subjects. However, none of the studies yet investigated the contribution of risk variants on CNS cells and their role in MS susceptibility.

This is the first study describing functional phenotypic differences in hiPSC-derived neurons from three twin pairs clinically discordant for MS. We have identified higher vesicular glutamate transporter VGLUT1 (*SLC17A7*) expression at protein and transcript level in hiPSC-derived mature neurons from three twins compared to their healthy siblings (Figures 36-37). The expression of VGLUT1 is directly correlate with the

number of vesicles available for glutamate loading and release (Wilson *et al*, 2005). However, the extracellular concentrations of glutamate measured in iPSC-derived neurons from two twin pairs were comparable. Additional glutamate release tests will be carried out using the intensity-based glutamate-sensing fluorescent reporter iGluSnFR (Marvin *et al*, 2013) and live imaging to confirm the findings. The detrimental role of glutamate excitotoxicity in MS pathogenesis has been largely described in both EAE and MS (Macrez *et al*, 2016; Pitt *et al*, 2000). Excessive activation of the glutamatergic pathway and altered glutamate homeostasis contribute to axonal and oligodendrocyte damage, eventually leading to neuroaxonal dysfunction, demyelination, and ultimately worsening clinical outcomes in MS (Azevedo *et al*, 2014). The increased expression of VGLUT1 has been linked (Daniels *et al*, 2011b; Wilson *et al*, 2005) to elevated glutamate release that overstimulates excitatory transmission and over-activates the axo-myelinic synapse (Micu *et al*, 2016), eventually leading to neuronal exhaustion and myelination defects. Promoting neuroprotection through modulation of excessive glutamate release may be an effective approach against neurodegeneration in MS.

In addition, we have investigated electrophysiology profiles of mature hiPSC-derived neurons from three twin pairs co-cultured with murine astrocytes to achieve efficient neuronal maturation. We identified a significant decrease in sodium (I_{Na}) and potassium (I_k) currents and decreased mature firing rate in neurons from MS patients. Potassium currents density deficiency may increase excitotoxicity due to the inability to repolarize the membrane potential. Loss of function of potassium Kv2.1 channels has been shown to decrease potassium current densities in hippocampal neurons of an Alzheimer's disease 3xTg-AD mouse model leading to neuronal excitability and increased ROS production (Frazzini *et al*, 2016). We could as well detect significantly decreased spontaneous synaptic activity (mixed excitatory and inhibitory postsynaptic currents) in neurons from two MS-affected twins compared to their healthy siblings. These results may indicate to the deficits in MS-specific neuronal electrophysiological properties, albeit additional experiments with a larger sample size are needed to corroborate the findings. To specifically analyse which voltage-gated ion channels may be implicated in the electrophysiological differences in MS neurons, we performed TaqMan array voltage-gated ion channels (VGICs) expression profiling of neurons from two twin pairs with the most notable electrophysiological differences. The two most downregulated genes in both

twin pairs were *CACNG3* and Potassium Two Pore Domain Channel Subfamily K Member 9 (*KCNK9* or *TASK-3*). *CACNG3* is reported to be significantly down-regulated in iPSC-derived motor neurons from ALS patients (Harjuhahto *et al*, 2020), while *TASK-3* knockout neurons showed deficiency in maintaining the repetitive action potential (AP) firing (Brickley *et al*, 2007). Interestingly, two-pore-domain potassium (K2P) channels have been described to play a role in regulating neuronal excitability, immune modulation, and neuroprotection (Luo *et al*, 2021). The ion channels expression profile in white matter lesions of progressive MS was described in details elsewhere (Boscia *et al*, 2021); however no data are available on *KCNK9* and *CACNG3* expression.

Thanks to the collaboration with Prof. Sergio Baranzini lab, we have performed a bulk RNA-sequencing on fibroblasts, iPSCs, NPCs, young and mature neurons from three MS discordant twin pairs to validate the findings of neuronal cell functional characterization. Principal component analysis showed the separation of the distinct cell populations, with perfectly overlaying fibroblasts and iPSCs clusters in the six samples, whereas NPCs and neuronal clusters showed discernible differences. 77 DEGs were identified in both NPCs and neuronal clusters between MS and healthy controls, with 18 shared genes. Notably, *CACNG3* down-regulation was also identified in both NPCs and neurons, reinforcing the TaqMan array VGICs expression data. Another gene downregulated in the neuronal cluster is *SLIT3*, as well found to be dysregulated in bulk NAWM MS tissue compared to NAWM of healthy donor (Kular *et al*, 2019). In addition, we have identified a significant down-regulation of *LPAR3*, *PRDX4*, and *SAT1* genes in the MS neuronal cluster. These genes closely regulate oxidative stress response, lipid peroxidation and ferroptosis. The strong evidence of the downregulation of genes playing a role in oxidative stress response in MS-specific neurons may justify the increased ROS levels upon TBHP exposure, as shown in the functional oxidative stress assay CellROX (Figure 44). Validation of *LPAR3*, *PRDX4*, and *SAT1* in hiPSC-derived neurons from MS patients upon oxidative stress exposure will be performed by RT-qPCR in the following experiments. We will as well validate *KDM5D* and *TMSB4Y* genes on available snRNAseq datasets from MS post-mortem tissue to further elucidate their role in MS pathogenesis. In summary, by performing bulk RNA-sequencing on various cell populations including fibroblasts, hiPSC, NPC and neurons from three twin pairs clinically discordant for MS, unprecedentedly, we could identify substantial differences

in the transcriptome profiles of MS NPC and neuronal populations, but not in fibroblasts or iPSCs, suggesting potential MS susceptibility to neuronal impairment. Identified DEGs can be used for target prioritization that might be more relevant in MS and are valuable discoveries for predicting specific drug-gene connections, signalling pathways and molecular mechanisms amenable to therapeutic targeting.

5. CONCLUSIONS AND FUTURE PERSPECTIVES

A comprehensive and well-characterized *in vitro* phenotypic drug screening of an *ad hoc* prioritized drug repurposing library was setup to identify compounds with therapeutic potential for PMS. The drug library was built by integration of different sources via a machine learning approach that accurately represents the domain knowledge in MS field. This strategy is effective in prioritizing the molecules with the greatest potential to influence the targeted phenotypes: neuroprotection and remyelination. The pharmacological screening was carried out on primary murine and hiPSC-derived neuronal and oligodendroglia cultures, a stepwise validation approach that should overcome the limitations of traditional drug screens based on a single cellular model. As a result, we identified six lead compounds with potentially novel targets for PMS. Two compounds, Bavisant and Casopitant, were validated in 2D cellular models including dose-response experiments on primary cortical neurons, human iPSC-derived neurons, and oligodendrocytes, confirming their neuroprotective and promyelinating efficacy. Both drugs were validated in 3D neural spheroids and EAE preclinical model of MS. Although no clinical evidence was observed in EAE, the therapeutic treatment with both drugs resulted in lower demyelination and axonal loss. Additional *in vivo* experiments will be performed testing compounds in the late chronic phase (after 40 days post-immunisation) and in combination with anti-inflammatory treatments (dexamethasone/teriflunomide). In addition, preliminary data were obtained on the compounds molecular targets, and their mechanism of action will be investigated in future studies. The next phase of research will focus on exploring the potential use of NK1R and HRH3 antagonists, and SIGMAR1 agonists for neuroprotection and remyelination. The data obtained on the mechanism of action and on the pharmacological properties of the compounds will translate into results that will de-risk consequent clinical research.

We as well took advantage of characterizing hiPSC lines from three discordant MS twins to evaluate potential functional and molecular differences in hiPSC-derived neurons. Functional characterization and RNA-sequencing revealed MS-specific phenotypes in hiPSC-derived neurons of MS-discordant twins, including dysregulated electrophysiology profiles, increased oxidative stress response, and molecular signature indicating neuronal vulnerability. The iPSC lines from three additional MS twin pairs

have been generated and will be included in the RNA molecular profiling panel. NPCs, NPC-derived neurons, and oligodendrocytes will be generated from a total of six twin pairs to validate the preliminary RNA-seq findings. The investigation of molecular differences in neurons from MS twin pairs will provide additional knowledge on the potential impact of genetic and epigenetic changes on neuronal susceptibility to damage in MS. Altogether, human induced pluripotent stem cell derived oligodendrocytes and neurons from healthy controls and MS patients provide a promising approach to study disease-specific human cells, non-assessable otherwise. The findings might have a useful impact on the basic understanding of neural damage and myelination processes not only in MS but also in other neurodegenerative diseases. Better knowledge of the underlying causes of progressive nerve damage and impaired myelin regeneration will eventually lead to the development of novel treatments for people with PMS.

6. MATERIALS AND METHODS

6.1 Animals

6.1.1 Ethics, Consent, and Permission

Mice were kept at the animal housing facility of the San Raffaele Institute, Milan. We were committed to minimising animal suffering and reducing the number of mice, following the directives of the Council of the European Community, 24 November 1986 (86/609 / EEC). All experimental protocols were approved by the Ethics Committee for Animal Testing of the Italian Ministry of Health and performed according to the Institute of Animal Health guidelines and the commission of the San Raffaele Institute (IACUC 1172). All mice used in the experiments belong to the C57BL/6J strain.

6.2 Preparation of the compounds

The 273 purchased compounds were received from the partner of the BRAVEinMS consortium IRBM (Pomezia, Italy). Prior, IRBM has validated the identity of the purchased molecules and controlled the purity of the compounds through mass spectrometry analysis. Furthermore, each compound was dissolved in DMSO at a concentration of 25mM and dispensed with a robotic system in 96 multi-well plates. Upon receipt in Martino lab, compounds were re-distributed within five identical replicate plates, 5 mM concentration and stored at -80°C.

6.3 Differentiation of primary murine cortical neurons and astrocytes

Primary cultures of murine cortical neurons were obtained from C57BL/6J female mice at gestation stage E16.5-E17.5. The cortices were washed three times with HBSS without phenol red (Hanks' Balanced Salt solution, Sigma) containing 5 mM HEPES (Sigma) and subsequently enzymatically dissociated for 30 minutes at 37°C, with one solution containing: trypsin 1.25 mg/ml (Sigma, dissolved in HBSS-phenol red, Euroclone), DNase 30 µg/ml (Sigma, dissolved in Neurobasal medium, Gibco), CaCl₂ 5mM (Sigma) in HBSS-phenol red. Afterwards, enzyme activity was stopped using a complete Neurobasal medium (Gibco), 1% L-Glutamine (Gibco), 1% penicillin-streptomycin (Gibco), 0.5X B27 supplement (Gibco); 10% FetalClone III Serum (FCIII) HyClone). Cortical neurons were seeded at a density of 30,000 cells/ well in a 96-well multiwell plate (Falcon) and 200,000 cells/coverglass in 24-well multiwell plate, coated with 100 µg/ml Poly-D-Lysine (Sigma) and 3.5 µg/ml laminin (Sigma) in PBS 1X. After 4 hours

from the seeding, the complete medium was replaced with a serum-free Neurobasal medium. Cultures were maintained in a humidified CO₂ incubator (5% CO₂, 37°C), and half of the medium was changed every four days. The cytotoxicity/neuroprotective assays were performed between 13-14 days in vitro (DIV). To culture primary astrocytes, the same protocol was applied, except that astrocyte culture was Minimal essential media (MEM, Gibco), 1% L-Glutamine (Gibco), 1% penicillin-streptomycin (Gibco), containing 10% FBS the whole maintenance period. Astrocytes were cultured in T75 flasks and were split/expanded until P3-P4.

6.4 Differentiation of Neuro2A cells

The murine neuroblastoma Neuro2A (ATCC) line was cultured in DMEM medium (Lonza) in the presence of penicillin/streptomycin (P/S, Gibco) and 10% fetal bovine serum (FBS, Corning) at 37 °C, 5% CO₂ conditions. For differentiation, the cells were plated at a density of 3×10^3 cells/well in 96-multiwell plates and maintained in the standard growth media for 24 h. The next day, the standard growth media were replaced with the differentiation media: 4.5 g/L DMEM-high glucose (Gibco), 0.01% FBS, 100U/ml P/S, 10 µM retinoic acid (RA, Sigma). The protocol was modified from (Kumar & Katyal, 2018). Experiments were performed after 5-7 days of differentiation.

6.5. iPSC generation

Skin biopsies from 6 twin pairs (MS patients and healthy controls) discordant for the disease have been previously collected and generated at Neuroimmunology laboratory, OSR. In detail, skin biopsies were first divided into pieces and then cultured in a sterile serum-rich medium until fibroblasts spread from the tissue and grew exponentially. Human fibroblasts were maintained in DMEM containing 10% FBS, 2 mM L-glutamine (Gibco), 1×10^{-4} M nonessential amino acids (Gibco), 1 mM sodium pyruvate (Sigma), and 0.5% penicillin-streptomycin (P/S, Gibco). The explants were screened for the presence of mycoplasma using a standard PCR kit. Fibroblasts were expanded and cryopreserved at 1-2 million cells per vial in FBS and 10% DMSO or seeded immediately for reprogramming. For iPSCs generation, fibroblasts within fourth passages were used to avoid replicative senescence.

For hiPSC generation, fibroblasts were infected with the CytoTune™-iPS 2.0 Sendai Reprogramming Kit (Life Technologies). After one week, the transduced fibroblasts were plated on a feeder layer of mitotically inactivated with mitomycin C (Sigma Aldrich)

mouse embryonic fibroblasts (MEFs) (2.5×10^4 cells/cm²) in a DMEM supplemented with 20% KnockOut serum replacement (KSR, Gibco), 2 mM L-glutamine (Gibco), 0.1 mM nonessential amino acids (Gibco), 1 mM sodium pyruvate (Sigma), 0.02 mM β -mercaptoethanol (Calbiochem), 1% penicillin-streptomycin (P/S, Gibco), and 10 ng/ml FGF2 (Peprotech). The medium was changed every day, and colonies appeared 3 to 4 weeks later. After approximately one month, colonies with the correct morphology were picked and transferred to a Matrigel-coated (feeders free) culture in mTeSR™ (StemCell Technologies) medium. Colonies that reached at least passage five were assessed: for the absence of Sendai virus via qRT-PCR, their effective pluripotency (expression of pluripotency markers OCT4, NANOG, SOX2 evaluated by immunocytochemistry and qRT-PCR), and for their ability to differentiate into the three main germ layers via embryoid bodies formation (differentiation to the mesoderm, endoderm and neuroectoderm potential).

6.5.1 hiPSC differentiation into neural progenitors (NPCs) and neurons

The glutamatergic neuron differentiation protocol was modified from (Qi *et al*, 2017). First, neural progenitor cells (NPCs) were generated from hiPSCs by dual-SMAD inhibition. Briefly, at day 0, iPSC colonies (confluent at 70-80%) were washed with PBS Dulbecco's w/o calcium w/o magnesium (Euroclone), and hiPSC maintenance medium (mTeSR™, StemCell Technologies) was replaced with neural induction medium composed by DMEM/F12 medium (Gibco) supplemented with 1X N2 (Gibco), 0.5X B27 without RA supplement (Gibco). Small molecules were added fresh every media change, including 10 μ M SB431542 (Miltenyi) and 500nM LDN 193189 (R&D). This medium was kept until day 4 ("induction"). On day 4, cells were split (1:3) using Accutase®/Accumax™ (StemCell Technologies) dissociated solution. The entire medium was replaced daily up to days 14-16 until rosette formation ("patterning") was observed. On day 14-16, cells were detached by Accutase®/Accumax™ and re-plated on 96- or 24-multiwell plates coated with 100 μ g/ml poly-L-ornithine (Sigma)/5 μ g/ml laminin (Sigma)/ 2 μ g/ml human recombinant fibronectin for terminal differentiation in Neurobasal medium (Gibco) supplemented with 0.5x B27 (Gibco), 1X GlutaMAX (Gibco), 1X penicillin-streptomycin (P/S, Gibco), 20ng/ml BDNF (Peprotech), 500 μ M dbcAMP (Sigma), 200 μ M ascorbic acid (Sigma), 1 μ M PD0325901 (Tocris), 5 μ M SU5402 (Biovision), 3 μ M CHIR (Tocris), 5 μ g/ml human recombinant insulin (Gibco)

supplemented with Rock inhibitor Y-27632 (Millipore) (1:3000) at the seeding to reduce dissociation induced apoptosis. Half of the differentiation medium was changed every 3-4 days, supplemented with 1 $\mu\text{g}/\text{ml}$ laminin (Sigma) and 1-2 μM DAPT (Tocris) until terminal maturation of neuronal population (MAP2⁺ cells). Cultures were characterised by immunocytochemistry and RT-qPCR, and neuroprotective experiments were performed on days 30-40 of differentiation.

6.5.2 hiPSC differentiation into hSOX10 oligodendrocytes

6.5.2.1 hSox10 inducible vector

The expression of *SOX10* is related to the administration of doxycycline, meaning that the reverse-tTA (rtTA) binds Tet operator (tetO) in the presence of effector doxycycline. The binding of doxycycline triggers a conformational switch in rtTA, which allows tetO binding and expression of SOX10 and GFP. 1 $\mu\text{g}/\text{ml}$ doxycycline (Sigma) was added before sorting and at day1 of oligodendrocyte induction.

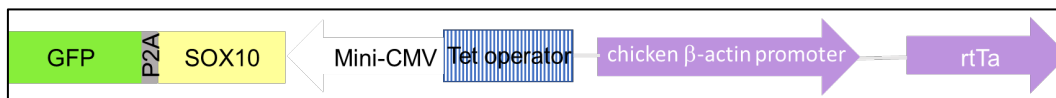


Figure. The map of inducible lentiviral *SOX10* plasmid.

6.5.2.2 Neural precursor generation

Neural precursors cells were generated from hiPSCs by Reinhardt differentiation protocol (Reinhardt *et al*, 2013). The expansion media for Reinhardt NPCs includes a base medium with freshly added supplements. Reinhardt base medium is a 1:1 mixture of DMEM/F12 (Gibco) and Neurobasal medium (Gibco), supplemented with 0.5X N2 (Gibco), 1X B27 without RA (Gibco), 1X GlutaMAX (Gibco), 1X penicillin-streptomycin (P/S, Gibco), supplemented with freshly added small molecules, including 3 μM CHIR (Tocris), 1 μM SAG (Millipore), 150 μM ascorbic acid (AA, Sigma) and 0.5X RevitaCell (RC, Gibco) when cells are being thawed or split.

6.5.2.3 hSOX10 oligodendrocyte differentiation

Reinhardt NPCs are plated on 50 $\mu\text{g}/\text{ml}$ polyornithine (Sigma)/10 $\mu\text{g}/\text{ml}$ laminin (Sigma) coated 96MW- 24MW- 6MW or T25 flasks in media consisting of DMEM/F12 (Gibco), 1X B27 without RA (Gibco), 0.5X N2 (Gibco), 1X GlutaMAX (Gibco), 1X penicillin-

streptomycin (Gibco), supplemented with 10ng T3 (Peprotech), 10ng rhPDGF (Peprotech), 10ng rhNT3 (Peprotech), 1 μ M SAG (Millipore), 10ng IGF-1 (Peprotech), 200 μ M AA (Sigma) and 1 μ g/ml doxycycline (Sigma) from days 1 to 3 of differentiation. From days five until days of 26 of differentiation, Neurobasal base media consisting of DMEM/F12, 1X B27 without RA, 0.5X N2, 1X GlutaMAX, 1X penicillin-streptomycin, supplemented with 60ng T3, 10ng rhNT3, 10ng IGF-1, 200 μ M AA, 100 μ M dbcAMP. 1 μ g/ml doxycycline was added until day 14 of differentiation. A freshly thawed aliquot of AA (ascorbic acid) was used for every medium change. 50% of media was changed three times a week during 26 days of differentiation.

6.6 3D neural spheroids (BrainSpheres)

Neural progenitor cells (NPCs) were derived from Induced Pluripotent Stem Cells (iPSC) by seven days neural induction (Neurobasal® Medium, Neural Induction Supplement, 50X, Gibco) followed by NPCs expansion (4-6 days). In detail, 70-80% confluent iPSC colonies were detached with Accutase® Cell Dissociation Reagent and plated on Matrigel (Corning) coated 6-well plate, with a density of 2.5-3 \times 10⁵ iPSCs per well, supplemented with RevitaCell™ (1:100), Gibco. On day 1 of iPSC seeding, the medium was changed to Neural Induction medium, followed by complete media change every other day. On day 7 of neural induction, NSCs (P0) were expanded in Neural Expansion medium consisting of Neurobasal® Medium, Advanced™ DMEM/F-12 (Gibco) and Neural Induction Supplement (Gibco). NSCs were detached with Accutase, and 2 \times 10⁶ cells were plated in a low attachment 6-well plate (Falcon Fisher Scientific) in a neural expansion medium. After 48h, the medium was changed to spheroids differentiation medium (Neurobasal electro medium (Gibco), 0.5X B27 supplement electro (Gibco), 1X Penicillin/Streptomycin/Glutamine (Gibco), 0.02 μ g/ml human recombinant GDNF (Peprotech), 0.02 μ g/ml human recombinant BDNF (Peprotech). The spheroids were differentiated and matured for twelve weeks under constant gyratory shaking (88 rpm, 19mm orbit diameter) in the cell culture incubator (37 °C, 5% CO₂). Half of the medium was exchanged three times a week.

6.6.1 Neuroprotective assay and sholl analysis of neurite outgrowth of 3D neural spheroids (BrainSpheres)

BrainSpheres were differentiated as described above. The day before the experiment, BrainSpheres were pre-treated with Casopitant 1 μM for 24h and then exposed to 0-50 μM -100 μM - μM of tert-butyl hydrogen peroxide (TBHP, Sigma) for two hours in Neurobasal medium deprived of antioxidants (0.5X B27 minus antioxidants, Gibco). After exposure to the stressor, BrainSpheres were seeded on 100 $\mu\text{g}/\text{ml}$ polyornitine/5 $\mu\text{g}/\text{ml}$ laminin-coated 4-well chamber slides (Nunc[®]Lab-Tek[®]II Chamber Slide[™]). After 72 h, the BrainSpheres were fixed in 4% PFA, stained with neuronal marker beta-III-Tubulin (1:1000, Biolegend) and astrocyte marker GFAP (1:500, Dako) as described above and imaged using a confocal microscope Mavig RS-G4. Neurite outgrowth was analysed using the Sholl ImageJ Software. For data analysis, the number of intersections from the spheroid centre was calculated. Significance was calculated using the area under the curve (AUC) analysis. ANOVA with Dunnett's post-test was performed comparing each treatment with the control ($p < 0.05$). Intersections were counted within 0.15 cm diameter.

6.7 Cytotoxic and neuroprotective assay on primary murine cortical neurons

To assess the neuroprotective activity of 160 selected non-toxic compounds on primary murine cortical neurons, 13DIV cultures were pre-treated with 1 μM compounds for 3 hours, followed by 24 hours chronic stimulation with 8 μM N-Methyl-D-aspartic acid (NMDA, Sigma) to induce neuronal damage. Each test plate included: a negative control (untreated), vehicle-treated control (0.02% vol/vol DMSO), a positive neurotoxic control - staurosporine 0.1 μM , a stressor - NMDA 8 μM , a positive neuroprotective control – 300 μM N-acetylcysteine (NAC, Sigma), and a combination of stressor + neuroprotective molecule (NMDA+NAC). Cell viability was measured with Cell Counting Kit-8 assay compared to NMDA-treated control.

In oxidative stress assay settings, primary murine cortical neurons (13DIV) cultures were pre-treated with 1 μM compounds for 3 hours, followed by 24 hours chronic stimulation with 20 μM TBHP to induce neuronal damage. Each test plate included: a negative control (untreated); vehicle-treated control (0.02% vol/vol DMSO); a positive neurotoxic control – either 0.1 μM staurosporine (Sigma) or TBHP 20 μM ; a positive neuroprotective control –2.5nM mitoquinone (MitoQ, MedChemExpress); and a

combination of stressor plus a neuroprotective molecule (TBHP + MitoQ). Cell viability was measured with Cell Counting Kit-8 assay and compared to TBHP-treated control.

6.8 Morphological integrity evaluation of primary murine cortical neurons

Neuronal structural integrity after NMDA-induced cytotoxicity was evaluated by MAP2 staining. Mouse cortical neurons (14DIV) cultured in MW96 plates were fixed with 4% paraformaldehyde (PFA, Sigma). Fixed cells were incubated with blocking solution (PBS 1X, donkey serum 5%, Triton 0.1%) for 1-hour, primary antibody (rabbit α -MAP2, 1:250, Millipore) was applied in the same solution overnight at +4°C. The following day cells were washed three times with PBS 1X + Triton 0.1% at RT and incubated with secondary antibody donkey anti-rabbit Alexa Fluor 555, (1:1000) (Molecular Probes, ab150074) diluted in PBS 1X + Triton 0.1% for one hour at RT. Nuclei were stained with 4'-6-diamidino-2-phenylindole (DAPI, DAKO). Microscopy was performed using ArrayScan™XTI (ThermoFisher) imaging platform. Fifteen images per well were acquired and analysed by CellProfiler. Total neurite length and the total number of non-trunk branches were analysed. The total neurite length and the number of branching were evaluated from 15 images/well; each compound or control was tested in triplicates. The total neurite length and the total number of branches were converted to a standardised Z-score using the formula: $X_{ij} = ((X_{ij} - \mu)/\sigma)$, where x_{ij} is the raw measurement of the compound located in well (i, j), and μ and σ are, respectively, the mean and the standard deviation of all measures of the plate (Malo *et al*, 2006).

6.9 Cytotoxic and neuroprotective assay on human hiPSC-derived neurons

Neuroprotective experiments were performed using hiPSC-derived glutamatergic neurons from three healthy controls lines cultured for 30-40 DIV. Cells were pre-treated for 24h with the drugs at 1 μ M, vehicle (DMSO) or 5nM Mito-Q as a positive control. The next day, cells were incubated with 100 μ M TBHP (Sigma) for two hours. The medium was replaced, and the viability was evaluated on the following day by the CCK8 viability assay kit (Dojindo). Cell viability was expressed as standardised Z score and compared to TBHP-treated cells.

6.10 Functional oxidative stress assay (CellROX)

ROS generation was determined using a CellROX Deep Red Kit (Life Technologies, Carlsbad, CA, USA). CellROX is a cell-permeable reagent, non-fluorescent or very

weakly fluorescent in a reduced state. At the same time, it exhibits a robust fluorogenic signal upon oxidation, therefore reflecting the ROS levels in the cell cytoplasm. In detail, NPCs from two twin pairs were seeded on a twenty-four-well plate and differentiated for 30-40 days to mature (MAP2+) neurons. The day before the experiment, cells were pre-treated with Casopitant 1 μ M for 24h. On the day of the experiment, CellROX Deep Red reagent was added to the samples at a final concentration of 1 μ M and incubated for 10 min at 37 °C in the dark. The cells were exposed to 100 μ M TBHP for two hours in a Neurobasal medium deprived of antioxidants (NB-AO). After exposure to the stressor, the medium was removed, and the cells were washed three times with PBS. Afterwards, cells were harvested with Accumax (Sigma) and stained with LIVE/DEAD™ Cell Stain Kit (Invitrogen). Subsequently, cells were fixed with 4% PFA and then subjected to flow cytometry using a FACS flow cytometer (BD Biosciences) (excitation/emission wavelengths: 640/665 nm for CellROX deep red, 375/512nm for LIVE/DEAD). Approximately 1×10^4 cells were analysed for each sample.

CellROX experiments in N2A were performed as follows: N2A cells were used 72h after Sigmar1 siRNA-silencing or non-transfected (mock-treated). Cells cultured in DMEM + 0.1% FBS were pre-treated with Casopitant 1 μ M for 3h. CellROX solution 1 μ M was added before addition of TBHP 50 μ M for 1h. After incubation at 37C, cells were stained with Hoescht nuclear staining (1:5000), washed with PBS 1x and FluoriBrite solution suitable for live imaging (DMEM without phenol red) was added to the cells. Live imaging was performed using ArrayScan™XTI (ThermoFisher) imaging platform.

6.11 Cytotoxic and neuroprotective assay on Neuro2A cell line

Neuroprotective experiments were performed using Neuro2A, a neuronal-like cell line differentiated for 5-7 days. Cells were pre-treated for three hours with 1 μ M of compounds, vehicle (DMSO), or the positive controls of neuroprotection 5nM Mito-Q or 200 μ M NAC. Cells were then incubated for two hours with 5 μ M of TBHP in a serum-deprived differentiation medium, and the viability was evaluated on the following day by CCK8 viability assay kit (Dojindo).

6.12 Cellular characterisation

6.12.1 Immunofluorescence

Cells were fixed with 4% paraformaldehyde (PFA, Sigma) for 10 minutes washed three times with PBS 1X. If the target antigen was nuclear, a pre-permeabilization protocol with 0.1% PBS-Triton X-100 (Sigma) for 30 min was followed, and subsequent washes were performed in 0.1% Tween-20 in PBS 1X and appropriate serum. In the case of a cytoplasmic antigen, pre-permeabilization was omitted. The possible non-specific binding sites for antibodies were blocked for one hour with a blocking solution consisting of PBS 1X+ 0.1% Triton X-100 and 5% normal goat serum (NGS, Sigma) or 5% donkey serum (DKS, Sigma) based on the species of secondary antibodies. In the case of a cell surface antigen, the detergent was omitted in the blocking phase and during washing. The primary antibodies were resuspended in the blocking solution, and then the slides/coverslips were incubated overnight at 4°C. The slides/coverslips were washed three times with PBS 1X + 0.1% Triton X-100. Secondary antibodies were resuspended in the same blocking solution, and the slides/coverslips were incubated for two hours in the dark at room temperature. Subsequently, three washes were carried out with PBS 1X+ 0.1% Triton X-100, and then nuclear labeling was performed by DAPI (DAKO) in PBS 1X (1:10000) for 5 min at room temperature. Three washes were performed with PBS 1X, and the slides/coverslips were mounted on a specimen slide with mounting solution (DAKO). The images were acquired with a LEICA SP5 confocal microscope at a magnification of 40X or 63X. The antibodies used for the characterization: Tuj1 (Mouse, 1:500, Biolegend); vGLUT1 (Guinea Pig, 1:100, Synaptic System); Glua1/2 (Rabbit, 1:100, Synaptic System); PAX6 (Rabbit, 1:300, Biolegend); GFAP (Rabbit, 1:500, DAKO); GFAP (Rat, 1:100, Millipore); MAP2 (Rabbit, 1:250, Millipore); Synapsin1 (Mouse, 1:200, Synaptic System); Synaptotagmin (Mouse, 1:200, Millipore);_Nestin (Mouse, 1:500, Millipore); SOX2 (Rabbit, 1:250, Abcam); NMDAR1 (Rabbit, 1:250, Invitrogen); MBP (Rat, 1:50, Millipore); GalC Mouse, 1:200, Millipore); O4 (Mouse, IgM, 1:200, Millipore); NK1R (Rabbit, 1:100, Novus Biological); SIGMAR1 (Rabbit, 1:100, Invitrogen); Anti-KDEL (Mouse, 1:200, ENZO), Histamine H3 (Rabbit, 1:200, Invitrogen). The secondary antibodies used for immunofluorescence were AlexaFluor, Invitrogen (1:1000):

6.12.2 BrainSpheres immunocytochemistry

BrainSpheres plated in Nunc slide chambers were washed three times for 5 min with PBS 1X and fixed with 4% PFA for one hour at room temperature, followed by two washing steps with PBS 1X. BrainSpheres were incubated for one hour in a blocking solution consisting of 5% normal goat serum (NGS) in PBS with 0.4% Triton-X100 (Sigma). BrainSpheres were then incubated for 48 h at 4C with a combination of primary antibodies (Tuj1 and GFAP) diluted in PBS containing 3% NGS and 0.1% Triton-X100. After incubation, BrainSpheres were washed three times for 15 minutes in PBS 1X and incubated one hour with secondary antibodies diluted in PBS with 3% NGS at room temperature. Subsequently, BrainSpheres were washed three times for 5 minutes each with PBS; the nuclei were stained with DAPI (1:10000, DAKO) for 10 min. BrainSpheres were mounted on glass slides by using Vectashield mounting medium. The images were taken using a Mavig RS-G4 confocal microscope.

6.12.3 EAE spinal cords immunohistochemistry

6.12.3.1 Hematoxylin and Eosin (H&E) staining

The sections were air-dried for several minutes to remove moisture, dehydrated with a series of EtOH, 5 minutes each (50%-70%-100%-50%-70%), then sections were stained with filtered 0.1% Mayer's Hematoxylin solution for 10 minutes in a 50 ml conical tube. Then, in a Coplin jar, sections were rinsed in cool running ddH₂O for 5 minutes and then dipped in 0.5% Eosin (1.5g dissolved in 300ml of 95% EtOH) 12 times. Later, sections were dipped in ddH₂O until the eosin stopped streaking. Next, sections were dipped in 95% for 60 seconds and in 100% EtOH for 10 minutes. Finally, sections were dipped in Xylene several times, synthetic resin mounting reagent (DPX) was added and mounted with coverglass.

6.12.3.2 Luxol fast blue staining

The Luxol Fast Blue Stain (LFB, myelin stain) is designed for staining myelin/myelinated axons and Nissl substance on formalin-fixed, paraffin-embedded tissue as well as frozen tissue. First, sections were rinsed with 100% ethyl alcohol and rinsed with ddH₂O afterwards. Secondly, slides were incubated with Luxol Fast Blue 0.1% Solution overnight at 56°-60°C. Slides were rinsed thoroughly in distilled water and

differentiated the section by dipping in 0.1% solution of lithium carbonate for 10-15 minutes. The staining was differentiated by repeatedly dipping in 70% EtOH until the myelin was stained blue and the background was clear. Slides were rinsed in distilled water and incubated with 0.8% periodic acid for 10 minutes, then rinsed again in distilled water followed by incubation with Schiff's Reagent at RT for 20'. Finally, slides were quickly rinsed in the washing solution, running tap water, and quickly dehydrated with three changes of absolute alcohol (50%-70%-100% ETOH). Slides were then mounted in synthetic resin (DPX).

6.12.3.3 Bielschowsky's silver stain

Bielschowsky's silver stain is used to stain axons and neurofibrils in the central nervous system. First, the slides were dehydrated with a series of EtOH, 5 minutes each (100%-70%-50%). Secondly, the sections were placed in the silver solution for 20 min and kept this solution aside after incubation. Then slides were washed 2X for 3 minutes in dH₂O and concentrated (32%) ammonium hydroxide solution was added dropwise with stirring to the silver nitrate solution. This allowed clearing the silver solution. After, the sections were incubated in previously treated ammonia solution silver solution for 15 minutes in the dark. Then sections were washed in ddH₂O containing 2-5 drops of 32% ammonium hydroxide solution for 2 minutes at room temperature. Finally, the development solution (20 ml 37% formaldehyde, 100 ml dH₂O, 1-2 drops of concentrated nitric acid and 0.5g citric acid) was added to the previously used silver solution and slides were immersed until the staining development. Then slides were rinsed with tap water, ddH₂O and exposed to 5% sodium thiosulfate solution to inactivate silver reaction. As the last step, slides were washed in dH₂O, dehydrated in 50%-70%-100% EtOH, and were mounted.

6.12.4 RNA extraction and reverse transcription

The RNA was extracted using the RNeasy mini-kit (74104, Qiagen) following the instructions given by the manual. DNase I treatment was performed to avoid genomic DNA contamination. RNA was eluted in 30µl of RNase-free water and quantified using the Nanodrop (Thermo Fisher Scientific). 1000ng/500ng of RNA was retrotranscribed with Superscript IV (Invitrogen) following the guidelines given in the manual using a mix of primer Oligo dT, random hexamers, dNTPs, 5x cDNA synthesis buffer, 0.1M DTT, RNase inhibitor and Superscript IV transcriptase. The reverse transcription program was performed following the protocol: 23°C-10', 55°C-10', 80°C-10' and 4°C in maintenance.

6.12.5 Polymerase Chain reaction (PCR) and Real-Time Polymerase Chain reaction (RT-qPCR)

The cDNA obtained from the Neuro2A cell line, mouse cortical neurons and human iPSC-derived neurons were used for the molecular characterization of neuronal differentiation and maturation genes by TaqMan RT-qPCR assay, for target validation by qPCR and siRNA experiments by SYBR green RT-qPCR. cDNA samples were stored at -20°C until the analyses were performed.

TaqMan analyses were performed with TaqMan™ Fast Advanced Master Mix on QuantStudio™ 3 System following the thermal cycle protocol: Hold 50°C for 2 minutes, hold 95°C 20 seconds, denature 95°C 1second, anneal/extend 60°C 20 seconds, repeated for 40 cycles, using 20ng of cDNA for each analysed sample. The relative fold gene expression analysis was done using the $2^{-\Delta\Delta CT}$ method. The following TaqMan probes were used for the characterization of the human neurons: GAPDH (Hs99999905_m1), PAX6 (Hs00240871_m1), NESTIN (Hs04187831_g1), SOX2 (Hs01053049_s1), TUBB3 (Hs00801390_s1), MAP2 (Hs00258900_m1), SLC17A7 (Hs00220404_m1).

Voltage-gated ion channels TaqMan array (Applied Biosystems, Catalog number: 4414099) was performed on hiPSC-derived neurons from two twin pairs CTR4-RR16 and CTR7-RR24 differentiated for 30 days and co-cultured for 30 days with primary murine astrocytes. cDNA templates were prepared as described above. Equal proportions of 10µl mix containing 10ng of cDNA resuspended in nuclease-free water and 10µl of TaqMan™ Fast Advanced Master Mix (Applied Biosystems) were added with precision multichannel pipette in the pre-designed plate. The plate was covered with MicroAmp Optical adhesive film, spined 1 minute at 1000 rpm and readout was performed on QuantStudio™ 3 System following the thermal cycle protocol: hold 95°C for 20 seconds, denature 95°C 1second, anneal/extend 60°C for 20 seconds, repeated for 40 cycles. The relative fold gene expression analysis was done using the $2^{-\Delta\Delta CT}$ method.

The siRNA experiment readout was performed by the real-time RT-qPCR consisting of SYBR Green reaction mix (Bio-Rad Laboratories Inc.), 0.05 µM of each forward and reverse primers, 5ng of cDNA and RNase-free water up to a volume of 20µl. The PCR thermal cycling was performed in QuantStudio™ 3 System following the protocol: hold

95°C for 2 minutes, denature 95°C for 5 seconds, anneal/extend at 62°C for 30 seconds, repeated for 40 cycles. The relative fold gene expression analysis was done using the $2^{-\Delta\Delta CT}$ method.

For the conventional PCR, the master mix (one per molecular target) was prepared at a final volume of 25µl which contained 5X cDNA synthesis buffer (Promega), 0.2 mM of dNTPs, 1.5 mM MgCl₂, 1 µM of forward and reverse primers, 0.5µl of GoTaq DNA polymerase (Promega) and 20-40 ng of cDNA. The PCR thermal cycling was performed in Eppendorf Mastercycler thermal cycler following the protocol: denaturation at 95°C for 2 minutes, followed by 35 cycles at 95°C for 30 seconds, annealing for 30seconds at 57°C for mSIGMAR1; at 59°C for hTACR1 pair1 and hSIGMAR1; at 60°C for hTACR1 pair2. The extension was 30 seconds or 1 minute at 72°C, and the final extension was at 72°C for 10 minutes. To determine the band size, the amplification products were run on 2% agarose gel and stained with Bioatlas Clear DNA stain. Following primer sequences were used:

TACR1 Human primers pair1

Forward GCCTGTTCTACTGCAAGTTCCAC

Reverse CACAGATGACCACTTTGGTGGC

product length = 156 bp

TACR1 Human primers pair 2

Forward AACCCCATCATCTACTGCTGC

Reverse ATTTCCAGCCCCTCATAGTCG

Product length = 107 bp

TACR1 Mouse

Forward GTTCATCCAGCAGGTCTACCTG

Reverse TCACCAGCACTGATGAAAGGGC

SIGMAR1 Human

Forward GTCCGAGTATGTGCTGCTCTTC

Reverse GAAGACCTCACTTTTGGTGGTGC

product length = 139/162 bp

SIGMAR1 Mouse

Forward GGACCATGAGCTTGCCTTCT

Reverse CCCAGTATCGTCCCGAATGG

Product length = 209 bp

HRH3 Human

Forward TCTTCCTGCTCAACCTCGCCAT

Reverse ACTACCAGCCACAGCTTGCAGA

product length = 127 bp

HRH3 Mouse

Forward CGAGCCCTGTGAGCCTG

Reverse GCAGAAGGCACCCACGAG

product length = 285 bp

6.12.6 Patch-clamp electrophysiology

To assess whether the hiPSC-derived neurons were mature and electrophysiologically functional, patch-clamp analyses were performed. Each slide containing neurons was placed on a recording chamber mounted on the worktable of the Olympus BX51WI optical microscope, equipped with differential interference contrast optics (DIC; Semrock, Rochester, NY). The cells were perfused continuously (2-3 ml/min) with artificial cerebrospinal fluid (ACSF) containing (in mM): 125 NaCl, 2.5 KCl, 1.25 NaH₂PO₄, 2 CaCl₂, 25 NaHCO₃, 1 MgCl₂ and 11 D-glucose, saturated with 95% O₂, 5% CO₂ (pH 7.3). Whole-cell patch-clamp recordings were made on individual cells using microelectrodes filled with an intracellular solution containing the following reagents (in mM): 124 KH₂PO₄, 2 MgCl₂, 10 NaCl, 10 HEPES, 0.5 EGTA, 2 Na₂-ATP, 0.02 Na-GTP (pH 7.2, titrated with KOH; peak resistance electrodes: 6-8 MΩ). All recordings were made with an amplifier MultiClamp 700B amplifier interfaced with a PC via Digidata A/D card 1440A (Molecular Devices, Sunnyvale, CA, USA). Data were recorded using pClamp10 software (Molecular Devices) analysed with Prism 5 (GraphPad Software, Inc., La Jolla, CA). Tracks in voltage- and current-clamp were sampled at the frequency of 10 kHz and filtered at 2 kHz cutoff frequency.

6.12.7 Glutamate release measure

Extracellular concentration of glutamate was measured in hiPSC-derived neurons at days 30, 40, and 50 of differentiation with luminescence-based Glutamate-Glo assay (Promega). In detail, 5µl of media was collected from three wells of MW96 plate

containing hiPSC-derived neurons before and immediately after the challenge with 60mM KCl solution and was diluted in 95µl of PBS 1x. The collected supernatants were kept at -20C until the readout was performed. The cell viability of the same wells used for normalization was measured by CellTiter-Glo assay (Promega). 10ml of CellTiter-Glo buffer and 1 vial of lyophilized substrate were mixed and added 1:1 ratio to the wells containing hiPSC-derived neurons. The plate was equilibrated for 30 minutes at room temperature and the luminescence readout was performed on Berthold Mithras luminometer. On the day of the glutamate readout, the Glutamate Detection reagent was prepared according to the manufacturer's protocol. In detail, 5ml Luciferin Detection solution, 55µl Reductase, 55µl Reductase Substrate, 100µl Glutamate Dehydrogenase, 275µl NAD were mixed, sufficient for 100 reactions in 96-well plates (50µl of supernatant + 50 µl of Glutamate Detection Reagent). The plate was shaken for 30-60 seconds and incubated for 60 minutes at room temperature. The luminescence readout was performed on Berthold Mithras luminometer. The glutamate titration curve was performed using twofold serial dilutions of 10mM glutamate prepared in PBS. Negative control (buffer only) was used to determine assay background.

6.12.8 Western blot and SDS-page analysis

To extract cellular proteins, cultured cells were collected, washed once with ice-cold PBS 1X, and solubilized in cell lysis buffer (RIPA Lysis Buffer: NaCl 150mM, 5mM EDTA, 50mM Tris pH 8.0, 1% NP-40 (IGEPAL CA-630), 0.5% sodium deoxycholate, 0.1% SDS in H₂O) with freshly added protease inhibitor (1:100) and phosphatase inhibitor (1:10). The protein content of cell lysates was quantified with bicinchoninic acid (BCA) assay (BCATM Protein Assay Kit, Thermo-Scientific). The equal amounts of proteins were diluted with Laemmli buffer 4X and loaded onto 10% (or 4-20%) Mini-PROTEAN[®] TGXTM precast gels (Bio-Rad). The Trans-Blot Turbo Transfer System was used to transfer proteins onto the nitrocellulose membrane. Proteins were visualized with reversible Ponceau staining and then were washed with ddH₂O. The membrane was then incubated with a blocking solution containing 5% skimmed milk in 0.1% TBS-Tween20. Primary antibody (anti-Sigmar1, 1:1000, Sigma) was diluted in 0.1% TBS-Tween20 solution containing 5% skimmed milk and incubated overnight with horizontal shaking at 4°C followed by three washes in 0.1% TBS-Tween (10 minutes each) on the next day. The secondary antibodies (anti-rabbit HRP, 1:3000, Bio-Rad) were prepared in the same

solution as primary antibodies and incubated for 1 hour at room temperature with horizontal shaking. The membrane was developed by Clarity Max™ Western ECL Substrate (Bio-Rad) and chemiluminescence signal was detected by ChemiDoc MP Imaging System (Bio-Rad). Densitometric analysis was performed with ImageLab (Bio-Rad Laboratories, Inc. Version 6.1.0 build 7). Beta-actin was used as a normaliser for quantitative analysis.

6.13 Small RNA interference

Neuro-2a cells were seeded 24h before transfection onto 24 well plates (100000 cells /well) in Dulbecco's minimal essential medium (DMEM) supplemented with 10% heat-inactivated fetal bovine serum (FBS) and 1X penicillin/streptomycin in a 5% CO₂ incubator at 37 °C. The next day, cells were transfected with 15 pmol SIGMAR1-siRNAs for 24-48-72h using Lipofectamine 3000 (Invitrogen) in media without serum. As a positive control of transfection, 60ng/well of GFP DNA was used. In detail, Lipofectamine 3000 Reagent was diluted in an Opti-MEM medium (Gibco). A master mix of control GFP DNA was prepared by diluting DNA in Opti-MEM Medium, with a P3000 reagent. The master mix of siRNA was prepared by diluting siRNA in an Opti-MEM medium to achieve the desired concentration. Diluted siRNA and DNA master mixes were added to each tube of diluted Lipofectamine 3000 Reagent (1:1 ratio) and incubated for 10-15 minutes at room temperature. Then DNA-lipid and siRNA-lipid complexes were added to cells. For confirmation of S1R knockdown, cells were harvested 24h-48h-72h post-transfection and lysed in RIPA buffer for western blot analyses or with RLT buffer for gene expression analyses. SIGMAR1 siRNA and non-targeting negative control siRNA (scrambled siRNA) were purchased from Eurofins.

Mouse Sigmar1 1 small interfering (si)RNA
sense, 5'-ACACGUGGAUGGUGGAGUA -3',
antisense, 3'-UGUGCACCUACCACCUCAU- 5'

Mouse Sigmar1_2 small interfering (si)RNA
sense, 5'-GGACAUACAUACUUGUACA -3',
antisense 3'-CCUGUAUGUAUGAACAUUGU-5'

Mouse Sigmar1_3 small interfering (si)RNA
Sense 5'-ACUUCGUCUUCUCUAGAGA-3',
Antisense 3'-UGAAGCAGAAGAGAUCUCU-5'

Negative controls

Non-Specific Control 1 (31% GC content) UAAUGUAUUGGAACGCAUA

Non-Specific Control 2 (47% GC content) AGGUAGUGUAAUCGCCUUG

6.14 Induction of MOG-EAE and clinical follow-up

Eight-week-old C57BL6/J female mice received a subcutaneous injection of 200µg MOG₃₅₋₅₅ peptide (ESPIKEM) emulsified in the complete Freund's adjuvant containing 200µg Mycobacteria tuberculosis (Beckton Dickinson). On days 0 and 2 post-immunisation, 200 ng pertussis toxin (Quadrantech Diagnostics LTD) were administered by intraperitoneal injection. Mice were weighed and scored for clinical signs daily according to a 5-score EAE scale. Casopitant (100 mg/kg) and Bavisant (30mg/kg) were administered by oral gavage in a therapeutic setting starting from day 14 post-immunisation, once or twice daily, until day 42 post-immunisation. Control animals received Methocell (0.5% methylcellulose) orally twice daily as a sham treatment. The grading system for clinical assessment of EAE was performed as follows : 0- healthy animal; 1- limp tail; 2-hind limb weakness; 3-partial paralysis of the hind limbs and urinary incontinence; 4-weakness of the forelimbs and complete paralysis of the hind limbs; 5-death/moribund (Miller & Karpus, 2007).

6.15 Signaling pathways network analysis via SPOKE

The Neighbourhood Explorer allows interactively finding and viewing specific “neighbourhoods” within SPOKE. The search can be restricted to a specific node and edge types and by edge value. The resulting network is displayed with colour-coding by node type, with detailed information for any node or edge popping up on mouseover. Sets of terminal nodes (“leaf” nodes) are grouped into rectangles that can be collapsed to simplify the view. The network can be extended further from any node(s) of interest by one or more additional rounds of searching. The drug query was performed by searching the compound by ChEMBL identifier, for example, ChEMBL1672054 for Casopitant, and ChEMBL2103862 for Bavisant, respectively, to limit the results to a reasonable number of nodes and edges the set options before submitting the search were selected. For the nodes selection included: “Compound”, “Disease”, “Gene”, “Protein”. The selection of the edge included: “Compound-binds-Protein”, “Compound-downregulates-Gene”, “Compound-upregulates-Gene”, “Disease-associated-Gene”, “Gene-encode-Protein”, “Gene-participates-biological process”.

The filter nodes included: the Compound max phase $\geq [\text{minPhase}]$ – a minimum value of the maximum clinical trial phase a compound has reached (for treating any disease) was set to 1. Compound-treats-Disease phase $\geq [\text{minPhase}]$ – minimum value of the maximum clinical trial phase the compound has reached as a treatment for the specific disease was set to 1 as well. All other search limits were used as default.

6.16 Statistical analyses

Statistical analyses were performed using a one-way ANOVA test followed by Dunnett multiple test adjustment corrections for a normally distributed data comparing more than two variables; a nonparametric Kruskal-Wallis test with Dunn's multiple comparison correction for a non-normally distributed data comparing more than two variables; Normality of data distribution was checked by Shapiro-Wilk normality test; False discovery rate correction was performed by Benjamini-Hochberg (Figure 5) or Benjamini, Krieger and Yekutieli (Figure 12) methods; Spearman's rank correlation performed for the correlation analyses; Pairwise comparisons were performed with the Mann-Whitney test for non-normally distributed data, and with unpaired t-test for a normally distributed data. P values ≤ 0.05 were considered significant. Statistics were generated using the GraphPad Prism 7.0 software.

7. REFERENCES

- 't Hart BA, Gran B & Weissert R (2011) EAE: imperfect but useful models of multiple sclerosis. *Trends Mol Med* 17: 119–125
- Abreu CM, Gama L, Krasemann S, Chesnut M, Odwin-Dacosta S, Hogberg HT, Hartung T & Pamies D (2018) Microglia Increase Inflammatory Responses in iPSC-Derived Human BrainSpheres. *Front Microbiol* 9: 1–12
- Absinta M, Lassmann H & Trapp BD (2020) Mechanisms underlying progression in multiple sclerosis. *Curr Opin Neurol* 33: 277–285
- Absinta M, Maric D, Gharagozloo M, Garton T, Smith MD, Jin J, Fitzgerald KC, Song A, Liu P, Lin JP, *et al* (2021) A lymphocyte–microglia–astrocyte axis in chronic active multiple sclerosis. *Nature* 597: 709–714
- Absinta M, Sati P, Masuzzo F, Nair G, Sethi V, Kolb H, Ohayon J, Wu T, Cortese ICM & Reich DS (2019) Association of Chronic Active Multiple Sclerosis Lesions with Disability in Vivo. *JAMA Neurol* 76: 1474–1483
- Absinta M, Sati P, Schindler M, Leibovitch EC, Ohayon J, Wu T, Meani A, Filippi M, Jacobson S, Cortese ICM, *et al* (2016) Persistent 7-tesla phase rim predicts poor outcome in new multiple sclerosis patient lesions. *J Clin Invest* 126: 2597–2609
- Airas L, Nylund M & Rissanen E (2018) Evaluation of microglial activation in multiple sclerosis patients using positron emission tomography. *Front Neurol* 9: 1–10
- Almsned F, Lipsky RH & Jafri MS (2021) Transcriptomic analysis of Multiple Sclerosis patient-derived monocytes by RNA-Sequencing for candidate gene discovery. *Informatics Med Unlocked* 23: 100563
- Alroughani R & Boyko A (2018) Pediatric multiple sclerosis: a review. *BMC Neurol* 18: 27
- Amin ND & Paşca SP (2018) Building Models of Brain Disorders with Three-Dimensional Organoids. *Neuron* 100: 389–405
- Amit B, Lama F, Boli F, J. DP, Aja R, Christine G, A. CP, Emmanuelle W, L. HS, Jiameng Z, *et al* (2010) Abnormal B-cell cytokine responses a trigger of T-cell-mediated disease in MS? *Ann Neurol* 67: 452–461
- Arun T, Tomassini V, Sbardella E, De Ruiter MB, Matthews L, Leite MI, Gelineau-Morel R, Cavey A, Vergo S, Craner M, *et al* (2013) Targeting ASIC1 in primary progressive multiple sclerosis: Evidence of neuroprotection with amiloride. *Brain* 136: 106–115
- Axelsson M, Malmeström C, Nilsson S, Haghighi S, Rosengren L & Lycke J (2011) Glial fibrillary acidic protein: A potential biomarker for progression in multiple sclerosis. *J Neurol* 258: 882–888

- Ayrignac X, Le Bars E, Duflos C, Hirtz C, Maleska Maceski A, Carra-Dallière C, Charif M, Pinna F, Prin P, Menjot de Champfleur N, *et al* (2020) Serum GFAP in multiple sclerosis: correlation with disease type and MRI markers of disease severity. *Sci Rep* 10: 1–6
- Azevedo CJ, Kornak J, Chu P, Sampat M, Okuda DT, Cree BA, Nelson SJ, Hauser SL & Pelletier D (2014) In vivo evidence of glutamate toxicity in multiple sclerosis. *Ann Neurol* 76: 269–278
- Baden P, De Cicco S, Yu C & Deleidi M (2019) Immune Senescence and Inflammaging in Neurological Diseases. *Handb Immunosenescence*: 2283–2303
- Balashov K (2020) Drugs in development for multiple sclerosis. *Pract Neurol*: 40–43
- Baldassari LE & Fox RJ (2018) Therapeutic Advances and Challenges in the Treatment of Progressive Multiple Sclerosis. *Drugs* 78: 1549–1566
- Baranzini SE, Mudge J, Velkinburgh JC Van, Khankhanian P, Khrebtukova I, Miller NA, Zhang L, Farmer AD, Bell CJ, W R, *et al* (2010a) Genome, epigenome and RNA sequences of monozygotic twins discordant for multiple sclerosis. *Nature* 464: 1351–1356
- Baranzini SE & Oksenberg JR (2017) The Genetics of Multiple Sclerosis: From 0 to 200 in 50 Years. *Trends Genet* 33: 960–970
- Baranzini SE, Srinivasan R, Khankhanian P, Okuda DT, Nelson SJ, Matthews PM, Hauser SL, Oksenberg JR & Pelletier D (2010b) Genetic variation influences glutamate concentrations in brains of patients with multiple sclerosis. *Brain* 133: 2603–2611
- de Barcelos IP, Troxell RM & Graves JS (2019) Mitochondrial dysfunction and multiple sclerosis. *Biology (Basel)* 8
- Bardy C, Van Den Hurk M, Eames T, Marchand C, Hernandez R V., Kellogg M, Gorris M, Galet B, Palomares V, Brown J, *et al* (2015) Neuronal medium that supports basic synaptic functions and activity of human neurons in vitro. *Proc Natl Acad Sci U S A* 112: E2725–E2734
- Bardy C, van den Hurk M, Kakaradov B, Erwin JA, Jaeger BN, Hernandez R V., Eames T, Paucar AA, Gorris M, Marchand C, *et al* (2016) Predicting the functional states of human iPSC-derived neurons with single-cell RNA-seq and electrophysiology. *Mol Psychiatry* 21: 1573–1588
- Barzegar M, Shaygannejad V, Mirmosayyeb O & Afshari A (2020) Progression to Secondary Progressive Multiple Sclerosis and its Early Risk Factors: A Population-based Study (2171). *Neurology* 94: 2171
- Bastianetto S, Ménard C & Quirion R (2015) Neuroprotective action of resveratrol. *Biochim Biophys Acta - Mol Basis Dis* 1852: 1195–1201
- Bauckneht M, Capitanio S, Raffa S, Roccatagliata L, Pardini M, Lapucci C, Marini C, Sambuceti G, Inglese M, Gallo P, *et al* (2019) Molecular imaging of multiple

- sclerosis: from the clinical demand to novel radiotracers. *EJNMMI Radiopharm Chem* 4: 6
- Belle AM, Enright HA, Sales AP, Kulp K, Osburn J, Kuhn EA, Fischer NO & Wheeler EK (2018) Evaluation of in vitro neuronal platforms as surrogates for in vivo whole brain systems. *Sci Rep* 8: 10820
- Beraki S, Litrus L, Soriano L, Monbureau M, To LK, Braithwaite SP, Nikolich K, Urfer R, Oksenberg D & Shamloo M (2013) A Pharmacological Screening Approach for Discovery of Neuroprotective Compounds in Ischemic Stroke. *PLoS One* 8: e69233
- Berer K, Gerdes LA, Cekanaviciute E, Jia X, Xiao L, Xia Z, Liu C, Klotz L, Stauffer U, Baranzini SE, *et al* (2017) Gut microbiota from multiple sclerosis patients enables spontaneous autoimmune encephalomyelitis in mice. *Proc Natl Acad Sci U S A* 114: 10719–10724
- Bezukladova S, Tuisku J, Matilainen M, Vuorimaa A, Nylund M, Smith S, Sucksdorff M, Mohammadian M, Saunavaara V, Laaksonen S, *et al* (2020) Insights into disseminated MS brain pathology with multimodal diffusion tensor and PET imaging. *Neurol - Neuroimmunol Neuroinflammation* 7: e691
- Bittner S, Oh J, Havrdová EK, Tintoré M & Zipp F (2021) The potential of serum neurofilament as biomarker for multiple sclerosis. *Brain* 144: 2954–2963
- Blaser H, Dostert C, Mak TW & Brenner D (2016) TNF and ROS Crosstalk in Inflammation. *Trends Cell Biol* 26: 249–261
- Boffa G, Massacesi L, Inglese M, Mariottini A, Capobianco M, Moiola L, Amato MP, Cottone S, Gualandi F, de Gobbi M, *et al* (2021) Long-term Clinical Outcomes of Hematopoietic Stem Cell Transplantation in Multiple Sclerosis. *Neurology* 96: e1215–e1226
- de Boni L, Gasparoni G, Haubenreich C, Tierling S, Schmitt I, Peitz M, Koch P, Walter J, Wüllner U & Brüstle O (2018) DNA methylation alterations in iPSC- and hESC-derived neurons: Potential implications for neurological disease modeling. *Clin Epigenetics* 10: 1–13
- Boscia F, Elkjaer ML, Illes Z & Kukley M (2021) Altered Expression of Ion Channels in White Matter Lesions of Progressive Multiple Sclerosis: What Do We Know About Their Function? *Front Cell Neurosci* 15: 1–40
- Bramow S, Frischer JM, Lassmann H, Koch-Henriksen N, Lucchinetti CF, Sørensen PS & Laursen H (2010) Demyelination versus remyelination in progressive multiple sclerosis. *Brain* 133: 2983–2998
- Brickley SG, Aller MI, Sandu C, Veale EL, Alder FG, Sambhi H, Mathie A & Wisden W (2007) TASK-3 Two-Pore Domain Potassium Channels Enable Sustained High-Frequency Firing in Cerebellar Granule Neurons. *J Neurosci* 27: 9329–9340
- Brooks WH & Renaudineau Y (2015) Epigenetics and autoimmune diseases: The X chromosome-nucleolus nexus. *Front Genet* 6: 22

- Brown DG & Wobst HJ (2020) Opportunities and Challenges in Phenotypic Screening for Neurodegenerative Disease Research. *J Med Chem* 63: 1823–1840
- Brown JWL, Coles A, Horakova D, Havrdova E, Izquierdo G, Prat A, Girard M, Duquette P, Trojano M, Lugaresi A, *et al* (2019) Association of Initial Disease-Modifying Therapy with Later Conversion to Secondary Progressive Multiple Sclerosis. *JAMA - J Am Med Assoc* 321: 175–187
- Cadavid D, Mellion M, Hupperts R, Edwards KR, Calabresi PA, Drulović J, Giovannoni G, Hartung H-P, Arnold DL, Fisher E, *et al* (2019) Safety and efficacy of opicinumab in patients with relapsing multiple sclerosis (SYNERGY): a randomised, placebo-controlled, phase 2 trial. *Lancet Neurol* 18: 845–856
- Campbell G & Mahad DJ (2018) Mitochondrial dysfunction and axon degeneration in progressive multiple sclerosis. *FEBS Lett* 592: 1113–1121
- Cantó E, Barro C, Zhao C, Caillier SJ, Michalak Z, Bove R, Tomic D, Santaniello A, Häring DA, Hollenbach J, *et al* (2019) Association Between Serum Neurofilament Light Chain Levels and Long-term Disease Course Among Patients With Multiple Sclerosis Followed up for 12 Years. *JAMA Neurol* 76: 1359–1366
- Cantuti-Castelvetri L, Fitzner D, Bosch-Queralt M, Weil M-T, Su M, Sen P, Ruhwedel T, Mitkovski M, Trendelenburg G, Lütjohann D, *et al* (2018) Defective cholesterol clearance limits remyelination in the aged central nervous system. *Science (80-)* 359: 684–688
- Capitani M & Sallese M (2009) The KDEL receptor: New functions for an old protein. *FEBS Lett* 583: 3863–3871
- Casanova B, Jarque I, Gascón F, Carlos Hernández-Boluda J, Pérez-Miralles F, De La Rubia J, Alcalá C, Sanz J, Mallada J, Cervelló A, *et al* Autologous hematopoietic stem cell transplantation in relapsing-remitting multiple sclerosis: comparison with secondary progressive multiple sclerosis.
- Cencioni MT, Mattoscio M, Magliozzi R, Bar-Or A & Muraro PA (2021) B cells in multiple sclerosis — from targeted depletion to immune reconstitution therapies. *Nat Rev Neurol* 17: 399–414
- Center HM, Sharma A, Bader G, Wang L, Himmelstein DS, Santaniello A, Parvin M & Baranzini SE (2015) Open Peer Review iCTNet2: integrating heterogeneous biological interactions to understand complex traits [version 2; referees: 2 approved].
- Cerqueira JJ, Compston DAS, Geraldès R, Rosa MM, Schmierer K, Thompson A, Tinelli M & Palace J (2018) Time matters in multiple sclerosis: can early treatment and long-term follow-up ensure everyone benefits from the latest advances in multiple sclerosis? *J Neurol Neurosurg Psychiatry* 89: 844–850
- Chambers SM, Fasano CA, Papapetrou EP, Tomishima M, Sadelain M & Studer L (2009) Highly efficient neural conversion of human ES and iPS cells by dual inhibition of SMAD signaling. *Nat Biotechnol* 27: 275–280

- Chang A, Nishiyama A, Peterson J, Prineas J & Trapp BD (2000) NG2-positive oligodendrocyte progenitor cells in adult human brain and multiple sclerosis lesions. *J Neurosci* 20: 6404–6412
- Chang A, Smith MC, Yin X, Fox RJ, Staugaitis SM & Trapp BD (2008) Neurogenesis in the chronic lesions of multiple sclerosis. *Brain* 131: 2366–2375
- Chataway J, De Angelis F, Connick P, Parker RA, Plantone D, Doshi A, John N, Stutters J, MacManus D, Prados Carrasco F, *et al* (2020) Efficacy of three neuroprotective drugs in secondary progressive multiple sclerosis (MS-SMART): a phase 2b, multiarm, double-blind, randomised placebo-controlled trial. *Lancet Neurol* 19: 214–225
- Chataway J, Schuerer N, Alsanousi A, Chan D, MacManus D, Hunter K, Anderson V, Bangham CRM, Clegg S, Nielsen C, *et al* (2014) Effect of high-dose simvastatin on brain atrophy and disability in secondary progressive multiple sclerosis (MS-STAT): a randomised, placebo-controlled, phase 2 trial. *Lancet (London, England)* 383: 2213–21
- Chen Y, Zhen W, Guo T, Zhao Y, Liu A, Rubio JP, Krull D, Richardson JC, Lu H & Wang R (2017) Histamine Receptor 3 negatively regulates oligodendrocyte differentiation and remyelination. *PLoS One* 12: e0189380
- Chesnut M, Paschoud H, Repond C, Smirnova L, Hartung T, Zurich MG, Hogberg HT & Pamiès D (2021) Human iPSC-derived model to study myelin disruption. *Int J Mol Sci* 22: 1–20
- Choi I-Y, Lee P, Adany P, Hughes AJ, Belliston S, Denney DR & Lynch SG (2018) In vivo evidence of oxidative stress in brains of patients with progressive multiple sclerosis. *Mult Scler* 24: 1029–1038
- Choi JH, Oh J, Lee MJ, Bae H, Ko SG, Nah SY & Cho IH (2021) Inhibition of lysophosphatidic acid receptor 1–3 deteriorates experimental autoimmune encephalomyelitis by inducing oxidative stress. *J Neuroinflammation* 18: 1–20
- Christodoulou C, Melville P, Scherl WF, MacAllister WS, Elkins LE & Krupp LB (2006) Effects of donepezil on memory and cognition in multiple sclerosis. *J Neurol Sci* 245: 127–136
- Ciotti JR & Cross AH (2018) Disease-Modifying Treatment in Progressive Multiple Sclerosis. *Curr Treat Options Neurol* 20
- Comi G (2013) Disease-modifying treatments for progressive multiple sclerosis. *Mult Scler J* 19: 1428–1436
- Constantinescu CS, Farooqi N, O'Brien K & Gran B (2011) Experimental autoimmune encephalomyelitis (EAE) as a model for multiple sclerosis (MS). *Br J Pharmacol* 164: 1079
- Costa J, Martins S, Ferreira PA, Cardoso AMS, Guedes JR, Peça J & Cardoso AL (2021) The old guard: Age-related changes in microglia and their consequences. *Mech*

- Cree BAC, Arnold DL, Chataway J, Chitnis T, Fox RJ, Pozo Ramajo A, Murphy N & Lassmann H (2021) Secondary Progressive Multiple Sclerosis: New Insights. *Neurology* 97: 378–388
- Cree BAC, Cutter G, Wolinsky JS, Freedman MS, Comi G, Giovannoni G, Hartung H-P, Arnold D, Kuhle J, Block V, *et al* (2020) Safety and efficacy of MD1003 (high-dose biotin) in patients with progressive multiple sclerosis (SPI2): a randomised, double-blind, placebo-controlled, phase 3 trial. *Lancet Neurol* 19: 988–997
- Cree BAC, Hollenbach JA, Bove R, Kirkish G, Sacco S, Caverzasi E, Bischof A, Gundel T, Zhu AH, Papinutto N, *et al* (2019) Silent progression in disease activity-free relapsing multiple sclerosis. *Ann Neurol* 85: 653–666
- Cunniffe N & Coles A (2021) Promoting remyelination in multiple sclerosis. *J Neurol* 268: 30–44
- Cunniffe N, Vuong KA, Ainslie D, Baker D, Beveridge J, Bickley S, Camilleri P, Craner M, Fitzgerald D, De La Fuente AG, *et al* (2021) Systematic approach to selecting licensed drugs for repurposing in the treatment of progressive multiple sclerosis. *J Neurol Neurosurg Psychiatry* 92: 295–302
- Dai H, Fu Q, Shen Y, Hu W, Zhang Z, Timmerman H, Leurs R & Chen Z (2007) The histamine H3 receptor antagonist clobenpropit enhances GABA release to protect against NMDA-induced excitotoxicity through the cAMP/protein kinase A pathway in cultured cortical neurons. *Eur J Pharmacol* 563: 117–123
- Dal-Bianco A, Grabner G, Kronnerwetter C, Weber M, Höftberger R, Berger T, Auff E, Leutmezer F, Trattnig S, Lassmann H, *et al* (2017) Slow expansion of multiple sclerosis iron rim lesions: pathology and 7 T magnetic resonance imaging. *Acta Neuropathol* 133: 25–42
- Daniels RW, Miller BR & DiAntonio A (2011a) Increased vesicular glutamate transporter expression causes excitotoxic neurodegeneration. *Neurobiol Dis* 41: 415–420
- Daniels RW, Miller BR & DiAntonio A (2011b) Increased vesicular glutamate transporter expression causes excitotoxic neurodegeneration. *Neurobiol Dis* 41: 415–420
- Danysz W & Parsons CG (2002) Neuroprotective potential of ionotropic glutamate receptor antagonists. *Neurotox Res* 4: 119–126
- Dendrou CA, Fugger L & Friese MA (2015) Immunopathology of multiple sclerosis. *Nat Rev Immunol* 15: 545–558
- Deshmukh M & Johnson EM (2000) Staurosporine-induced neuronal death: multiple mechanisms and methodological implications. *Cell Death Differ* 7: 250–261
- Domingues HS, Portugal CC, Socodato R & Relvas JB (2016) Oligodendrocyte,

- astrocyte, and microglia crosstalk in myelin development, damage, and repair. *Front Cell Dev Biol* 4: 1–16
- Dong XX, Wang Y & Qin ZH (2009) Molecular mechanisms of excitotoxicity and their relevance to pathogenesis of neurodegenerative diseases. *Acta Pharmacol Sin* 30: 379–387
- Dugas JC, Tai YC, Speed TP, Ngai J & Barres BA (2006) Functional Genomic Analysis of Oligodendrocyte Differentiation. *J Neurosci* 26: 10967–10983
- Dutta R, McDonough J, Yin X, Peterson J, Chang A, Torres T, Gudz T, Macklin WB, Lewis DA, Fox RJ, *et al* (2006) Mitochondrial dysfunction as a cause of axonal degeneration in multiple sclerosis patients. *Ann Neurol* 59: 478–489
- Eapen PM, Rao CM & Nampoothiri M (2019) Crosstalk between neurokinin receptor signaling and neuroinflammation in neurological disorders. *Rev Neurosci* 30: 233–243
- Ehrenreich H, Fischer B, Norra C, Schellenberger F, Stender N, Stiefel M, Sirén AL, Paulus W, Nave KA, Gold R, *et al* (2007) Exploring recombinant human erythropoietin in chronic progressive multiple sclerosis. *Brain* 130: 2577–2588
- Ehrlich M, Mozafari S, Glatza M, Starost L, Velychko S, Hallmann A-L, Cui Q-L, Schambach A, Kim K-P, Bachelin C, *et al* (2017) Rapid and efficient generation of oligodendrocytes from human induced pluripotent stem cells using transcription factors. *Proc Natl Acad Sci U S A* 114: E2243–E2252
- Eleuteri C, Olla S, Veroni C, Umeton R, Mechelli R, Romano S, Buscarinu MC, Ferrari F, Calò G, Ristori G, *et al* (2017) A staged screening of registered drugs highlights remyelinating drug candidates for clinical trials. *Sci Rep* 7: 1–15
- Elliott C, Belachew S, Wolinsky JS, Hauser SL, Kappos L, Barkhof F, Bernasconi C, Fecker J, Model F, Wei W, *et al* (2019) Chronic white matter lesion activity predicts clinical progression in primary progressive multiple sclerosis. *Brain* 142: 2787–2799
- Enders M, Heider T, Ludwig A & Kuerten S (2020) Strategies for Neuroprotection in Multiple Sclerosis and the Role of Calcium. *Int J Mol Sci* 21
- Eschborn M, Pawlitzki M, Wirth T, Nelke C, Pfeuffer S, Schulte-Mecklenbeck A, Lohmann L, Rolfes L, Pape K, Eveslage M, *et al* (2021) Evaluation of Age-Dependent Immune Signatures in Patients With Multiple Sclerosis. *Neurol - Neuroimmunol Neuroinflammation* 8: e1094
- Eshaghi A, Prados F, Brownlee WJ, Altmann DR, Tur C, Cardoso MJ, De Angelis F, van de Pavert SH, Cawley N, De Stefano N, *et al* (2018) Deep gray matter volume loss drives disability worsening in multiple sclerosis. *Ann Neurol* 83: 210–222
- Everett K V., Chioza B, Aicardi J, Aschauer H, Brouwer O, Callenbach P, Covanis A, Dulac O, Eeg-Olofsson O, Feucht M, *et al* (2007) Linkage and association analysis of CACNG3 in childhood absence epilepsy. *Eur J Hum Genet* 2007 154 15: 463–

- Faissner S & Gold R (2019) Progressive multiple sclerosis: latest therapeutic developments and future directions. *Ther Adv Neurol Disord* 12
- Faissner S, Mishra M, Kaushik DK, Wang J, Fan Y, Silva C, Rauw G, Metz L, Koch M & Yong VW (2017) Systematic screening of generic drugs for progressive multiple sclerosis identifies clomipramine as a promising therapeutic. *Nat Commun* 8
- Fambiatos A, Jokubaitis V, Horakova D, Kubala Havrdova E, Trojano M, Prat A, Girard M, Duquette P, Lugaresi A, Izquierdo G, *et al* (2020) Risk of secondary progressive multiple sclerosis: A longitudinal study. *Mult Scler J* 26: 79–90
- Fard MK, Van der Meer F, Sánchez P, Cantuti-Castelvetri L, Mandad S, Jäkel S, Fornasiero EF, Schmitt S, Ehrlich M, Starost L, *et al* (2017) BCAS1 expression defines a population of early myelinating oligodendrocytes in multiple sclerosis lesions. *Sci Transl Med* 9: 1–13
- Farsetti A, Mitsuhashi T, Desvergne B, Robbins J & Nikodem VM (1991) Molecular basis of thyroid hormone regulation of myelin basic protein gene expression in rodent brain. *J Biol Chem* 266: 23226–23232
- De Feo D, Merlini A, Brambilla E, Ottoboni L, Laterza C, Menon R, Srinivasan S, Farina C, Garcia Manteiga JM, Butti E, *et al* (2017) Neural precursor cell–secreted TGF- β 2 redirects inflammatory monocyte-derived cells in CNS autoimmunity. *J Clin Invest* 127: 3937–3953
- Feys P, Lamers I, Francis G, Benedict R, Phillips G, LaRocca N, Hudson LD & Rudick R (2017) The Nine-Hole Peg Test as a manual dexterity performance measure for multiple sclerosis. *Mult Scler J* 23: 711–720
- Filippi M (2000) Enhanced magnetic resonance imaging in multiple sclerosis. *Mult Scler* 6: 320–326
- Filippi M, Bar-Or A, Piehl F, Preziosa P, Solari A, Vukusic S & Rocca MA (2018) Multiple sclerosis. *Nat Rev Dis Prim* 4: 1–27
- Fox RJ, Coffey CS, Conwit R, Cudkowicz ME, Gleason T, Goodman A, Klawiter EC, Matsuda K, McGovern M, Naismith RT, *et al* (2018) Phase 2 Trial of Ibudilast in Progressive Multiple Sclerosis. *N Engl J Med* 379: 846–855
- Fox RJ, Cronin T, Lin J, Wang X, Sakaie K, Ontaneda D, Mahmoud SY, Lowe MJ & Phillips MD (2011) Measuring myelin repair and axonal loss with diffusion tensor imaging. *Am J Neuroradiol* 32: 85–91
- Franco R, Rivas-Santisteban R, Casanovas M, Lillo A, Saura CA & Navarro G (2020) Adenosine A2A Receptor Antagonists Affects NMDA Glutamate Receptor Function. Potential to Address Neurodegeneration in Alzheimer’s Disease. *Cells* 9
- Frederiksen HR, Doehn U, Tveden-Nyborg P & Freude KK (2021) Non-immunogenic Induced Pluripotent Stem Cells, a Promising Way Forward for Allogenic Transplantations for Neurological Disorders. *Front Genome Ed* 0: 30

- Freedman DH (2019) Hunting for New Drugs with AI. *Nature* 576: S49–S53
- Frischer JM, Weigand SD, Guo Y, Kale N, Parisi JE, Pirko I, Mandrekar J, Bramow S, Imke M, Bruck W, *et al* (2015) Clinical and Pathological Insights into the Dynamic Nature of the White Matter Multiple Sclerosis Plaque. *Ann Neurol* 78: 710–721
- Fusaki N, Ban H, Nishiyama A, Saeki K & Hasegawa M (2009) Efficient induction of transgene-free human pluripotent stem cells using a vector based on Sendai virus, an RNA virus that does not integrate into the host genome. *Proc Jpn Acad Ser B Phys Biol Sci* 85: 348–62
- Galvin VC, Yang S, Lowet AS, Datta D, Duque A, Arnsten AF & Wang M (2021) M1 receptors interacting with NMDAR enhance delay-related neuronal firing and improve working memory performance. *Curr Res Neurobiol* 2: 100016
- Garcia-Leon JA, Vitorica J & Gutierrez A (2019) Use of human pluripotent stem cell-derived cells for neurodegenerative disease modeling and drug screening platform. *Future Med Chem* 11: 1305–1322
- Gautier HOB, Evans KA, Volbracht K, James R, Sitnikov S, Lundgaard I, James F, Lao-Peregrin C, Reynolds R, Franklin RJM, *et al* (2015) Neuronal activity regulates remyelination via glutamate signalling to oligodendrocyte progenitors. *Nat Commun* 6: 8518
- Geddes JW, Bondada V & Pang Z (2000) Mechanisms of 3-Nitropropionic Acid Neurotoxicity. *Mitochondrial Inhib Neurodegener Disord*: 107–120
- Genc B, Bozan HR, Genc S & Genc K (2018) Stem Cell Therapy for Multiple Sclerosis. *Adv Exp Med Biol* 1084: 145–174
- Gerdes LA, Janoschka C, Eveslage M, Mannig B, Wirth T, Schulte-Mecklenbeck A, Lauks S, Glau L, Gross CC, Tolosa E, *et al* (2020) Immune signatures of prodromal multiple sclerosis in monozygotic twins. *Proc Natl Acad Sci U S A* 117: 21546–21556
- Gh Popescu BF & Lucchinetti CF (2012) Meningeal and cortical grey matter pathology in multiple sclerosis. *BMC Neurol* 12
- Ghaffari LT, Starr A, Nelson AT & Sattler R (2018) Representing diversity in the dish: Using patient-derived in vitro models to recreate the heterogeneity of neurological disease. *Front Neurosci* 12: 1–18
- Ghirotto B, Oliveira DF, Cipelli M, Basso PJ, de Lima J, Breda CNS, Ribeiro HC, Silva CCC, Sertié AL, Oliveira AER, *et al* (2022) MS-Driven Metabolic Alterations Are Recapitulated in iPSC-Derived Astrocytes. *Ann Neurol*
- Gianfrancesco M & Barcellos L (2016) Obesity and Multiple Sclerosis Susceptibility: A Review. *J Neurol Neuromedicine* 1: 1–5
- Giovannoni G, Butzkueven H, Dhib-Jalbut S, Hobart J, Kobelt G, Pepper G, Sormani MP, Thalheim C, Traboulsee A & Vollmer T (2016) Brain health: time matters in multiple sclerosis. *Mult Scler Relat Disord* 9: S5–S48

- Giovannoni G, Popescu V, Wuerfel J, Hellwig K, Iacobescu E, Jensen MB, García-Domínguez JM, Sousa L, Rossi N De, Hupperts R, *et al* (2022) Smouldering multiple sclerosis: the ‘real MS’. *Ther Adv Neurol Disord* 15: 175628642110667
- Göbel K, Ruck T & Meuth SG (2018) Cytokine signaling in multiple sclerosis: Lost in translation. *Mult Scler J* 24: 432–439
- Goldschmidt T, Antel J, König FB, Brück W & Kuhlmann T (2009) Remyelination capacity of the MS brain decreases with disease chronicity. *Neurology* 72: 1914 LP – 1921
- Görlach A, Bertram K, Hudecova S & Krizanova O (2015) Calcium and ROS: A mutual interplay. *Redox Biol* 6: 260–271
- Granziera C, Wuerfel J, Barkhof F, Calabrese M, De Stefano N, Enzinger C, Evangelou N, Filippi M, Geurts JJG, Reich DS, *et al* (2021) Quantitative magnetic resonance imaging towards clinical application in multiple sclerosis. *Brain* 144: 1296–1311
- Green AJ, Gelfand JM, Cree BA, Bevan C, Boscardin WJ, Mei F, Inman J, Arnow S, Devereux M, Abounasr A, *et al* (2017) Clemastine fumarate as a remyelinating therapy for multiple sclerosis (ReBUILD): a randomised, controlled, double-blind, crossover trial. *Lancet* 390: 2481–2489
- Greenfield AL & Hauser SL (2018) B-cell Therapy for Multiple Sclerosis: Entering an era. *Ann Neurol* 83: 13–26
- Griffiths L, Reynolds R, Evans R, Bevan RJ, Rees MI, Gveric D, Neal JW & Howell OW (2020) Substantial subpial cortical demyelination in progressive multiple sclerosis: have we underestimated the extent of cortical pathology? *Neuroimmunol Neuroinflammation*: 51–67
- Guan JZ, Guan WP, Maeda T, Guoqing X, GuangZhi W & Makino N (2015) Patients with multiple sclerosis show increased oxidative stress markers and somatic telomere length shortening. *Mol Cell Biochem* 400: 183–187
- Guney E, Menche J, Vidal M & Barábasi A-L (2016) Network-based in silico drug efficacy screening. *Nat Commun* 7: 10331
- Guttenplan KA, Weigel MK, Prakash P, Wijewardhane PR, Hasel P, Rufen-Blanchette U, Münch AE, Blum JA, Fine J, Neal MC, *et al* (2021) Neurotoxic reactive astrocytes induce cell death via saturated lipids. *Nature* 599: 102–107
- Guyton MK, Das A, Samantaray S, Wallace GC, Butler JT, Ray SK & Banik NL (2010) Calpeptin attenuated inflammation, cell death, and axonal damage in animal model of multiple sclerosis. *J Neurosci Res* 135: NA-NA
- Hackett JT & Ueda T (2015) Glutamate Release. *Neurochem Res* 40: 2443–60
- Hagemeyer K, Brück W & Kuhlmann T (2012) Multiple sclerosis - remyelination failure as a cause of disease progression. *Histol Histopathology* 27: 277–287
- Hametner S, Wimmer I, Haider L, Pfeifenbring S, Brück W & Lassmann H (2013) Iron

- and neurodegeneration in the multiple sclerosis brain. *Ann Neurol* 74: 848–861
- Hampton DW, Amor S, Story D, Torvell M, Bsibsi M, van Noort JM & Chandran S (2020) HspB5 Activates a Neuroprotective Glial Cell Response in Experimental Tauopathy. *Front Neurosci* 14: 574
- Harjuhaahto S, Rasila TS, Molchanova SM, Woldegebriel R, Kvist J, Konovalova S, Sainio MT, Pennonen J, Torregrosa-Muñumer R, Ibrahim H, *et al* (2020) ALS and Parkinson's disease genes CHCHD10 and CHCHD2 modify synaptic transcriptomes in human iPSC-derived motor neurons. *Neurobiol Dis* 141: 104940
- Harris VK, Stark J, Vyshkina T, Blackshear L, Joo G, Stefanova V, Sara G & Sadiq SA (2018) Phase I Trial of Intrathecal Mesenchymal Stem Cell-derived Neural Progenitors in Progressive Multiple Sclerosis. *EBioMedicine* 29: 23–30
- Harris VK, Stark JW, Yang S, Zanker S, Tuddenham J & Sadiq SA (2021) Mesenchymal stem cell-derived neural progenitors in progressive MS. *Neurol - Neuroimmunol Neuroinflammation* 8: e928
- Hartung DM (2021) Health economics of disease-modifying therapy for multiple sclerosis in the United States. *Ther Adv Neurol Disord* 14: 1–9
- Hayashi T & Su T-P (2007) Sigma-1 Receptor Chaperones at the ER- Mitochondrion Interface Regulate Ca²⁺ Signaling and Cell Survival. *Cell* 131: 596–610
- Hayashi T & Su TP (2004) Sigma-1 receptors at galactosylceramide-enriched lipid microdomains regulate oligodendrocyte differentiation. *Proc Natl Acad Sci U S A* 101: 14949–14954
- He H, Hu Z, Xiao H, Zhou F & Yang B (2018) The tale of histone modifications and its role in multiple sclerosis. *Hum Genomics* 2018 121 12: 1–12
- Hecker M, Fitzner B, Jäger K, Bühring J, Schwartz M, Hartmann A, Walter M & Zettl UK (2021) Leukocyte Telomere Length in Patients with Multiple Sclerosis and Its Association with Clinical Phenotypes. *Mol Neurobiol* 58: 2886–2896
- Hedegaard A, Monzón-Sandoval J, Newey SE, Whiteley ES, Webber C & Akerman CJ (2020a) Pro-maturational Effects of Human iPSC-Derived Cortical Astrocytes upon iPSC-Derived Cortical Neurons. *Stem Cell Reports* 15: 38–51
- Hedegaard A, Monzón-Sandoval J, Newey SE, Whiteley ES, Webber C & Akerman CJ (2020b) Pro-maturational Effects of Human iPSC-Derived Cortical Astrocytes upon iPSC-Derived Cortical Neurons. *Stem Cell Reports* 15: 38–51
- Heß K, Starost L, Kieran NW, Thomas C, Vincenten MCJ, Antel J, Martino G, Huitinga I, Healy L & Kuhlmann T (2020) Lesion stage-dependent causes for impaired remyelination in MS. *Acta Neuropathol* 140: 359–375
- Himmelstein DS, Lizee A, Hessler C, Brueggeman L, Chen SL, Hadley D, Green A, Khankhanian P & Baranzini SE (2017) Systematic integration of biomedical knowledge prioritizes drugs for repurposing. *Elife* 6: 1–35

- Högel H, Rissanen E, Barro C, Matilainen M, Nylund M, Kuhle J & Airas L (2020) Serum glial fibrillary acidic protein correlates with multiple sclerosis disease severity. *Mult Scler J* 26: 210–219
- Howell OW, Reeves CA, Nicholas R, Carassiti D, Radotra B, Gentleman SM, Serafini B, Aloisi F, Roncaroli F, Magliozzi R, *et al* (2011) Meningeal inflammation is widespread and linked to cortical pathology in multiple sclerosis. *Brain* 134: 2755–2771
- Huntemann N, Rolfes L, Pawlitzki M, Ruck T, Pfeuffer S, Wiendl H & Meuth SG (2021) Failed, Interrupted, or Inconclusive Trials on Neuroprotective and Neuroregenerative Treatment Strategies in Multiple Sclerosis: Update 2015–2020 Springer International Publishing
- Hunter SF, Bowen JD & Reder AT (2016) The direct effects of fingolimod in the central nervous system: Implications for relapsing multiple sclerosis. *CNS Drugs* 30: 135–147
- Imeri F, Stepanovska Tanturovska B, Zivkovic A, Enzmann G, Schwalm S, Pfeilschifter J, Homann T, Kleuser B, Engelhardt B, Stark H, *et al* (2021) Novel compounds with dual S1P receptor agonist and histamine H3 receptor antagonist activities act protective in a mouse model of multiple sclerosis. *Neuropharmacology* 186: 108464
- Imitola J, Chitnis T & Khoury SJ (2006) Insights into the molecular pathogenesis of progression in multiple sclerosis: Potential implications for future therapies. *Arch Neurol* 63: 25–33
- Ingelfinger F, Gerdes LA, Kavaka V, Krishnarajah S, Friebel E, Galli E, Zwicky P, Furrer R, Peukert C, Dutertre C-A, *et al* (2022) Twin study reveals non-heritable immune perturbations in multiple sclerosis. *Nature*: 1–7
- Ingwersen J, Aktas O, Kuery P, Kieseier B, Boyko A & Hartung H (2012) Fingolimod in multiple sclerosis : Mechanisms of action and clinical efficacy. *Clin Immunol* 142: 15–24
- Isonaka R, Hiruma H & Kawakami T (2011) Inhibition of axonal transport caused by tert-butyl hydroperoxide in cultured mouse dorsal root ganglion neurons. *J Mol Neurosci* 45: 194–201
- Jafari R, Almqvist H, Axelsson H, Ignatushchenko M, Lundbäck T, Nordlund P & Molina DM (2014) The cellular thermal shift assay for evaluating drug target interactions in cells. *Nat Protoc* 9: 2100–2122
- Jäkel S, Agirre E, Mendanha Falcão A, van Bruggen D, Lee KW, Knuesel I, Malhotra D, ffrench-Constant C, Williams A & Castelo-Branco G (2019) Altered human oligodendrocyte heterogeneity in multiple sclerosis. *Nature* 566: 543–547
- Jakkula E, Leppä V, Sulonen AM, Varilo T, Kallio S, Kemppinen A, Purcell S, Koivisto K, Tienari P, Sumelahti ML, *et al* (2010) Genome-wide Association Study in a High-Risk Isolate for Multiple Sclerosis Reveals Associated Variants in STAT3 Gene. *Am J Hum Genet* 86: 285–291

- Jang H, Ma YJ, Chang EY, Fazeli S, Lee RR, Lombardi AF, Bydder GM, Corey-Bloom J & Du J (2021) Inversion Recovery Ultrashort TE MR Imaging of Myelin is Significantly Correlated with Disability in Patients with Multiple Sclerosis. *Am J Neuroradiol* 42: 868–874
- Jangi S, Gandhi R, Cox LM, Li N, Von Glehn F, Yan R, Patel B, Mazzola MA, Liu S, Glanz BL, *et al* (2016) Alterations of the human gut microbiome in multiple sclerosis. *Nat Commun* 7
- Janssen B, Vugts DJ, Windhorst AD & Mach RH (2018) PET imaging of microglial activation - Beyond targeting TSPO. *Molecules* 23: 1–14
- Johnson MB, Young AD & Marriott I (2017) The Therapeutic Potential of Targeting Substance P/NK-1R Interactions in Inflammatory CNS Disorders. *Front Cell Neurosci* 10: 1–14
- Kalia L V., Kalia SK & Salter MW (2008) NMDA Receptors in Clinical Neurology: Excitatory Times Ahead. *Lancet Neurol* 7: 742
- Kalinowski A, Cutter G, Bozinov N, Hinman JA, Hittle M, Motl R, Odden M & Nelson LM (2021) The timed 25-foot walk in a large cohort of multiple sclerosis patients. *Mult Scler J*: 1–11
- Kam MK, Lee DG, Kim B, Lee H-S, Lee S-R, Bae YC & Lee D-S (2019) Peroxiredoxin 4 ameliorates amyloid beta oligomer-mediated apoptosis by inhibiting ER-stress in HT-22 hippocampal neuron cells. *Cell Biol Toxicol* 35: 573–588
- Kamiloglu S, Sari G, Ozdal T & Capanoglu E (2020) Guidelines for cell viability assays. *Food Front* 1: 332–349
- Kapoor R, Furby J, Hayton T, Smith KJ, Altmann DR, Brenner R, Chataway J, Hughes RA & Miller DH (2010) Lamotrigine for neuroprotection in secondary progressive multiple sclerosis: a randomised, double-blind, placebo-controlled, parallel-group trial. *Lancet Neurol* 9: 681–688
- Kappos L, Bar-Or A, Cree BACC, Fox RJ, Giovannoni G, Gold R, Vermersch P, Arnold DL, Arnould S, Scherz T, *et al* (2018) Siponimod versus placebo in secondary progressive multiple sclerosis (EXPAND): a double-blind, randomised, phase 3 study. *Lancet* 391: 1263–1273
- Karunakaran I & van Echten-Deckert G (2017) Sphingosine 1-phosphate – A double edged sword in the brain. *Biochim Biophys Acta - Biomembr* 1859: 1573–1582
- Kaunzner UW & Gauthier SA (2017) MRI in the assessment and monitoring of multiple sclerosis: an update on best practice. *Ther Adv Neurol Disord* 10: 247–261
- Kepp O, Galluzzi L, Lipinski M, Yuan J & Kroemer G (2011) Cell death assays for drug discovery. *Nat Rev Drug Discov* 10: 221–237
- Kipp M (2020) Does Siponimod Exert Direct Effects in the Central Nervous System? *Cells* 9: 1–17

- Klistorner A & Barnett M (2021) Remyelination Trials: Are We Expecting the Unexpected? *Neurol Neuroimmunol neuroinflammation* 8: 4–9
- Koch M, Kingwell E, Rieckmann P, Tremlett H, UBC MS Clinic Neurologists UMC, Adams D, Craig D, Daly L, Devonshire V, Hashimoto S, *et al* (2010) The natural history of secondary progressive multiple sclerosis. *J Neurol Neurosurg Psychiatry* 81: 1039–43
- Koch MW, Sage K, Kaur S, Kim J, Cerchiaro G, Yong VW, Cutter GR & Metz LM (2021) Repurposing Domperidone in Secondary Progressive Multiple Sclerosis. *Neurology* 96: e2313 LP-e2322
- Kočovská E, Gaughran F, Krivoy A & Meier U-C (2017) Vitamin-D Deficiency As a Potential Environmental Risk Factor in Multiple Sclerosis, Schizophrenia, and Autism. *Front psychiatry* 8: 47
- Krysko KM, Henry RG, Cree BAC, Lin J, Caillier S, Santaniello A, Zhao C, Gomez R, Bevan C, Smith DL, *et al* (2019) Telomere Length Is Associated with Disability Progression in Multiple Sclerosis. *Ann Neurol* 86: 671–682
- Kuhle J, Kropshofer H, Haering DA, Kundu U, Meinert R, Barro C, Dahlke F, Tomic D, Leppert D & Kappos L (2019) Blood neurofilament light chain as a biomarker of MS disease activity and treatment response. *Neurology* 92: E1007–E1015
- Kuhlmann T, Ludwin S, Prat A, Antel J, Brück W & Lassmann H (2017) An updated histological classification system for multiple sclerosis lesions. *Acta Neuropathol* 133: 13–24
- Kuhlmann T, Miron V, Cuo Q, Wegner C, Antel J & Brück W (2008) Differentiation block of oligodendroglial progenitor cells as a cause for remyelination failure in chronic multiple sclerosis. *Brain* 131: 1749–1758
- Kuijlaars J, Oyelami T, Diels A, Rohrbacher J, Versweyveld S, Meneghello G, Tuefferd M, Verstraelen P, Detrez JR, Verschuuren M, *et al* (2016) Sustained synchronized neuronal network activity in a human astrocyte co-culture system. *Sci Reports* 2016 6: 1–14
- Kular L, Needhamsen M, Adzemovic MZ, Kramarova T, Gomez-Cabrero D, Ewing E, Piket E, Tegnér J, Beck S, Piehl F, *et al* (2019) Neuronal methylome reveals CREB-associated neuro-axonal impairment in multiple sclerosis. *Clin Epigenetics* 11: 1–20
- Kumar M & Katyal A (2018) Data on retinoic acid and reduced serum concentration induced differentiation of Neuro-2a neuroblastoma cells. *Data Br* 21: 2435–2440
- Kutzelnigg A & Lassmann H (2005) Cortical lesions and brain atrophy in MS. *J Neurol Sci* 233: 55–59
- Kutzelnigg A, Lucchinetti CF, Stadelmann C, Brück W, Rauschka H, Bergmann M, Schmidbauer M, Parisi JE & Lassmann H (2005) Cortical demyelination and diffuse white matter injury in multiple sclerosis. *Brain* 128: 2705–2712
- Lassmann H (2018) Multiple sclerosis pathology. *Cold Spring Harb Perspect Med* 8: 1–

- Lassmann H & van Horssen J (2016) Oxidative stress and its impact on neurons and glia in multiple sclerosis lesions. *Biochim Biophys Acta - Mol Basis Dis* 1862: 506–510
- Lassmann H, Van Horssen J & Mahad D (2012) Progressive multiple sclerosis: Pathology and pathogenesis. *Nat Rev Neurol* 8: 647–656
- Laterza C, Merlini A, De Feo D, Ruffini F, Menon R, Onorati M, Fredrickx E, Muzio L, Lombardo A, Comi G, *et al* (2013) iPSC-derived neural precursors exert a neuroprotective role in immune-mediated demyelination via the secretion of LIF. *Nat Commun* 2013 41 4: 1–16
- Lee Y, Morrison BM, Li Y, Lengacher S, Farah MH, Hoffman PN, Liu Y, Tsingalia A, Jin L, Zhang PW, *et al* (2012) Oligodendroglia metabolically support axons and contribute to neurodegeneration. *Nature* 487: 443–448
- de Leeuw SM, Davaz S, Wanner D, Milleret V, Ehrbar M, Gietl A & Tackenberg C (2021) Increased maturation of iPSC-derived neurons in a hydrogel-based 3D culture. *J Neurosci Methods* 360: 109254
- Leist TP & Weissert R (2011) Cladribine: Mode of Action and Implications for Treatment of Multiple Sclerosis. *Clin Neuropharmacol* 34
- Leray E, Yaouanq J, Le Page E, Coustans M, Laplaud D, Oger J & Edan G (2010) Evidence for a two-stage disability progression in multiple sclerosis. *Brain* 133: 1900–1913
- Li BS, Sun MK, Zhang L, Takahashi S, Ma W, Vinade L, Kulkarni AB, Brady RO & Pant HC (2001) Regulation of NMDA receptors by cyclin-dependent kinase-5. *Proc Natl Acad Sci U S A* 98: 12742–12747
- Li C, Xiao L, Liu X, Yang W, Shen W, Hu C, Yang G & He C (2013) A functional role of NMDA receptor in regulating the differentiation of oligodendrocyte precursor cells and remyelination. *Glia* 61: 732–749
- Li J, Cao F, Yin H liang, Huang Z jian, Lin Z tao, Mao N, Sun B & Wang G (2020) Ferroptosis: past, present and future. *Cell Death Dis* 2020 112 11: 1–13
- Li N, Kulkarni P, Badrinarayanan A, Kefelegn A, Manoukian R, Li X, Prasad B, Karasu M, McCarty WJ, Knutson CG, *et al* (2021) P-glycoprotein Substrate Assessment in Drug Discovery: Application of Modeling to Bridge Differential Protein Expression Across In Vitro Tools. *J Pharm Sci* 110: 325–337
- Li Y, Sun H, Chen Z, Xu H, Bu G & Zheng H (2016) Implications of GABAergic neurotransmission in Alzheimer's disease. *Front Aging Neurosci* 8: 31
- Licht-Mayer S, Campbell GR, Canizares M, Mehta AR, Gane AB, McGill K, Ghosh A, Fullerton A, Menezes N, Dean J, *et al* (2020) Enhanced axonal response of mitochondria to demyelination offers neuroprotection: implications for multiple sclerosis. *Acta Neuropathol* 140: 143–167

- Liddelow SA, Guttenplan KA, Clarke LE, Bennett FC, Bohlen CJ, Schirmer L, Bennett ML, Münch AE, Chung W-SS, Peterson TC, *et al* (2017) Neurotoxic reactive astrocytes are induced by activated microglia. *Nature* 541: 481–487
- Lisak RP, Benjamins JA, Nedelkoska L, Barger JL, Ragheb S, Fan B, Ouamara N, Johnson TA, Rajasekharan S & Bar-Or A (2012) Secretory products of multiple sclerosis B cells are cytotoxic to oligodendroglia in vitro. *J Neuroimmunol* 246: 85–95
- Lisak RP, Nedelkoska L & Benjamins JA (2020) Sigma-1 receptor agonists as potential protective therapies in multiple sclerosis. *J Neuroimmunol* 342: 577188
- Lisak RP, Nedelkoska L, Benjamins JA, Schalk D, Bealmear B, Touil H, Li R, Muirhead G & Bar-Or A (2017) B cells from patients with multiple sclerosis induce cell death via apoptosis in neurons in vitro. *J Neuroimmunol* 309: 88–99
- Liu Y, Beyer A & Aebersold R (2016) On the Dependency of Cellular Protein Levels on mRNA Abundance. *Cell* 165: 535–550
- Liu Y, Castano D, Girolamo F, Trigueros-Motos L, Bae HG, Neo SP, Oh J, Narayanaswamy P, Torta F, Rye KA, *et al* (2022) Loss of ABCA8B decreases myelination by reducing oligodendrocyte precursor cells in mice. *J Lipid Res* 63: 100147
- Liu Y, Tak PW, Aarts M, Rooyakkers A, Liu L, Ted WL, Dong CW, Lu J, Tymianski M, Craig AM, *et al* (2007) NMDA receptor subunits have differential roles in mediating excitotoxic neuronal death both in vitro and in vivo. *J Neurosci* 27: 2846–2857
- Lorscheider J, Buzzard K, Jokubaitis V, Spelman T, Havrdova E, Horakova D, Trojano M, Izquierdo G, Girard M, Duquette P, *et al* (2016) Defining secondary progressive multiple sclerosis. *Brain* 139: 2395–2405
- Lotfi Shahreza M, Ghadiri N, Mousavi SR, Varshosaz J & Green JR (2018) A review of network-based approaches to drug repositioning. *Brief Bioinform* 19: 878–892
- Lu F, Selak M, O'Connor J, Croul S, Lorenzana C, Butunoi C & Kalman B (2000) Oxidative damage to mitochondrial DNA and activity of mitochondrial enzymes in chronic active lesions of multiple sclerosis. *J Neurol Sci* 177: 95–103
- Lubetzki C, Zalc B, Williams A, Stadelmann C & Stankoff B (2020) Remyelination in multiple sclerosis: from basic science to clinical translation. *Lancet Neurol* 19: 678–688
- Lublin F, Miller DH, Freedman MS, Cree BAC, Wolinsky JS, Weiner H, Lubetzki C, Hartung H-P, Montalban X, Uitdehaag BMJ, *et al* (2016) Oral fingolimod in primary progressive multiple sclerosis (INFORMS): a phase 3, randomised, double-blind, placebo-controlled trial. *Lancet* 387: 1075–1084
- Luchetti S, Fransen NL, van Eden CG, Ramaglia V, Mason M & Huitinga I (2018) Progressive multiple sclerosis patients show substantial lesion activity that correlates with clinical disease severity and sex: a retrospective autopsy cohort analysis. *Acta*

- Luo Y, Huang L, Liao P & Jiang R (2021) Contribution of Neuronal and Glial Two-Pore-Domain Potassium Channels in Health and Neurological Disorders. *Neural Plast* 2021
- Machado-Santos J, Saji E, Tröscher AR, Paunovic M, Liblau R, Gabriely G, Bien CG, Bauer J & Lassmann H (2018) The compartmentalized inflammatory response in the multiple sclerosis brain is composed of tissue-resident CD8⁺ T lymphocytes and B cells. *Brain* 141: 2066–2082
- Macrez R, Stys PK, Vivien D, Lipton SA & Docagne F (2016) Mechanisms of glutamate toxicity in multiple sclerosis: biomarker and therapeutic opportunities. *Lancet Neurol* 15: 1089–102
- Magliozzi R, Howell O, Vora A, Serafini B, Nicholas R, Puopolo M, Reynolds R & Aloisi F (2007) Meningeal B-cell follicles in secondary progressive multiple sclerosis associate with early onset of disease and severe cortical pathology. *Brain* 130: 1089–1104
- Malo N, Hanley JA, Cerquozzi S, Pelletier J & Nadon R (2006) Statistical practice in high-throughput screening data analysis. *Nat Biotechnol* 24: 167–175
- Mannino A, Lithander FE, Dunlop E, Hoare S, Shivappa N, Daly A, Phillips M, Pereira G, Sherriff J, Lucas RM, *et al* (2022) A proinflammatory diet is associated with an increased likelihood of first clinical diagnosis of central nervous system demyelination in women. *Mult Scler Relat Disord* 57
- Manousi A, Göttle P, Reiche L, Cui QL, Healy LM, Akkermann R, Gruchot J, Schira-Heinen J, Antel JP, Hartung HP, *et al* (2021) Identification of novel myelin repair drugs by modulation of oligodendroglial differentiation competence. *EBioMedicine* 65
- Mansilla MJ, Presas-Rodríguez S, Teniente-Serra A, González-Larreategui I, Quirant-Sánchez B, Fondelli F, Djedovic N, Iwaszkiewicz-Grześ D, Chwojncki K, Miljković Đ, *et al* (2021) Paving the way towards an effective treatment for multiple sclerosis: advances in cell therapy. *Cell Mol Immunol* 18: 1353–1374
- Mao P, Manczak M, Shirendeb UP & Reddy PH (2013) MitoQ, a mitochondria-targeted antioxidant, delays disease progression and alleviates pathogenesis in an experimental autoimmune encephalomyelitis mouse model of multiple sclerosis. *Biochim Biophys Acta - Mol Basis Dis* 1832: 2322–2331
- Marschallinger J, Iram T, Zardeneta M, Lee SE, Lehallier B, Haney MS, Pluvinaige J V., Mathur V, Hahn O, Morgens DW, *et al* (2020) Lipid-droplet-accumulating microglia represent a dysfunctional and proinflammatory state in the aging brain. *Nat Neurosci* 23: 194–208
- Marvin JS, Borghuis BG, Tian L, Cichon J, Harnett MT, Akerboom J, Gordus A, Renninger SL, Chen TW, Bargmann CI, *et al* (2013) An optimized fluorescent probe for visualizing glutamate neurotransmission. *Nat Methods* 10: 162

- Matthews PM (2019) Chronic inflammation in multiple sclerosis — seeing what was always there. *Nat Rev Neurol* 15: 582–593
- McGinley MP & Cohen JA (2021) Sphingosine 1-phosphate receptor modulators in multiple sclerosis and other conditions. *Lancet* 398: 1184–1194
- Meca-Lallana V, Berenguer-Ruiz L, Carreres-Polo J, Eichau-Madueño S, Ferrer-Lozano J, Forero L, Higuera Y, Téllez Lara N, Vidal-Jordana A & Pérez-Miralles FC (2021) Deciphering Multiple Sclerosis Progression. *Front Neurol* 12: 1–14
- Mehta SR, Tom CM, Wang Y, Bresee C, Rushton D, Mathkar PP, Tang J & Mattis VB (2018) Human Huntington’s Disease iPSC-Derived Cortical Neurons Display Altered Transcriptomics, Morphology, and Maturation. *Cell Rep* 25: 1081-1096.e6
- Mehta V, Pei W, Yang G, Li S, Swamy E, Boster A, Schmalbrock P & Pitt D (2013) Iron Is a Sensitive Biomarker for Inflammation in Multiple Sclerosis Lesions. *PLoS One* 8: 1–10
- Mei F, Fancy SPJJ, Shen Y-AA, Niu J, Zhao C, Presley B, Miao E, Lee S, Mayoral SR, Redmond SA, *et al* (2014) Micropillar arrays as a high-throughput screening platform for therapeutics in multiple sclerosis. *Nat Med* 20: 954–960
- Meinl E, Krumbholz M, Derfuss T, Junker A & Hohlfeld R (2008) Compartmentalization of inflammation in the CNS: A major mechanism driving progressive multiple sclerosis. *J Neurol Sci* 274: 42–44
- Mendiola AS, Ryu JK, Bardehle S, Meyer-Franke A, Ang KKH, Wilson C, Baeten KM, Hanspers K, Merlini M, Thomas S, *et al* (2020) Transcriptional profiling and therapeutic targeting of oxidative stress in neuroinflammation. *Nat Immunol* 21: 513–524
- Mertens J, Paquola ACM, Ku M, Hatch E, Böhnke L, Ladjevardi S, McGrath S, Campbell B, Lee H, Herdy JR, *et al* (2015) Directly Reprogrammed Human Neurons Retain Aging-Associated Transcriptomic Signatures and Reveal Age-Related Nucleocytoplasmic Defects. *Cell Stem Cell* 17: 705–718
- Metz LM, Al Malik Y, Makkawi S, Zedde A & Cerchiaro G (2020) Quetiapine is Not Tolerable to People with MS in Doses Potentially Required to Enhance Myelin Repair (2868). *Neurology* 94
- Michel L, Touil H, Pikor NB, Gommerman JL, Prat A & Bar-Or A (2015) B cells in the multiple sclerosis central nervous system: Trafficking and contribution to CNS-compartmentalized inflammation. *Front Immunol* 6: 1–12
- Micu I, Plemel JR, Lachance C, Proft J, Jansen AJ, Cummins K, van Minnen J & Stys PK (2016) The molecular physiology of the axo-myelinic synapse. *Exp Neurol* 276: 41–50
- Miller SD & Karpus WJ (2007) Experimental autoimmune encephalomyelitis in the mouse. *Curr Protoc Immunol* Chapter 15: Unit 15.1
- Minthorn E, Mencken T, King AG, Shu A, Rominger D, Gontarek RR, Han C, Bambal

- R & Davis CB (2008) Pharmacokinetics and brain penetration of casopitant, a potent and selective neurokinin-1 receptor antagonist, in the ferret. *Drug Metab Dispos* 36: 1846–1852
- Miraglia L, Pagliaruso S, Bordini E, Martinucci S & Pellegatti M (2010) Metabolic disposition of casopitant, a potent neurokinin-1 receptor antagonist, in mice, rats, and dogs. *Drug Metab Dispos* 38: 1876–1891
- Mishra A & Lal G (2021) Neurokinin receptors and their implications in various autoimmune diseases. *Curr Res Immunol* 2: 66–78
- Mizuno T, Zhang G, Takeuchi H, Kawanokuchi J, Wang J, Sonobe Y, Jin S, Takada N, Komatsu Y & Suzumura A (2008) Interferon-gamma directly induces neurotoxicity through a neuron specific, calcium-permeable complex of IFN- gamma receptor and AMPA GluR1 receptor. *FASEB J* 22: 1797–1806
- Montalban X, Hauser SL, Kappos L, Arnold DL, Bar-Or A, Comi G, de Seze J, Giovannoni G, Hartung H-P, Hemmer B, *et al* (2017) Ocrelizumab versus Placebo in Primary Progressive Multiple Sclerosis. *N Engl J Med* 376: 209–220
- Montalban X, Leist TP, Cohen BA, Moses H, Campbell J, Hicking C & Dangond F (2018) Cladribine tablets added to IFN- β in active relapsing MS. *Neurol Neuroimmunol NeuroInflammation* 5
- Morgan BP, Gommerman JL & Ramaglia V (2021) An “Outside-In” and “Inside-Out” Consideration of Complement in the Multiple Sclerosis Brain: Lessons From Development and Neurodegenerative Diseases. *Front Cell Neurosci* 14: 1–22
- Mori T, Hayashi T, Hayashi E & Su TP (2013) Sigma-1 Receptor Chaperone at the ER-Mitochondrion Interface Mediates the Mitochondrion-ER-Nucleus Signaling for Cellular Survival. *PLoS One* 8
- Mozafari S & Baron-Van Evercooren A (2021) Human stem cell-derived oligodendrocytes: From humanized animal models to cell therapy in myelin diseases. *Semin Cell Dev Biol* 116: 53–61
- Mozafari S, Starost L, Manot-Saillet B, Garcia-Diaz B, Xu YKT, Roussel D, Levy MJF, Ottoboni L, Kim KP, Schöler HR, *et al* (2020) Multiple sclerosis iPSC-derived oligodendroglia conserve their properties to functionally interact with axons and glia in vivo. *Sci Adv* 6: 1–15
- Nagel D, Wessel-carpenter N, Parri R, Sims R, George J, Hill E, Winkler M, Dutta-passecker P, Schröder O & Bader BM Functional phenotypic characterization of iPSC-neurons from Alzheimer ’ s disease patients carrying PS-1 mutation in drug screening and disease modeling. 4
- Naismith RT, Bermel RA, Coffey CS, Goodman AD, Fedler J, Kearney M, Klawiter EC, Nakamura K, Narayanan S, Goebel C, *et al* (2021) Effects of Ibudilast on MRI Measures in the Phase 2 SPRINT-MS Study. *Neurology* 96: e491 LP-e500
- Najm FJ, Madhavan M, Zaremba A, Shick E, Karl RT, Factor DC, Miller TE, Nevin ZS,

- Kantor C, Sargent A, *et al* (2015) Drug-based modulation of endogenous stem cells promotes functional remyelination in vivo. *Nature* 522: 216–220
- Navari RM (2008) Casopitant, a neurokinin-1 receptor antagonist with anti-emetic and anti-nausea activities. *Curr Opin Investig Drugs* 9: 774–785
- Nave K-A (2010a) Myelination and the trophic support of long axons. *Nat Rev Neurosci* 11: 275–283
- Nave K-A (2010b) Myelination and support of axonal integrity by glia. *Nature* 468: 244–52
- Nessler S, Stadelmann C, Bittner A, Schlegel K, Gronen F, Brueck W, Hemmer B & Sommer N (2006) Suppression of autoimmune encephalomyelitis by a neurokinin-1 receptor antagonist—a putative role for substance P in CNS inflammation. *J Neuroimmunol* 179: 1–8
- Neumann B, Baror R, Zhao C, Segel M, Dietmann S, Rawji KS, Foerster S, McClain CR, Chalut K, van Wijngaarden P, *et al* (2019) Metformin Restores CNS Remyelination Capacity by Rejuvenating Aged Stem Cells. *Cell Stem Cell* 25: 473-485.e8
- Neumann B, Foerster S, Zhao C, Bodini B, Reich DS, Bergles DE, Káradóttir RT, Lubetzki C, Lairson LL, Zalc B, *et al* (2020) Problems and Pitfalls of Identifying Remyelination in Multiple Sclerosis. *Cell Stem Cell* 26: 617–619
- Nicaise AM, Wagstaff LJ, Willis CM, Paisie C, Chandok H, Robson P, Fossati V, Williams A & Crocker SJ (2019) Cellular senescence in progenitor cells contributes to diminished remyelination potential in progressive multiple sclerosis. *Proc Natl Acad Sci U S A* 116: 9030–9039
- Nicholas RS, Heaven ML, Middleton RM, Chevli M, Pulikottil-Jacob R, Jones KH & Ford D V. (2020) Personal and societal costs of multiple sclerosis in the UK: A population-based MS Registry study. *Mult Scler J - Exp Transl Clin* 6
- Nicholls D & Attwell D (1990) The release and uptake of excitatory amino acids. *Trends Pharmacol Sci* 11: 462–8
- Nicholls DG & Budd SL (1998) Mitochondria and neuronal glutamate excitotoxicity. *Biochim Biophys Acta - Bioenerg* 1366: 97–112
- Nishri Y, Fainstein N, Goldfarb S, Hampton D, Macrini C, Meinl E, Chandran S & Ben-Hur T (2021) Modeling compartmentalized chronic immune-mediated demyelinating CNS disease in the Biozzi ABH mouse. *J Neuroimmunol* 356: 577582
- O’Gorman C, Lucas R & Taylor B (2012) Environmental risk factors for multiple sclerosis: A review with a focus on molecular mechanisms. *Int J Mol Sci* 13: 11718–11752
- Odawara A, Katoh H, Matsuda N & Suzuki I (2016) Physiological maturation and drug responses of human induced pluripotent stem cell-derived cortical neuronal networks in long-term culture. *Sci Rep* 6: 1–14

- Ohl K, Tenbrock K & Kipp M (2016) Oxidative stress in multiple sclerosis: Central and peripheral mode of action. *Exp Neurol* 277: 58–67
- de Oliveira DM, de Oliveira EML, Ferrari M de FR, Semedo P, Hiyane MI, Cenedeze MA, Pacheco-Silva A, Câmara NOS & Peron JPS (2015) Simvastatin ameliorates experimental autoimmune encephalomyelitis by inhibiting Th1/Th17 response and cellular infiltration. *Inflammopharmacology* 23: 343–354
- Olla S, Steri M, Formato A, Whalen MB, Corbisiero S & Agresti C (2021) Combining Human Genetics of Multiple Sclerosis with Oxidative Stress Phenotype for Drug Repositioning. *Pharmaceutics* 13: 2064
- Olsson T, Barcellos LF & Alfredsson L (2016) Interactions between genetic, lifestyle and environmental risk factors for multiple sclerosis. *Nat Rev Neurol* 13: 26–36
- Oost W, Talma N, Meilof JF & Laman JD (2018) Targeting senescence to delay progression of multiple sclerosis. *J Mol Med* 96: 1153–1166
- Ozawa Y (2010) Pieces of the Parkinson's puzzle. *Nat Rev Neurosci* 11: 787–787
- Öztürk Z, O'Kane CJ & Pérez-Moreno JJ (2020) Axonal Endoplasmic Reticulum Dynamics and Its Roles in Neurodegeneration. *Front Neurosci* 14: 48
- Palmer AL & Ousman SS (2018) Astrocytes and aging. *Front Aging Neurosci* 10: 1–14
- Pamies D, Barreras P, Block K, Makri G, Kumar A, Wiersma D, Smirnova L, Zang C, Bressler J, Christian KM, *et al* (2017) A human brain microphysiological system derived from induced pluripotent stem cells to study neurological diseases and toxicity. *ALTEX* 34: 362–376
- Papadopoulos D, Magliozzi R, Mitsikostas DD, Gorgoulis VG & Nicholas RS (2020) Aging, Cellular Senescence, and Progressive Multiple Sclerosis. *Front Cell Neurosci* 14: 1–11
- Passier R, Orlova V & Mummery C (2016) Complex Tissue and Disease Modeling using hiPSCs. *Cell Stem Cell* 18: 309–321
- Patrikios P, Stadelmann C, Kutzelnigg A, Rauschka H, Schmidbauer M, Laursen H, Sorensen PS, Brück W, Lucchinetti C & Lassmann H (2006) Remyelination is extensive in a subset of multiple sclerosis patients. *Brain* 129: 3165–3172
- Patsopoulos NA, Baranzini SE, Santaniello A, Shoostari P, Cotsapas C, Wong G, Beecham AH, James T, Replogle J, Vlachos IS, *et al* (2019) Multiple sclerosis genomic map implicates peripheral immune cells and microglia in susceptibility. *Science (80-)* 365: 100–106
- Patti F, Visconti A, Capacchione A, Roy S, Trojano M, Amato MP, Cocco E, Danni MC, Filippi M, Gasperini C, *et al* (2020) Long-term effectiveness in patients previously treated with cladribine tablets: a real-world analysis of the Italian multiple sclerosis registry (CLARINET-MS). *Ther Adv Neurol Disord* 13: 1–10
- Perrera V & Martello G (2019) How Does Reprogramming to Pluripotency Affect

Genomic Imprinting? *Front Cell Dev Biol* 7

- Perriot S, Mathias A, Perriard G, Canales M, Jonkmans N, Merienne N, Meunier C, El Kassar L, Perrier AL, Laplaud D-A, *et al* (2018) Human Induced Pluripotent Stem Cell-Derived Astrocytes Are Differentially Activated by Multiple Sclerosis-Associated Cytokines. *Stem Cell Reports* 11: 1199–1210
- Petrou P, Kassis I, Levin N, Paul F, Backner Y, Benoliel T, Oertel FC, Scheel M, Hallimi M, Yaghmour N, *et al* (2020) Beneficial effects of autologous mesenchymal stem cell transplantation in active progressive multiple sclerosis. *Brain* 143: 3574–3588
- Philipp M (2016) Substance P and Antagonists of the Neurokinin-1 Receptor in Neuroinflammation Associated with Infectious and Neurodegenerative Diseases of the Central Nervous System. *J Neurol Neuromedicine* 1: 29–36
- Pitt D, Werner P & Raine CS (2000) Glutamate excitotoxicity in a model of multiple sclerosis. *Nat Med* 6: 67–70
- Plemel JR, Liu W-Q & Yong VW (2017) Remyelination therapies: a new direction and challenge in multiple sclerosis. *Nat Rev Drug Discov* 16: 617–634
- Pluchino S, Smith JA & Peruzzotti-Jametti L (2020) Promises and Limitations of Neural Stem Cell Therapies for Progressive Multiple Sclerosis. *Trends Mol Med* 26: 898–912
- Ponath G, Lincoln MR, Levine-Ritterman M, Park C, Dahlawi S, Mubarak M, Sumida T, Airas L, Zhang S, Isitan C, *et al* (2018) Enhanced astrocyte responses are driven by a genetic risk allele associated with multiple sclerosis. *Nat Commun* 9: 5337
- Pushpakom S, Iorio F, Eyers PA, Escott KJ, Hopper S, Wells A, Doig A, Guilliams T, Latimer J, McNamee C, *et al* (2019) Drug repurposing: progress, challenges and recommendations. *Nat Rev Drug Discov* 18: 41–58
- Qi Y, Zhang XJ, Renier N, Wu Z, Atkin T, Sun Z, Ozair MZ, Tchieu J, Zimmer B, Fattahi F, *et al* (2017) Combined small-molecule inhibition accelerates the derivation of functional cortical neurons from human pluripotent stem cells. *Nat Biotechnol* 35: 154–163
- Qian L & Tcw J (2021) Human iPSC-Based Modeling of Central Nerve System Disorders for Drug Discovery. *Int J Mol Sci* 22: 1–36
- Quartara L, Altamura M, Evangelista S & Maggi CA (2009) Tachykinin receptor antagonists in clinical trials. *Expert Opin Investig Drugs* 18: 1843–1864
- Raghu P, Joseph A, Krishnan H, Singh P & Saha S (2019) Phosphoinositides: Regulators of Nervous System Function in Health and Disease. *Front Mol Neurosci* 12: 208
- Ramagopalan S V, Dobson R, Meier UC & Giovannoni G (2010) Multiple sclerosis: risk factors, prodromes, and potential causal pathways. *Lancet Neurol* 9: 727–739
- Rankin KA, Mei F, Kim K, Shen YAA, Mayoral SR, Desponts C, Lorrain DS, Green AJ, Baranzini SE, Chan JR, *et al* (2019) Selective estrogen receptor modulators enhance

- CNS remyelination independent of estrogen receptors. *J Neurosci* 39: 2184–2194
- Reich DS, Lucchinetti CF & Calabresi PA (2018) Multiple Sclerosis. *N Engl J Med* 378: 169–180
- Reinhardt P, Glatza M, Hemmer K, Tsytsyura Y, Thiel CS, Höing S, Moritz S, Parga JA, Wagner L, Bruder JM, *et al* (2013) Derivation and Expansion Using Only Small Molecules of Human Neural Progenitors for Neurodegenerative Disease Modeling. *PLoS One* 8
- Reinke EK, Johnson MJ, Ling C, Karman J, Lee J, Weinstock J V, Sandor M & Fabry Z (2006) Substance P receptor mediated maintenance of chronic inflammation in EAE. *J Neuroimmunol* 180: 117–125
- Renner H, Grabos M, Becker KJ, Kagermeier TE, Wu J, Otto M, Peischard S, Zeuschner D, Tsytsyura Y, Disse P, *et al* (2020) A fully automated high-throughput workflow for 3d-based chemical screening in human midbrain organoids. *Elife* 9: 1–39
- Riss TL, Moravec RA, Niles AL, Duellman S, Benink HA, Worzella TJ & Minor L (2016) Cell Viability Assays. *Assay Guid Man*
- Rist JM & Franklin RJM (2008) Taking ageing into account in remyelination-based therapies for multiple sclerosis. *J Neurol Sci* 274: 64–67
- Rivellini C, Quattrini A & Previtali SC (2021) JAB1 deletion in oligodendrocytes causes senescence-induced inflammation and neurodegeneration in mice.
- Rocamonde B, Paradells S, Barcia JM, Barcia C, García Verdugo JM, Miranda M, Romero Gómez FJ & Soria JM (2012) Neuroprotection of lipoic acid treatment promotes angiogenesis and reduces the glial scar formation after brain injury. *Neuroscience* 224: 102–115
- Rosenkranz SC, Shaposhnykov AA, Träger S, Engler JB, Witte ME, Roth V, Vieira V, Paauw N, Bauer S, Schwencke-Westphal C, *et al* (2021) Enhancing mitochondrial activity in neurons protects against neurodegeneration in a mouse model of multiple sclerosis. *Elife* 10: 1–60
- Rossi S, Motta C, Studer V, Macchiarulo G, Volpe E, Barbieri F, Ruocco G, Buttari F, Finardi A, Mancino R, *et al* (2014) Interleukin-1 β causes excitotoxic neurodegeneration and multiple sclerosis disease progression by activating the apoptotic protein p53. *Mol Neurodegener* 9: 56
- Rumah KR, Linden J, Fischetti VA & Vartanian T (2013) Isolation of *Clostridium perfringens* Type B in an Individual at First Clinical Presentation of Multiple Sclerosis Provides Clues for Environmental Triggers of the Disease. *PLoS One* 8
- Ruscio A Di, Patti F, Welner RS, Tenen DG, Amabile G, Di Ruscio A, Patti F, Welner RS, Tenen DG & Amabile G (2015) Multiple sclerosis: Getting personal with induced pluripotent stem cells. *Cell Death Dis* 6: e1806-7
- Ryskamp DA, Korban S, Zhemkov V, Kraskovskaya N & Bezprozvanny I (2019) Neuronal sigma-1 receptors: Signaling functions and protective roles in

neurodegenerative diseases. *Front Neurosci* 13: 1–20

- Santra M, Zhang ZG, Yang J, Santra S, Santra S, Chopp M & Morris DC (2014) Thymosin β 4 Up-regulation of MicroRNA-146a Promotes Oligodendrocyte Differentiation and Suppression of the Toll-like Proinflammatory Pathway. *J Biol Chem* 289: 19508–19518
- Saraste M, Bezukladova S, Matilainen M, Sucksdorff M, Kuhle J, Leppert D & Airas L (2021a) Increased serum glial fibrillary acidic protein associates with microstructural white matter damage in multiple sclerosis: GFAP and DTI. *Mult Scler Relat Disord* 50
- Saraste M, Bezukladova S, Matilainen M, Tuisku J, Rissanen E, Sucksdorff M, Laaksonen S, Vuorimaa A, Kuhle J, Leppert D, *et al* (2021b) High serum neurofilament associates with diffuse white matter damage in MS. *Neurol Neuroimmunol neuroinflammation* 8: 1–11
- Särkijärvi S, Kuusisto H, Paalavuo R, Levula M, Airla N, Lehtimäki T, Kaprio J, Koskenvuo M & Elovaara I (2006) Gene expression profiles in Finnish twins with multiple sclerosis. *BMC Med Genet* 7: 1–10
- Satoh JI, Tabunoki H & Yamamura T (2009) Molecular network of the comprehensive multiple sclerosis brain-lesion proteome. *Mult Scler* 15: 531–541
- Scalfari A, Neuhaus A, Daumer M, Muraro PA & Ebers GC (2014) Onset of secondary progressive phase and long-term evolution of multiple sclerosis. *J Neurol Neurosurg Psychiatry* 85: 67–75
- Scalfari A, Romualdi C, Nicholas RS, Mattoscio M, Magliozzi R, Morra A, Monaco S, Muraro PA & Calabrese M (2018) The cortical damage, early relapses, and onset of the progressive phase in multiple sclerosis. *Neurology* 90: e2107 LP-e2118
- Schirmer L, Velmeshev D, Holmqvist S, Kaufmann M, Werneburg S, Jung D, Vistnes S, Stockley JH, Young A, Steindel M, *et al* (2019) Neuronal vulnerability and multilineage diversity in multiple sclerosis. *Nature* 573: 75–82
- Schmitz K, Brunkhorst R, de Bruin N, Mayer CA, Häussler A, Ferreiros N, Schiffmann S, Parnham MJ, Tunaru S, Chun J, *et al* (2017) Dysregulation of lysophosphatidic acids in multiple sclerosis and autoimmune encephalomyelitis. *Acta Neuropathol Commun* 5: 42
- Schreiber K, Magyari M, Sellebjerg F, Iversen P, Garde E, Madsen CG, Börnsen L, Romme Christensen J, Ratzner R, Siebner HR, *et al* (2017) High-dose erythropoietin in patients with progressive multiple sclerosis: A randomized, placebo-controlled, phase 2 trial. *Mult Scler* 23: 675–685
- Schwartzbach CJ, Grove RA, Brown R, Tompson D, Then Bergh F & Arnold DL (2017) Lesion remyelinating activity of GSK239512 versus placebo in patients with relapsing-remitting multiple sclerosis: a randomised, single-blind, phase II study. *J Neurol* 264: 304–315

- Scott LJ & Figgitt DP (2004) Mitoxantrone: A review of its use in multiple sclerosis. *CNS Drugs* 18: 379–396
- Sedel F, Papeix C, Bellanger A, Touitou V, Lebrun-Frenay C, Galanaud D, Gout O, Lyon-Caen O & Tourbah A (2015) High doses of biotin in chronic progressive multiple sclerosis: A pilot study. *Mult Scler Relat Disord* 4: 159–169
- Seewann A, Vrenken H, Valk P, Blezer ELA, Knol DL, Castelijns JA, Polman CH, Pouwels PJW, Barnhof F & Ceurts JGG (2009) Diffusely abnormal white matter in chronic multiple sclerosis. *Ann Neurol* 66: 601–609
- Seminary ER, Santarriaga S, Wheeler L, Mejaki M, Abrudan J, Demos W, Zimmermann MT, Urrutia RA, Fee D, Barkhaus PE, *et al* (2020) Motor Neuron Generation from iPSCs from Identical Twins Discordant for Amyotrophic Lateral Sclerosis. *Cells* 2020, Vol 9, Page 571 9: 571
- Severa M, Zhang J, Giacomini E, Rizzo F, Etna MP, Cruciani M, Garaci E, Chopp M & Coccia EM (2019) Thymosins in multiple sclerosis and its experimental models: moving from basic to clinical application. *Mult Scler Relat Disord* 27: 52
- Shameer K, Glicksberg BS, Hodos R, Johnson KW, Badgeley MA, Readhead B, Tomlinson MS, O'Connor T, Miotto R, Kidd BA, *et al* (2018) Systematic analyses of drugs and disease indications in RepurposeDB reveal pharmacological, biological and epidemiological factors influencing drug repositioning. *Brief Bioinform* 19: 656–678
- Sharma A, Sances S, Workman MJ & Svendsen CN (2020) Multi-lineage Human iPSC-Derived Platforms for Disease Modeling and Drug Discovery. *Cell Stem Cell* 26: 309–329
- Shen H, Kihara T, Hongo H, Wu X, Kem WR, Shimohama S, Akaike A, Niidome T & Sugimoto H (2010) Neuroprotection by donepezil against glutamate excitotoxicity involves stimulation of $\alpha 7$ nicotinic receptors and internalization of NMDA receptors. *Br J Pharmacol* 161: 127–139
- Shepard CJ, Cline SG, Hinds D, Jahanbakhsh S, Prokop JW, Cj S, Sg C & Prokop JS (2019) Breakdown of multiple sclerosis genetics to identify an integrated disease network and potential variant mechanisms. *Physiol Genomics* 51: 562–577
- Sherman SP & Bang AG (2018) High-throughput screen for compounds that modulate neurite growth of human induced pluripotent stem cell-derived neurons. *Dis Model Mech* 11: dmm031906
- Shirani A, Okuda DT & Stüve O (2016) Therapeutic Advances and Future Prospects in Progressive Forms of Multiple Sclerosis. *Neurotherapeutics* 13: 58–69
- Sim FJ, Zhao C, Penderis J & Franklin RJM (2002) The Age-Related Decrease in CNS Remyelination Efficiency Is Attributable to an Impairment of Both Oligodendrocyte Progenitor Recruitment and Differentiation. *J Neurosci* 22: 2451–2459
- Simon KC, Munger KL & Ascherio A (2012) Vitamin D and multiple sclerosis. *Curr*

- Singh S, Dallenga T, Winkler A, Roemer S, Maruschak B, Siebert H, Brück W & Stadelmann C (2017) Relationship of acute axonal damage, Wallerian degeneration, and clinical disability in multiple sclerosis. *J Neuroinflammation* 14: 1–15
- Singhal NK, Li S, Arning E, Alkhayer K, Clements R, Sarcyk Z, Dassanayake RS, Brasch NE, Freeman EJ, Bottiglieri T, *et al* (2015) Changes in Methionine Metabolism and Histone H3 Trimethylation Are Linked to Mitochondrial Defects in Multiple Sclerosis. *J Neurosci* 35: 15170–15186
- Smith JA, Nicaise AM, Ionescu R-B, Hamel R, Peruzzotti-Jametti L & Pluchino S (2021) Stem Cell Therapies for Progressive Multiple Sclerosis. *Front Cell Dev Biol* 9: 1751
- Souren NY, Gerdes LA, Lutsik P, Gasparoni G, Beltrán E, Salhab A, Kümpfel T, Weichenhan D, Plass C, Hohlfeld R, *et al* (2019) DNA methylation signatures of monozygotic twins clinically discordant for multiple sclerosis. *Nat Commun* 10: 2094
- Spain R, Powers K, Murchison C, Heriza E, Wings K, Yadav V, Cameron M, Kim E, Horak F, Simon J, *et al* (2017) Lipoic acid in secondary progressive MS. *Neurol Neuroimmunol NeuroInflammation* 4
- Staerk J, Dawlaty MM, Gao Q, Maetzel D, Hanna J, Sommer CA, Mostoslavsky G & Jaenisch R (2010) Reprogramming of human peripheral blood cells to induced pluripotent stem cells. *Cell Stem Cell* 7: 20–24
- Stanislaus R, Gilg AG, Singh AK & Singh I (2005) N-acetyl-L-cysteine ameliorates the inflammatory disease process in experimental autoimmune encephalomyelitis in Lewis rats. *J Autoimmune Dis* 2: 5–7
- Stankoff B, Mrejen S, Tourbah A, Fontaine B, Lyon-Caen O, Lubetzki C & Rosenheim M (2007) Age at onset determines the occurrence of the progressive phase of multiple sclerosis. *Neurology* 68: 779–781
- Starkov AA (2008) The Role of Mitochondria in Reactive Oxygen Species Metabolism and Signaling. *Ann N Y Acad Sci* 1147: 37–52
- Starost L, Lindner M, Herold M, Xu YKT, Drexler HCA, Heß K, Ehrlich M, Ottoboni L, Ruffini F, Stehling M, *et al* (2020) Extrinsic immune cell-derived, but not intrinsic oligodendroglial factors contribute to oligodendroglial differentiation block in multiple sclerosis. *Acta Neuropathol* 140: 715–736
- Steinman L (1996) Multiple sclerosis: A coordinated immunological attack against myelin in the central nervous system. *Cell* 85: 299–302
- Stüber C, Pitt D & Wang Y (2016) Iron in multiple sclerosis and its noninvasive imaging with quantitative susceptibility mapping. *Int J Mol Sci* 17
- Subedi L, Ji E, Shin D, Jin J, Yeo JH & Kim SY (2017) Equol, a dietary daidzein gut metabolite attenuates microglial activation and potentiates neuroprotection in vitro. *Nutrients* 9: 1–16

- Sucksdorff M, Matilainen M, Tuisku J, Polvinen E, Vuorimaa A, Rokka J, Nylund M, Rissanen E & Airas L (2020) Brain TSPO-PET predicts later disease progression independent of relapses in multiple sclerosis. *Brain* 143: 3318–3330
- Szeliga M (2020) Peroxiredoxins in neurodegenerative diseases. *Antioxidants* 9: 1–19
- Takahashi K, Tanabe K, Ohnuki M, Narita M, Ichisaka T, Tomoda K & Yamanaka S (2007) Induction of Pluripotent Stem Cells from Adult Human Fibroblasts by Defined Factors. *Cell* 131: 861–872
- Takahashi K & Yamanaka S (2006) Induction of Pluripotent Stem Cells from Mouse Embryonic and Adult Fibroblast Cultures by Defined Factors. *Cell* 126: 663–676
- Takenaka S, Fujisawa T & Ichijo H (2020) Apoptosis signal-regulating kinase 1 (ASK1) as a therapeutic target for neurological diseases. *Expert Opin Ther Targets*
- Takewaki D, Suda W, Sato W, Takayasu L, Kumar N, Kimura K, Kaga N, Mizuno T, Miyake S, Hattori M, *et al* (2020) Alterations of the gut ecological and functional microenvironment in different stages of multiple sclerosis. *Proc Natl Acad Sci U S A* 117: 22402–22412
- Tang X, Zhou L, Wagner AM, Marchetto MCN, Muotri AR, Gage FH & Chen G (2013) Astroglial cells regulate the developmental timeline of human neurons differentiated from induced pluripotent stem cells. *Stem Cell Res* 11: 743–757
- Thebault S, Abdoli M, Fereshtehnejad SM, Tessier D, Tabard-Cossa V & Freedman MS (2020) Serum neurofilament light chain predicts long term clinical outcomes in multiple sclerosis. *Sci Rep* 10: 1–11
- Thompson AJ, Baranzini SE, Geurts J, Hemmer B & Ciccarelli O (2018) Multiple sclerosis. *Lancet (London, England)* 391: 1622–1636
- Thompson AJ, Carroll W, Ciccarelli O, Comi G, Cross A, Donnelly A, Feinstein A, Fox RJ, Helme A, Hohlfeld R, *et al* (2022) Charting a global research strategy for progressive MS-An international progressive MS Alliance proposal. *Mult Scler* 28: 16–28
- Tiscornia G, Vivas EL & Belmonte JCI (2011) Diseases in a dish: modeling human genetic disorders using induced pluripotent cells. *Nat Med* 2011 1712 17: 1570–1576
- Tombaugh TN (2006) A comprehensive review of the Paced Auditory Serial Addition Test (PASAT). *Arch Clin Neuropsychol* 21: 53–76
- Toritsuka M, Yoshino H, Makinodan M, Ikawa D, Kimoto S, Yamamuro K, Okamura K, Akamatsu W, Okada Y, Matsumoto T, *et al* (2021) Developmental dysregulation of excitatory-to-inhibitory GABA-polarity switch may underlie schizophrenia pathology: A monozygotic-twin discordant case analysis in human iPS cell-derived neurons. *Neurochem Int* 150: 105179
- Tourbah A, Lebrun-Frenay C, Edan G, Clanet M, Papeix C, Vukusic S, De Sèze J, Debouverie M, Gout O, Clavelou P, *et al* (2016) MD1003 (high-dose biotin) for the

- treatment of progressive multiple sclerosis: A randomised, double-blind, placebo-controlled study. *Mult Scler* 22: 1719–1731
- Townshend RF, Shao Y, Wang S, Cortez CL, Esfahani SN, Spence JR, O’Shea KS, Fu J, Gumucio DL & Taniguchi K (2020) Effect of Cell Spreading on Rosette Formation by Human Pluripotent Stem Cell-Derived Neural Progenitor Cells. *Front Cell Dev Biol* 8: 1072
- Tsai AP, Lin PBC, Dong C, Moutinho M, Casali BT, Liu Y, Lamb BT, Landreth GE, Oblak AL & Nho K (2021) INPP5D expression is associated with risk for Alzheimer’s disease and induced by plaque-associated microglia. *Neurobiol Dis* 153: 105303
- Tutuncu M, Tang J, Zeid NA, Kale N, Crusan DJ, Atkinson EJ, Siva A, Pittock SJ, Pirko I, Keegan BM, *et al* (2012) Onset of progressive phase is an age-dependent clinical milestone in multiple sclerosis. *Mult Scler J* 19: 188–198
- Uccelli A, Benvenuto F, Laroni A & Giunti D (2011) Neuroprotective features of mesenchymal stem cells. *Best Pract Res Clin Haematol* 24: 59–64
- Upadhayay S & Mehan S (2021) Targeting Nrf2/HO-1 anti-oxidant signaling pathway in the progression of multiple sclerosis and influences on neurological dysfunctions. *Brain Disord* 3: 100019
- Uphaus T, Steffen F, Muthuraman M, Ripfel N, Fleischer V, Groppa S, Ruck T, Meuth SG, Pul R, Kleinschmitz C, *et al* (2021) NfL predicts relapse-free progression in a longitudinal multiple sclerosis cohort study: Serum NfL predicts relapse-free progression. *EBioMedicine* 72
- Uzawa A, Mori M, Masuda H, Ohtani R, Uchida T, Aoki R & Kuwabara S (2020) Peroxiredoxins are involved in the pathogenesis of multiple sclerosis and neuromyelitis optica spectrum disorder. *Clin Exp Immunol* 202: 239–248
- Vilisaar J, Kawabe K, Braitch M, Aram J, Furtun Y, Fahey AJ, Chopra M, Tanasescu R, Tighe PJ, Gran B, *et al* (2015) Reciprocal Regulation of Substance P and IL-12/IL-23 and the Associated Cytokines, IFN γ /IL-17: A Perspective on the Relevance of This Interaction to Multiple Sclerosis. *J neuroimmune Pharmacol Off J Soc NeuroImmune Pharmacol* 10: 457–467
- Villoslada P (2016) Neuroprotective therapies for multiple sclerosis and other demyelinating diseases. *Mult Scler Demyelinating Disord* 1
- Vivash L & OBrien TJ (2016) Imaging Microglial Activation with TSPO PET: Lighting Up Neurologic Diseases? *J Nucl Med* 57: 165–168
- Volpato V & Webber C (2020) Addressing variability in iPSC-derived models of human disease: Guidelines to promote reproducibility. *DMM Dis Model Mech* 13
- Vrenken H, Seewann A, Knol DL, Polman CH, Barkhof F & Geurts JJG (2010) Diffusely abnormal white matter in progressive multiple sclerosis: In vivo quantitative MR imaging characterization and comparison between disease types. *Am J Neuroradiol*

31: 541–548

- Walton C, King R, Rechtman L, Kaye W, Leray E, Marrie RA, Robertson N, La Rocca N, Uitdehaag B, van der Mei I, *et al* (2020) Rising prevalence of multiple sclerosis worldwide: Insights from the Atlas of MS, third edition. *Mult Scler* 26: 1816–1821
- Wang J, Zhao J, Cui X, Mysona BA, Navneet S, Saul A, Ahuja M, Lambert N, Gazaryan IG, Thomas B, *et al* (2019) The molecular chaperone sigma 1 receptor mediates rescue of retinal cone photoreceptor cells via modulation of NRF2. *Free Radic Biol Med* 134: 604–616
- Wang Q, Yu S, Simonyi A, Sun GY & Sun AY (2005) Kainic acid-mediated excitotoxicity as a model for neurodegeneration. *Mol Neurobiol* 31: 3–16
- Waslo C, Bourdette D, Gray N, Wright K & Spain R (2019) Lipoic Acid and Other Antioxidants as Therapies for Multiple Sclerosis. *Curr Treat Options Neurol* 21
- Weisler RH, Pandina GJ, Daly EJ, Cooper K & Gassmann-Mayer C (2012) Randomized clinical study of a histamine H3 receptor antagonist for the treatment of adults with attention-deficit hyperactivity disorder. *CNS Drugs* 26: 421–434
- Westerlind H, Ramanujam R, Uvehag D, Kuja-Halkola R, Boman M, Bottai M, Lichtenstein P & Hillert J (2014) Modest familial risks for multiple sclerosis: a registry-based study of the population of Sweden. *Brain* 137: 770–8
- Wheeler MA, Clark IC, Tjon EC, Li Z, Zandee SEJ, Couturier CP, Watson BR, Scalisi G, Alkawai S, Rothhammer V, *et al* (2020) MAFG-driven astrocytes promote CNS inflammation. *Nature* 578: 593–599
- Wheeler MA, Jaronen M, Covacu R, Zandee SEJ, Scalisi G, Rothhammer V, Tjon EC, Chao CC, Kenison JE, Blain M, *et al* (2019) Environmental Control of Astrocyte Pathogenic Activities in CNS Inflammation. *Cell* 176: 581-596.e18
- Whitford KL, Marillat V, Stein E, Goodman CS, Tessier-Lavigne M, Chédotal A & Ghosh A (2002) Regulation of cortical dendrite development by Slit-Robo interactions. *Neuron* 33: 47–61
- Wilson NR, Kang J, Hueske E V., Leung T, Varoqui H, Murnick JG, Erickson JD & Liu G (2005) Presynaptic regulation of quantal size by the vesicular glutamate transporter VGLUT1. *J Neurosci* 25: 6221–6234
- Witte ME, Mahad DJ, Lassmann H & van Horssen J (2014) Mitochondrial dysfunction contributes to neurodegeneration in multiple sclerosis. *Trends Mol Med* 20: 179–187
- Woodard CM, Campos BA, Kuo SH, Nirenberg MJ, Nestor MW, Zimmer M, Mosharov E V., Sulzer D, Zhou H, Paull D, *et al* (2014) iPSC-derived dopamine neurons reveal differences between monozygotic twins discordant for parkinson's disease. *Cell Rep* 9: 1173–1182
- Wu C, Zhao W, Yu J, Li S, Lin L & Chen X (2018) Induction of ferroptosis and mitochondrial dysfunction by oxidative stress in PC12 cells. *Sci Rep* 8: 1–11

- Yadav SK, Ito N, Soin D, Ito K & Dhib-Jalbut S (2021) Dimethyl Fumarate Suppresses Demyelination and Axonal Loss through Reduction in Pro-Inflammatory Macrophage-Induced Reactive Astrocytes and Complement C3 Deposition. *J Clin Med* 10: 857
- Yamanaka S (2020) Pluripotent Stem Cell-Based Cell Therapy-Promise and Challenges. *Stem Cell* 27: 523–531
- Yan K, Balijepalli C, Desai K, Gullapalli L & Druyts E (2020) Epidemiology of pediatric multiple sclerosis: A systematic literature review and meta-analysis. *Mult Scler Relat Disord* 44: 102260
- Yan X-Y, Zhang S-W & Zhang S-Y (2016) Prediction of drug–target interaction by label propagation with mutual interaction information derived from heterogeneous network. *Mol Biosyst* 12: 520–531
- Yang C, Hao Z, Zhang L, Zeng L & Wen J (2015) Sodium channel blockers for neuroprotection in multiple sclerosis. *Cochrane Database Syst Rev* 2015
- Yang H, Shen H, Li J & Guo L-W (2019) SIGMAR1/Sigma-1 receptor ablation impairs autophagosome clearance. *Autophagy* 15: 1539–1557
- Yanwu Y, Meiling G, Yunxia Z, Qiukui H & Birong D (2020) Mesenchymal stem cells in experimental autoimmune encephalomyelitis model of multiple sclerosis: A systematic review and meta-analysis. *Mult Scler Relat Disord* 44: 102200
- Yoshino J, Baur JA & Imai S ichiro (2018) NAD⁺Intermediates: The Biology and Therapeutic Potential of NMN and NR. *Cell Metab* 27: 513–528
- Zamvil SS & Steinman L (2002) Cholesterol-lowering statins possess anti-inflammatory activity that might be useful for treatment of MS. *Neurology* 59: 970 LP – 971
- Zeis T, Howell OW, Reynolds R & Schaeren-Wiemers N (2018) Molecular pathology of Multiple Sclerosis lesions reveals a heterogeneous expression pattern of genes involved in oligodendroglioneogenesis. *Exp Neurol* 305: 76–88
- Zhan J, Mann T, Joost S, Behrangi N, Frank M & Kipp M (2020) The Cuprizone Model: Dos and Do Nots. *Cells* 9
- Zhang G, Murthy KD, Binti Pare R & Qian Y (2020) Protective effect of Tβ4 on central nervous system tissues and its developmental prospects. *Eur J Inflamm* 18: 205873922093455
- Zhang M, Ni Y, Zhou Q, He L, Meng H, Gao Y, Huang X, Meng H, Li P, Chen M, *et al* (2021a) 18F-florbetapir PET/MRI for quantitatively monitoring myelin loss and recovery in patients with multiple sclerosis: A longitudinal study. *EClinicalMedicine* 37
- Zhang X, Huang N, Xiao L, Wang F & Li T (2021b) Replenishing the Aged Brains: Targeting Oligodendrocytes and Myelination? *Front Aging Neurosci* 13: 1–11
- Ziemssen T, Tolley C, Bennett B, Kilgariff S, Jones E, Pike J, Tomic D, Piani-Meier D

& Lahoz R (2020) A mixed methods approach towards understanding key disease characteristics associated with the progression from RRMS to SPMS: Physicians' and patients' views. *Mult Scler Relat Disord* 38

Ziff OJ, Clarke BE, Taha DM, Crerar H, Luscombe NM & Patani R (2022) Meta-analysis of human and mouse ALS astrocytes reveals multi-omic signatures of inflammatory reactive states. *Genome Res* 32: 71–84

